An Investigation of the Wetting Behaviour of Evaporating Drops

Samuel David

A thesis submitted for the degree of Doctor of Philosophy.
The University of Edinburgh.
October 2007

Acknowledgements

I would like to thank all those people who made this thesis possible and an enjoyable experience for me. First of all, I would like to express my deepest sense of gratitude to my supervisor Dr. Khellil Sefiane for his patient guidance, encouragement and excellent advice throughout this study.

I am also indebted to Lounès Tadrist for the opportunity to work at the University of Edinburgh.

I am thankful to Gavin Dunn, Pr Stephen Wilson and Dr Brian Duffy from the University of Strathclyde for their collaboration, especially in the elaboration of the mathematical model.

I am thankful to Pr Martin Shanahan from the University of Bordeaux for his comments and suggestions on binary mixture drops.

I would like to thank Jack and Ross for reading and editing my thesis and all the members of Sefiane's group: Yavor, Dario and Chris.

Finally, I would like to express my gratitude to EPSRC for financing of my study.

List of Publications

Journal Papers Resulting from the Project

1. S. David, K. Sefiane and L. Tadrist, Experimental Investigation of the Effect of Thermal Properties of the Substrate in the Wetting and Evaporation of Sessile Drops, Colloids and Surfaces A: Physicochemical and Engineering Aspects, 298, 108-114, 2007.

2. S. David, K. Sefiane and M. E. R. Shanahan On the Dynamics of Wetting of Water-Methanol Volatile Sessile Drops on Smooth Substrates, Defect and Diffusion Forum, 258/260, 469-473, 2006.

3. S. David, K. Sefiane and L. Tadrist, Experimental Investigation of the Effect of the Ambient Gas on Evaporating Sessile Drops, Defect and Diffusion Forum, 258/260, 461-468, 2006.

4. G. J. Dunn, S. K. Wilson, B. R. Duffy, S. David and K. Sefiane , The effect of the thermal conductivity of the substrate on droplet evaporation, 14th European Conference on Mathematics for Industry (ECMI 2006) Proceedings published by Springer, in press.

5. G. J. Dunn, S. K. Wilson, B. R. Duffy, S. David and K. Sefiane, A mathematical model of the evaporation of a thin sessile liquid droplet: comparison between experiment and theory, submitted to Colloids and Surfaces A.

6. G. J. Dunn, S. K. Wilson, B. R. Duffy, S. David and K. Sefiane, Influence of the Thermal Conductivity of the Substrate on Drop Evaporation, to be submitted to Journal of Fluid Mechanics.

7. S. David, K. Sefiane, G. J. Dunn, S. K. Wilson and B. R. Duffy, Drop Evaporation Under Reduced Pressure, to be submitted to Physics of Fluids.

Conference Presentations Resulting from the Project

1. 1.G. J. Dunn, S. K. Wilson, B. R. Duffy, S. David and K. Sefiane, 7th European Coating Symposium, Paris, France, 12-14 September 2007 (abstract submitted).

2. G. J. Dunn, S. K. Wilson, B. R. Duffy, S. David and K. Sefiane, 10th UK National Heat Transfer Conference, Edinburgh, 10-11 September 2007 (abstract accepted).

3. G. J. Dunn, S. K. Wilson, B. R. Duffy, S. David and K. Sefiane, 20th Scottish Fluid Mechanics Meeting, St. Andrews, 25 May 2007.

4. G. J. Dunn, S. K. Wilson, B. R. Duffy, S. David and K. Sefiane, 17th British Applied Mathematics Colloquium, Bristol, 17-19 April 2007.

5. K. Sefiane, S. David, G. J. Dunn, S. K. Wilson and B. R. Duffy, Analysis of the diffusion model for sessile drops evaporating under reduced pressure and the influence of the properties of the substrate and ambient atmosphere, International Workshop on Bubble and Drop Interfaces, Granada, Spain, 25-28 March 2007. (Invited keynote lecture, to be published in Advances in Colloid and Interface Science.)

6. S. David, K. Sefiane, G. J. Dunn, S. K. Wilson and B. R. Duffy, Influence of the substrate thermal conductivity on evaporating sessile drops under reduced pressure, ibid.

7. S. David, K. Sefiane and L. Tadrist, Experimental Investigation of the Effect of the Ambient Gas on Evaporating Sessile Drops, Second International Conference on Diffusion in Solids and Liquids, Aveiro, Portugal, 25-28 July, 2006.

8. S. David, K. Sefiane and M. E. R. Shanahan, On the Dynamics of Wetting of Water-Methanol Volatile Sessile Drops on Smooth Substrates", ibid.

9. G. J. Dunn, S. K. Wilson, B. R. Duffy, S. David and K. Sefiane, 16th British Applied Mathematics Colloquium, Keele, 24-27 April 2006.

10. S. David and K. Sefiane, 27th European Chemistry at Interfaces Conference, Loughborough, 27 June - 1 July 2005.

11. G. J. Dunn, S. K. Wilson, B. R. Duffy, S. David and K. Sefiane, 15th British Applied Mathematics Colloquium, Liverpool, 4-7 April 2005.

Contents

List of figures

List of tables

Introduction

Wettability is a fundamental phenomenon that plays a crucial role in a huge variety of practical situations ranging from technological applications such as printing, heat-transfer devices and various coating processes to a variety of biological and geophysical situations. For example, understanding wetting is key to the successful use of many detergents, emulsifiers, wetting agents, textile-processing chemicals, pesticides, herbicides and cosmetics. Other applications in which wetting plays an important role are found in the semi-conductors industry (in which cleaning and drying semi-conductor wafers is a key issue), the oil industry (in which wetting plays an important role in the recovery of oil), and heat transfer (in which the presence of fluid drops and/or films can have a dramatic effect on overall heat-transfer rates). In the particular case of sessile droplets, three phases co-exist: solid (substrate), liquid (drop) and gas (environment). A full understanding of the physics and controlling mechanisms for evaporating sessile drops requires a thorough analysis of heat and mass transfers across each interface as well as the interaction between different phases.

The aim of the present project is to carry out an experimental investigation of the wetting behaviour of an evaporating drop, a prototype problem for a wide range of physical situations in which wetting plays an important role. This work has also been undertaken in close collaboration with Gavin Dunn, PhD student at the University of Strathclyde (Department of Applied Mathematics) under the supervisions of Pr. S. Wilson and Dr B. Duffy. In a joint effort between our group in Edinburgh and Strathclyde group, a mathematical model for the case of sessile droplets with a pinned triple line was developed.

The topic of wetting and evaporation has been subject to an increasing interest by researchers in recent years. The extensive experimental investigations undertaken by various authors [1–6] gave insight in the physics of the wetting process during evaporation and the interaction between the two phenomena. Many of these investigations adopted the case of the spontaneous evaporation of liquid drops on substrates [1, 4, 7]. In these situations heat is brought from the ambient to allow the evaporation process to take place. Deegan *et al.* [1, 6] investigated the evaporation of pinned sessile drops and the ring stain formation. H. Hu *et al.* [7, 8] investigated the case where the droplet is small enough to be regarded as having a spherical cap shape and the contact line is pinned, the evaporation is considered mainly to be diffusion limited and can

be regarded as quasi-steady-state process. In the case of a droplet of water on a glass substrate, the model shows that at the initial contact angle of 40° the temperature increases from the top to the edge of the droplet, while at a contact angle of 10°, the temperature decreases. They suggest that this reversal of temperature-gradients direction occurs because at early times, the longer conduction path from the bottom of the glass to the top of the drop makes the temperature lower at the top than elsewhere, while at long times the faster rate at the edge makes it cooler there. In the case of binary mixtures, few investigations have been performed [9–11]. Rowan *et al.* [9] investigated the wetting behaviour of a 1-propanol and water mixture. The results of this work show two distinct trends of wetting behaviour: one for mixtures with mole fractions of less than 0.39 propanol (the contact angle decreased at a steady rate for the period required for total evaporation) and one for mixtures with mole fractions more than 0.39 propanol (appearance of instabilities around the droplet periphery). Sefiane *et al.* [10] and Yu *et al.* [11] both investigated water-ethanol mixture but on rough and smooth substrates respectively. Their works were focused on the influence of the mixture concentration but also on the differences between the pure components and the binary mixtures. Another important field of research in the case of sessile drops is the influence of the surface roughness on the wetting behaviour. Many works [12–18] have been performed in order to establish a relation between the surface topography of the substrate and the wetting (apparent contact angle) of the drops. One of the first theories taking into account the surface heterogeneities has been introduced by Wenzel [12, 13] and Cassie and Baxter [14] where coefficients characterising the surface roughness were added in the Young-Dupré equation. In the last 20 years, with the apparition of new technologies, important works have been undertaken in the elaboration of micro patterned surfaces [17–25] in order to control the wetting.

The present work is focused on the experimental investigation of the wetting behaviour of evaporating sessile drops. The experimental investigation could be divided into four cases. First the study of the influence of the substrate surface roughness on wetting, second the wetting behaviour of evaporating binary mixture drops, then the limiting effect in the evaporation process and finally the substrate thermal conductivity influence.

In the first chapter, a brief introduction to the main physics involved in the process of evaporative sessile droplets is presented. Firstly the notion of wettability (i.e the interaction between liquids and solids) is introduced. Particular interest is given to surface tensions, contact angles and sessile drop profiles in the case of partial wetting. Secondly the evaporation process is

explained in three parts: the interface phenomenon, the cooling effect and the mass diffusion in the surrounding gas.

In the second chapter, a literature review of the last 30 years in the area of volatile sessile drops is summarized. Both experimental and theoretical studies relevant to the present research are presented. First, there is a short presentation of the primary instants of the drop corresponding to its deposition on the substrate surface. Then the review will dwell upon various and important investigations done on the evaporation of sessile droplets, with experimental and theoretical works discussed in two different sections for clarity. Finally, recent works on rough surfaces and binary drops mixtures are introduced. In the following chapter 3, the actual work is introduced with a presentation of the experimental process.

Chapter 3 presents all the mains instruments used during the experimental work. A full description of the drop shape analyser (an apparatus which allows the injection and deposition of the drops), the image analysis software and the environmental chamber are given. Further details concerning each experimental preparations and procedures will be explained in the corresponding chapters.

The first experimental investigation to be presented in chapter 4, is a study of the effect of structured surfaces on the wetting behaviour. This was examined by using a substrate made of hydrophobic polymers patterned with structured defects. The topography of the substrate was measured using a profilometer. Six different surfaces with holes/pillars every 200 μm and depth/height from 1 to 200 μm were investigated. The results show a strong pinning of the contact line on surfaces with larger defects. The pinning/depinning phenomenon of the contact line of water drops on the various substrates was investigated to elucidate the role played by roughness on the dynamics of moving contact lines. The analysis of the results suggests that the competition between the unbalanced Young force and the anchoring forces of the defects may be dominating the pinning/depinning process. Noticeable "stick-slip" behaviour of the contact line was observed for substrates with larger defects.

In chapter 5, the experimental study of the wetting behaviour of evaporating binary mixture liquids are presented. Indeed multicomponent droplets are present in several industrial applications, such as crop-dusting where the wettability and the evaporation of herbicides on targeted surfaces is crucial. In cooling technologies binary systems are also frequently encountered when using binary refrigerants as cooling fluids. The understanding of wettability associated

with phase change behaviour is essential for these applications. In this chapter 5 we present the results of an experimental investigation of binary drops by using Methanol-Water and DMSO-Water drops deposited on a smooth silicon substrate with Nitrogen as the ambient gas. For each mixture, three different compositions have been prepared. First, details on the choice of the studied liquids and their preparation are given. Then the experimental results are presented and analysed before being discussed. In the next three chapters (6, 7, 8), a serious of studies of the heat and mass transfers mechanisms involved in the evaporation process is presented.

As mentioned above, the present project was in close collaboration with G. Dunn from Strathclyde University in the elaboration of a mathematical model, chapter 6 summarizes this work. The mathematical model developed assumes spherical cap like droplets with a constant diameter. Due to the axisymmetry of the problem, a 2D model is thought to be sufficient to describe the major mechanism and the underlying physics of the phenomenon. The evaporation of the drop is solely driven by the diffusion of its vapour into the ambient gas. In the next two chapters (7, 8), the mathematical model is compared to the experimental results where the evaporation process and the role played by the substrate thermal conductivity are investigated.

First, in chapter 7, the results of an experimental study of evaporating sessile drops in a controlled environment are presented. The experimental setup allowed the investigation of the evaporation rate of sessile drops under reduced pressure (40 to 1000 $mbar$) and various ambient gases. Sessile drops of initial volume 2.5 μL are deposited on substrates and left to evaporate in a controlled atmosphere. The effect of reducing pressure on the evaporation rate as well as changing the ambient gas is studied. Three different gases are used; namely Helium, Nitrogen and Carbon Dioxide. The role of vapour diffusion as a limiting mechanism for evaporation is studied and the experimental results are compared to the mathematical model.

In chapter 8, two mains investigations on the influence of substrate thermal properties are presented. In all experiments, four different materials based on their thermal conductivity have been used. The first investigation has been undertaken at atmospheric pressure. The experiments have been performed with three liquids (Water, Acetone and Methanol) for various drop sizes. In the second investigation, Water drops ($R = 1.35\ mm$) are used and evaporating in an atmosphere for a range of pressures (from 40 $mbar$ to 1000 $mbar$). Three gases were used: Helium, Nitrogen and Carbon Dioxide. The above mentioned conditions will allow us to investigate the precise role played by substrates thermal properties in the evaporation of drops. These experimental data are also compared to the results obtained with the mathematical model.

Following the results obtained in the last three chapters, where the non uniformity of the temperature in the drop has been observed, additional temperature measurements have been undertaken using infrared thermography. Chapter 9 presents preliminary infra-red (IR) measurements of the interfacial temperature of three liquids: Water, Methanol and FC72 (coolant liquid) respectively, where unexpected observations have been made.

Chapter 1
Theory

In this chapter, a brief introduction to the main physics involved in the process of volatile sessile droplets is presented. Firstly, the notion of wettability (i.e the interaction between liquids and solids) is introduced. Particular interest is given to surface tensions, contact angles and sessile drop profiles. Secondly the evaporation process is explained in three parts: the interface phenomenon, the cooling effect and the mass diffusion in the surrounding gas.

1.1 Wettability

1.1.1 Surface tension

Definition

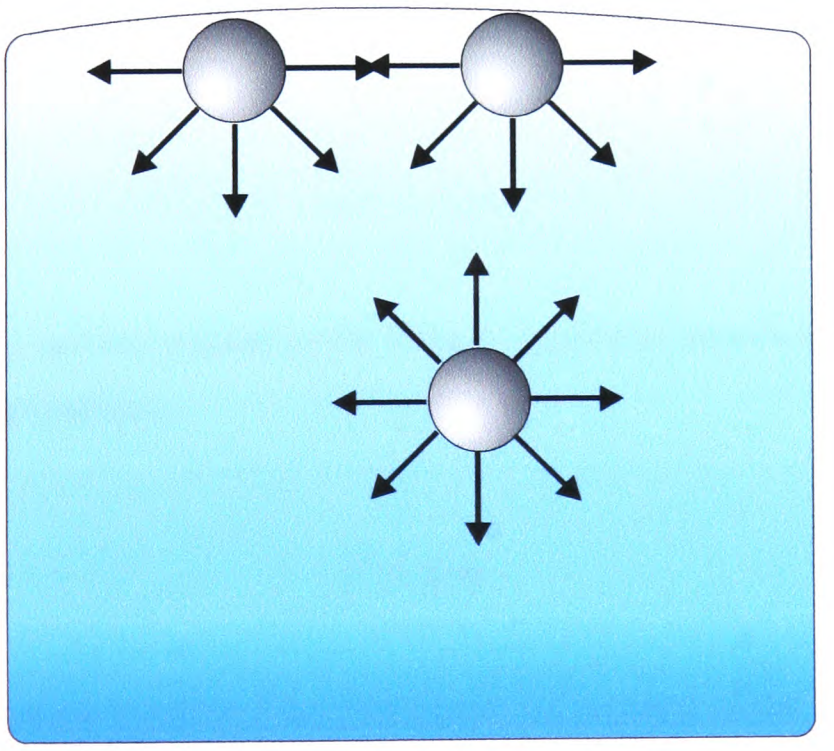

Figure 1.1: *Intermolecular forces between molecules in the bulk fluid and on the fluid surface.*

The origin of the surface tension is due to various intermolecular forces (Van der Waals forces, hydrogen bonds, electrostatic forces., etc). In the bulk of the liquid, each molecule is attracted

by the neighbouring liquid molecules, the resulting force is then zero. At the interface (see Figure 1.1), the attraction by the molecules in the liquid is greater than that from the molecules in the surrounding medium (air has a lower density). Therefore all the interfacial molecules are subject to an inward force which can be balanced only by the resistance of the liquid to compression. Thus the liquid squeezes itself to minimize its surface.

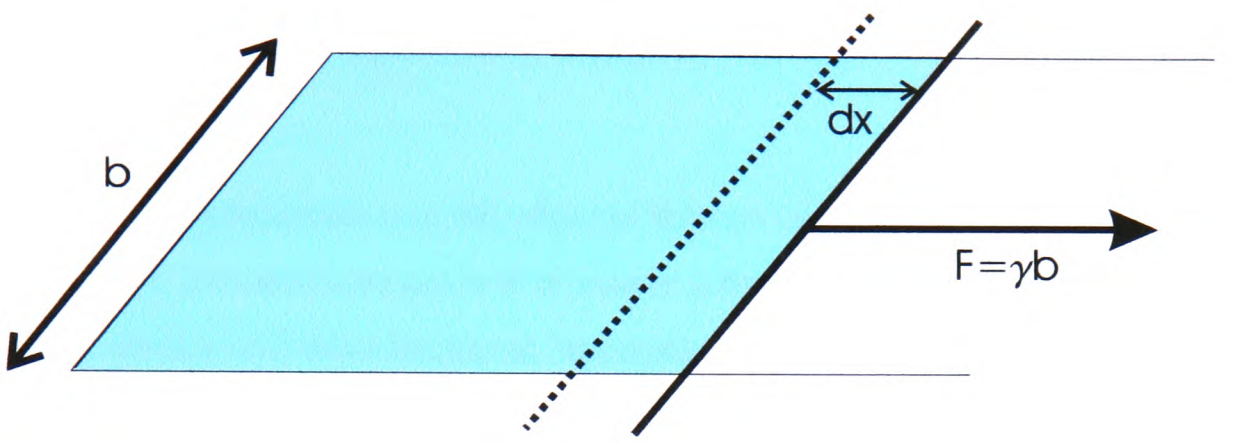

Figure 1.2: *Illustration of the relation between the work needed to increase a surface of a quantity dA and the surface tension γ.*

Another way to define the surface tension is the work done per unit area. Figure 1.2 illustrates this definition. A liquid film is spanned over a frame. To increase the surface area by moving the slider a distance dx, work has to be done. This work dW is proportional to the increase in surface area dA. We have:

$$dW = \gamma dA \tag{1.1}$$

We can also define the surface tension as the force F applied to maintain the slider in position and balance the surface tension:

$$F = 2\gamma b \tag{1.2}$$

The unit of surface tension is either $J.m^{-2}$ or $N.m^{-1}$. For most of the liquids the values are between $0.015\ N.m^{-1}$ and $0.08\ N.m^{-1}$. So they are usually given in $mN.m^{-1}$.

Temperature and concentration influences

For a narrow temperature range, the surface tension γ_T decreases linearly with the temperature T:

$$\gamma_T = \gamma_0 \left(1 - k_0 T\right) \tag{1.3}$$

where k is particular to each liquid, this is a property equivalent to the boiling point, density, etc... [26].

This variation with temperature is at the origin of thermocapillary convection (Marangoni convection). Indeed, if a temperature gradient is present at the interface, an interfacial force towards higher surface tension will drive the liquid into motion.

Laplace law

The Laplace law relates the pressure difference between the two phases and the curvature of the surface ($P_2 - P_2$), see Figure 1.3:

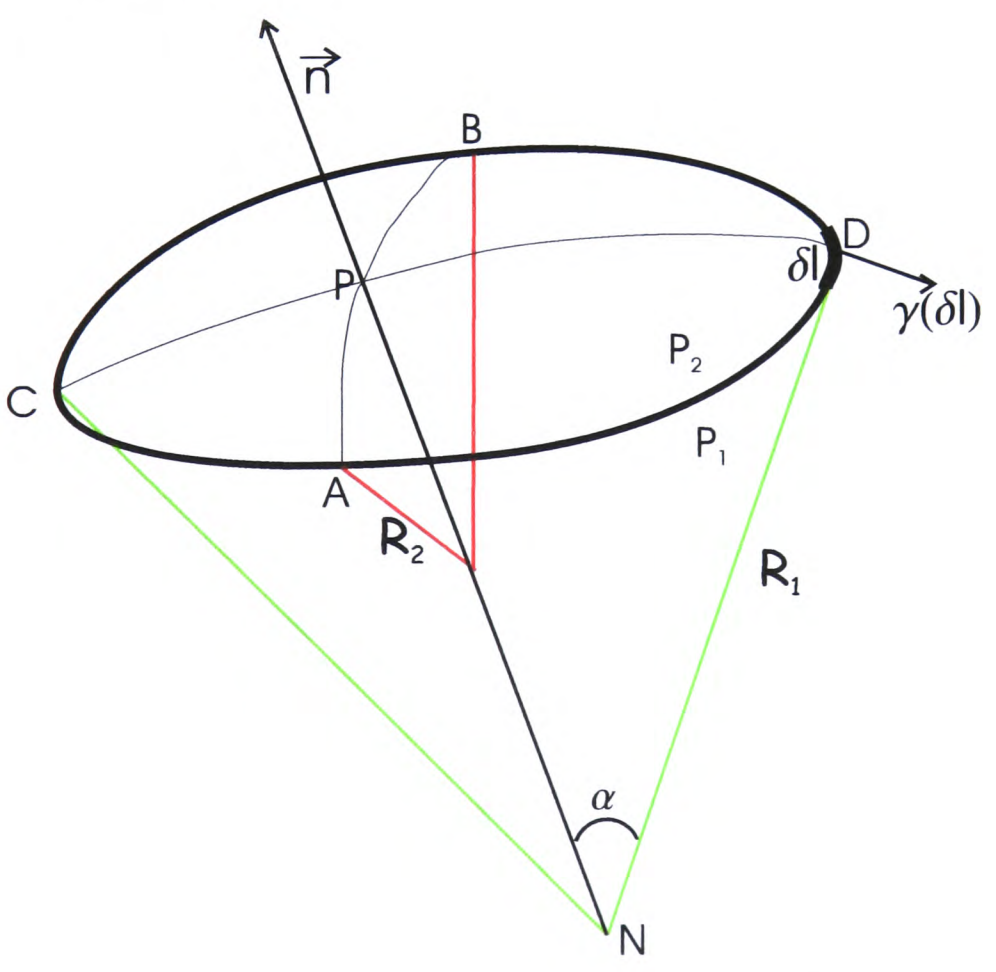

Figure 1.3: *Small interface element between two phases 1 and 2. R_1 and R_2 are the curvature radii.*

Take a point P on the surface and draw a line around it where the distance to P is a constant d. Through P take any two cuts that are perpendicular to each other (APB and CPD). The radii of curvature in P is R_1 and R_2. At A, consider a small segment of the line δl. As explained in Figure 1.2, the surface tension pulls with a force $\gamma\delta l$. The projection of the force on PN is:

$$\gamma\delta l \ \sin\alpha = \gamma\alpha\delta l = \gamma\delta l\frac{d}{R_1} \tag{1.4}$$

$\sin\alpha \simeq \alpha$ for small angles. The sum of the four vertical components at points A, B, C and D is

$$\gamma\delta l\left(\frac{2d}{R_1}+\frac{2d}{R_2}\right) \tag{1.5}$$

This expression is independent of the choice of AB and CD. Integration over one quarter of the borderline gives the total vertical force:

$$\gamma d^2\left(\frac{1}{R_1}+\frac{1}{R_2}\right) \tag{1.6}$$

At equilibrium, this downward force must be balanced by an equal force in the opposite direction. This is caused by an increase in pressure $P_2 - P_1$ on the concave side of $\pi d^2(P_2 - P_1)$. By equating both forces, we obtain:

$$\pi d^2(P_2-P_1) = \gamma d^2\left(\frac{1}{R_1}+\frac{1}{R_2}\right) \qquad \Rightarrow \qquad \Delta P = \frac{2\gamma}{r_m} \tag{1.7}$$

ΔP is the pressure difference between the two phases and r_m is the mean curvature defined by:

$$\frac{1}{r_m} = \frac{1}{2}\left(\frac{1}{r_1}+\frac{1}{r_2}\right) \tag{1.8}$$

One consequence of this relationship is described by Defay in [27]: "*The only surfaces which have to be considered in dealing with systems where gravitational effects can be neglected, are those of constant mean curvature*".

1.1.2 Contact angle

Definition

In the case of a liquid drop deposited on a solid substrate, three phases are present, see Figure 1.4. Therefore three surface tensions need to be considered: solid-liquid (γ_{SL}), solid-gas (γ_{SV}) and liquid-gas (γ_{LV}). For an ideal surface and at equilibrium (no evaporation and isolated system), the Young-Dupré equation gives the relation between the equilibrium contact angle (θ_{eq}) the drop makes with the surface and the three surface tensions as:

$$\gamma_{SV} = \gamma_{SL} + \gamma_{LV} \cos(\theta_{eq}) \tag{1.9}$$

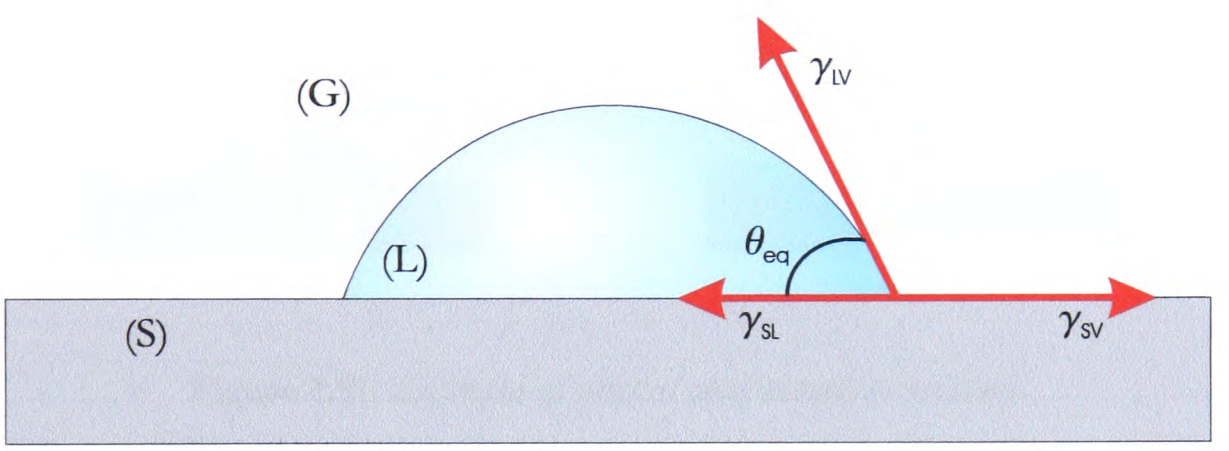

Figure 1.4: *Illustration of a three phase model: sessile drop deposited on a substrate.*

This expression can be obtained from other mechanical or thermodynamics principles. One example is to derive the equation from thermodynamics [28]; a small displacement of the triple line (corresponding to a change of the wetted area ΔA) results in a variation of the surface free energy:

$$\Delta G = \Delta A(\gamma_{SL} - \gamma_{SV}) + \Delta A \gamma_{LV} cos(\theta - \Delta\theta) \tag{1.10}$$

At equilibrium,

$$lim_{\Delta A \to 0} \frac{\Delta G}{\Delta A} = 0 \tag{1.11}$$

$\Delta\theta/\Delta A$ behaves as a second-order differential, so we finally obtain:

$$\gamma_{SL} - \gamma_{SV} + \gamma_{LV} cos\theta = 0 \tag{1.12}$$

If the three tensions are known, the wetting state of the fluid follows directly. In the case of a substrate with a low surface tension, a droplet with a finite contact angle will minimize the free energy of the system; resulting in partial wetting. To characterise the wetting state, the spreading coefficient S is usually used. It represents the surface free energy difference between partial and complete wetting;

$$S = \gamma_{SV} - \gamma_{SL} - \gamma_{LV} \tag{1.13}$$

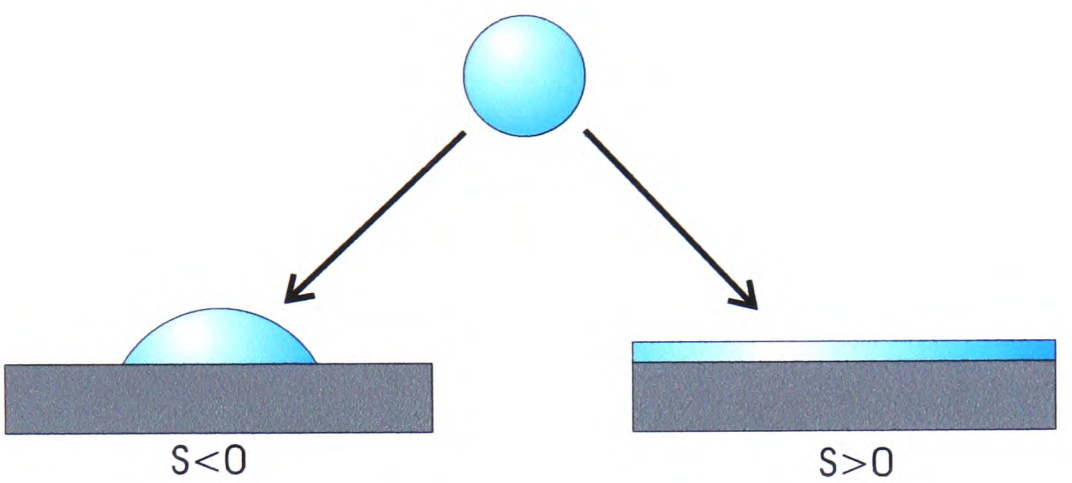

Figure 1.5: *Example of partial and complete wetting.*

If $S \geq 0$, the liquid wets completely the solid surface, see Figure 1.5. If $S < 0$, the liquid drop does not spread and forms a spherical cap with a finite contact angle determined by Equation 1.9:

$$\cos(\theta_{eq}) = \frac{\gamma_{SV} - \gamma_{SL}}{\gamma_{LV}} \tag{1.14}$$

Real surfaces

On real surfaces, the equilibrium contact angle is not unique. Surface irregularities and other chemical inhomogeneities lead to contact angle hysteresis. This corresponds to a succession of metastable states that differ in energy and are separated by energy barriers [29]. This range of equilibrium contact angles is limited by the advancing contact angle θ_{adv} and the receding contact angle θ_{rec}. In the case of a sessile drop, when we increase the volume of the drop, the angle at which the contact will start to move is θ_{adv}. On the opposite, if we decrease the volume, θ_{rec} corresponds to the angle when the triple line starts to recede. Due to the existence

of multiple apparent contact angles, interest has been focused on the apparent contact angle corresponding to the global energy minimum [30] (metastable state with the lowest energy). On both rough and heterogeneous surfaces, a correlation between this contact angle (θ_{app}) and the ideal contact angle (θ_{eq}) exists. On a rough surface and if the surface roughness is small compare to the drop size, the relation is given by the Wenzel equation [12, 13]:

$$\cos\theta_{app} = r\cos\theta_{eq} \tag{1.15}$$

where r is the ratio between the true and the apparent surface area of the solid ($r \geq 1$). This relationship shows that surface roughness makes the contact angle far from $90\,°$. For an angle greater than $90\,°$, the surface roughness increases the contact angle and vice versa for $\theta_{eq} < 90\,°$. On heterogeneous surfaces θ_{app} is related to θ_{eq} through the Cassie-Baxter equation [14]:

$$\cos\theta_{app} = f_1\cos\theta_{eq1} + f_2\cos\theta_{eq2} \tag{1.16}$$

where the subscripts 1 and 2 refer to the two surface components. f_1 and f_2 are surface ratios and θ_{eq1} and θ_{eq2} are the corresponding equilibrium contact angles.

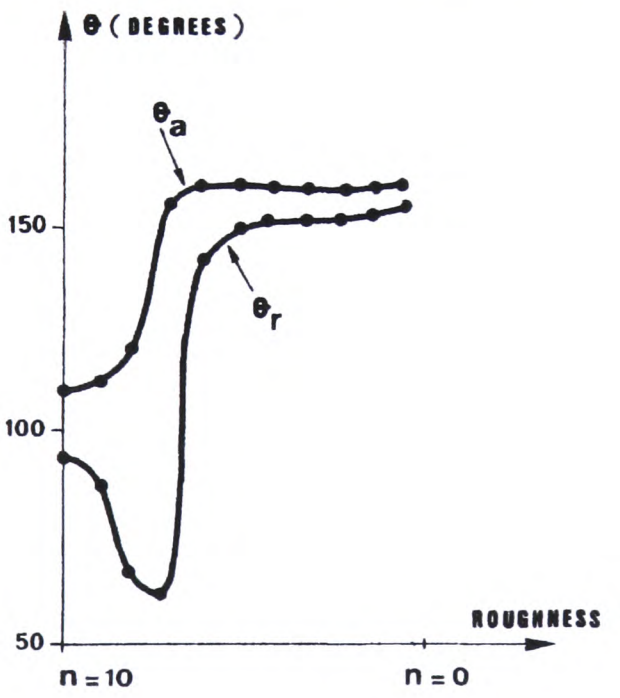

Figure 1.6: *Advancing and receding contact angles evolution on a wax substrate as a function of surface roughness state (obtained by successive heating n of the substrates in an oven) , from [31]*

Dynamic contact angle

The dynamic contact angle [1] represents the value of the contact angle when the three phase line is in motion. It can be divided in two categories: advancing and receding contact angles. The advancing angle corresponds to the contact angle when the three phase line is moving over and wetting the surface or "pushing" away the gas phase, while the receding angle corresponds to the contact angle when the three phase line is withdrawn over a pre-wetted surface or "pushing" away the liquid phase. It means that in the case of receding contact angle a thin wetted film is left behind. These two cases are represented in figures 1.7 and 1.8.

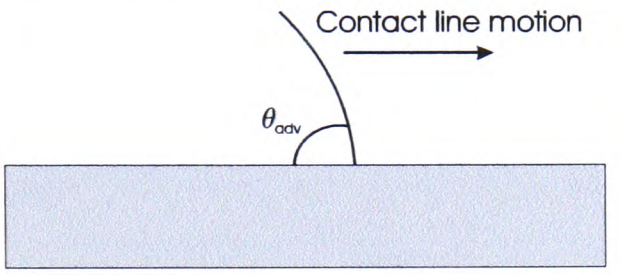

Figure 1.7: *Advancing contact angle.*

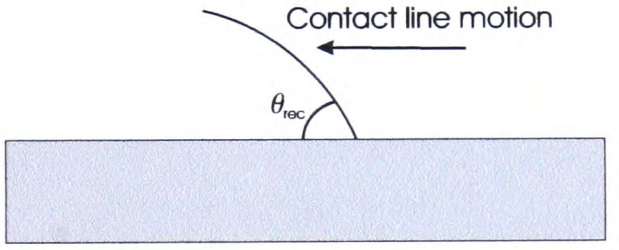

Figure 1.8: *Receding contact angle.*

The dynamic contact angle is influenced by the the surface roughness and by the velocity of the triple line. It has been shown by Lam *et al.* [32] that for low velocities the values of the advancing and receding contact angles could be considered as constant.

1.1.3 Sessile drop profile

Definition

To define the sessile drop profile, the competition between surface tension forces and gravity forces have to be considered. A way to characterise the predominant force is by using the dimensionless Bond number Bo:

[1] The present definition is limited to the case of partial wetting.

$$Bo = \frac{\rho g r}{\gamma} = \frac{Gravity}{Surface \quad Tension} \tag{1.17}$$

where ρ is the density, g the acceleration due to gravity, r a representative length scale (typically the drop base radius in the case of a sessile drop) and γ the liquid-gas surface tension. For smaller drops, surface tensions forces dominate. As a result, the surface mean curvature is constant and the drop profile has a spherical cap shape. For larger drops, the top of the drop is flattened due to gravity forces.

Another way to indicate the predominance of either gravity or surface tension is the capillary length κ^{-1}. When the characteristic length is greater than κ^{-1} the gravity forces cannot be neglected.

$$\kappa^{-1} = \sqrt{\frac{\gamma}{\rho g}} \tag{1.18}$$

The typical values for common liquids are between $1.5\ mm$ and $2\ mm$; but $2.7\ mm$ for Water because of its high surface tension, $72\ mN.m^{-1}$ (due to hydrogen bonds).

Profile equations

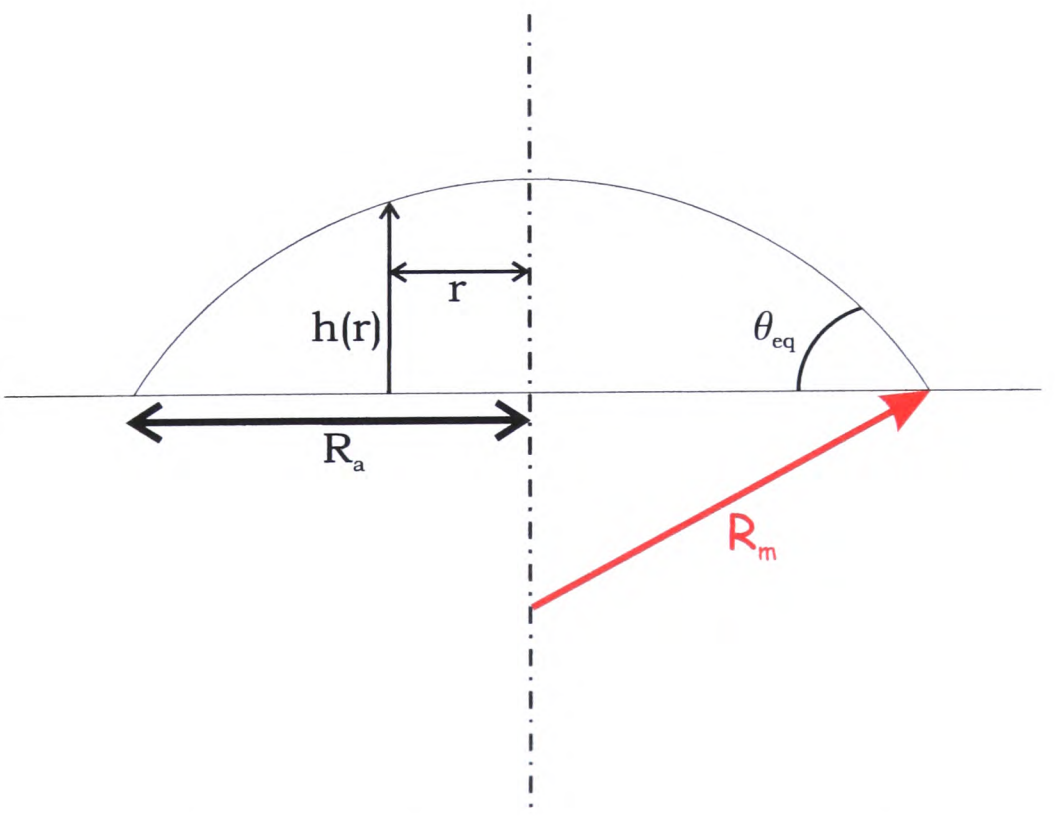

Figure 1.9: *Parameters defining the sessile drop profile.*

For the case of relatively small droplet ($R_a < \kappa^{-1}$), gravity forces are negligible, the sessile droplet profile can be considered as a spherical cap. In figure 1.9 all the parameters are represented. R_m is the radius of the sphere to which the spherical cap belongs, R_a is the drop base radius, $h(r)$ its height at a distance r from the centre and θ_{eq} its contact angle. Hence we can express $h(r)$ as follows:

$$h(r) = \sqrt{\frac{R_a^2}{\sin^2\theta_{eq}} - r^2} - \frac{R_a}{\tan\theta_{eq}} \tag{1.19}$$

and for the volume V and the surface A, we have:

$$V = \frac{\pi R_a^3 (1-\cos\theta_{eq})^2 (2+\cos\theta_{eq})}{3\sin^3\theta_{eq}} \tag{1.20}$$

$$A = \frac{2\pi R_a^2}{1+\cos\theta_{eq}} \tag{1.21}$$

For larger drops ($R_a > \kappa^{-1}$), the top of the drop is flattened due to gravity forces. The maximum height $h(0)$ of the drop is [33]:

$$h(0) = 2\kappa^{-1}\sin\left(\frac{\theta_{eq}}{2}\right) \tag{1.22}$$

1.2 Evaporation

1.2.1 Definition

At the difference of boiling, evaporation is a surface phenomenon. It is the result of a net mass transfer process between the liquid and the gas. We can describe this process by using the kinetic theory. At the liquid-gas interface, molecules from both the liquid and the gas cross the interface. If the liquid vapour pressure is at saturation, the mass transfer balance is zero. But if the vapour pressure is lower than the saturated value, there is a net mass transfer towards the gas.

From the kinetic theory, the Hertz-Knudsen equation gives an expression of the mass flux $\mathbf{J}_{\mathbf{mol}}$

at the interface, Prosperetti [34]:

$$\mathbf{J_{mol}} = \alpha\sqrt{\frac{k_B T_{int}}{2\pi M}}(\rho_v^{eq}(T_{int}) - \rho_{int})\mathbf{n} \tag{1.23}$$

where α is the accommodation coefficient, M the molecular weight, k_B the Boltzmann constant, $\rho_v^{eq}(T_{int})$ the density of the gas at equilibrium at the interface, ρ_{int} the actual density at the interface, $\mathbf{n}$ the outward normal to the interface. J_{mol} is proportional to the deviation from the saturated volume density.

$$v_{th} = \alpha\sqrt{\frac{k_B T_{int}}{2\pi M}}, \tag{1.24}$$

is a typical kinetic velocity of the process.

The energy consumed by transferring the molecules from the liquid phase to the gas phase is the latent heat of evaporation and result in a temperature decrease. Indeed only the molecules of highest energy cross the interface, thus the remaining molecules have lower average kinetic energy and so the temperature decreases. This is called evaporative cooling. Previous works (see [28]) show that a correlation exists between latent heat of evaporation and surface tension (it is dependent on the size of the molecule).

If evaporation was the unique process, molecules would rapidly accumulate at the interface and the saturated vapour pressure would be reached. In the configuration of a sessile droplet surrounded by a non-saturated ambient gas, departure from equilibrium is generated by the diffusion of the molecules near the interface ($\rho_{sat}(T)$) towards the ambient gas (ρ_∞).

To see if the limiting process is either diffusion or evaporation at the interface, we use the kinetic Péclet number Pe_k which is a dimensionless number comparing the two timescales:

$$Pe_k = \frac{v_{th} l}{D_{AB}} \tag{1.25}$$

where l is a characteristic length [35] and D_{AB} the diffusion coefficient.

1.2.2 Diffusion

Diffusion coefficients depend upon composition, temperature and pressure. The following is only about mass diffusion in binary system. Any perturbations which modify the equilibrium composition of a binary system generate a diffusive flow which is proportional to the gradient in chemical potential $(d\mu_A/dz)$. However, for ideal gases we have the following relationship between the chemical potential μ_A and its composition x_A:

$$\mu_A = \mu_A^0 + RTln(x_A), \tag{1.26}$$

we can hence consider that the diffusion is also proportional to the composition gradient.

At low to moderate pressures, the diffusion coefficients for a binary gas has been found independently by both Chapman and Enskog, [26]: from the kinetic theory, we can express the average molecular speed $\bar{C}$ by Maxwell's formula, see [36]:

$$\bar{C} = \left(\frac{8k_B N_A T}{\pi M}\right)^{1/2} \tag{1.27}$$

where k_B is the Boltzmann's constant. If we assume the molecules to be rigid and spherical, then the mean free path is:

$$l = \frac{k_B T}{\pi\sqrt{2}d^2 p} \tag{1.28}$$

where d is the effective molecular diameter and p the pressure. By substituting $\bar{C}$ and l in the expression of diffusion coefficient (see equation A.3 in Appendix A for more details), we obtain:

$$D_{AB} = (2\eta a)\,\bar{C}l \qquad \Rightarrow \qquad D_{AB} = \frac{(\pi k_B)^{3/2}}{d^2}\left(\frac{N_A}{M}\right)^{1/2}\frac{T^{3/2}}{p} \tag{1.29}$$

We can first notice that the diffusion coefficient varies as $T^{3/2}$ and p^{-1} and does not depend on the composition.

For a more accurate result, they also take into account that molecules are not really hard spheres, and also the differences in molecular sizes, and hence express the diffusion coefficient as:

$$D_{AB} = \frac{0.00266T^{3/2}}{PM_{AB}^{1/2}\sigma_{AB}^{2}\Omega_D} \tag{1.30}$$

where D_{AB} is the diffusion coefficient ($cm^2.s^{-1}$), T is the temperature (K), P is the pressure (bar), σ_{AB} is the characteristic length (A) and Ω_D is the diffusion collision integral (dimensionless).

The main physics involved in the evaporation of sessile drops have been presented. In particular, attentions have been given on the wettability and evaporation process phenomena. This will give the reader a better comprehension of the thesis. In the following chapter, a literature review of the main works on the subject is presented.

Chapter 2
Literature review

In the last 30 years a lot of interest has been shown in the area of volatile sessile drops. Many experimental and theoretical works have been reported. In the present chapter, the main studies relevant to the present research are presented. First, there is a short presentation of the primary instants of the drop corresponding to its deposition on the substrate surface. Then the review will dwell upon various and important investigations done on the evaporation of sessile droplets. In order to clarify the presentation, experimental and theoretical works are discussed in two different sections. Finally, recent works on rough surfaces and binary drops mixtures are introduced.

2.1 Drop deposition

When a liquid drop is placed on a solid surface, it may spread out and wet completely the surface (zero contact angle) or establish a finite equilibrium contact angle ($\theta_{eq} > 0$). Extensive researches [3, 37–44] have been undertaken on the hydrodynamic aspect of the problem. In the case of small drops, the gravity is negligible, the spreading is the result of a competition between the driving force (departure from equilibrium) and the friction between the layers of the liquid and the solid. When $S > 0$ (complete wetting), it has been shown that a precursor film is formed at the periphery of the drop. The spreading law, independent of S, can be expressed as follows $R(t) \sim t^n$ where the power n is of the order of $1/10$ [3, 37, 44].

One practical example of the study of droplet spreading has been performed by De Coninck *et al.* [45]. For partial wetting, they developed a molecular-kinetic model of friction with the solid that predicts the dynamic contact angle. Hence from experimental results it is possible to characterise some properties of the surface at the microscopic scale.

In the following section, all the investigations reported are for the non-wetting case. It means that when the drop is deposited on the substrate surface the equilibrium contact angle is reached instantly.

2.2 Evaporation

Picknett *et al.* [4] were first to show the presence of two distinct modes of evaporation. Drops resting on a substrate surface could evaporate either at a constant contact angle (no hysteresis) or at a constant contact area (presence of contact angle hysteresis), see Figures 2.1 and 2.2.

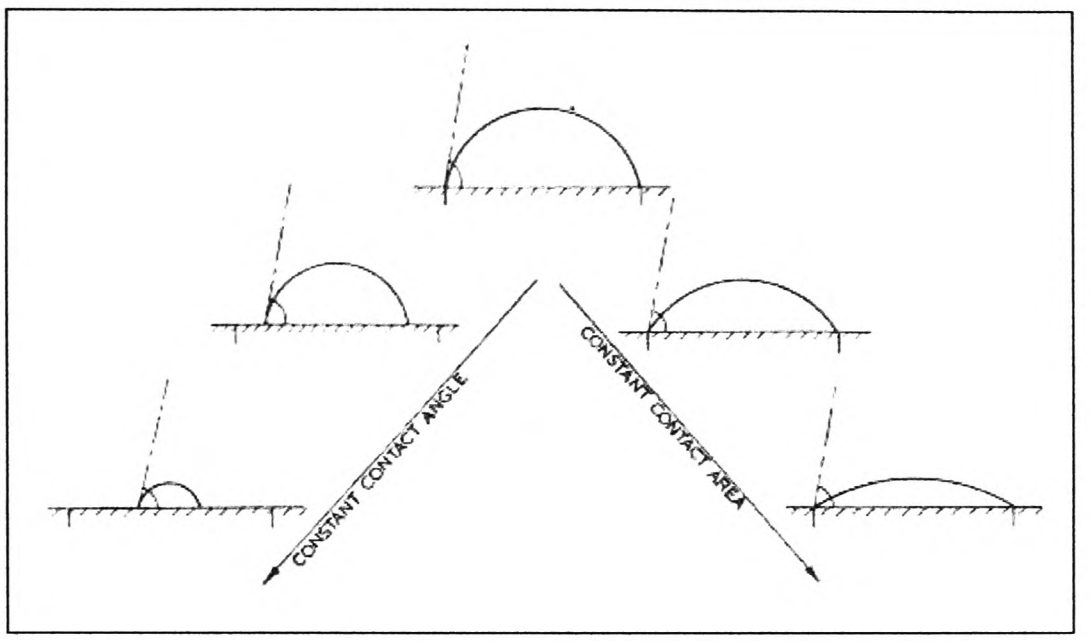

Figure 2.1: *The two modes of evaporation of drop resting on a surface [4].*

Their experiments [4] were conducted with methyl acetoacetate drops resting on a small convex lens covered with a thin layer of PTFE. In Figure 2.2, examples of experimental results for both modes are represented. In section 2.3, a presentation of the model introduced by these authors is given. A similar investigation on the modes of evaporation have been later performed by Shanahan *et al.* [2].

Shanahan *et al.* [2] have worked on the influence of evaporation on contact angle. They looked at the evolution of water and n-decane evaporating drops deposited on various substrates (namely polyethylene, PTFE and glass). In the first stage of their experiments, the surrounding atmosphere is saturated by the vapour of the test liquid, then the drop is allowed to evaporate. Their results have shown that the whole experimental process until the disappearance of the drop could be divided into four stages, see Figures 2.3 and 2.4. This result is independent of the couple solid/liquid. The first stage, describes the saturated atmosphere, all drop parameters are almost constant (saturation is not perfect). When evaporation starts, the drop base diameter remains constant and the contact angle decreases until reaching the "receding value" θ_R (stage II). In the third stage, the contact angle is now constant and the diameter recedes. Finally at the end of the lifetime of the drop, all parameters decrease until the drop vanishes (stage IV).

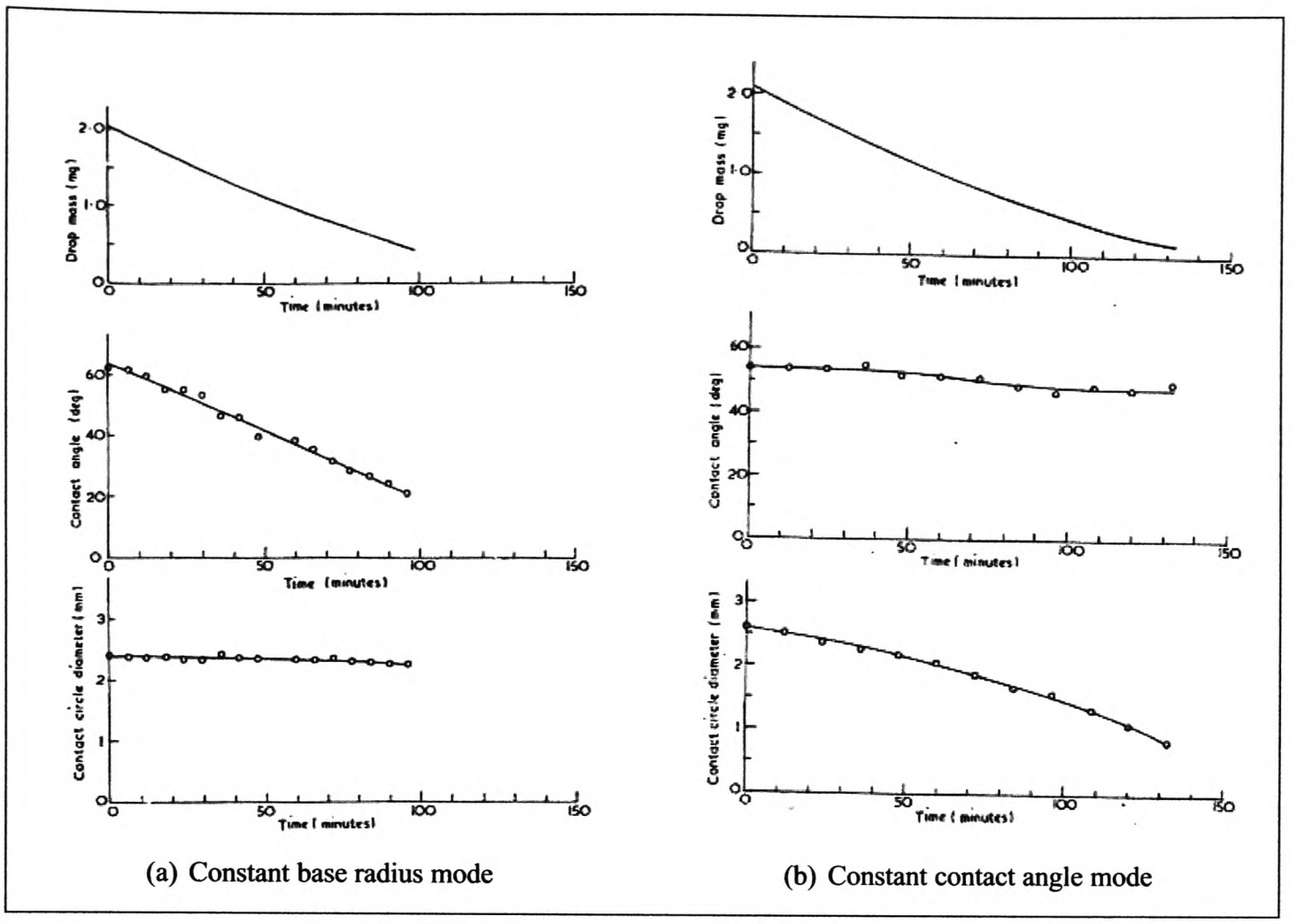

Figure 2.2: *Experimental results showing the two extreme modes of evaporation [4].*

These modes of evaporation are influenced by the substrate surface roughness. On a relatively rough substrate, the triple contact line will be pinned to the substrate. In this particular case where the contact base radius remains constant many investigations have been performed [46–49]. All these studies have been performed with water drops but other substrates were used.

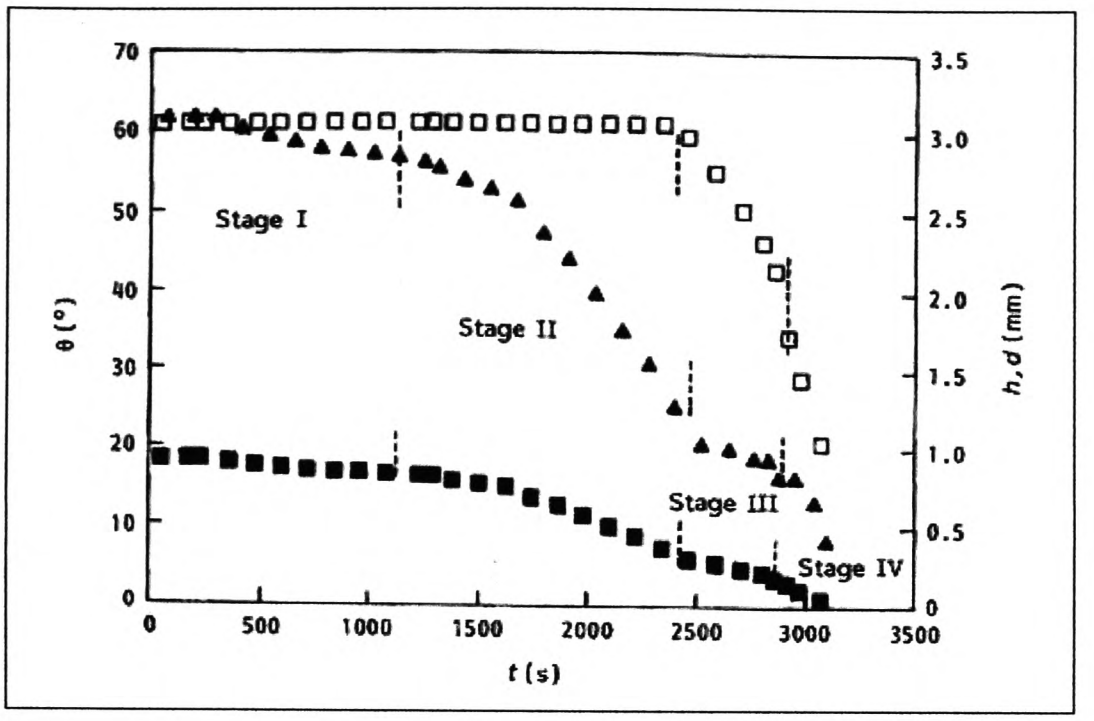

Figure 2.3: *Evolution in time of the drop height h, drop base diameter d and contact angle θ, for a drop of water on polished epoxy [2].*

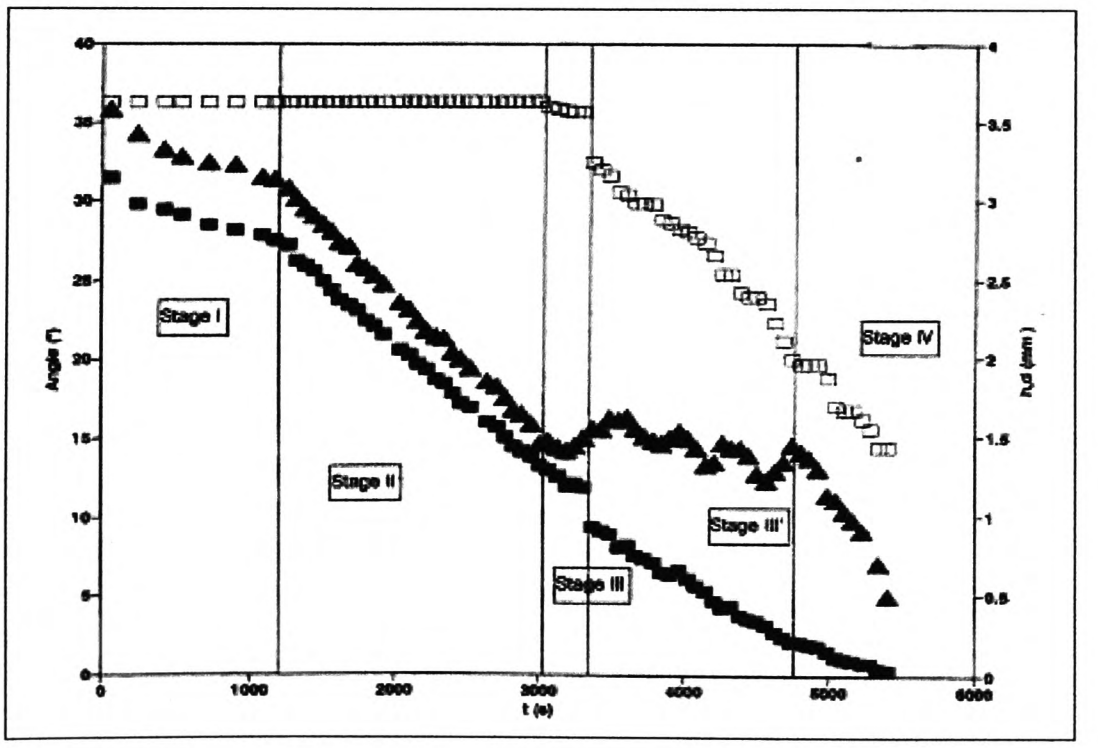

Figure 2.4: *Evolution in time of the drop height h, drop base diameter d and contact angle θ, for a drop of n-decane on PTFE [2].*

In their work, Birdi *et al.* [46] have studied the evaporation rate of water drops resting on PTFE by measuring the mass evolution in time. They have shown that the triple line is pinned during the evaporation process. In this case the rate of evaporation is constant (see Figure 2.5) and increases linearly with the drop base radius (see Figure 2.6). This is an important result which will be further discussed.

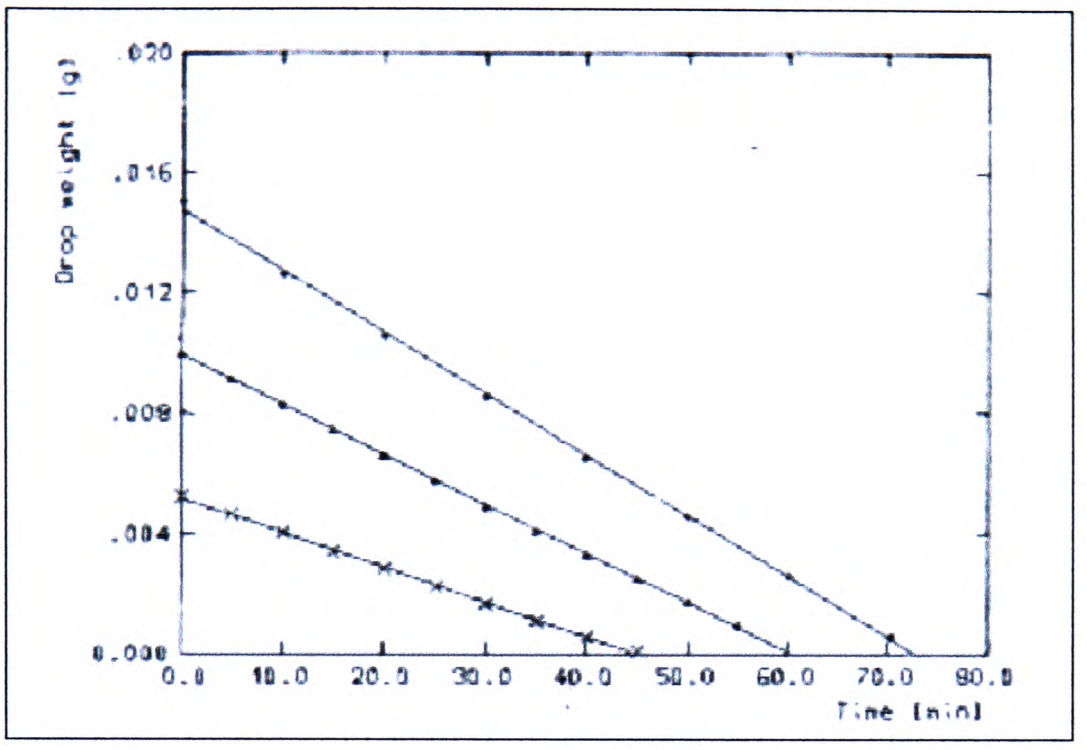

Figure 2.5: *Mass evolution of various water drops sizes deposited on PTFE substrate [46].*

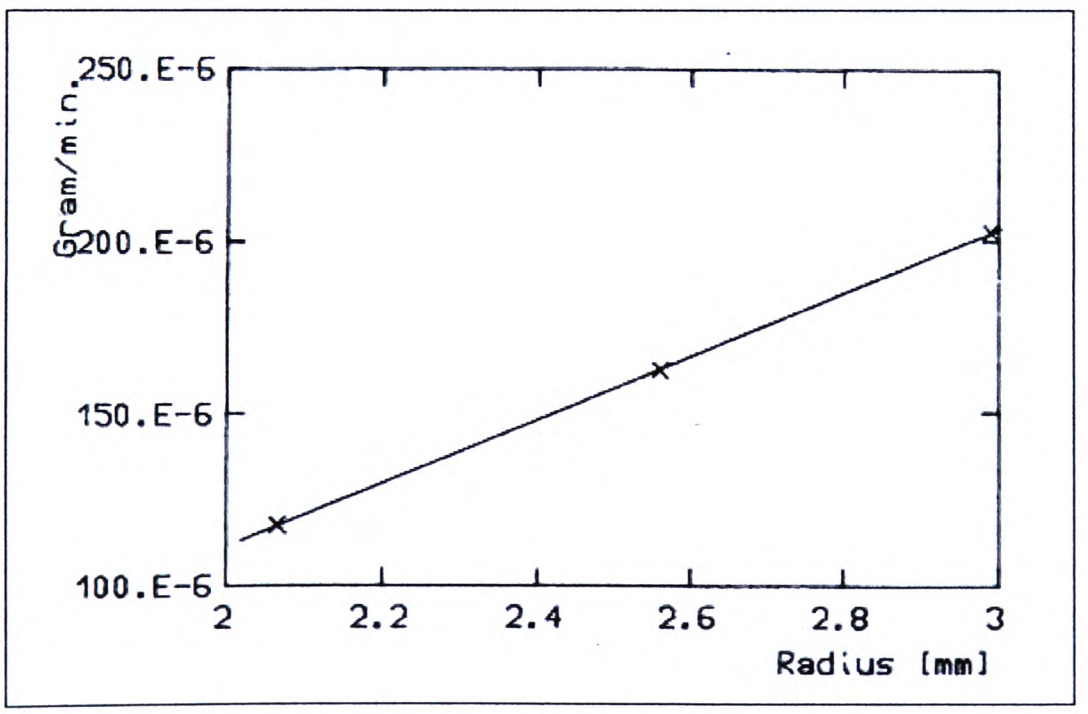

Figure 2.6: *Evaporation rate plotted against the drop base radius [46].*

Rowan *et al.* [47] deposited relatively small water drops (base radius ranging from 0.293 to $0.585\ mm$) on PMMA (polymethylmethacrylate) and let them freely evaporate (50% humdity

and $T = 21.5°C$). Through optical measurements they determined the drop profile and deduced the mass loss in time. From 85° (initial contact angle) to 40° the triple line is pinned, then the drop starts to shrink. In conclusion it was found that at the difference of the previous study, the rate of mass loss is proportional to the height and not to the base radius when the triple line is pinned.

Barthwal *et al.* [48] performed their experiments with glass and polycarbonate substrates. The surface roughness of substrate surfaces were measured with a profilometer and found to be $0.15\mu m$ for glass and $0.04\mu m$ for polycarbonate. The drops were left evaporating in the ambient air with temperature and humidity respectively around $27 - 28°C$ and $61 - 63\%$. To determine the evaporation rate, the drops were placed on a microbalance and an optical technique was used to measure the drop profile parameters (radius and conatct angle). Barthwal *et al.* showed that throughout the evaporation process the contact base radius remains constant and a linear decrease in drop mass is observed, see Figures 2.7, 2.8, 2.9 and 2.10.

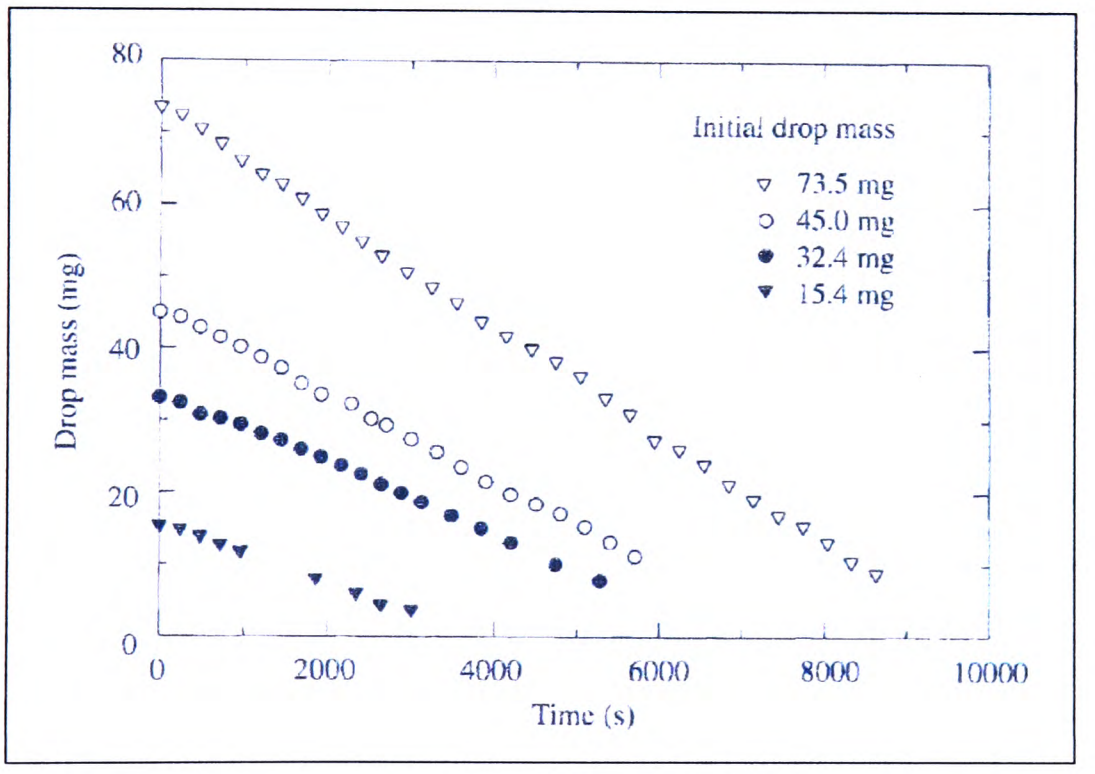

Figure 2.7: *Mass vs time for water drops deposited on glass [48].*

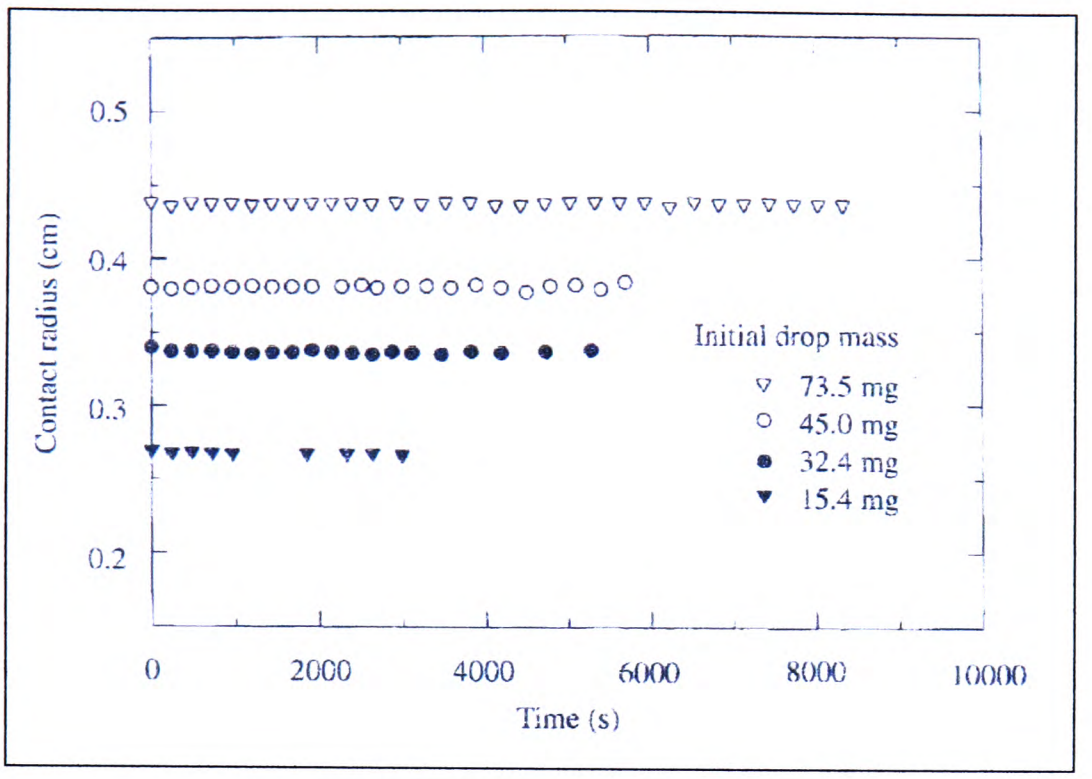

Figure 2.8: *Contact radius vs time for water drops deposited on glass [48].*

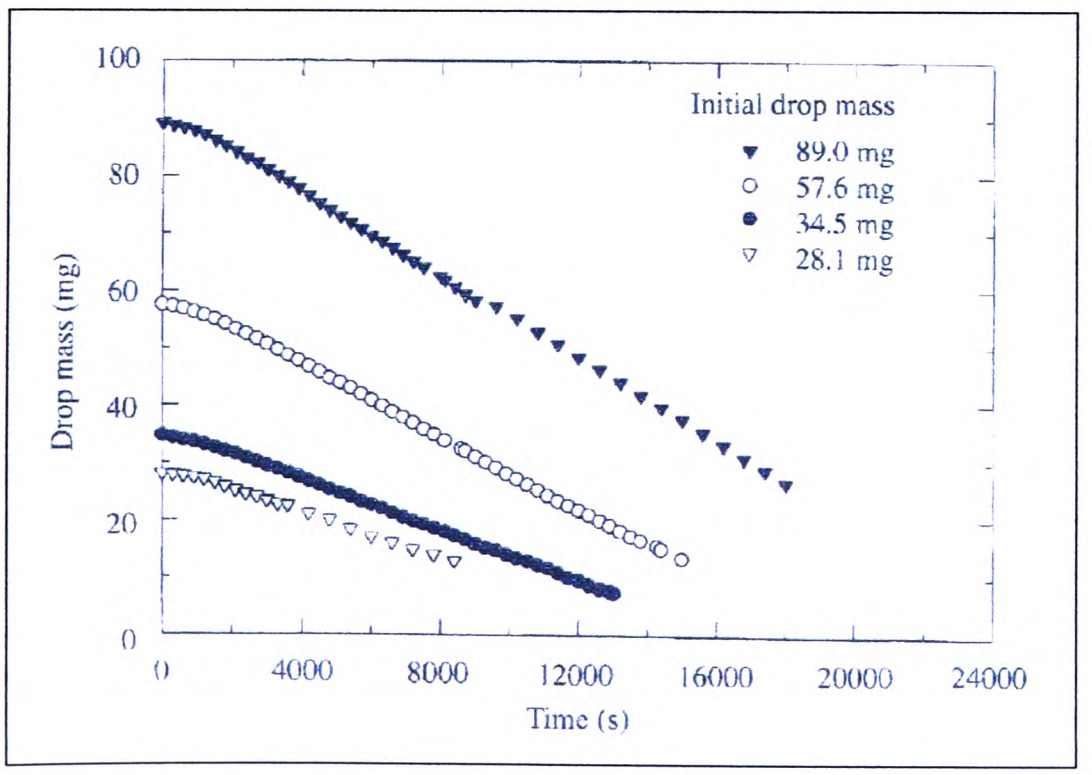

Figure 2.9: *Mass vs time for water drops deposited on polycarbonate [48].*

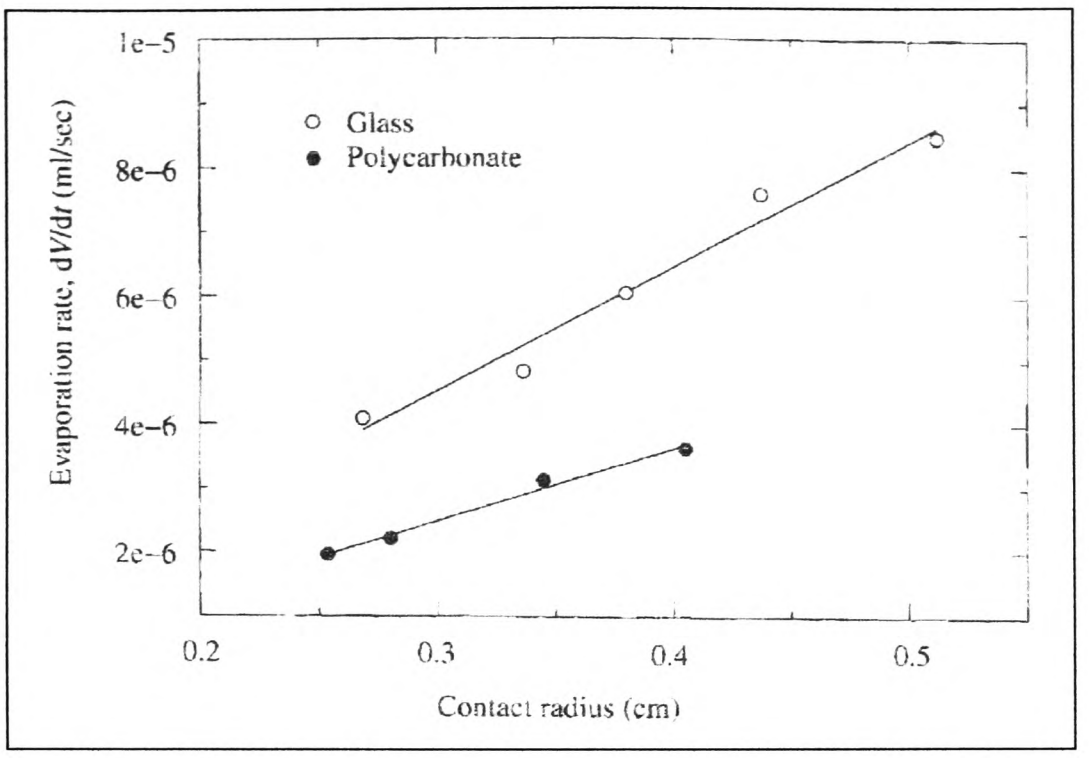

Figure 2.10: *Evolution of the evaporation rate for different drop sizes deposited on glass and polycarbonate [48].*

Finally, in their study on the ring like stain formation, Deegan *et al.* [49] have confirmed that in the case of evaporating pinned drops, the evaporation rate is proportional to the drop base radius R (see Figure 2.12). Their work was on water drops contaminated with surfactant free polystyrene microspheres resting on a microscope slide. There was no heating and the evaporation took place into dry air. To determine the evaporation rate, they measured the mass in time. They have performed these measurements for different drop sizes (see Figure 2.11). Further details on the evaporation process and theory are given in section 2.3. They [49] have shown that in the range of investigated sizes, the evaporation rate is linear with drops base radius.

In the absence of pinning, one example is the investigation performed by Erbil *et al.* [50].

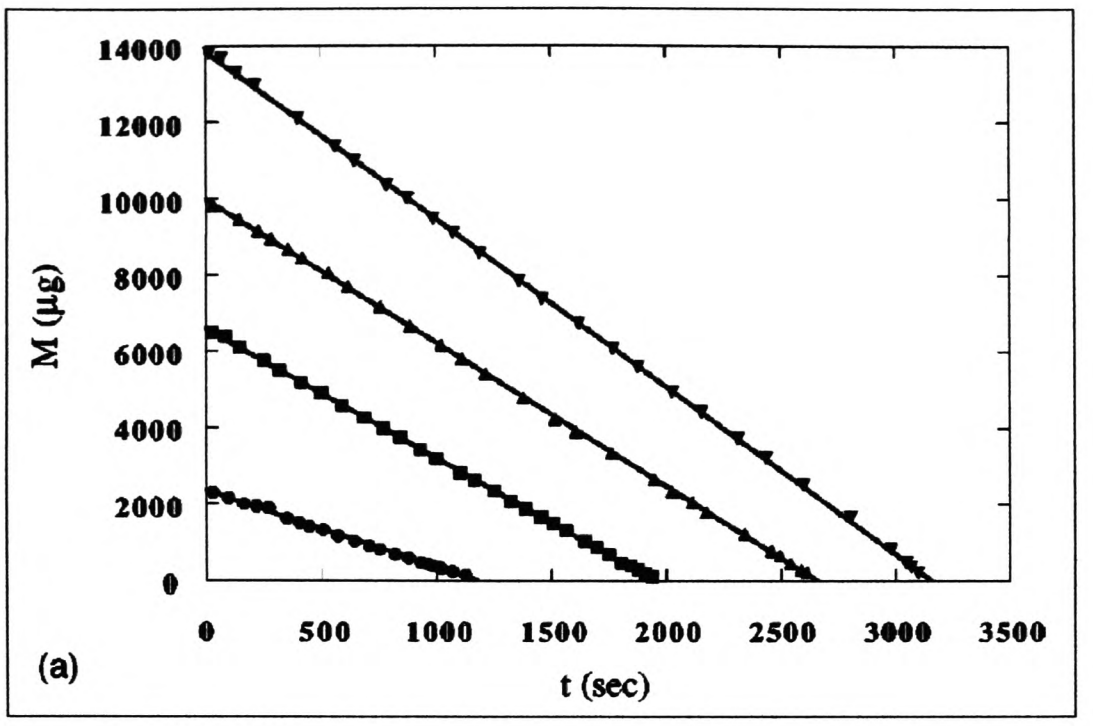

Figure 2.11: *Evaporation rate against drop base radius [49].*

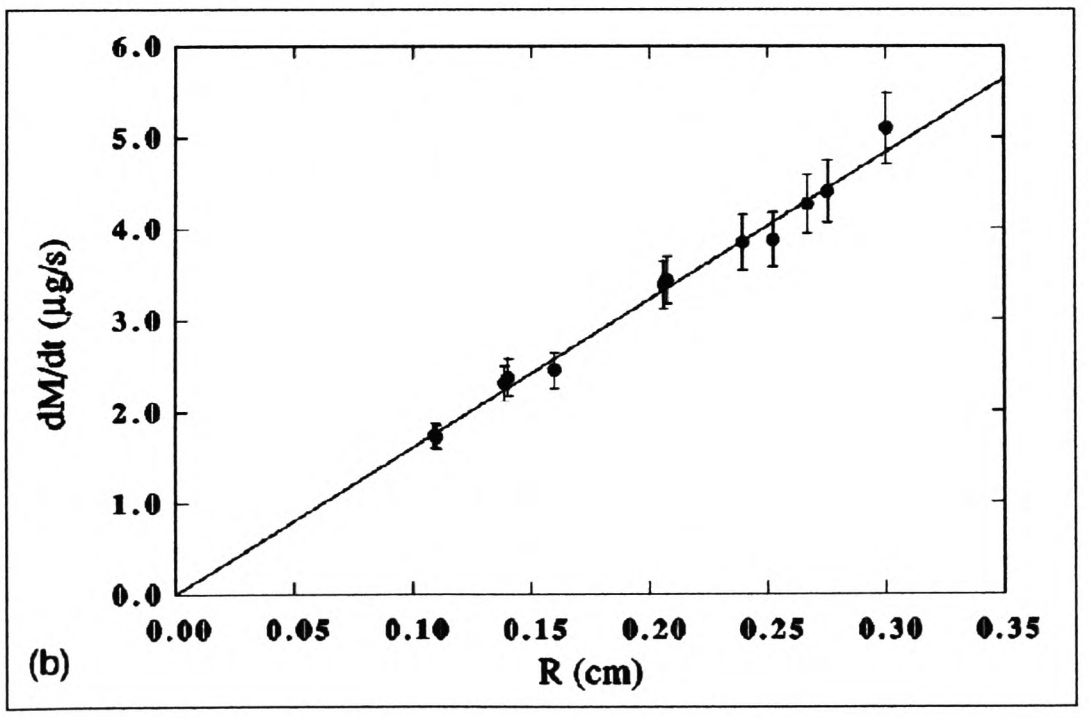

Figure 2.12: *Mass evolution for various initial volumes [49].*

Erbil *et al.* [50] have studied evaporating drops of four different liquids (namely butanol, toluene, nonane and octane) deposited on PTFE. There was no heating and no pinning of the contact line was observed. The evaporation process occurred at an almost constant contact angle. Figures 2.13 and 2.14 summarize their main results. They showed that for each liquid, the time dependence of the square drop base radius r_b^2 and the the two-thirds power of the volume $V_c^{2/3}$ are linear.

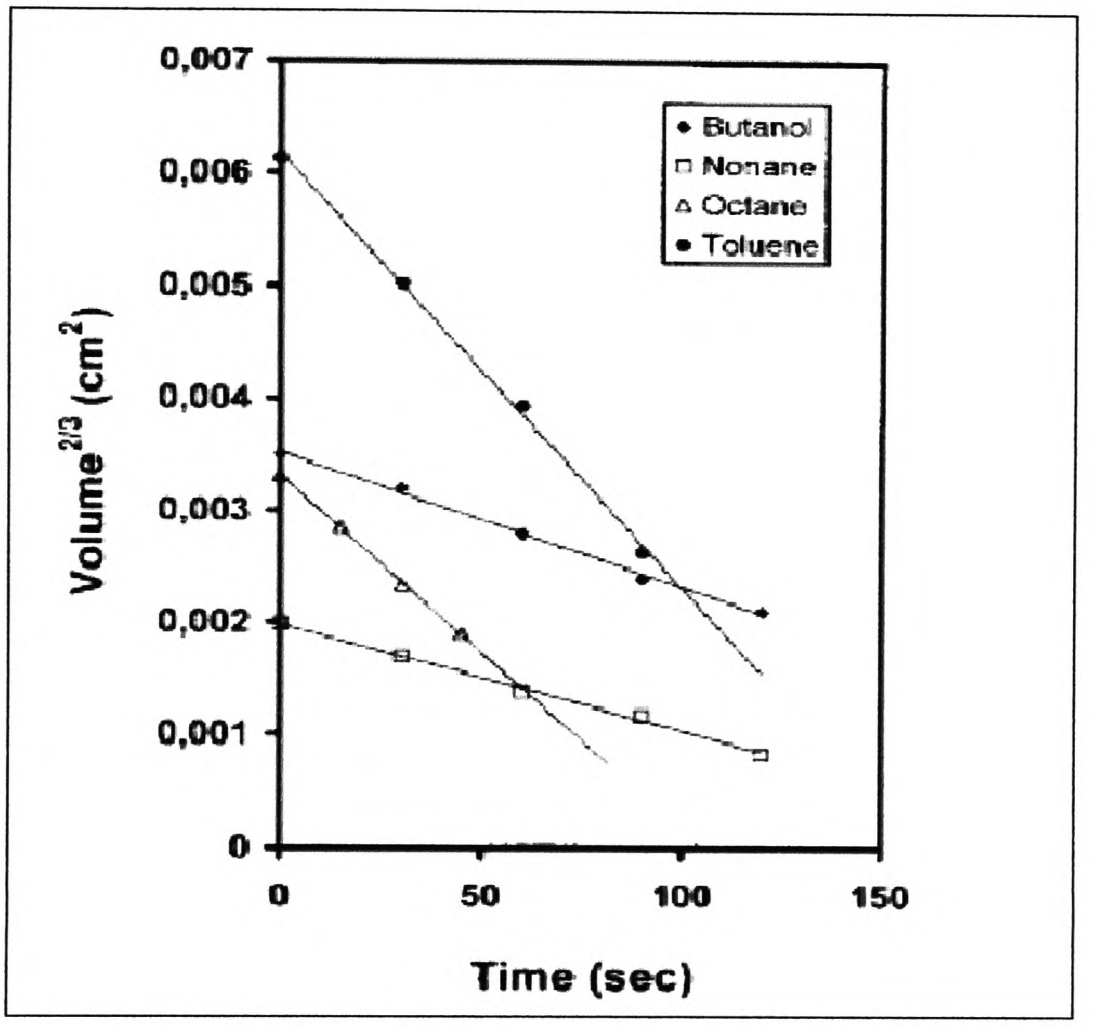

Figure 2.13: $V_c^{2/3}$ *vs time for four different liquids [50].*

They then compared the trend of $V_c^{2/3}$ to three models: Picknett *et al.* [4], Rowan *et al.* [51] and Shanahan *et al.* [2] (see Figure 2.15).

They considered the drops small enough to be regarded as a spherical cap, the expression of dV_c/dt is:

$$-\frac{dV_c}{dt} = \frac{4\pi R_s D}{\rho_L}(c_s - c_\infty) f(\theta) \tag{2.1}$$

where R_s is the sphere radius and with the expression of $f(\theta)$ depending on each model, see model section 2.3 for further details.

It was concluded that the Picknett and Bexon model was the best fit to their results (see Figure

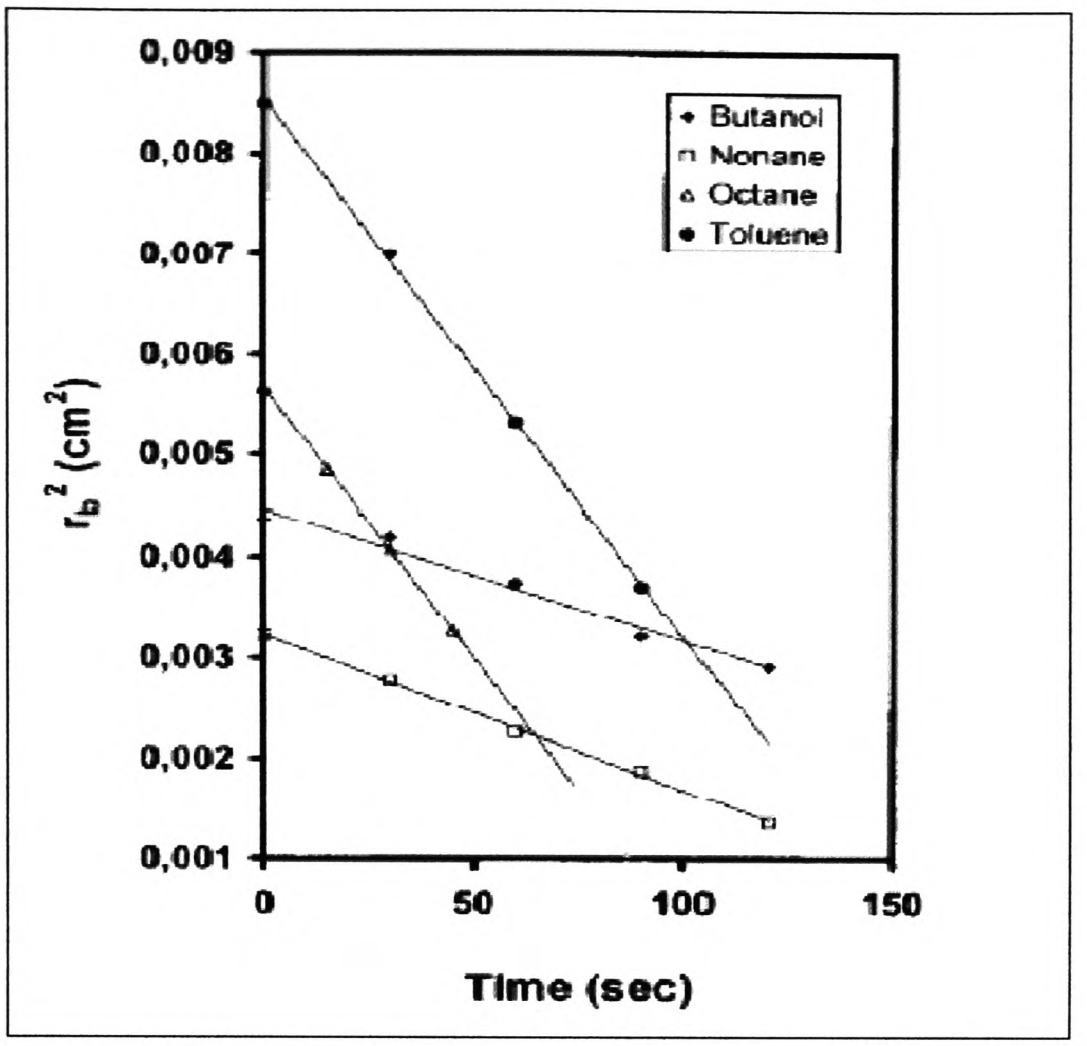

Figure 2.14: *r_b^2 vs time for four different liquids [50].*

2.15) and estimated that the free surface cooling was up to 2.2^oC.

H. Y. Erbil along with Y. Avci [52] worked also on the determination of the mass diffusion coefficient D of toluene into air. Two methods were used: the thin glass tube and sessile drop on PTFE. To control the ambient temperature, the tube and the sessile drop were housed in a cell. Each experiment was run for five different temperatures. To calculate D, the experimental results were compared to the theory. In the case of the thin tube, the Fick's law was used and stated that:

$$\frac{\partial h}{\partial t} = \frac{D}{\rho}\frac{M_w P_T}{hRT} ln\left(\frac{P_T}{P_T - P_{vs}}\right) = \frac{K}{h} \tag{2.2}$$

where

$$K = \frac{DM_w P_T}{\rho RT} ln\left(\frac{P_T}{P_T - P_{vs}}\right) \tag{2.3}$$

so by integrating equation 2.2, the time dependence of the height is given by:

$$h^2 = h_i^2 + 2Kt \tag{2.4}$$

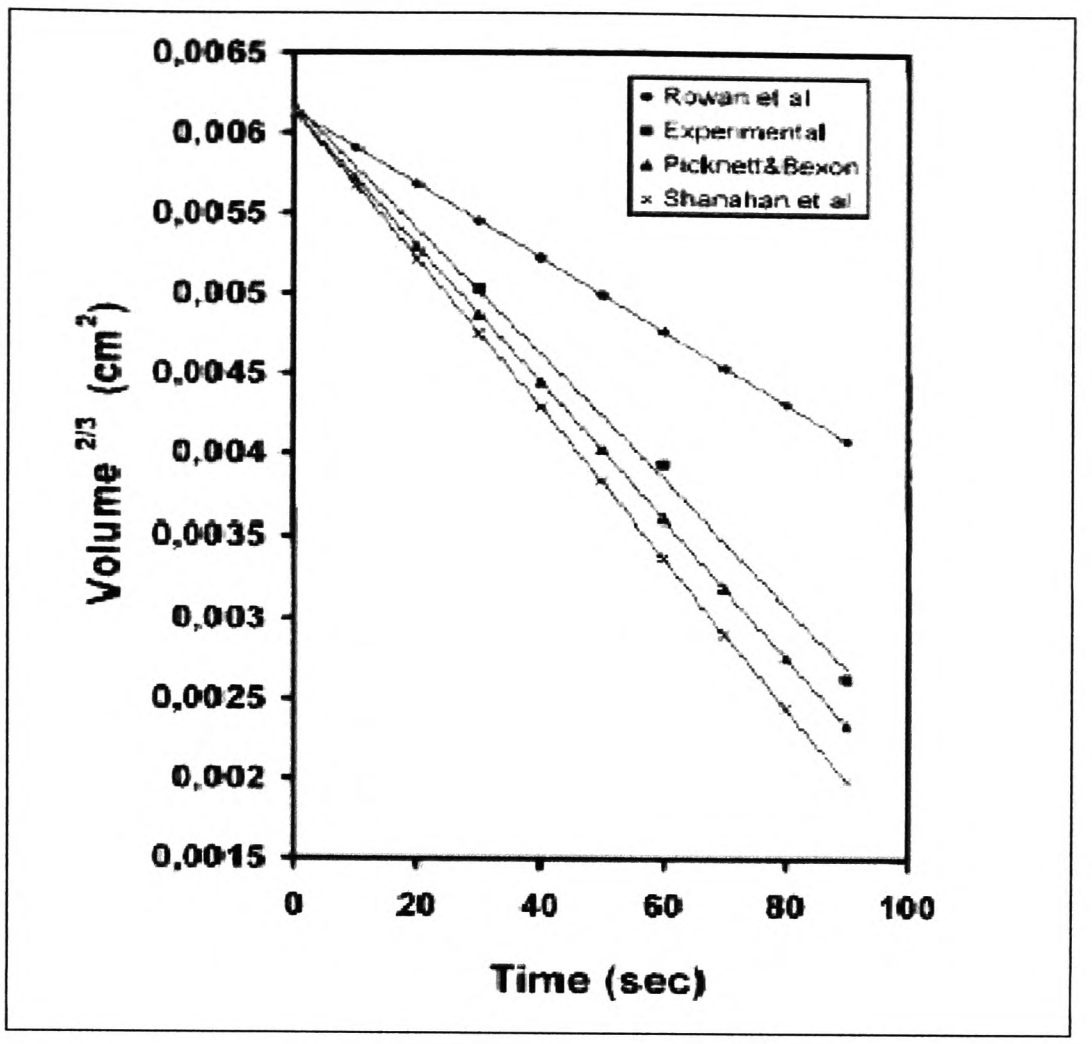

Figure 2.15: *Comparison with multiple models in the case of Toluene [50].*

They finally obtained D by plotting $h^2(t)$.

For the sessile drop case, they used the theory developed by Picknett and Bexon [4] which shows that:

$$V_c^{2/3} = V_{ci}^{2/3} - \frac{2}{3} f(\theta) K t \tag{2.5}$$

And then by plotting $V_c^{2/3}(t)$ they obtained D.

Using the thin tube and sessile drop methods they found relatively the same value for the mass diffusion coefficient. However a discrepancy for the temperature dependence of the diffusion coefficient ($D \propto T^{3.17}$) with the literature was observed. Indeed it usually accepted that $D \propto T^{1.5-2}$.

Finally, two works performed by di Marzo *et al.* [53–57] and Crafton *et al.* [58] where heated substrates were used are presented.

di Marzo *et al.* [53–57] investigated evaporating droplets in order to cool hot surfaces. They conducted various experimental works and developed different models (see section 2.3). In

1996, di Marzo *et al.* [54] looked at the influence of the contact angle on evaporation. Their experiment consisted in adding surfactant to water drops to reduce surface tension. Three surfactants concentrations were used (0 ppm, 100 ppm and 1000 ppm) which lead to three different initial contact angles of water-surfactants drops on stainless steel: 90°, 55° and 20° (see Figure 2.16).

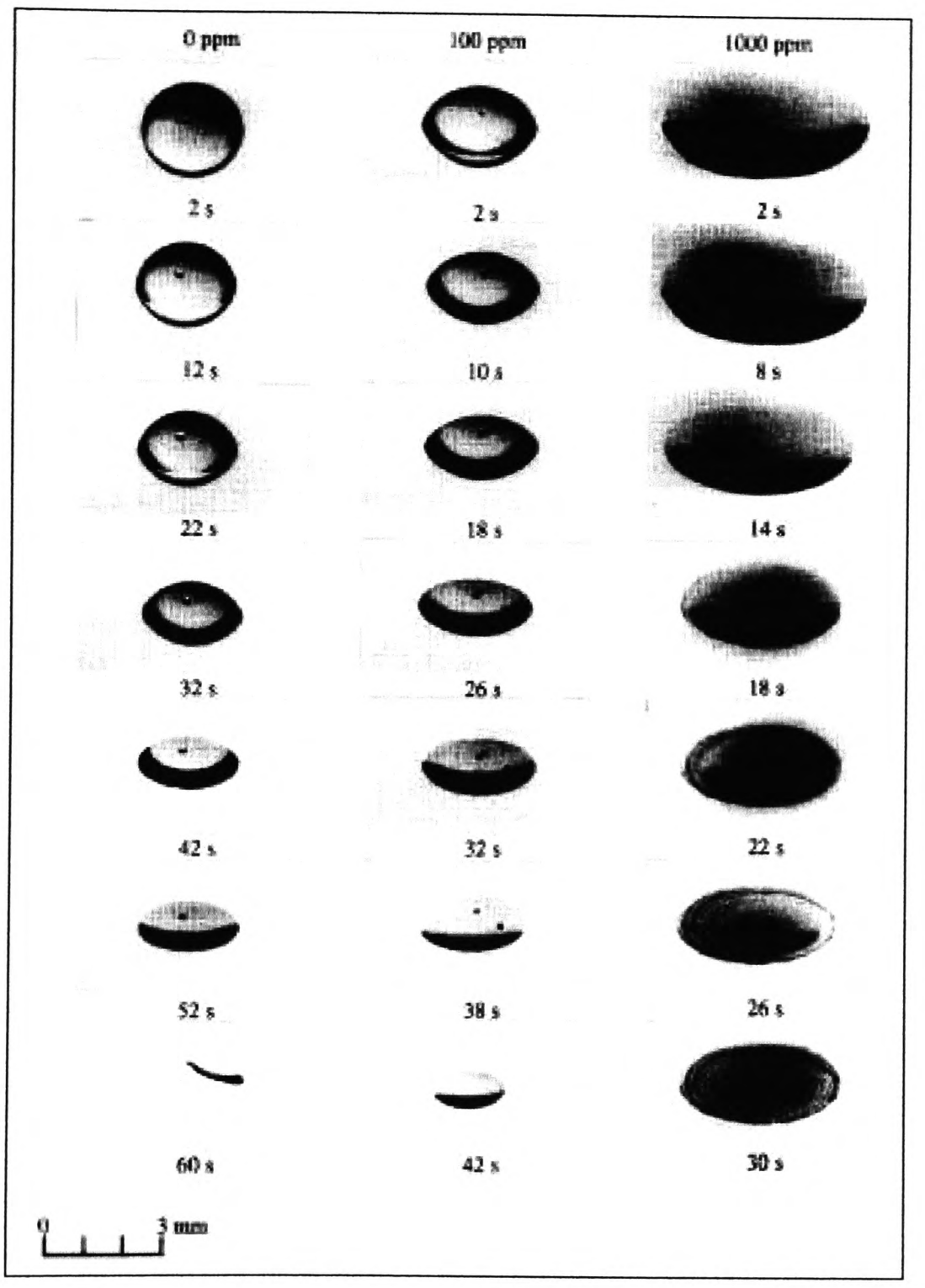

Figure 2.16: *Evaporation of three water surfactant solutions (0 ppm, 100 ppm and 1000 ppm) deposited on stainless steel surface at* 80° *[54].*

It has been shown that increasing the surfactant concentration of identical initial volumes results in a thinner droplet with a larger base diameter. This leads respectively to a larger heat transfer

area and heat transfer enhancement . As a consequence the surface cooling rises by 110% going from 90° to 20° in contact angle.

Crafton *et al.* [58] realised an experimental study on evaporating sessile droplets on heated substrates. The two liquids used for the experiment were water and n-heptane. Their initial volumes were 0.45 mm^3 (corresponding drop base radius is 1 mm) and 2.5 mm^3 respectively (corresponding drop base radius is 5 mm). The substrates used were copper and aluminium, both of which have high thermal conductivities. The temperature did not exceed the saturation value: from 60 to 90^oC for water and from 60 to 75^oC for heptane.

It is worth mentioning (see Figures 2.17, 2.18, 2.19 and 2.20) that water and heptane behave differently during the evaporation process. While water drops evaporate with a constant base diameter (Figure 2.17), heptane drops shrink at a relatively constant contact angle (Figure 2.20).

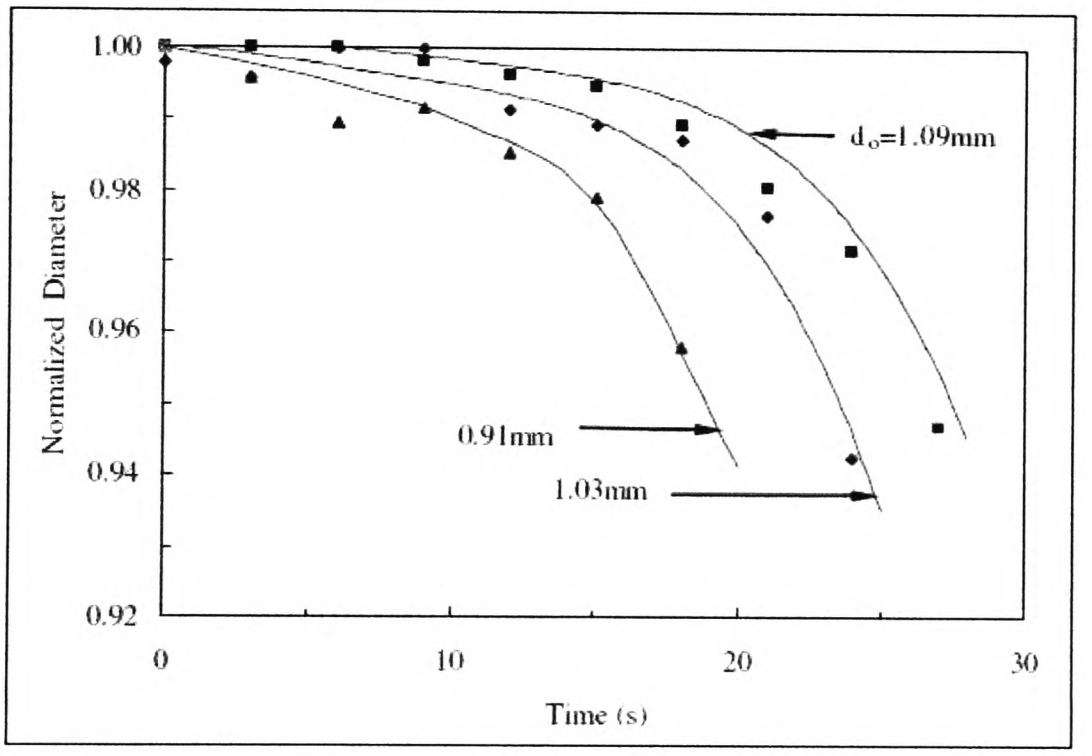

Figure 2.17: *Water drops normalized diameter against time for three sizes [58].*

Figures 2.19 and 2.20 show that the initial contact angle is independent of the drop volume. In the case of water drop, Crafton *et al.* [58] found that the evaporation rate is constant throughout the lifetime of the drop. This important result confirms that the evaporation rate is a linear function of the drop base radius at any substrate temperature (see Figure 2.21).

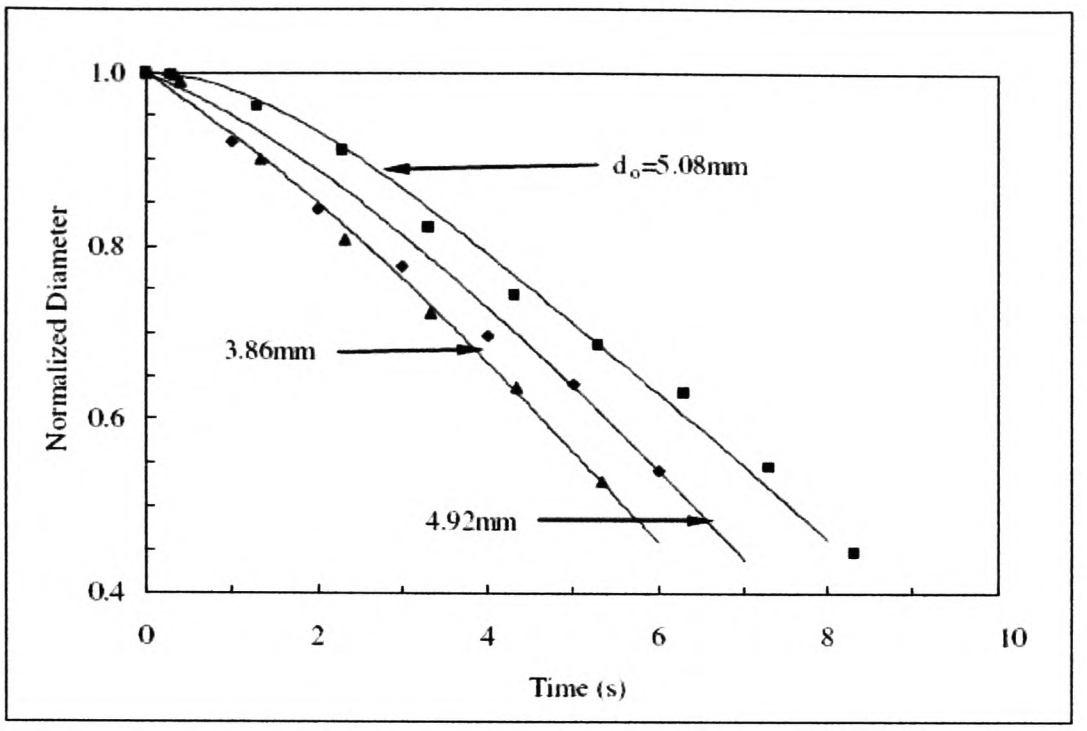

Figure 2.18: *Heptane drops normalized diameter against time for three sizes [58].*

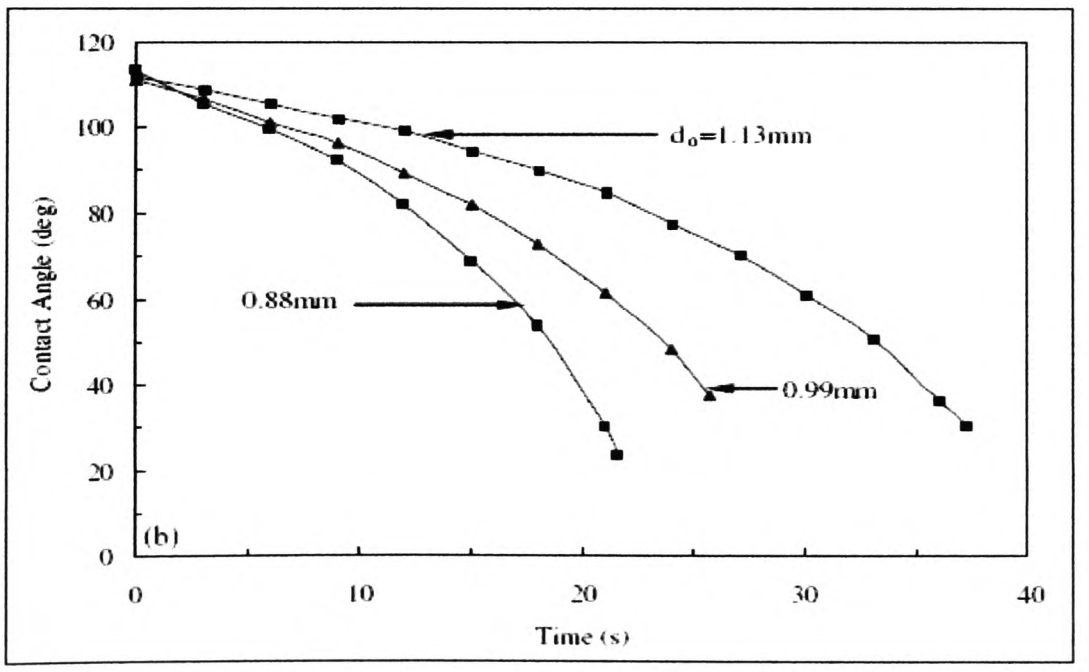

Figure 2.19: *Water drops contact angle against time for three sizes [58].*

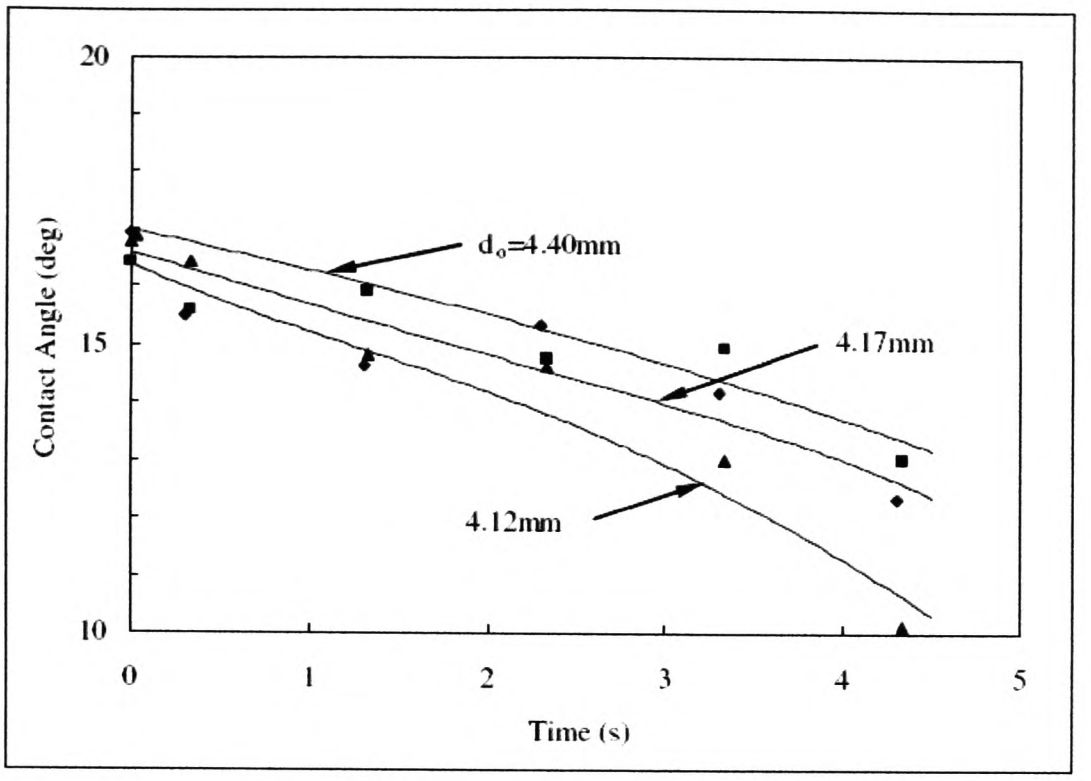

Figure 2.20: *Heptane drops contact angle against time for three sizes [58].*

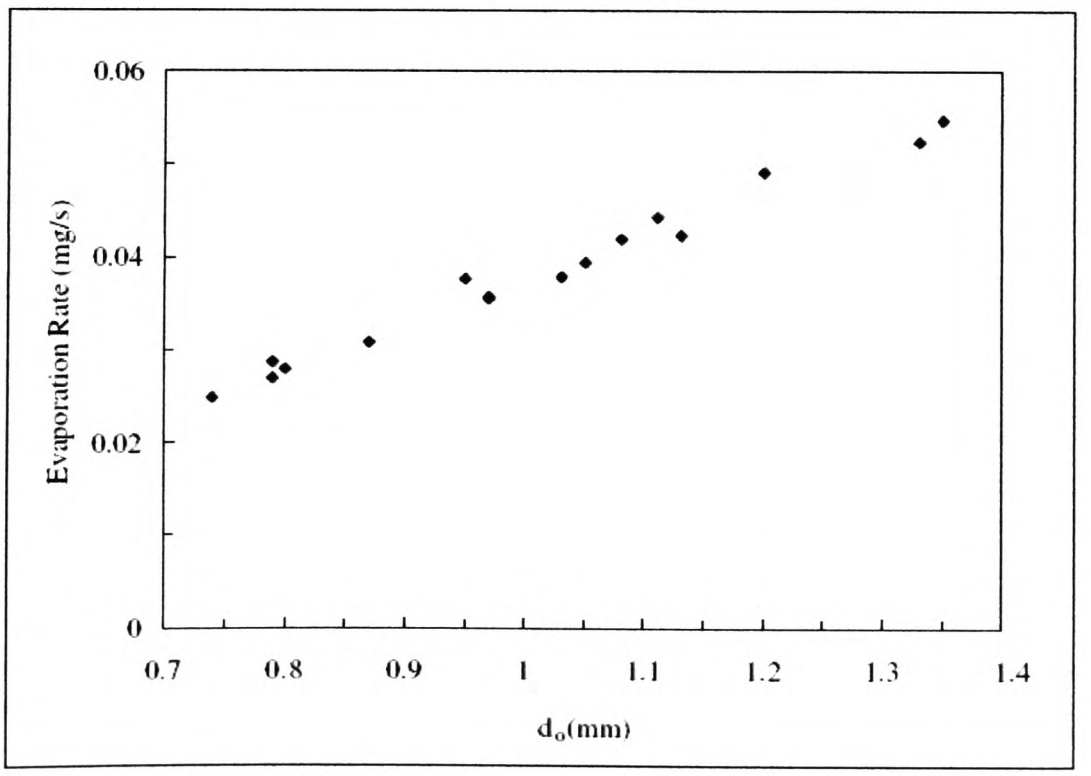

Figure 2.21: *Sessile drop evaporation rate as a function of drop base radius [58].*

2.3 Theoretical models

To determine theoretically the evaporation rate of sessile drops, Picknett *et al.* [4] used the analogy between diffusive flux and electrostatic potential. Hence to determine the evaporation rate of a sessile droplet the evaluation of the capacitance of an equiconvex lens of the same size is needed:

$$-\frac{dV}{dt} = \frac{2\pi D}{\rho_L} C_x (c_{sat} - c_\infty) \tag{2.6}$$

where C_x is the capacitance. As the analytical expression of C_x is rather complicated, they expressed two polynomial fits for small and large contact angles:

$$\frac{C}{R} = 0.6366\theta + 0.09591\theta^2 - 0.06144\theta^3 \qquad for \quad 0 \leq \theta \leq 0.175 \tag{2.7}$$

and

$$\frac{C}{R} = 0.00008957 + 0.6333\theta + 0.1160\theta^2 - 0.08878\theta^3 + 0.01033\theta^4 \qquad for \quad 0.175 \leq \theta \leq \pi \tag{2.8}$$

In Figure 2.22, the model is illustrated for the two modes of evaporation. Compared to the constant base radius mode, when the triple line is not pinned (constant contact angle), the evaporation rate diminishes much more and the lifetime of the drop becomes longer.

Following their experimental results (see section 2.2) Shanahan *et al.* [2] developed a model to describe stage II where the drop base radius is constant. They assumed that the diffusion of the vapour into the surrounding atmosphere is purely radial. Then for the concentration gradient they obtained:

$$\frac{dC}{dR} = \frac{C_{sat} cos\theta}{ln(1 - cos\theta)} \frac{1}{R(R - Rgcos\theta)} \tag{2.9}$$

where R_g is the radius of the spherical cap, hence the expression of the evaporation is given by:

$$\frac{dV}{dt} = \frac{DA}{\rho_L} \frac{dC}{dR}\bigg|_{R_g} = \frac{2\pi R_g D}{\rho_L} \frac{cos\theta}{ln(1 - cos\theta)} (c_{sat} - c_\infty) \tag{2.10}$$

They found a good agreement between experimental and theoretical results, and also suggested that the model could be used to estimate the diffusion coefficient.

Rowan *et al.* [47] compared their experimental results exposed in section 2.2 to a simple analytical model. The drop was left evaporating in a non saturated atmosphere with no heating. The contact base radii are less than 1 mm, hence the drops are regarded as spherical caps. The

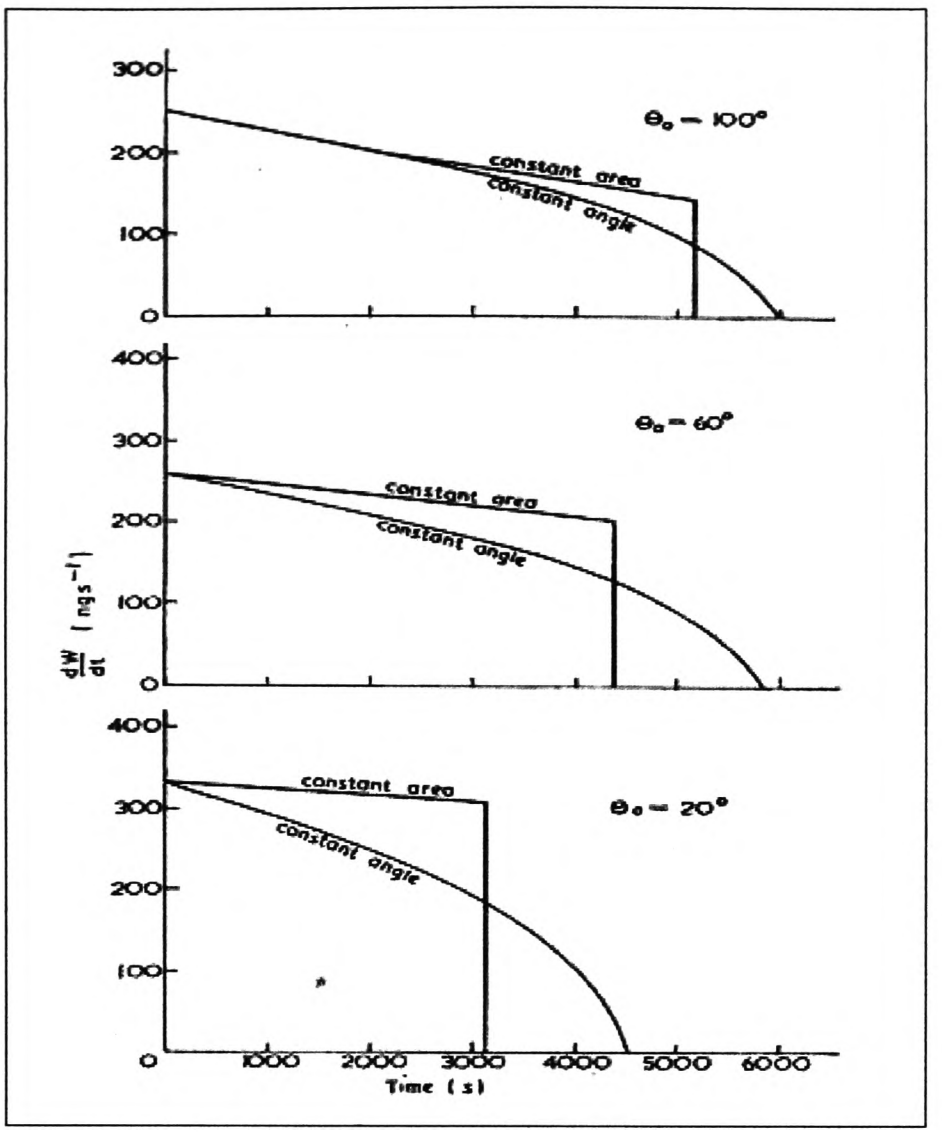

Figure 2.22: *Theoretical evaporation rates for methyl acetoacetate drops resting on a surface at* $22 - 23°C$ *for the two modes of evaporation [4].*

authors [47] followed Birdi *et al.* works [46] which considered that the evaporation is governed by the Fick's law but took into account the full spherical cap geometry by distinguishing the radii of curvature at the contact line: R and r_0.

$$\frac{dV}{dt} = -\frac{D}{\rho}\int \nabla C.dS \tag{2.11}$$

where ρ is the density of the liquid. The integral is taken over the liquid-gas interface. They considered that the concentration gradient is radially outward and equal to $(c_\infty - c_0)/R$, hence:

$$\frac{dV}{dt} = \frac{2\pi D(c_\infty - c_0)}{\rho}h = -\lambda h \tag{2.12}$$

and by using Equations 1.20,

$$\frac{d\theta}{dt} = -\frac{\lambda sin^3\theta}{\pi r_0^2(1 - cos\theta)} \tag{2.13}$$

This is integrated to give:

$$F(\theta) = ln[tan(\theta/2)] + \frac{1 - cos\theta}{sin^2\theta} = \frac{-2\lambda(t - t_0)}{\pi r_0^2} \tag{2.14}$$

Finally, they plotted $F(\theta)$ (see Figure 2.23), and gave an expression for the straight part ($90° - 30°$) as follows:

$$F(\theta) = -1.592 + 1.632\theta \tag{2.15}$$

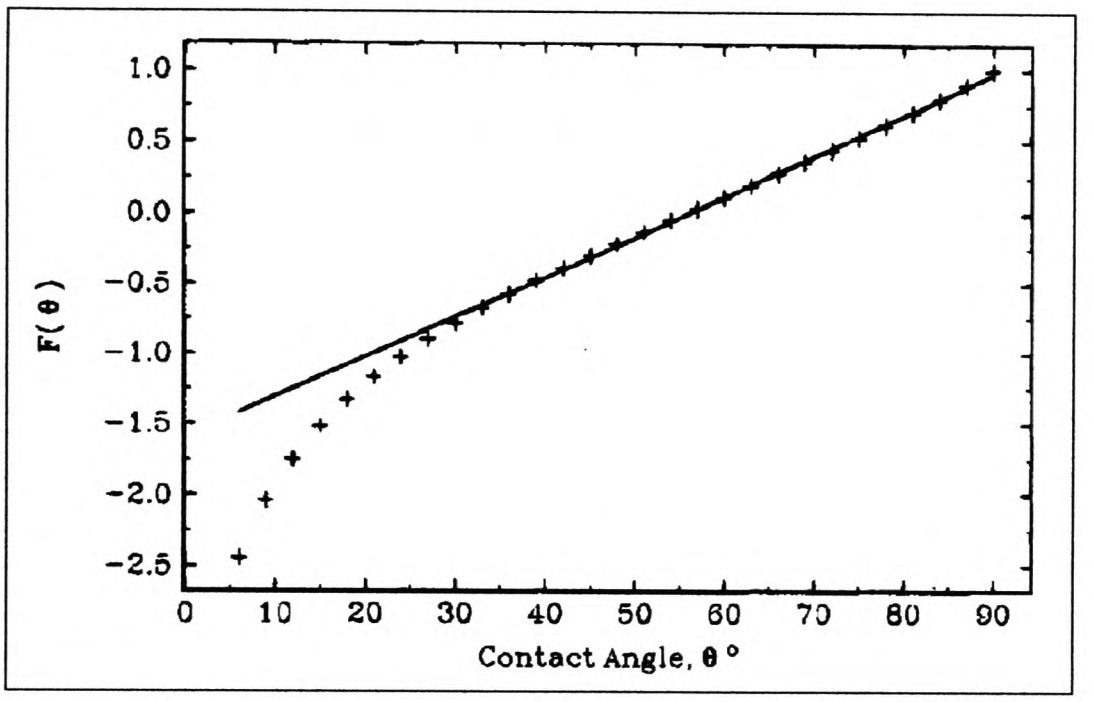

Figure 2.23: *Approximation of $F(\theta)$ as a straight line over the range $90° - 30°$ [47].*

Deegan *et al.* [1, 49] have investigated the ring formation left by particles dispersed in evaporating drops. This is basically the formation of coffee ring stain for example, see Figure 2.24. When coffee dries, residual particles are darker at the edge of the stain, giving the ring like shape. Their experimental results showed that two conditions were necessary for ring formation: triple line pinning and stronger evaporation at the edge.

In the case of evaporating sessile drops with a fixed triple line, an outward, radial flow must replenish the evaporated liquid at the perimeter of the droplet. As illustrated in Figure 2.25, if the contact line is not pinned, the surface minimization will lead to a diminution of the drop base radius. While with a pinned triple line, the force generates an outward flow.

To model the local mass flux, J, Deegan *et al.* used the electrostatic analogy of a spherical cap with a constant potential (constant vapour concentration) solved by Lebedev [59]. It shows that

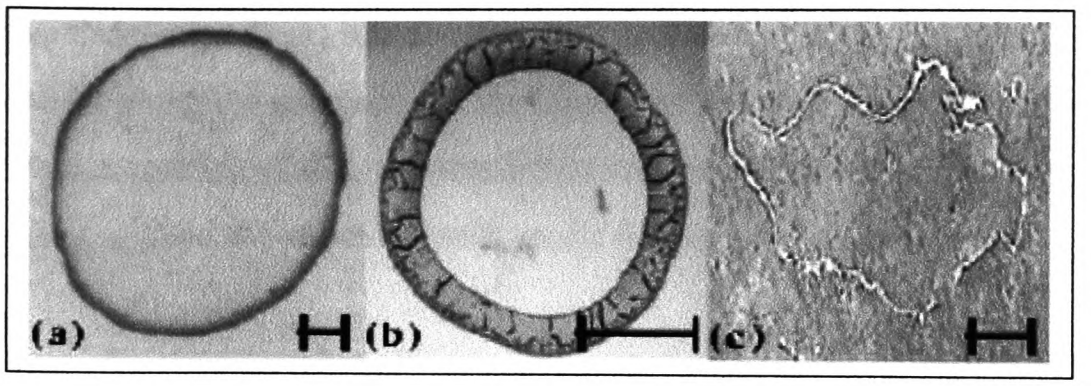

Figure 2.24: *Examples of ring formations: (a) coffee stain, (b) dried colloidal microsphere and (c) salt deposit. The bar corresponds to* 1 *cm [49].*

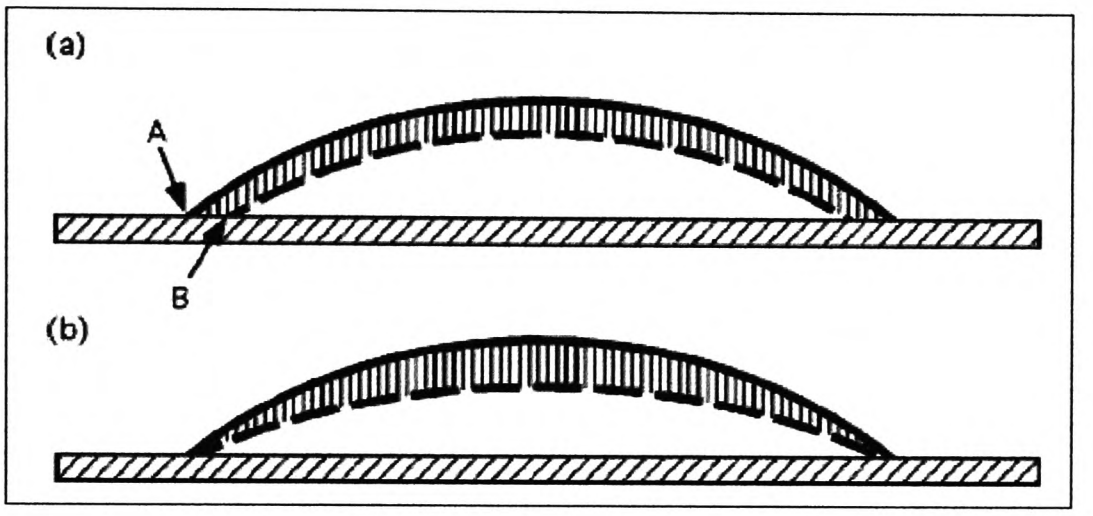

Figure 2.25: *Illustration of the liquid-gas interface motion (from solid to dashed line) in the case of both pinned and non pinned contact line [49].*

the current (J) diverges near the edge (triple line).

$$J(r,t)(R-r)^{-\lambda} \tag{2.16}$$

As the change in volume exactly compensated by the evaporation, we have:

$$\frac{dM}{dt} = \rho \frac{d}{dt} \int_0^R dr' 2\pi r' h(r',t) = \int_0^R dr' 2\pi r' J_S(r',t) \sqrt{1 + \left(\frac{\partial}{\partial r'} h(r',t)\right)^2} \tag{2.17}$$

Black *et al.* [5] elaborated a numerical model considering internal fluid motion. They studied evaporating water drops deposited on heated surfaces. The drop base diameter is less than 1 mm and so they reasonably simulated the drop shape as spherical. The numerical simulation ends when the contact angle approaches the receding value. Compared to previous models, Black *et al.* took into account the fluid motion within the drop. They justified it by the presence of buoyant and thermocapillary convection. The buoyant convection is due to temperature

gradient (and so density gradient) into the drop bulk and thermocapillary convection as a result of thermal gradient along the interface. At the liquid-gas interface, the mass flux is the product of the mass transfer coefficient, h_m, and the difference between the saturated vapour density at the interface, $\rho_{vap,sat}$, and the vapour density in the ambient gas $\rho_{vap,\infty}$:

$$\frac{dm}{dt} = h_m \left(\rho_{vap,sat}(T) - \rho_{vap,\infty}\right) \tag{2.18}$$

To determine the mass transfer coefficient h_m they used the analogy between heat and mass transfer:

$$h_m = \frac{h_{nc}}{\rho_{air} c_{p,air} Le^{2/3}} \tag{2.19}$$

where h_{nc} is the heat transfer coefficient, $c_{p,air}$ the heat capacity of air and Le the dimensionless Lewis number.

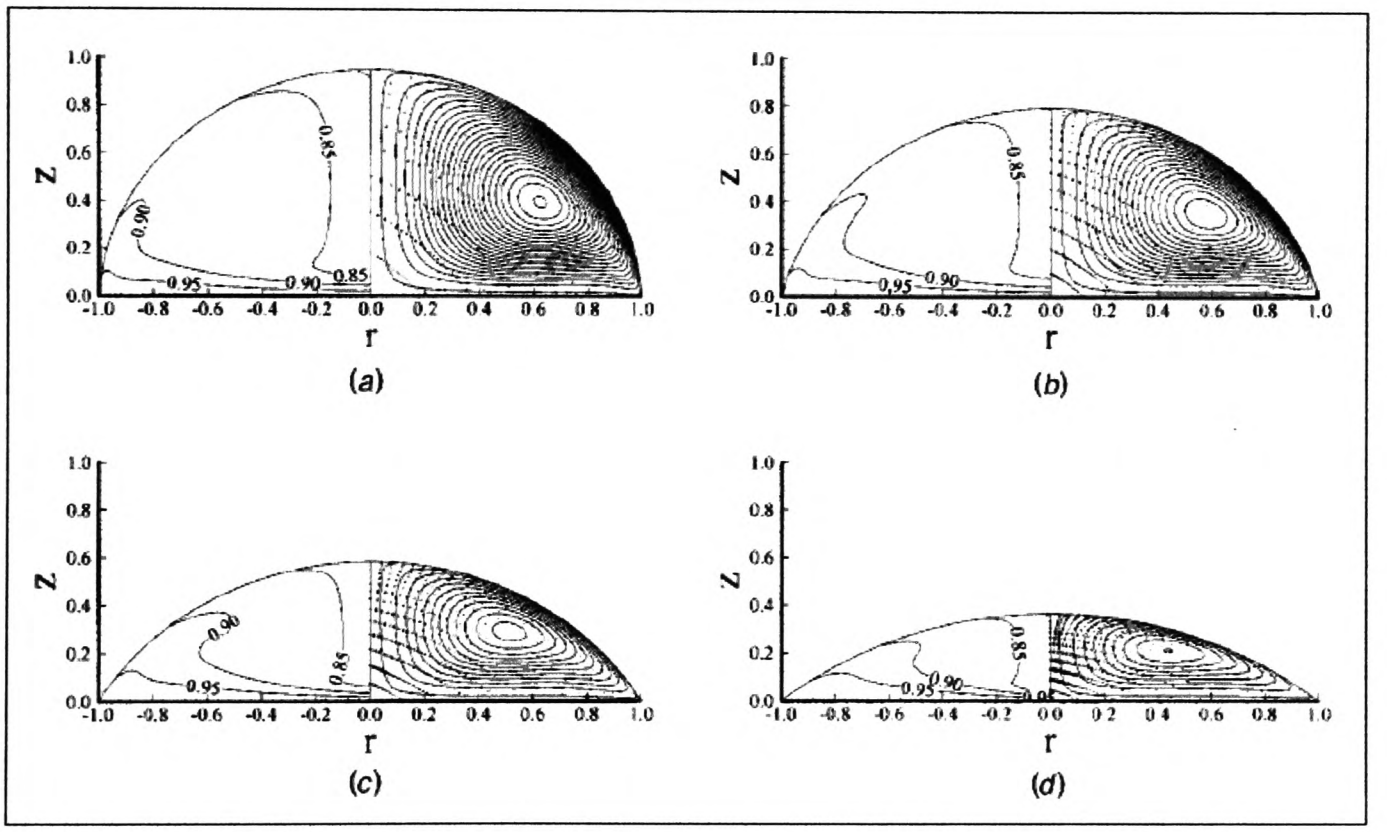

Figure 2.26: *Black et al. [5] numerical results of an evaporative drop deposited on a* 100*deg heated surface, with a* 90*deg initial contact angle. (a) 5 ms, (b) 20 ms, (c) 40 ms and (d) 60 ms.*

To underline the influence of fluid motion onto the evaporation rate, the numerical results are compared to a model where fluid motion is absent and replaced by a simple conduction model. In Figure 2.27, the comparison between the two models is presented. It is clearly shown that in the absence of fluid motion, the temperatures within the drop are underestimated and so the evaporation rate.

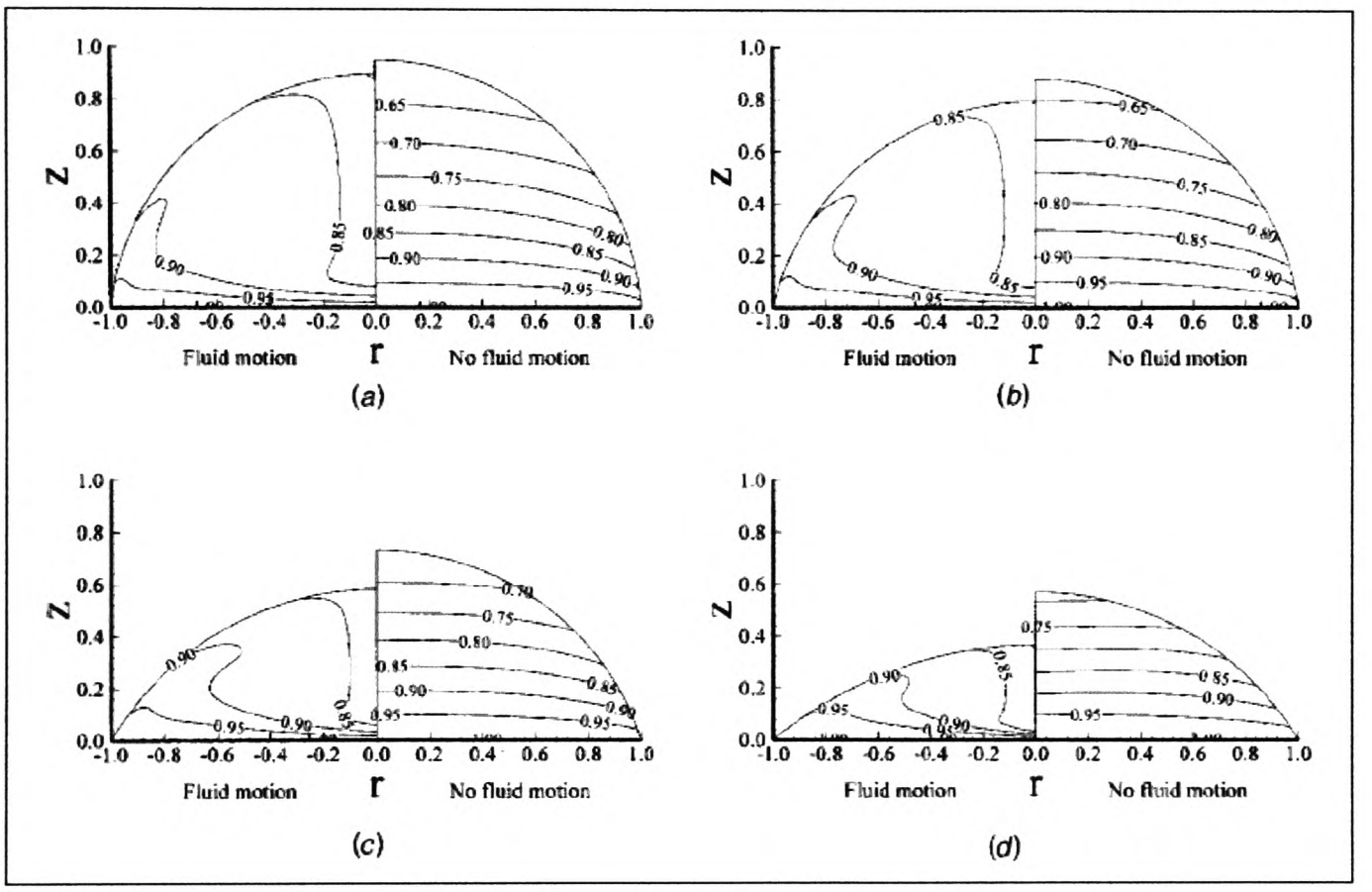

Figure 2.27: *Isotherms contours comparison between the model with fluid motion and the model without fluid motion. (a)10 ms, (b) 20 ms, (c) 40 ms and (d) 60 ms.*

Hu and Larson investigated [7, 8, 60] the evaporation of droplets resting on a substrate. They investigated small enough droplets to be regarded as spherical cap shape, with a pinned contact line, in the absence of heating and diffusion limited evaporation (which can be considered as a quasi-steady-state process due to a short equilibrium time).

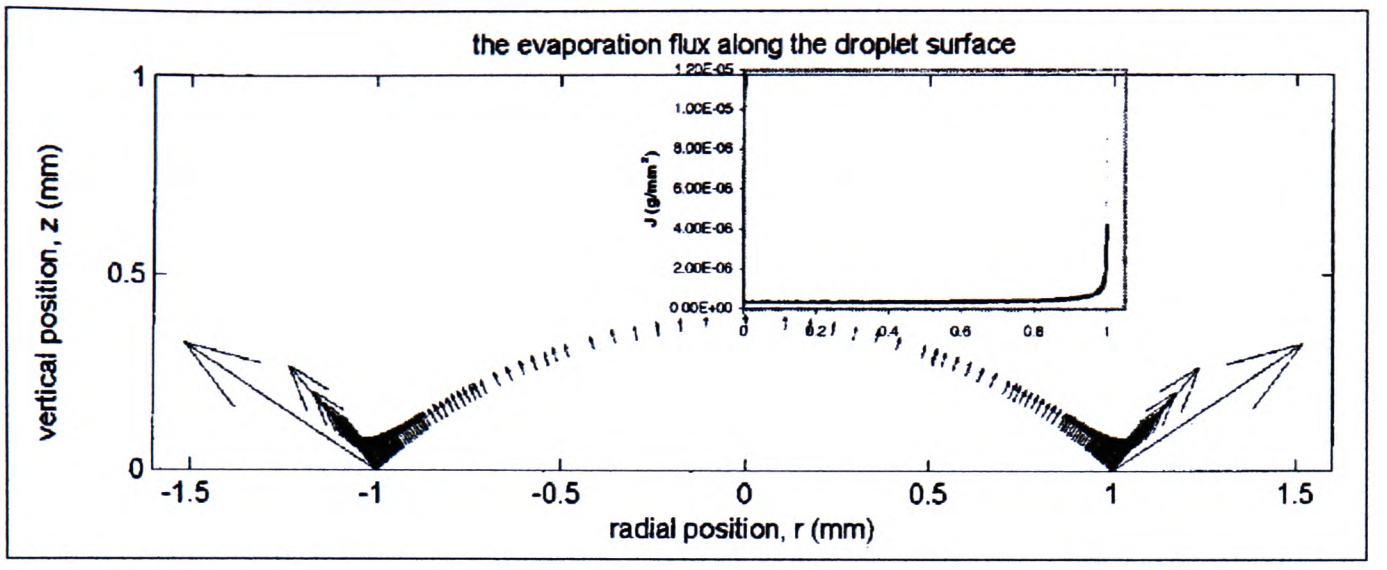

Figure 2.28: *Distribution obtained by the FEM analysis of the evaporation flux along the drop upper surface [7]. The insert show the magnitude of the evaporation flux.*

In their earlier work [7], a simple model is developed for the evaporation flux distribution along the liquid-gas interface. They first used a finite element method to build up the vapour concentration and the evaporation flux. They found that the evaporation flux was not uniform along the liquid-gas interface and became singular at the periphery of the drop (see Figure 2.28). They also showed that a good fit could be the expression developed by Deegan *et al.* [1, 6]:

$$(\vec{J}.\vec{n}) = J_0(1-\tilde{r}^2)^{-\lambda(\theta)} \tag{2.20}$$

where $\lambda(\theta) = 1/2 - \theta/2$ is a fitting parameter representing the non uniformity of the evaporation flux along the interface and $\tilde{r} \equiv r/R$ (r radial position along the droplet and R the contact line radius). For initial contact angle lower than $40°$ the FEM analysis showed that the evaporation rate was almost constant. An approximate expression was also established:

$$J(r,t) = \frac{Dc_v(1-H)}{R}(0.27\theta^2 + 1.30)(0.6381 - 0.2239(\theta - \frac{\pi}{4})^2)(1-\tilde{r}^2)^{-\lambda(\theta)} \tag{2.21}$$

$$-\dot{m}(t) = \pi RD(1-H)c_v(0.27\theta^2 + 1.30) \tag{2.22}$$

where θ is the contact angle, D is the vapor diffusivity, c_v the saturated vapor concentration, H the relative humidity and t the time.

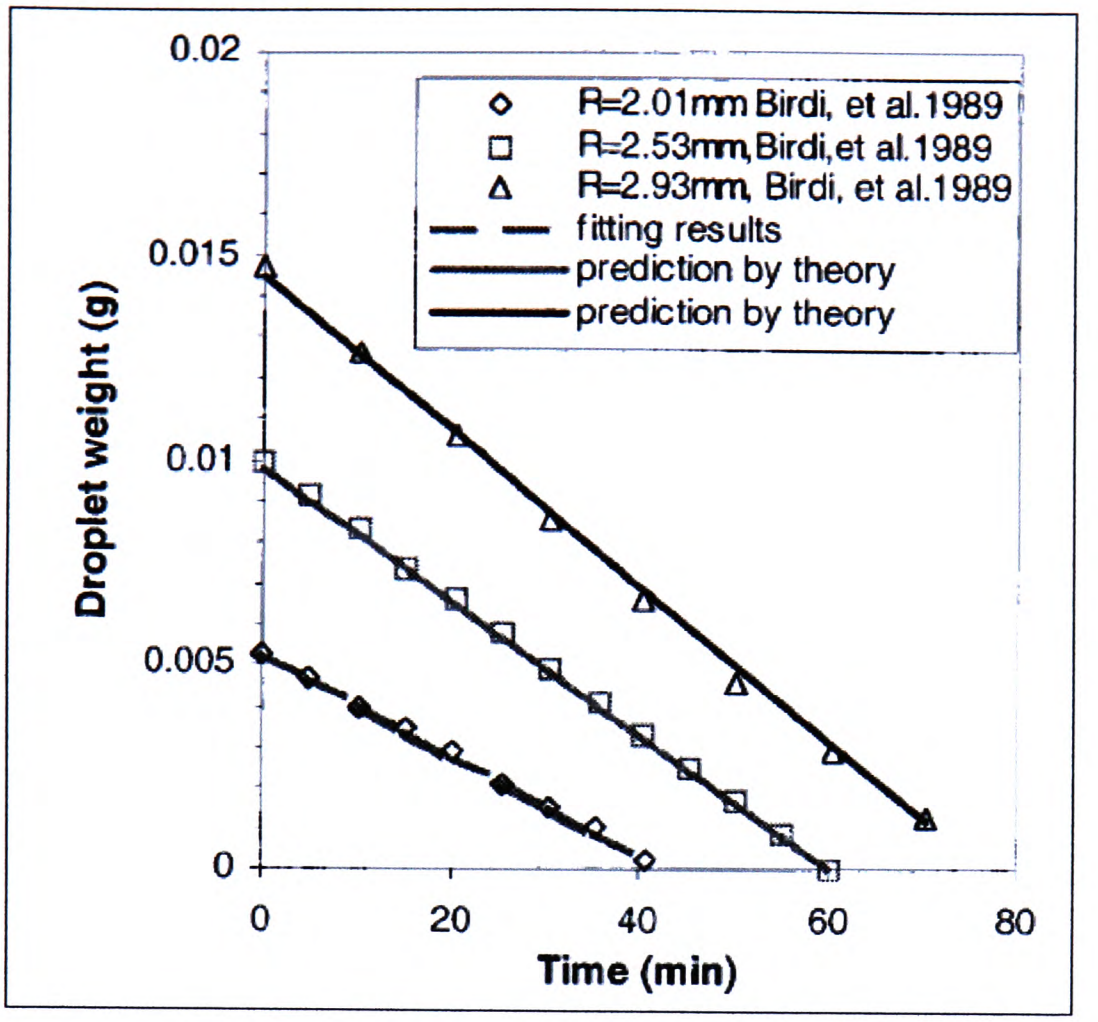

Figure 2.29: *Comparison between the model and previous experimental results.*

Their model is in good agreement with previous experimental works, see Figure 2.31(a).

More recently, Hu *et al.* [8, 60] looked at the flow pattern in an evaporating sessile drop. They first neglected the Marangoni stresses [8] and the validation of the application of the lubrification theory for low capillary numbers. Indeed they compared the lubrication analytical solution to a FEM analysis and showed good agreement.

In Figure 2.31, we can see a similar outward flow at each evaporating time (or contact angle). This is mainly due to the evaporation flux distribution and the pinning of the triple line. Indeed as explained by previous research [1], to maintain the position of the contact line a flow from the centre of the drop is necessary.

Following the validation of the lubrification theory, Marangoni stresses due to interfacial thermal gradient were taken into account. A simple analytical solution was applied to obtain evaporation flux and temperature profiles along the interface and used as boundary conditions. Then a FEM analysis was performed to build up both the vapour concentration and thermal and flow fields into the drop. The study showed that the theory was acceptable for contact angle less than

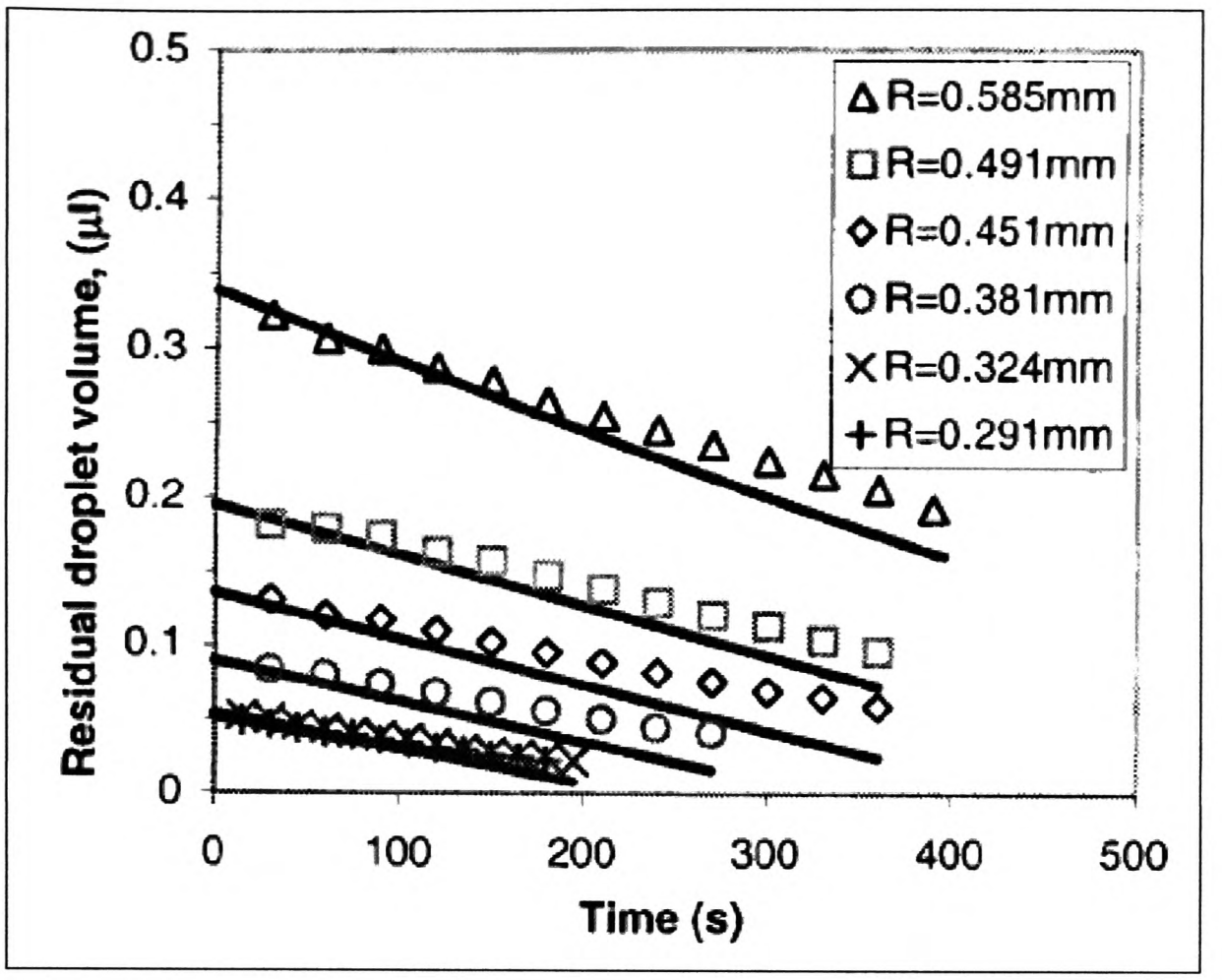

Figure 2.30: *Comparison between the model and previous experimental results.*

40°.

In Figure 2.32, the difference with the model with no Marangoni stresses is obvious. Near the interface the fluid flow is now going from the edge to the top of the drop. This is driven by the shear stress at the interface. In Figure 2.32(b) we can see that the streamlines could be assimilated as convection cells.

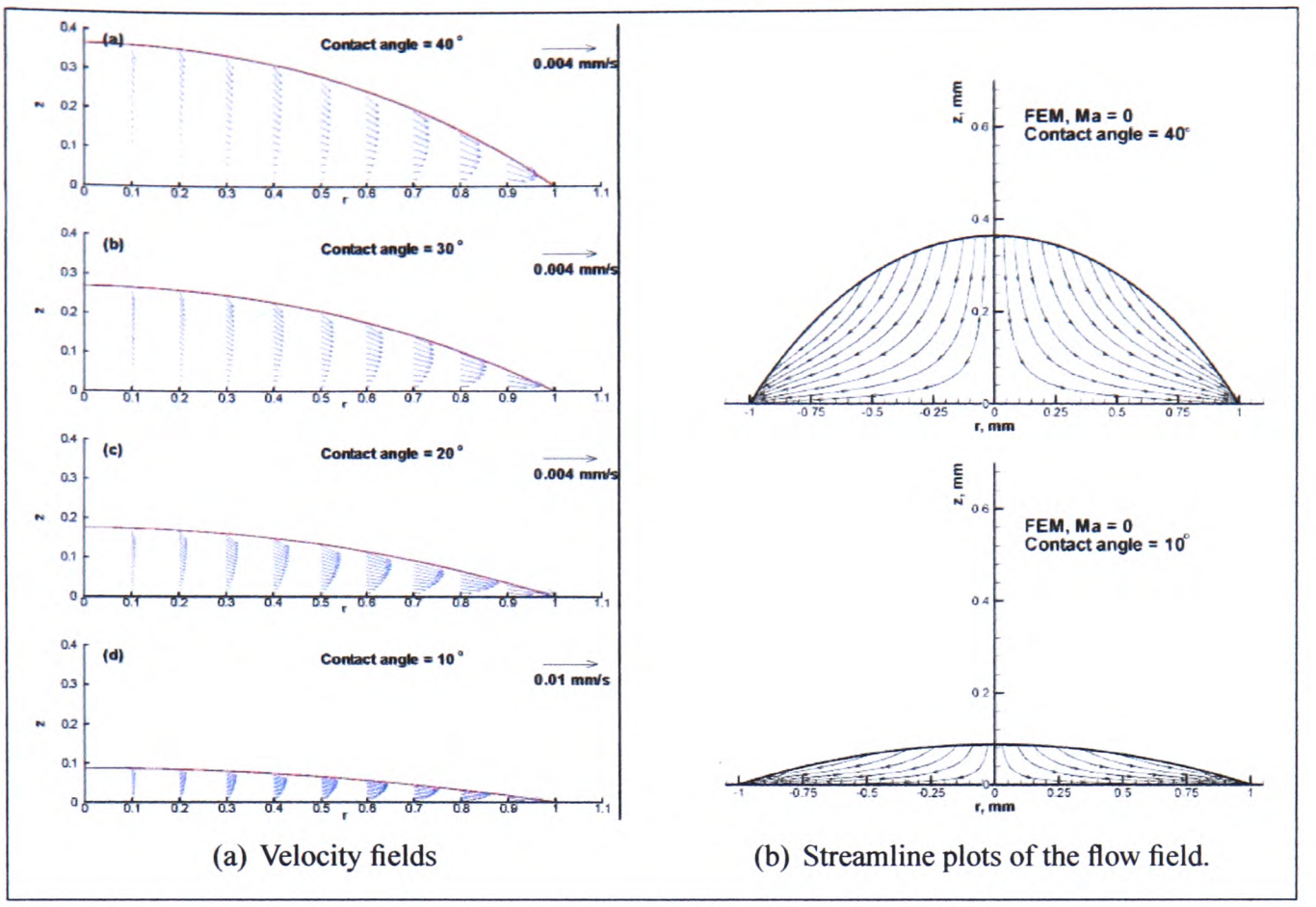

(a) Velocity fields

(b) Streamline plots of the flow field.

Figure 2.31: *Velocity fields and streamline plots of the flow field obtained by the FEM analysis in the absence of Marangoni stresses.*

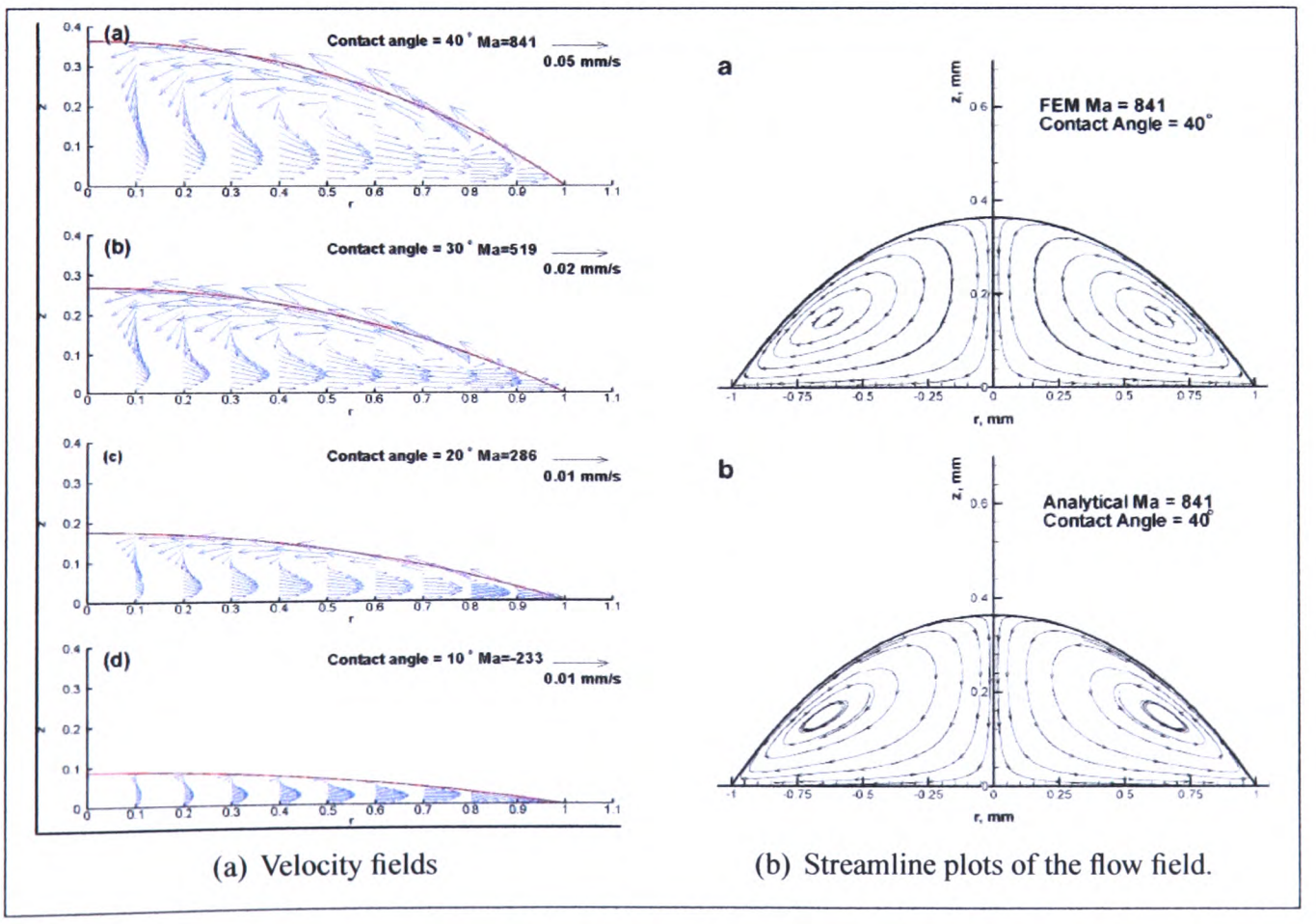

(a) Velocity fields

(b) Streamline plots of the flow field.

Figure 2.32: *Velocity fields and streamline plots of the flow field obtained by the FEM analysis considering Marangoni stresses.*

2.4 Binary mixture drops

Little research has been done on the study of evaporation of binary mixture drops [9–11]. In 2000, Rowan *et al.* [9] investigated an azeotropic mixture, 1-propanol and water. The drops were placed on PMMA substrate and freely evaporated at room temperature. They reported two main results, depending on either 1-propanol or water was in excess (with respect to the azeotropic value). When propanol was in excess, the drop evolution could be divided into two stages. First the triple line was pinned, the contact angle decreased, then the drop shrunk, both the contact and the drop base radius decreased, see Figure 2.33.

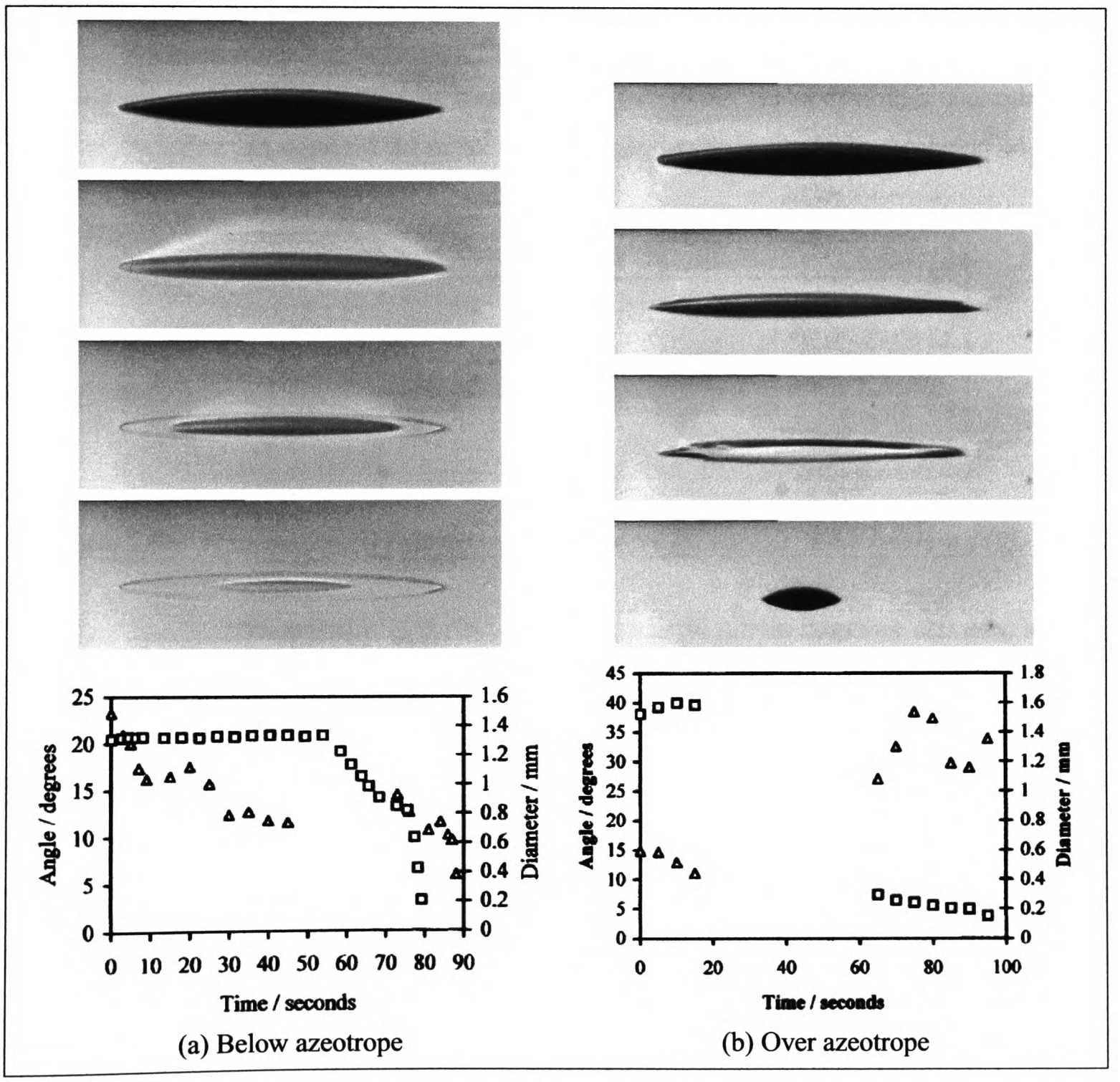

(a) Below azeotrope (b) Over azeotrope

Figure 2.33: *Propanol-water mixture microdroplet on PMMA substrate [9].*

However, if water was in excess, the evaporating drop behaved in a very different manner. In the early stage, the contact angle decreased and measurement became impossible. Great instabilities appeared at the periphery of the drop followed by the formation of single or multiple droplets, see the two image sequences in Figure 2.33. It is thought that the remaining droplet is pure water. To explain the formation of strong instabilities, they advanced a competition between local minima and maxima surface tension at the interface which will induce an undulating triple line.

Sefiane *et al.* [10] have studied the evaporation of water-ethanol binary drops resting on rough PTFE substrates. The drops were left evaporating in a chamber in order to control the ambient pressure. By using an optical technique, they recorded the drop profile in time and deduced the evaporation rate. In Figure 2.34, pictures of the initial contact angles at various concentrations are illustrated. As expected the initial contact angle diminishes with the concentration in ethanol.

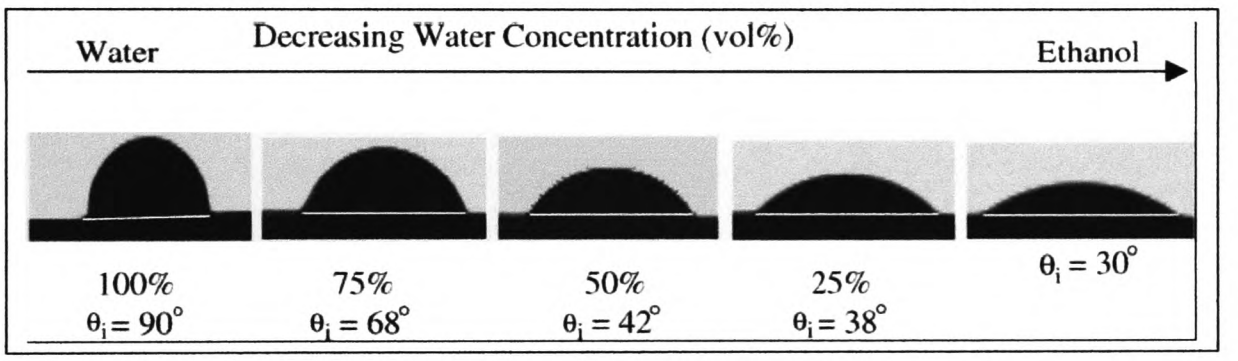

Figure 2.34: *Photographies of the initial contact angle for various concentrations [10].*

They also measured the evolution of the dynamic contact angle and the drop base diameter, see Figures 2.35 and 2.36.

At the difference of pure components (water and ethanol), where the drop profile evolves monotonously, the evaporation of binary mixtures could be divided in three stages, see Figure 2.37. From the evaporation rate measurements they showed that the more volatile component evaporates completely in the first stage. For concentrations in ethanol over 75% the contact angle behaves as the one of pure ethanol in the first stage and the one of pure water in the last stage. Hence they explained that as ethanol evaporates it diffuses to the interface and modify the interfacial surface tension.

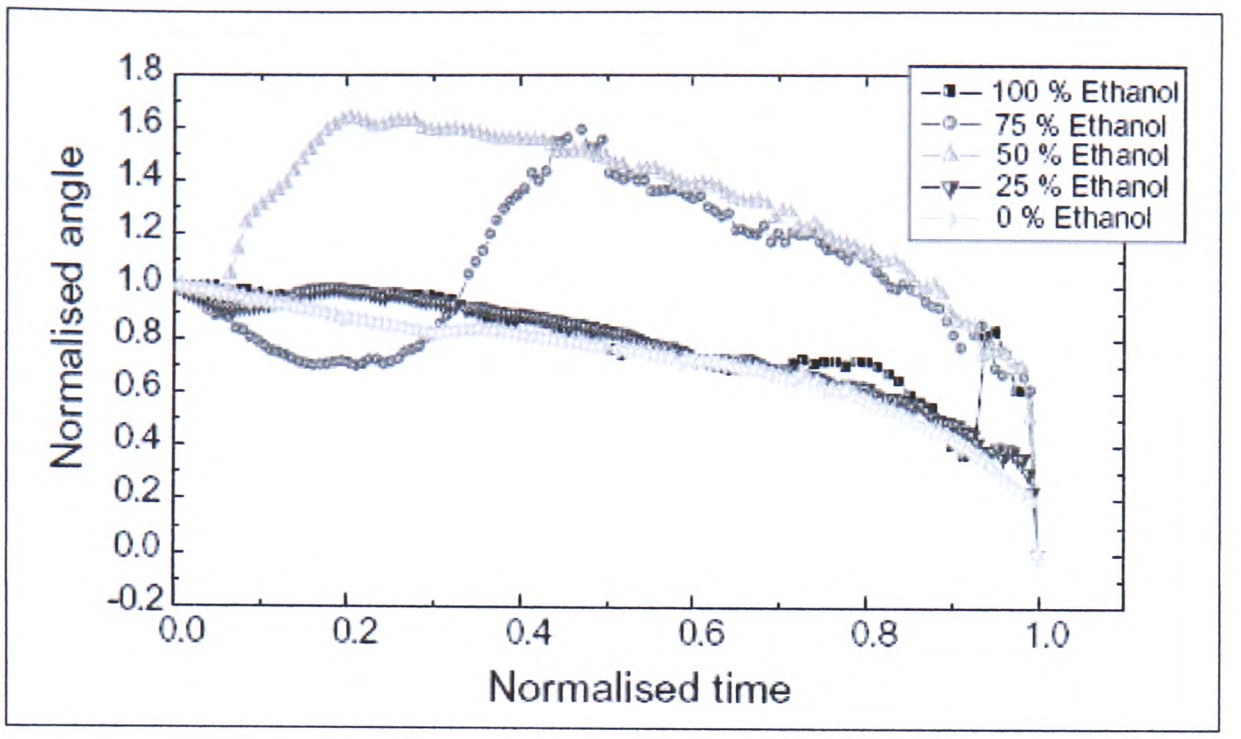

Figure 2.35: *Time dependence of the contact angle for three mixtures and the two pures components [10].*

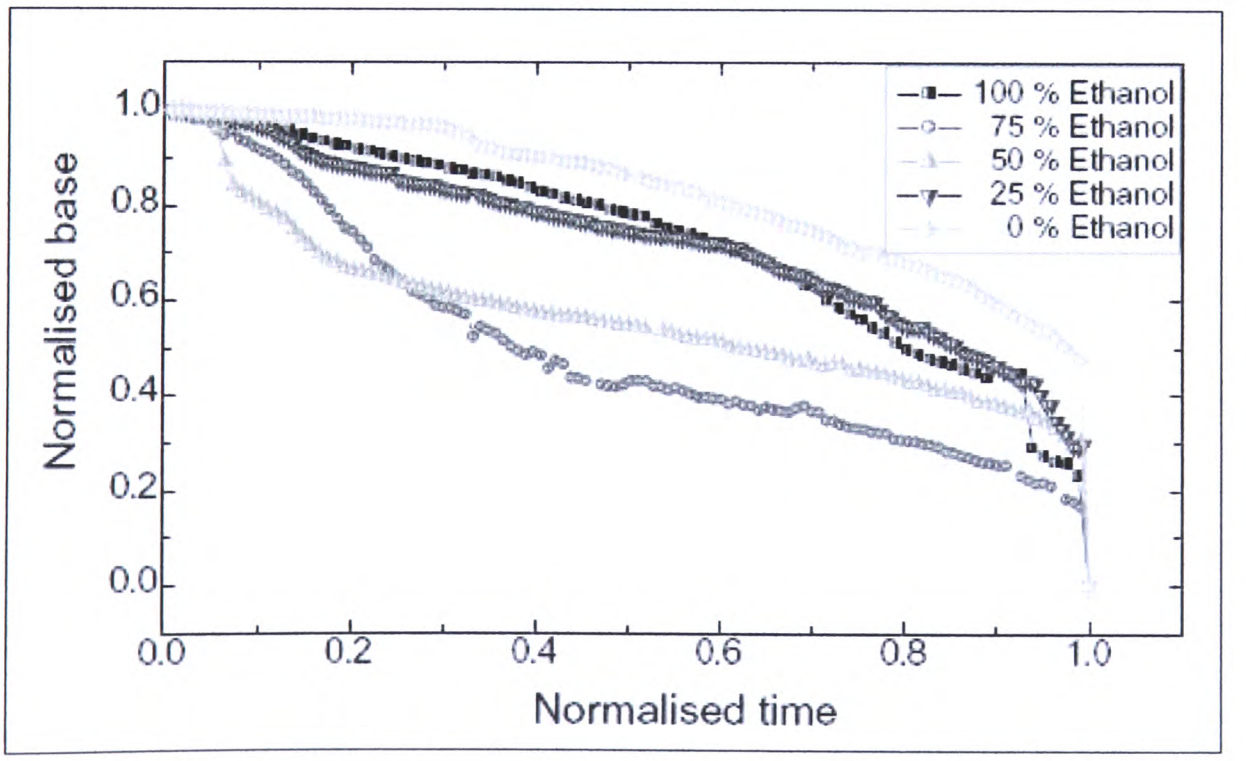

Figure 2.36: *Time dependence of the base diameter for three mixtures and the two pures components [10].*

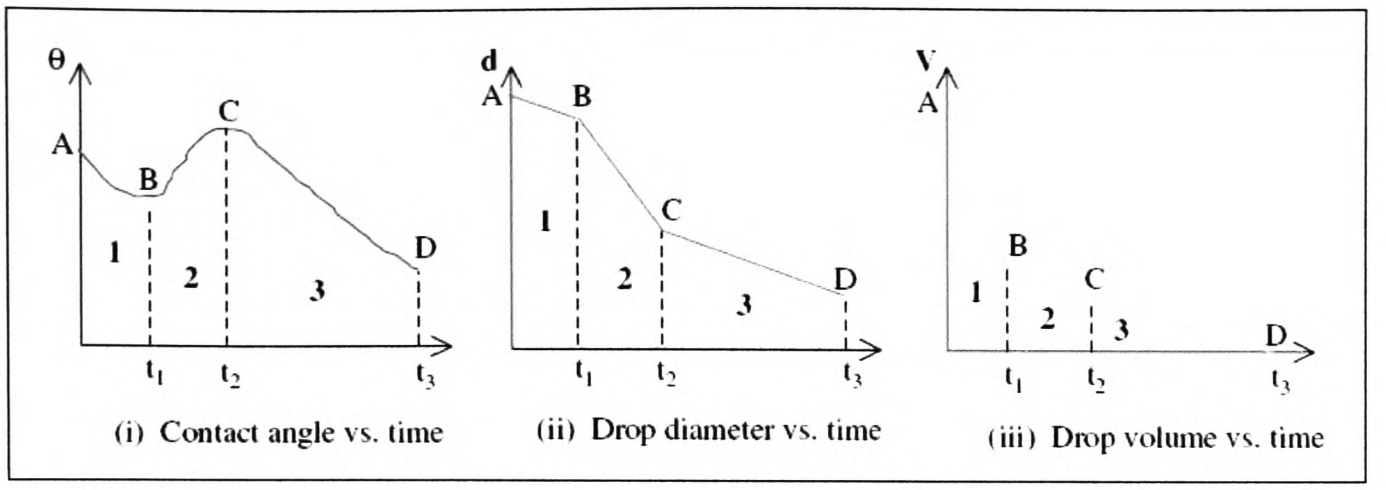

Figure 2.37: *Simplified evolution of drop contact angle, diameter and volume [10].*

Recently, Yu *et al.* [11] investigated the evaporation of microdroplets of ethanol-water mixtures on gold surfaces. Compared to Sefiane *et al.* [10] experiment, the surface (gold coated on a microscope slide) should not be considered as rough. Identical volumes ($2 \pm 0.3\ \mu L$) from various compositions (25%, 50% and 75% in volume) were deposited and left to evaporate in the ambient air ($T = 22.7 \pm 1.5°C$ and $H = 40 - 50\%$). By plotting the initial contact angle against the composition, a near linear relationship was found (see Figure 2.38). They used it as a direct correlation between the interfacial tension and the liquid bulk composition. In Figure 2.38 the variation in time of the contact angle and contact area are presented.

They first noticed a difference between pure components and binary mixtures. While the evaporation process of pure water or ethanol drops could be divided in two stages (as shown in many others studies): pinning and shrinking. At the beginning, water-ethanol mixtures experienced an increase in contact angle and a diminution in the solid-liquid contact area. It could be due to the highest evaporation of ethanol which increases the concentration of water and thus the surface tension.

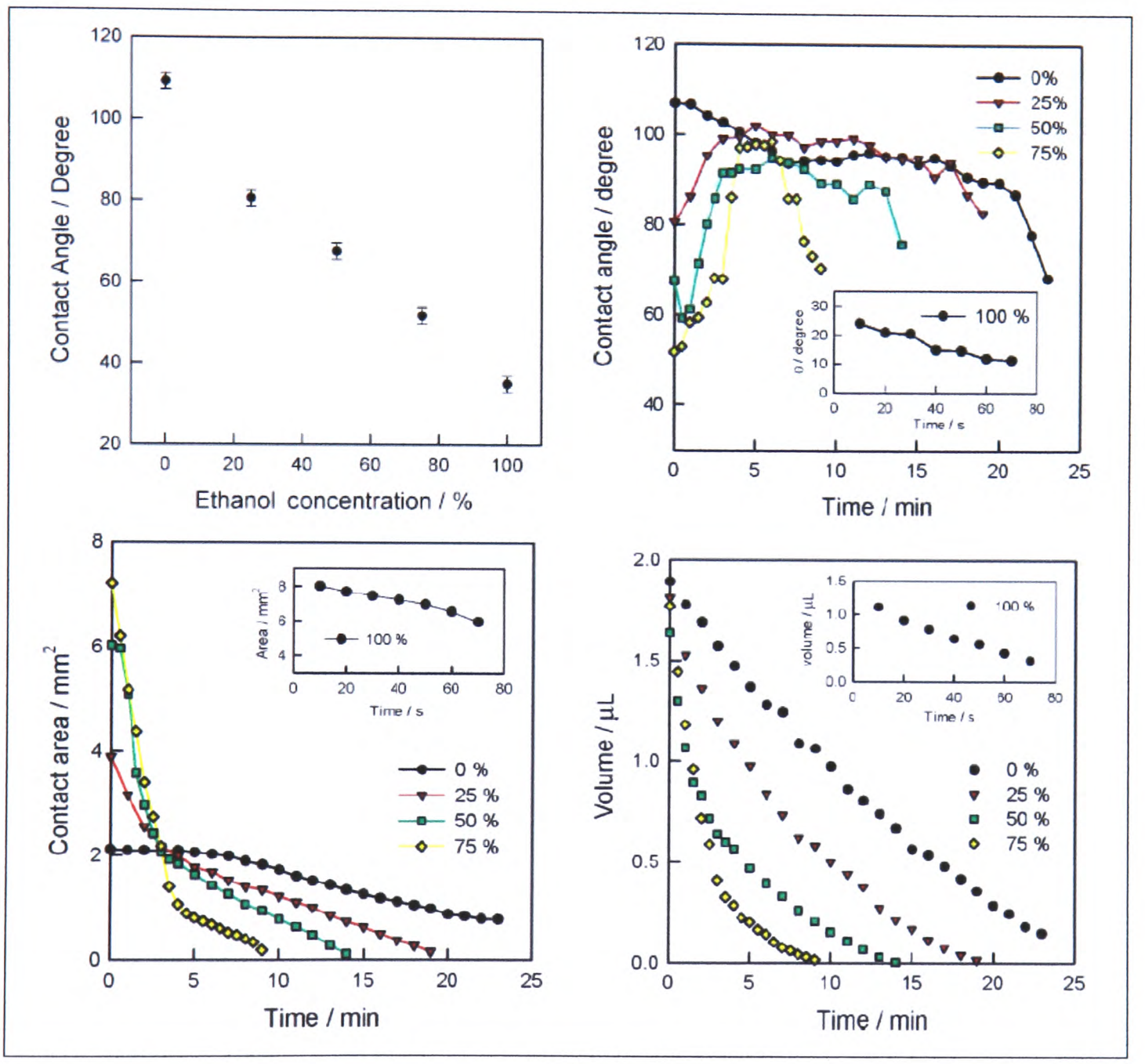

Figure 2.38: *Example of initial sessile drop at different water-methanol concentration*

2.5 Surface roughness

As mentioned in the previous chapter, ideal surfaces are very rare. The most noticeable effect is the non unique contact angle equilibrium as suggests the Young-Dupré equation (see Equation 1.9 page 10). Real surfaces are not perfectly flat and smooth. One of the first theories taking into account the surface heterogeneities has been introduced by Wenzel [12, 13] and Cassie and Baxter [14]. Later, Johnson and Dettre [29, 31] worked on the study of contact angle hysteresis on idealized rough surfaces comparing experimental results to a simple model. Over the last decades, many researches focused on patterned surfaces where structures were especially designed to create super repellent surfaces [17–25].

In their experiment, Johnson and Dettre [29, 31], made controlled surface roughness by successive heating in an oven. Both advancing and receding contact angles were plotted as a function of surface roughness (or number of heat treatments), see Figure 2.39. For low surface roughness, the advancing contact angle increases with r while the receding contact angle decreases. But over a given surface roughness, both advancing and receding contact angles increase abruptly and reach a maximum value.

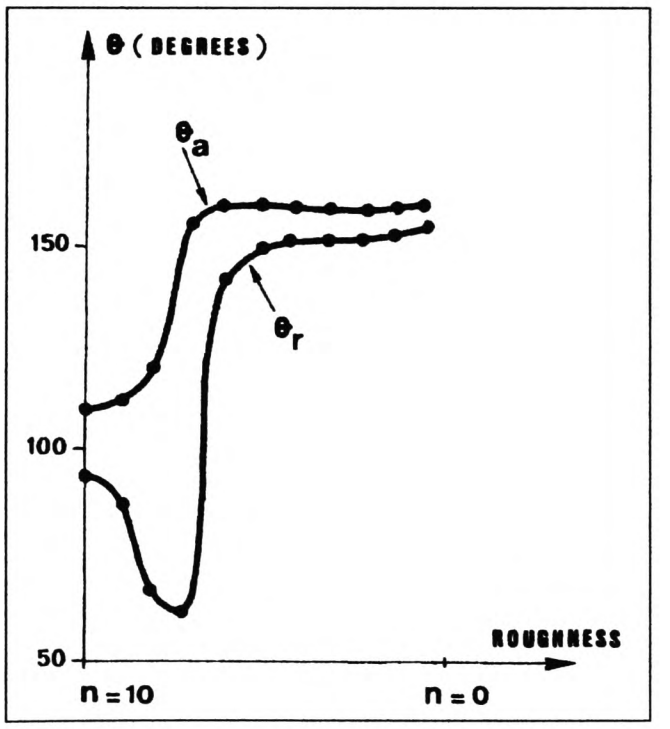

Figure 2.39: *Advancing receding contact angles evolution on a wax substrate as a function of surface roughness (number of heat treatment), from [31].*

Extensive work on the study of contact angle hysteresis, particularly the apparent contact angle for non ideal surfaces, have been performed by Marmur *et al.* [15, 16, 30, 61–68].

Marmur *et al.* [67] have shown the limit of the Wenzel theory, i.e the relation between the

apparent contact angle and the intrinsic contact angle θ_{eq}. However in the particular case of "sawtooth" surfaces and if the drop size is much larger than the roughness scale, it is found that the Wenzel equation is valid (see figure 2.40).

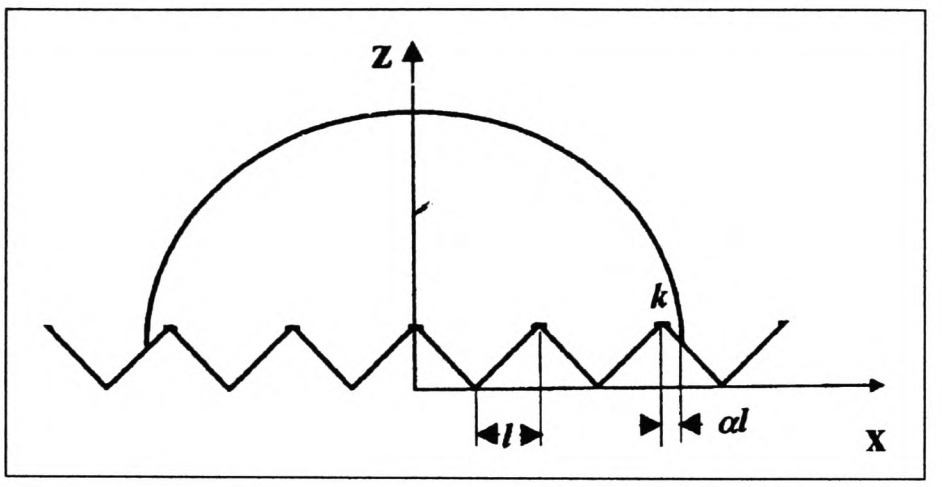

Figure 2.40: *Geometry of a "sawtooth" surface used by Marmur et al. [67]*

The same author [68] discussed in the case of rough surfaces, the competition between "homogeneous" and "heterogeneous" wetting. This problem underlines the difference between wetting on rough surfaces in the absence (or not) of air trapped into the grooves between the solid and the liquid and on the transition from one regime to the other.

In a more recent paper, Marmur *et al.* [30] developed a new method to measure the apparent contact angle at the global energy minimum on rough surfaces. The substrate was placed on a vibrating stage in order to reach the "global energy minimum" (see Figure 2.41). This was done for various surface roughnesses with a scale lower than the drop size (see Figure 2.42). The obtained results show that, independently of the surface state, a good agreement between the measurement and the value calculated using the Wenzel equation is found. In order to control perfectly the surface roughness, design of micro patterns were realised.

As can be seen in Figure 2.43, natural surfaces such as lotus leaf are very hydrophobic (contact angle over 170^o). Many works attempted to reproduce such surfaces and new commercial products based on this property have been produced: self-cleaning paints and glass windows are few examples [17, 69].

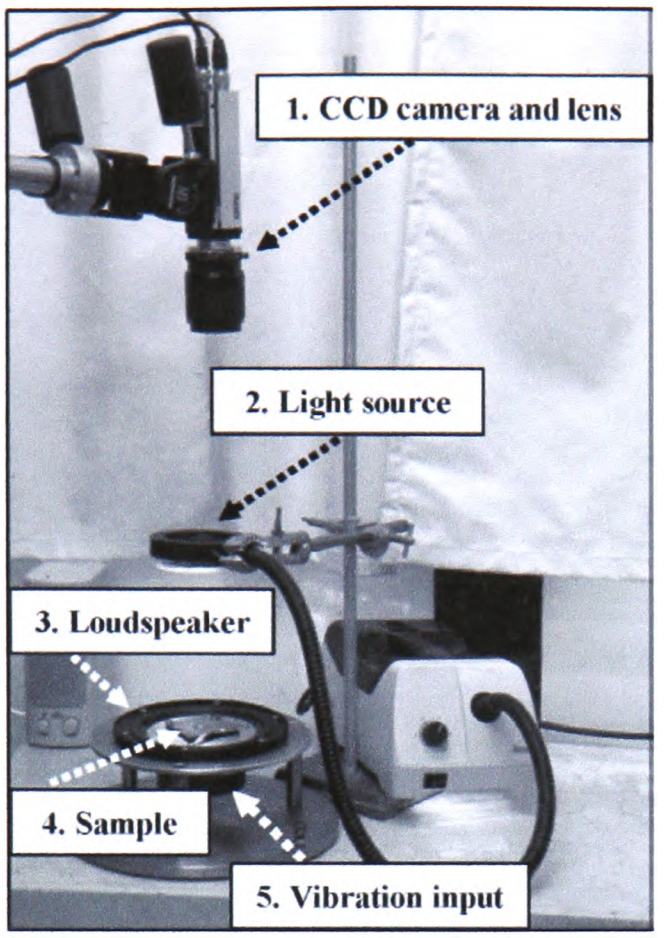

Figure 2.41: *Experimental set up used by Marmur et al. to determine the apparent contact angle corresponding to the "global energy minimum" [67].*

Queré *et al.* [17, 18, 24, 70, 71] have shown that the main parameter characterising the surface hydrophobicity is not r but the fraction of solid actually in contact with the liquid. Such surface roughness allows air to be trapped between the liquid and the substrate, while the liquid is suspended on the tips of the spikes. Since the area of real liquid-substrate contact is highly reduced, the contact angle of the drop was determined almost solely by the surface tension of the liquid, leading to a very large contact angle.

McCarthy *et al.* [22, 23] worked on the dynamic aspect of hydrophobic surfaces. The surfaces studied contained posts of different sizes, shapes and spacings, see Figures 2.44 and 2.45. They showed that square posts with a width less than 32 μm are "ultrahydrophobic" with a large contact angle hysteresis. The contact angles were independent of the post height from 20 to 120 μm. Finally, increasing the distance between posts and changing the shape from square to staggered rhombus, star, or indented square caused increases in receding contact angles.

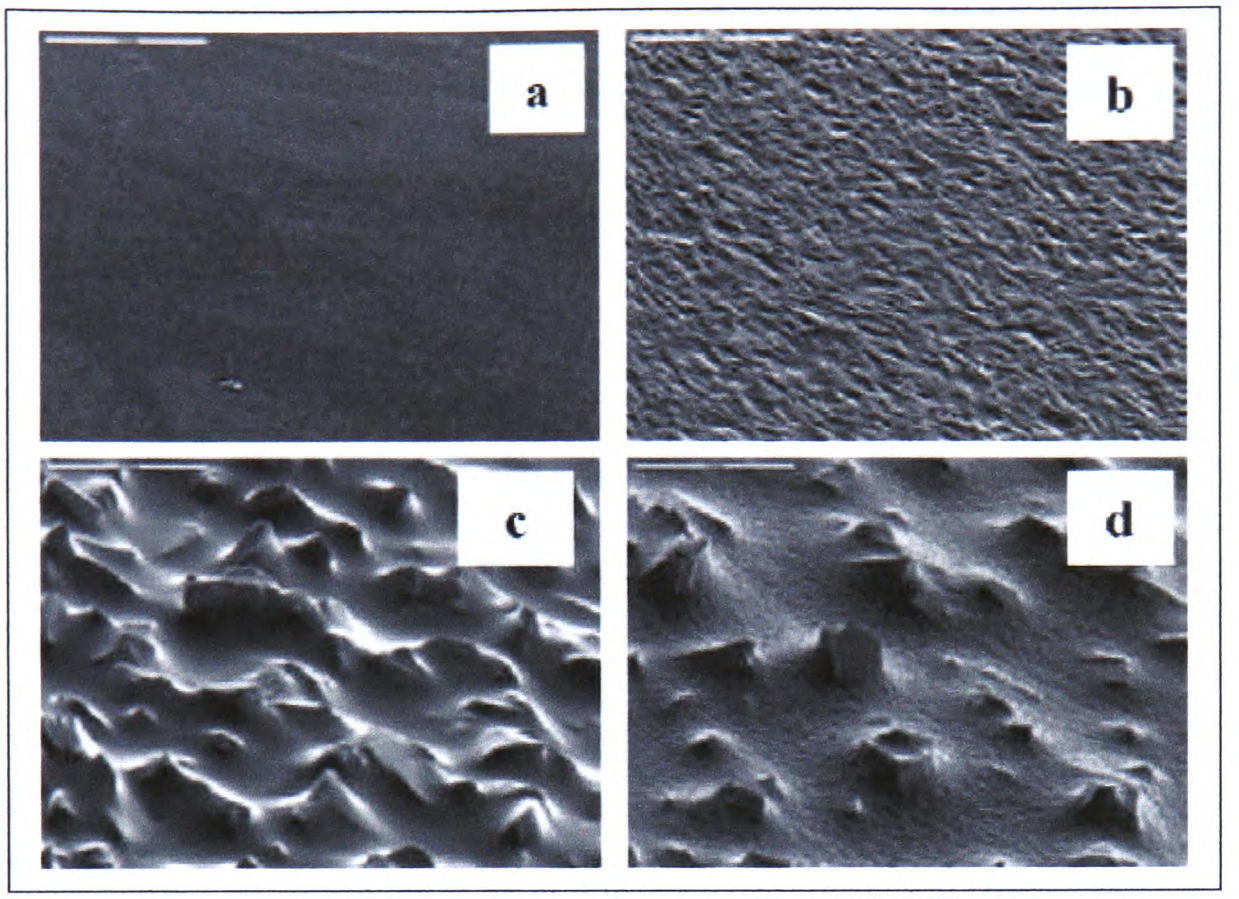

Figure 2.42: *Substrates surfaces photographies of the four samples used in the "global energy minimum" experiment [67].*

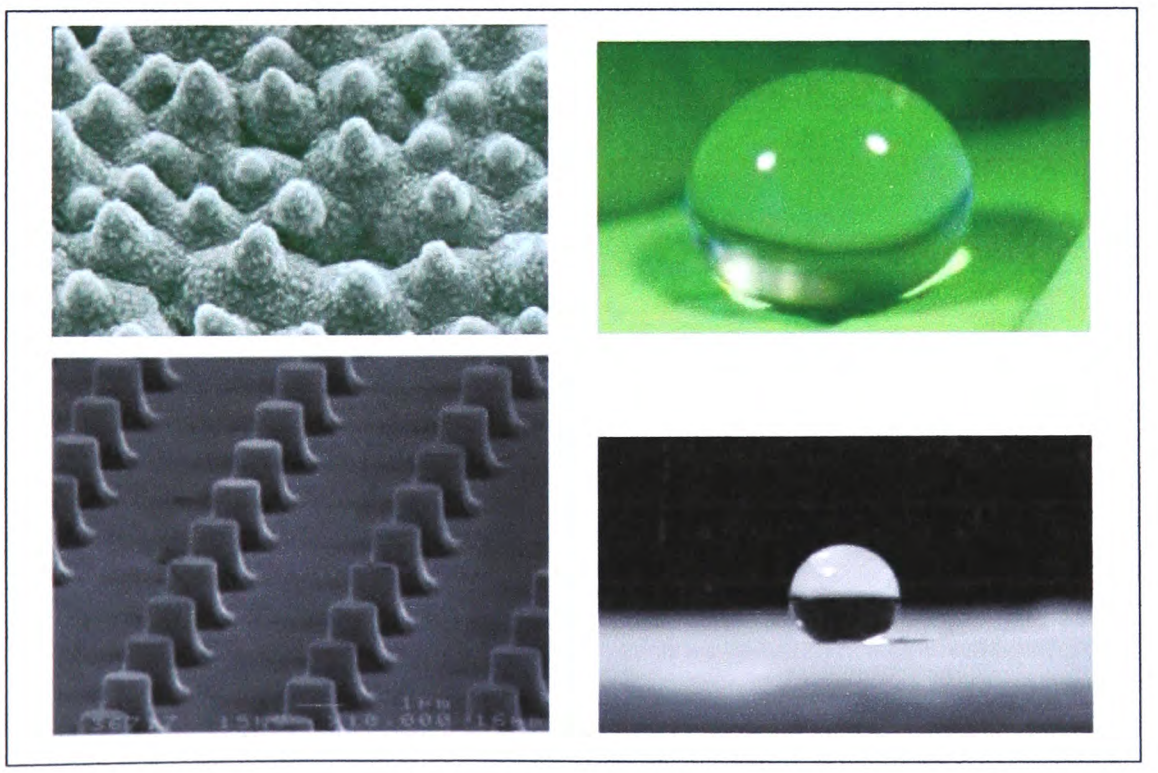

Figure 2.43: *Examples of natural and patterned super water repellent surfaces. Top pictures illustrate a lotus leaf (micro analysis on the left) [69]. Below, micro structured surfaces designed in order to increase considerably the surface hydrophobicity [18, 70].*

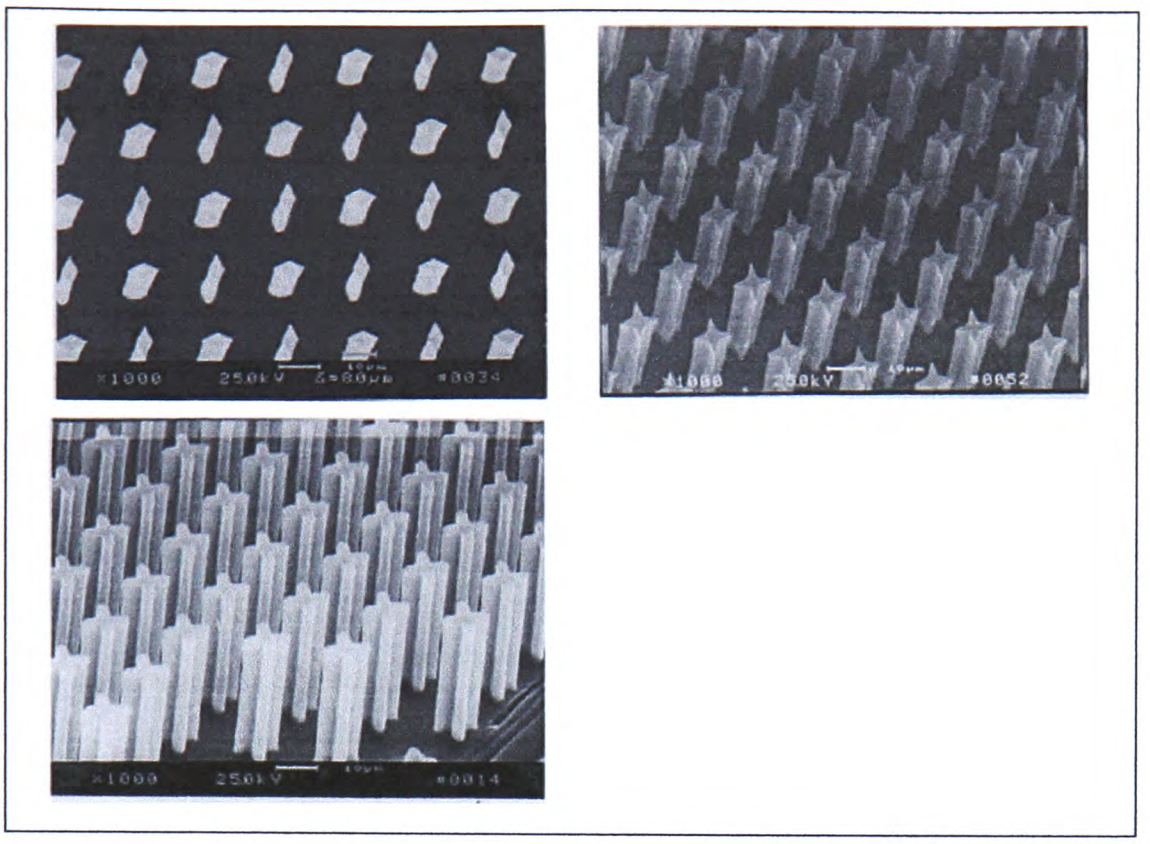

Figure 2.44: *Examples of natural and patterned super water repellent surfaces. Top pictures illustrate a lotus leaf (micro analysis on the left) [69]. Below, micro structured surfaces designed in order to increase considerably the surface hydrophobicity [18, 70].*

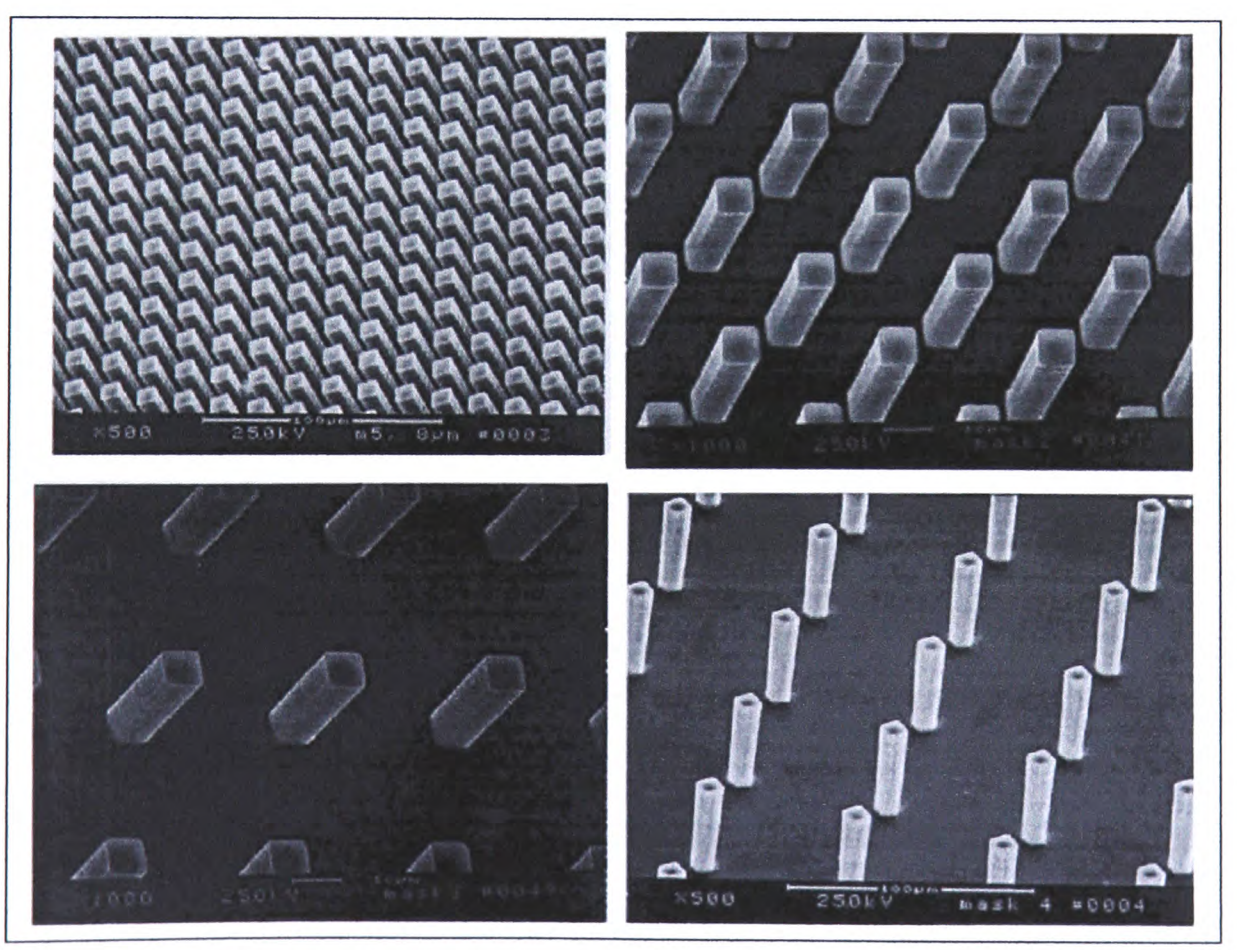

Figure 2.45: *SEM surfaces containing* 8 μm $\times$ 8 μm *square posts with different spacings [23]*

Chapter 3
Experimental overview

All the experiments which are presented in the following chapters are based on the study of sessile drop profiles. In order to deposit and study the wettability of sessile drops, a drop shape analyser was used. In this chapter all the common equipments used for the experiments are presented. Further details concerning each experimental preparations and processes will be explained in corresponding chapters.

3.1 Drop shape analyser

The DSA100 from Krüss (Krüss GmbH, Hamburg, Germany) is an apparatus especially designed for measuring contact angles. It is composed of both the hardware part (camera, dosing system, stage...) and the software part (image analysis, dosing controller...).

1. Hardware description (see Figure 3.1):

   - a sample table with up to three manually controlled axes,
   - a video system composed of a CCD camera (up to 25 frames/sec), a camera tilt and a light source. The magnification and focus are manually controlled.
   - a manual or PC-controlled dosing system: unit driven by a step motor.

2. Software description (see Figure 3.2):

   - dosing system controller, can generate drops of controlled volume, and deposit them automatically on the substrate. This is very important for the experiments reproducibility,
   - imaging controller, composed of a sharpness assistant, brightness and contrast settings
   - movie recorder, the frequency is up to 25 frames/sec. There is the possibility to program a video sequence in several steps with different single frame frequencies and recording times,

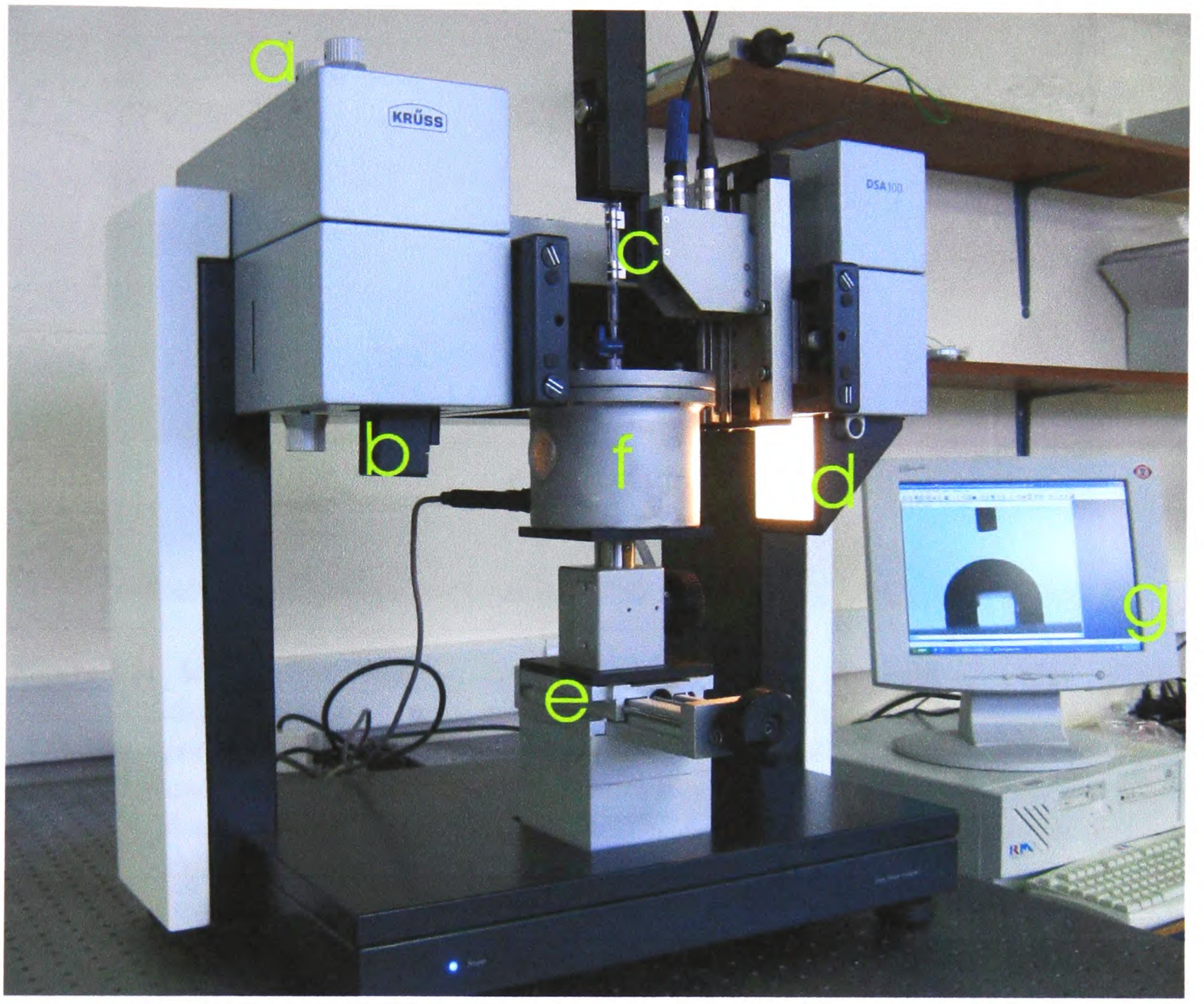

Figure 3.1: *Photography of the DSA100 apparatus mounted with the low pressure chamber: (a) focus and magnification assistant; (b) CCD camera; (c) PC-controlled dosing system; (d) light source; (e) three manually controlled axis stage; (f) low pressure chamber and (g) PC monitor.*

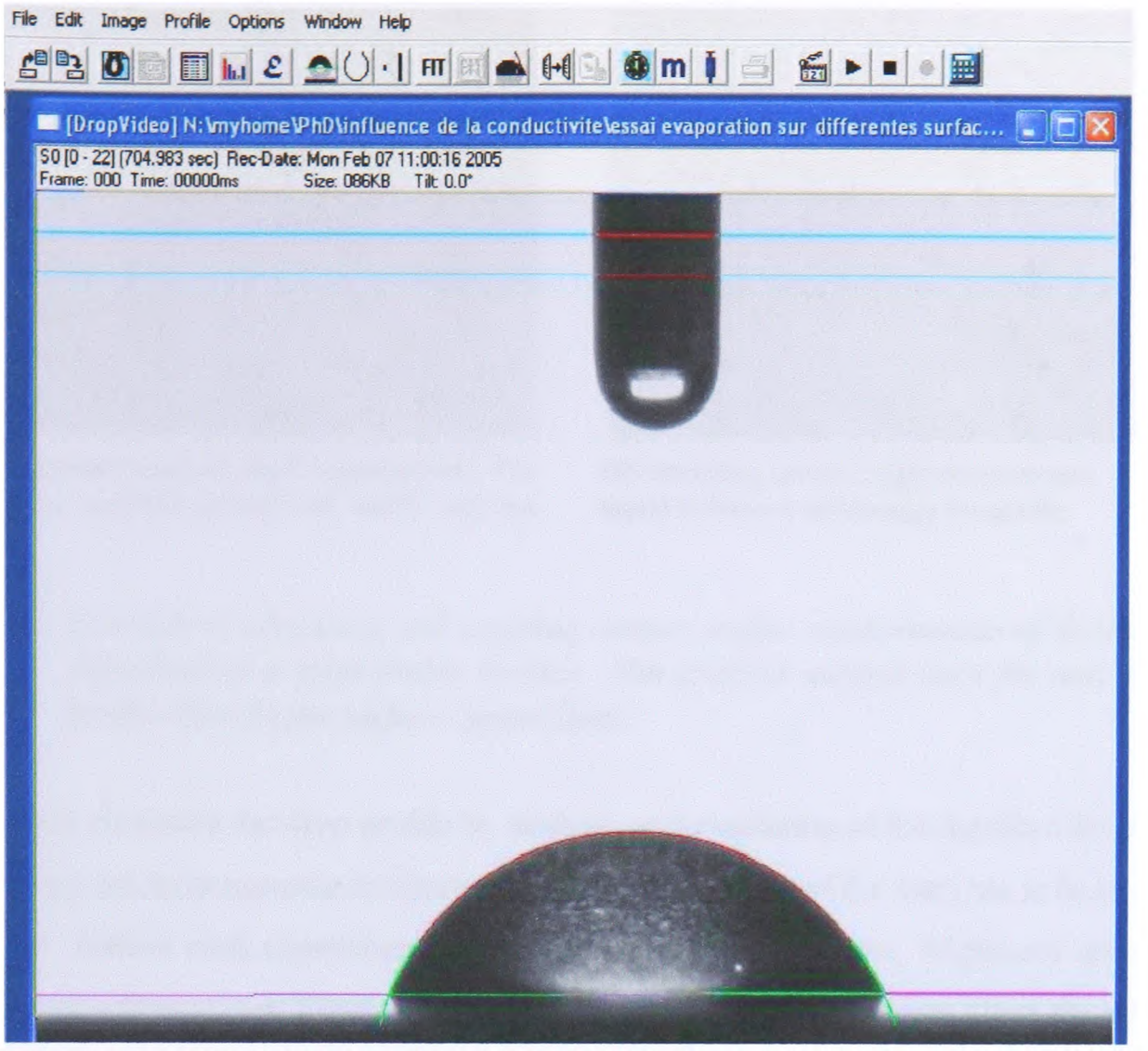

Figure 3.2: *Screen capture of the DSA100 analysis software. Example of a Water droplet deposited on a Titanium substrate. The green lines close to the triple line are the polynomial function fit, the red line is the drop profile according to the grey level analysis and the horizontal bottom line is the base line (which could be chosen both automatically and manually). The two top red lines on the needle serve to define the magnification factor by measuring its diameter.*

- contact angle measurement software, the package has four different methods to determine the drop shape. The first method fits the complete profile of a sessile drop with a general conic section equation. The second fits only the drop near the contact line with a polynomial function (see Figure 3.2), used primarily to measure advancing and receding contact angles (see Figures 3.3(a) and 3.3(b)). With the third method, the profile is fitted to a segment of a circle, it is accurate only for small drops, where there is no gravitation effect. The last method, Young-Laplace, is the most accurate (the complete drop contour is evaluated and includes a correction for gravitational effect) but is only reliable for contact angles above 30 °.

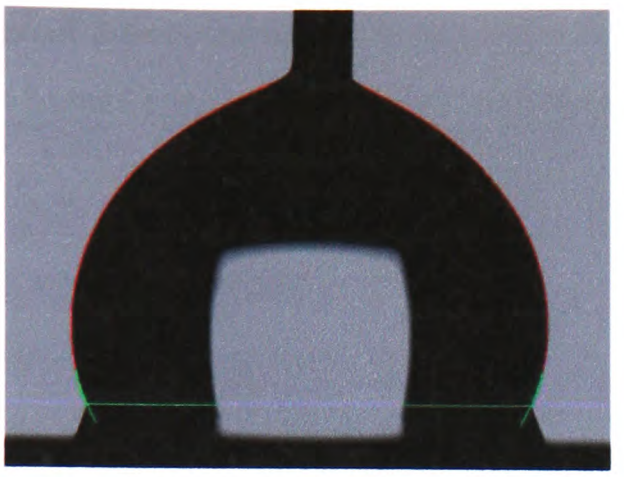

(a) Advancing contact angle measurement. The liquid is supplied through the needle into the drop.

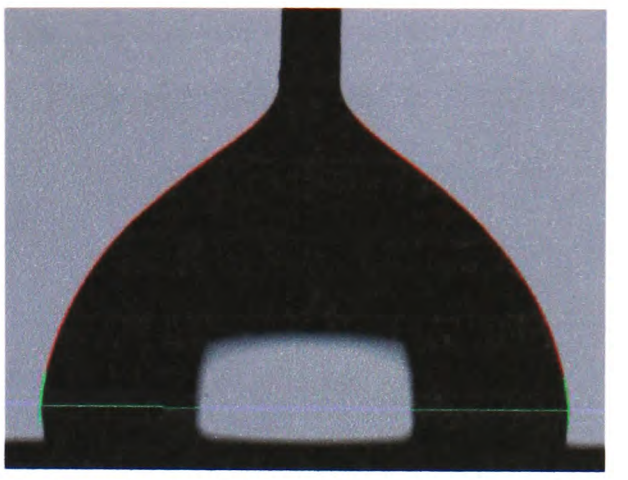

(b) Receding contact angle measurement. The liquid is drained out through the needle.

Figure 3.3: *Example of advancing and receding contact angles measurements of Water droplet deposited on a hydrophibic surface. The analysis method used fits only the drop profile close to the surface (green line).*

The DSA100 measures the drop profile by analysis and evaluation of the digitized drop image. In order to get the most accurate measurements, the video image of the drop has to be as optimal as possible. Before each experiment, three settings, image sharpness, brightness and camera tilt have to be adjusted (see Figures 3.4(a) and 3.4(b)). Tilting the camera alters the reflection of the drop on the substrate surface and eases the baseline determination.

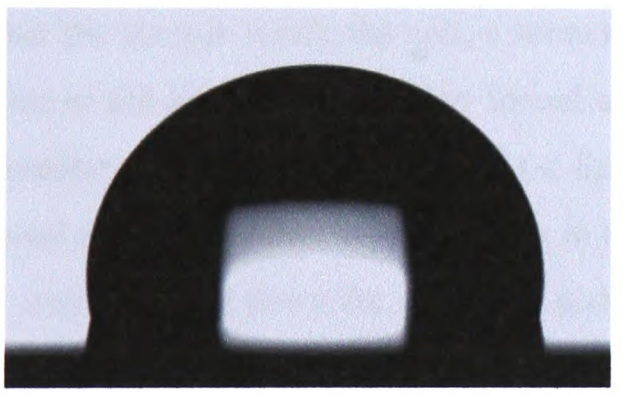

(a) Example of an optimum optical settings adjustment. The drop edge is sharp and the reflection of the drop on the substrate surface is distinct.

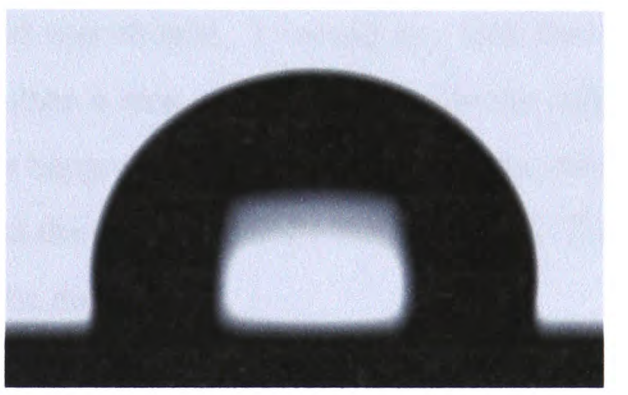

(b) Example of poor adjustments: fuzzy edges and undectable reflected drop on the substrate surface. It generates great difficulties to determine the drop baseline and profile.

Figure 3.4: *Optical settings*

Measurements uncertainties

In all the presented investigations, the DSA100 goniometer has been used to measure the contact angle and drop base diameter and therefore the drop volume has been determined. It is considered that the uncertainties measurements on the drop base radius is $\pm 5\%$ and $\pm 0.5^{\circ}$ in

the case of the contact angle. It means that in the case of a drop with a diameter of 2.7 mm and with a contact angle of 60° the uncertainty on the volume measurement is

$$\frac{\mathrm{d}V}{V}12\% \tag{3.1}$$

where

$$\mathrm{d}V = \frac{\partial V}{\partial r}\mathrm{d}r + \frac{\partial V}{\partial \theta}\mathrm{d}\theta \quad \text{and} \quad V = \frac{\pi R_a^3(1-\cos\theta_{eq})^2(2+\cos\theta_{eq})}{3\sin^3\theta_{eq}} \tag{3.2}$$

3.2 Low pressure chamber

The low pressure chamber is a cell, cylindrical in shape, connected to a vacuum pump and a gas supply. It was designed to be used with the DSA100 apparatus. Two optical windows are positioned on two opposite sides to allow simultaneous lighting and video recording. On the top a valve is connected to the injection system.

Pressure in the cell can be varied from 40 mbar to atmospheric pressure. During the experiment, the highest pressure variation/fluctuation occurs at lowest pressures and does not exceed 10%. The accuracy of the pressure gauge is 1 mbar for the range studied.

To place the sample inside the cell, a screwable lid was chosen. To avoid any leak the needle is sealed to the lid. This restriction forced us to place a step motor stage inside the cell. The drop generated, due to its tiny volume ($< 8\mu L$), is hanged to the needle nozzle. The only way to deposit it on a substrate is to put/bring in contact the surface and the hanging drop. The step motor moves up and down the sample to pick up the drop.

As the cell dimensions are much larger than the drop volume, the pressure will not be affected by the evaporated liquid (liquid partial pressure much smaller than the ambient pressure).

The biggest inconvenience occurs when the pressure is reduced. By pumping out the gas, the remaining liquid in the needle could be drained into the cell. To avoid this problem the low pressure cell must be used according to the following well defined steps:

1. after having well thightened the lid, air is removed from the chamber by reducing the pressure to its minimum (5 mbar),
2. the chamber is filled with the experimental gas (Helium, Nitrogen or Carbon Dioxide)

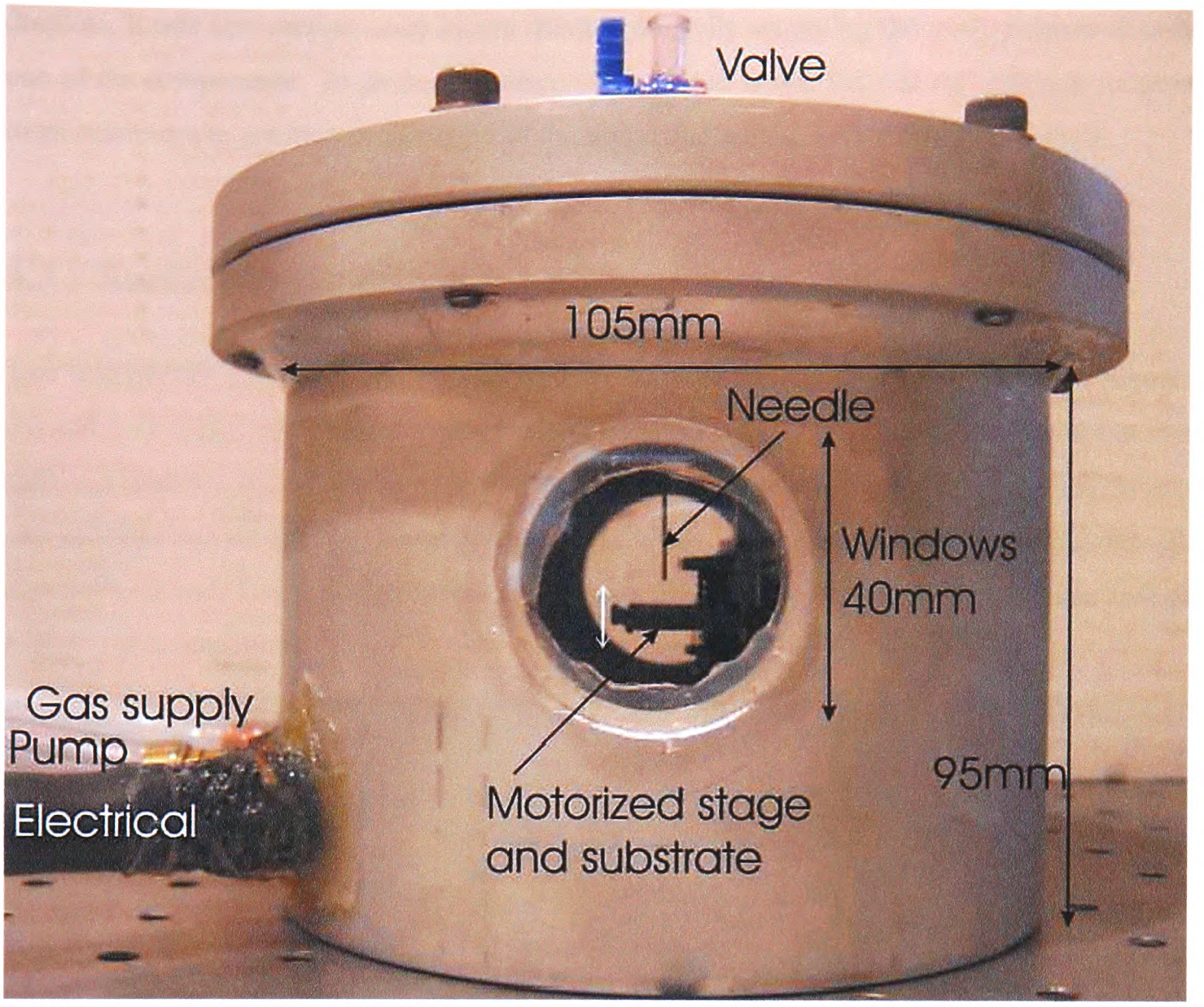

Figure 3.5: *Photography of the low pressure chamber. Two windows sealed with silicon paste are placed at half height. The valve on the top connects the injection pump (see Figure 3.1) to the needle. The chamber is also connected to the vacuum pump, gas supply and step motor power supply.*

until the pressure reaches the atmospheric value,

3. the droplet of controlled volume is deposited onto the substrate,

4. all remaining liquid in the needle is drained back into the syringe and the valve is closed. This step ensures that there is no liquid left,

5. the pressure is reduced to the desired value.

Another advantage of this chamber is the possibility of getting a saturated atmosphere. This has many uses, for example, this is very convenient in the determination of surface energy. Static contact angle and hanging drop profile measurements have to be done on non-evaporative

droplets. It was also used to study binary mixture drops by saturating the atmosphere with only one of the components. To proceed, a reservoir is placed inside the cell and pressure reduced to its minimum to enhance evaporation of the liquid and hence, saturate the atmosphere.

3.3 Surface analysis

Two instruments have been used to characterise the substrate surfaces (see analysis in Figures 3.6 and 3.7). These two equipments are complementary as they characterise the surface at two different scales: a New View 100 from Zygo Corp which uses scanning white light interferometry (SWLI) and an Atomic Force Microscope (AFM) which uses contact force microscopy. The SWLI is able to analyse a surface 1 cm^2 area, give resolution, and AFM a surface area of 1 mm^2, give resolution.

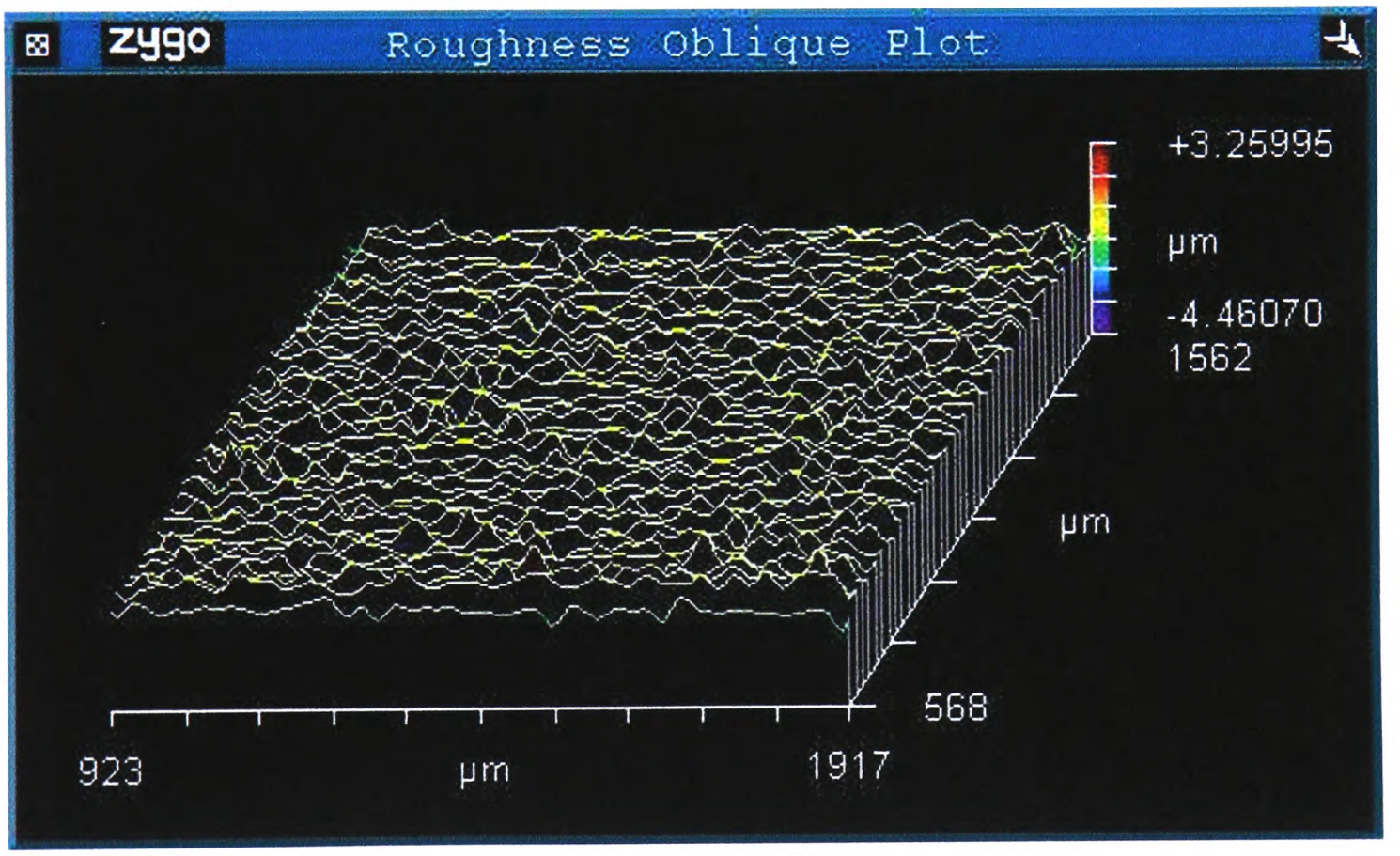

Figure 3.6: *Example of a surface roughness profile (Aluminium sample) obtained with the microscope interferometer. This 3D plot is the result of 3D interferogram which is transformed by frequency domain analysis. Indeed, an incoming light is split inside an interferometer, one beam going to an internal reference surface and the other to the surface analysed. After reflection, the beams recombine inside the interferometer, undergoing constructive and destructive interference and producing the light and dark fringe pattern.*

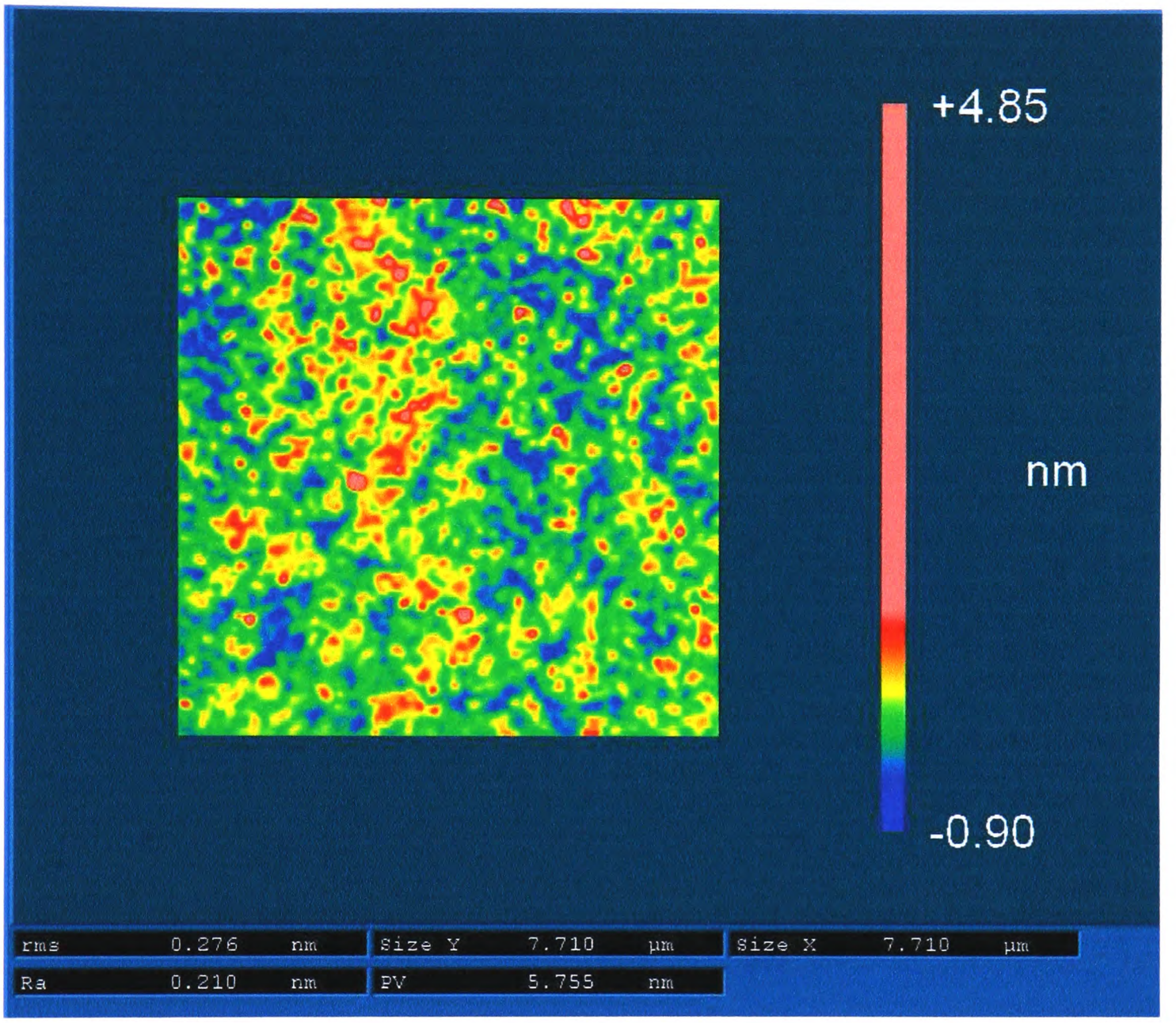

Figure 3.7: *Example of a surface roughness profile (silicon wafer coated with a very thin layer of PDMS) characterised with the AFM. The AFM consists of a microscale cantilever with a sharp tip (probe) at its end that is used to scan the specimen surface. When the tip is brought into proximity of a sample surface, forces between the tip and the sample lead to a deflection of the cantilever. Depending on the situation, forces that are measured in AFM include mechanical contact force, Van der Waals forces, capillary forces, chemical bonding, electrostatic forces, magnetic forces (see Magnetic force microscope (MFM)), etc. Typically, the deflection is measured using a laser spot reflected from the top of the cantilever into an array of photodiodes.*

3.4 Laboratory room description

The laboratory is equipped with an air conditioning unit to maintain a constant temperature. A weather station is also installed to measure the temperature, pressure and humidity. To minimize the perturbations the DSA100 apparatus is placed on an anti-vibration table.

3.5 Syringes and needles

Needles: Depending on the experiment a range of syringes and needles are used. All the needles were from Hamilton (Hamilton Company, Bonaduz, Switzerland), Kel-F hub needle type in stainless steel with a blunt point. There were three gauges:

larger diameter, details, which is used for surface tension measurement. The greater the diameter, the greater the hanging drop generated is,

medium diameter, gauge 22 s (inner diameter=0.15 mm and outer diameter=0.72 mm), used for most of the experiments,

smaller diameter, gauge 26 (inner diameter=0.10 mm and outer diameter=0.46 mm), used to produce the smallest drop and for the advancing and receding contact angle measurements (see Figures 3.3 page 58). It minimizes the needle intrusion effect on the drop.

Syringes One type of syringes were used, "Gastight 1725LT, 250 μL" from Hamilton Company. The inner diameter is 2.304 mm. Combined with the injection pump, it allows to generate drops at 7 $\mu L/min$ at the lowest rate.

Cleaning procedure: It is best to segregate syringes and needles according to the type of solvent they dispense. Nevertheless, as many liquids were used for the experiments, a perfect cleaning of both the syringe and the needle is needed. The following procedure is adopted:

1. Remove the syringe plunger and wash its tip in the alcohol. Slowly pour 50 mL of Methanol through the syringe body and needle (in a one-way flow into the top of the syringe, out of its bottom). This will flush the system of lightly adsorbed contaminants.
2. Flush 50 mL of deionised water through the syringe in exactly the same way as the alcohol.

3. Flush the water by pushing air through with the plunger, repeatedly removing and reinserting it. Remove the plunger and dry all in an oven at $50\,°C$ for four hours.

3.6 Common experimental procedure

3.6.1 Cleaning

Before running any experiment, all substrates were cleaned. As a large range of substrates have been used particular cleaning processes have been elaborated. Furhter details will be explained in each chapter. Nevertheless the basic steps could be summarised as follow:

1. substrate immersed in an ultrasonic bath for 5 to 10 minutes. Due to the high volatility and hazard, great care is taken by placing the bath in fume cupboard. The ultrasonic bath by its vibrations enhances the cleaning effect. The main solvent used is Acetone. It is particularly useful because it is inexpensive and moderately polar allowing it to dissolve a wide range of organic substances.
2. rinsing with Deionised Water,
3. drying in an oven or with Nitrogen flow.

3.6.2 Experimental Procedure

In this section all common steps to the experimental procedure for all experiments are presented:

1. adjust the three optical settings to get the optimal image (see Figures 3.4(a) and 3.4(b) page 58),
2. define the appropriate video recording time,
3. drop deposition on the substrate and start recording,
4. movie analysis

Chapter 4
Structured surfaces

The first experimental investigation to be presented is on the study of the effect of a structured surface on the wetting behaviour. This was examined by using a substrate made of hydrophobic materials patterned with structured defects. The topography of the substrate was measured using a profilometer. Four different surfaces with holes/pillars every 200 μm and depth/height from 1 to 11 μm were investigated.

4.1 Experimental conditions

Two kinds of patterned surfaces have been prepared: "holes" and "pillars" respectively. As the "holes" surfaces served as a mould to prepare the "pillars" surfaces, they had to be prepared previously. First a mask had to be designed where square holes have been pierced every 200 μm and photoresist was coated on $10 \times 10 \times 1$ mm glass samples. Then, providing a light source, at each hole site the thermoresist convertible from an unexposed state to an exposed state when heated to a temperature in excess of a threshold temperature by exposure to radiation from the light source. Depending on the exposure time, the depth of the holes will vary. The exposure time didn't exceed 30 s which corresponds to a depth of 11 μm. Each sample has been surface analysed with a ZYGO profilometre, top view of all the samples are represented in Figure 4.1. The patterned surface is only present in the centre part of the samples, it means that the deposition of the drops had to be carefully positioned. These surfaces are very fragile, no heat has to be applied and only Water drops could be used as other liquids might dissolve the photoresist.

To prepare the substrates with pillars, the previous samples were used as a mould. As these patterned surfaces cannot be made of photoresist, they were made in PDMS (Polydimethyl-siloxane) which is a polymer with an external hydrophobic surface which makes it difficult for polar solvents to wet. The "holes" samples were placed in a petri dish and a solution with the PDMS was poured on them. After 12 hours the liquid has hardened and the "pillars" samples

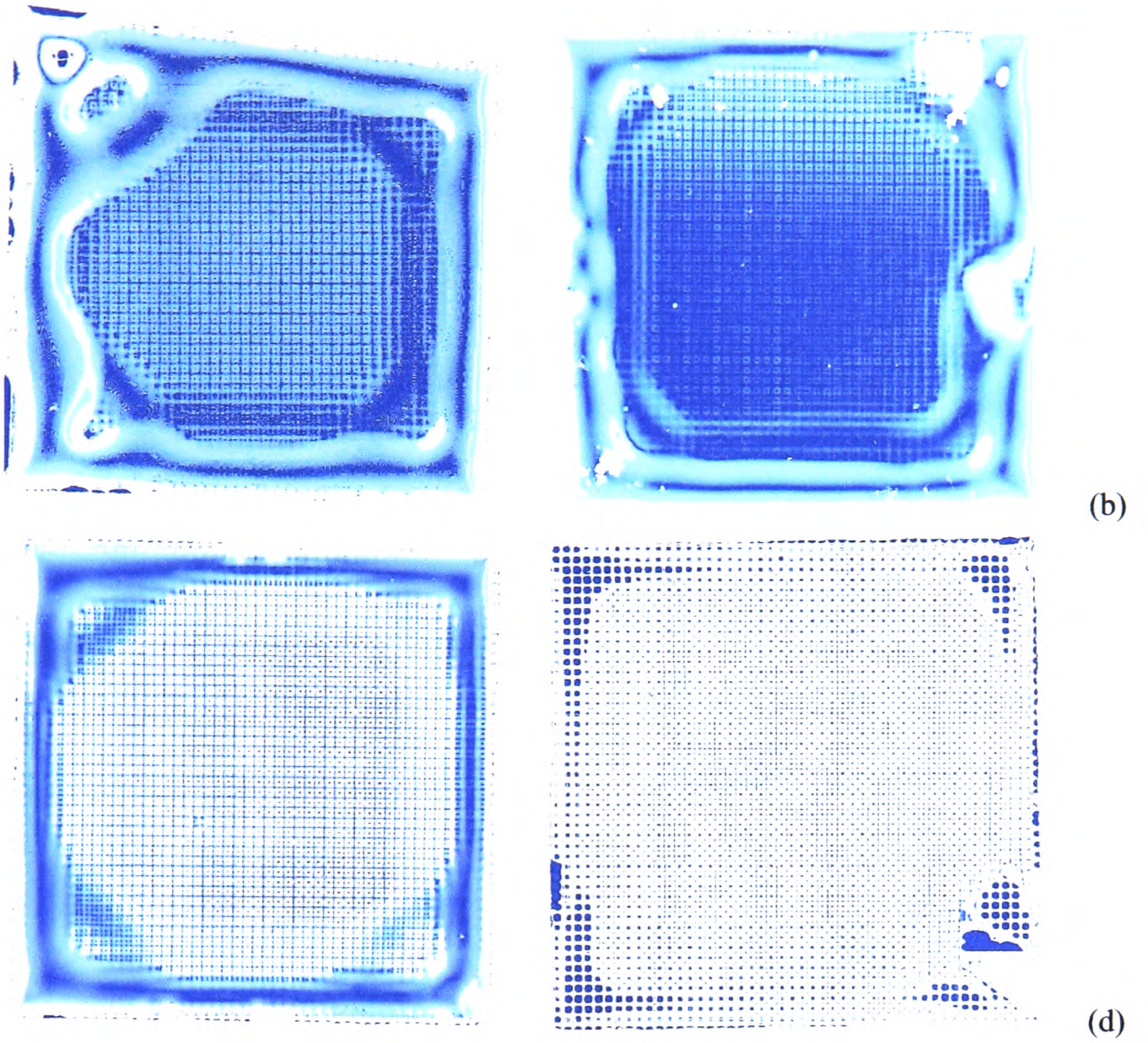

Figure 4.1: *Surface analysis of the four samples used in the present study.*

were ready. The samples obtained by this procedure are the exact "copy" of the "holes" samples. Topography analysis with the ZYGO profilometer confirmed that the shape of the pillars is identical to the shape of the holes and their heights are equal to the holes depths. As these samples are in PDMS any liquids but solvents like alkanes could be used.

Sample	a	b	c	d
Depth/Height (mm)	1.2	4	6	11

Table 4.1: *Sample properties.*

Pure deionised Water has been used in all the experiments.

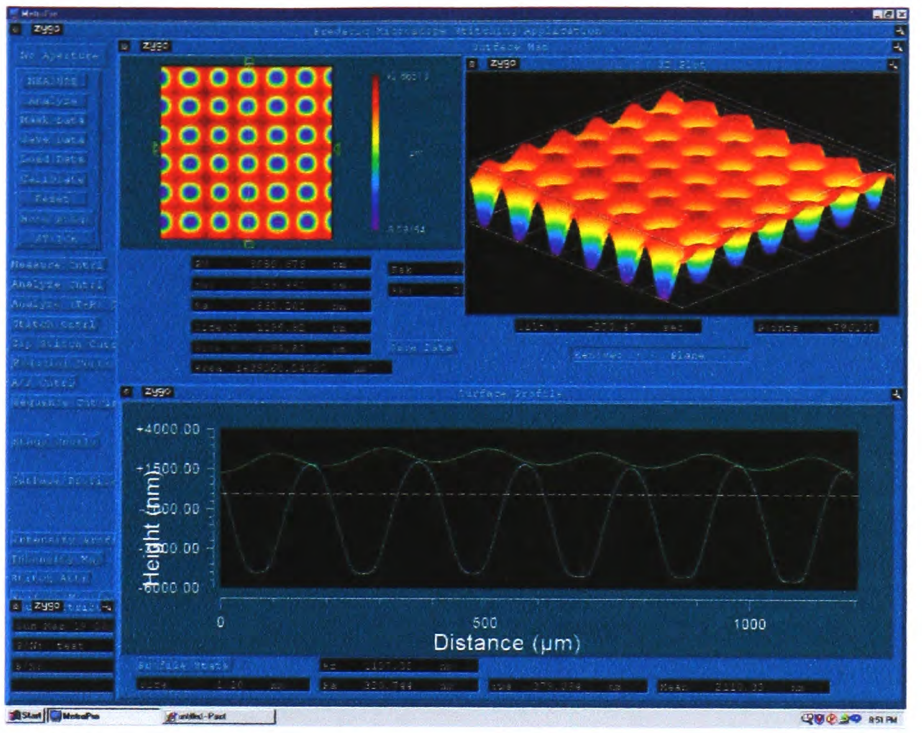

Figure 4.2: *Surface analysis of a "holes" surface performed with the ZYGO profilometre.*

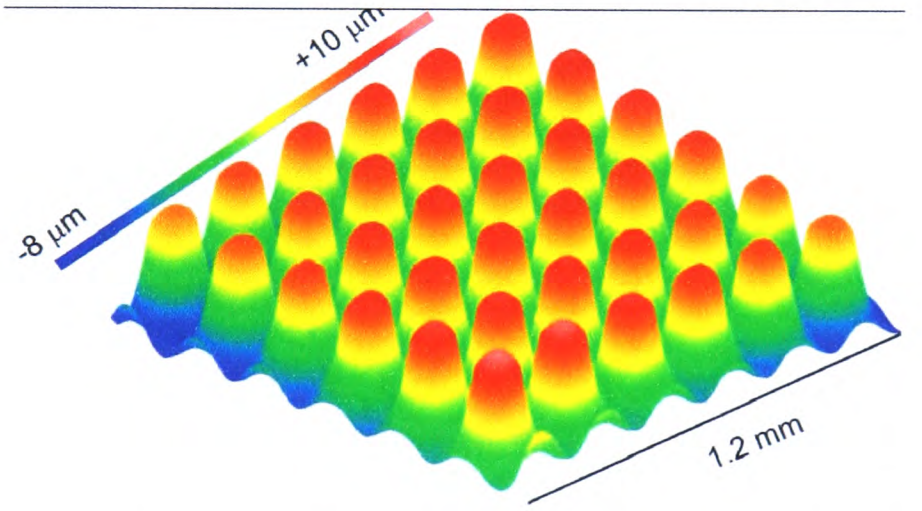

Figure 4.3: *Surface analysis of a "pillars" surface performed with the ZYGO profilometre.*

4.2 Results and analysis

Initially, the aim of this study was to investigate the influence of the evaporation rate on the receding contact angle value. As it was explained in the first two chapters, in the first stage of the evaporation process there is a diminution of the contact angle while the base radius remains constant. The value of the contact angle at the triple line depinning corresponds to the receding contact angle. To proceed, the experiments were performed in the environmental chamber where greater evaporation rates were achieved by reducing the ambient pressure. Unfortunately the experiment was unsuccessful. Because of the design of the environmental chamber (see details in section 3.2 page 59), the reduction of the ambient pressure had to be performed after the drop deposition. Hence the air trapped between the drop and the substrate (i.e the air trapped

into the holes) expanded with reduced pressure and deformed the drop.

Therefore it was decided to investigate the influence of the surface roughness on the advancing and receding contact angles by pumping out/in liquid from/into the drop. Basically, after the drop deposition the needle was introduced into the drop and the liquid was consistently injected/pumped out while the drop base diameter and the contact angle variations were recorded (see Figure 4.4).

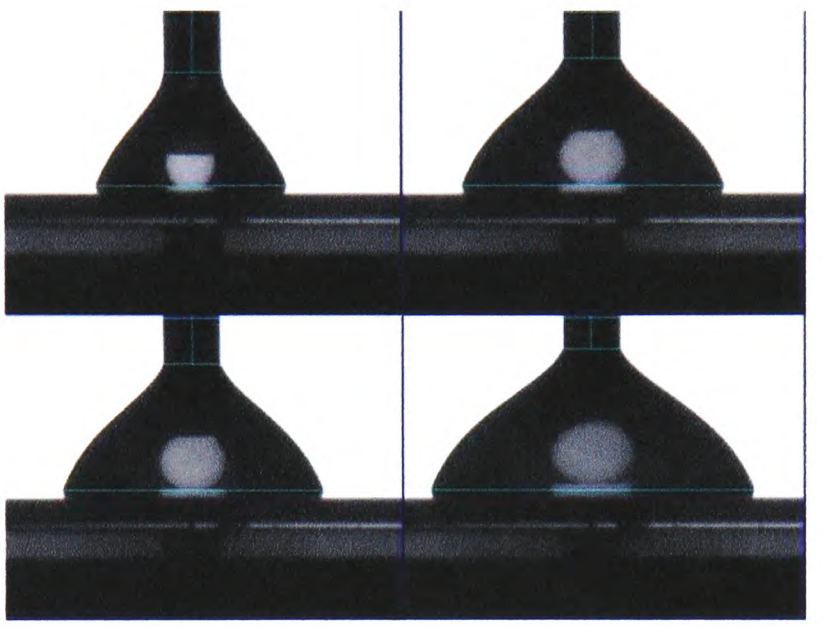

Figure 4.4: *Advancing contact angles.*

First, the advancing and receding contact angles measurements have been undertaken on the smooth substrate, see Figure 4.5. In the first part, the drop base diameter increases constantly, it corresponds to the advancing contact angle. Its value is pretty much constant, around 88 °. The obtention of consistent measurement of the receding contact angle was more challenging.

Then, the measurements have been undertaken on the the four different substrates (a), (b), (c) and (d) (see properties in Table 4.1). These contact angles evolutions are represented in Figures 4.6, 4.7, 4.8 and 4.9. On each Figure, the case corresponding to the fastest base line velocity is represented on the left graph while the slowest case is represented on the right graph.

Only in the case of the least deep holes (case (a) represented in Figure 4.6), the advancing contact angle doesn't seem affected by the structure of the substrate. It could also be seen on the evolution of the base diameter. For the case (a), the base diameter increases smoothly in comparison to the other three cases where the base diameter evolution is composed of multiple "steps". These steps correspond to a succession of triple line jump. Actually, the triple line is anchored by the surface defects and when the advancing contact angle reaches its maximum

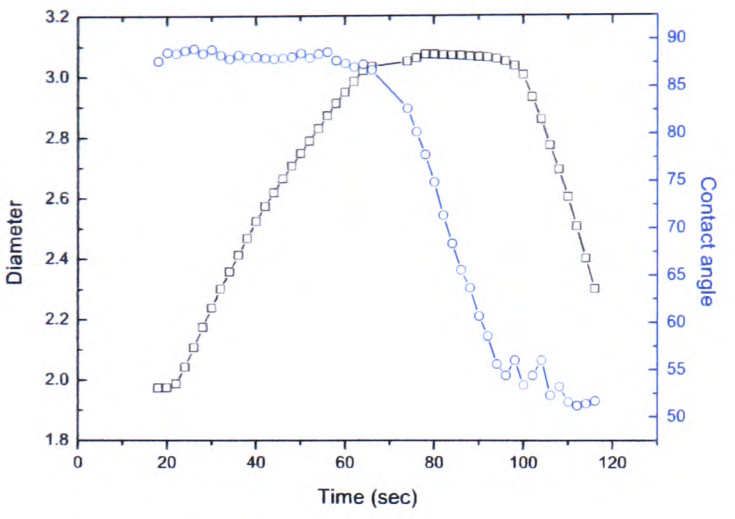

Figure 4.5: *Smooth sample covered with a photoresist: Evolution in time of the drop base diameter and contact angle. Base line velocity:* $0.71\ mm/min$.

value, the triple line "jump" to the next defect. As the jump is an instant phenomenon, the sudden increase of the base diameter corresponds to a decrease of the contact angle while when the triple line is pinned the contact angle increases. For each case, the values of the advancing contact angle are of the same order, between $80\,^{\circ}$ and $95\,^{\circ}$ and their behaviour are very similar. Over $4\ \mu m$ deep holes, increasing the depth doesn't seem to influence the contact angle. The velocity of the triple line seems to have little influence on the behaviour of the advancing contact angle. Only with the surface (b) (see Figure 4.7), the variation of the advancing contact angle changes with the velocity of the triple line. At the lowest velocity, the advancing contact angle and the base diameter behave similarly as a smooth surface: no variation of the advancing contact angle and no "steps".

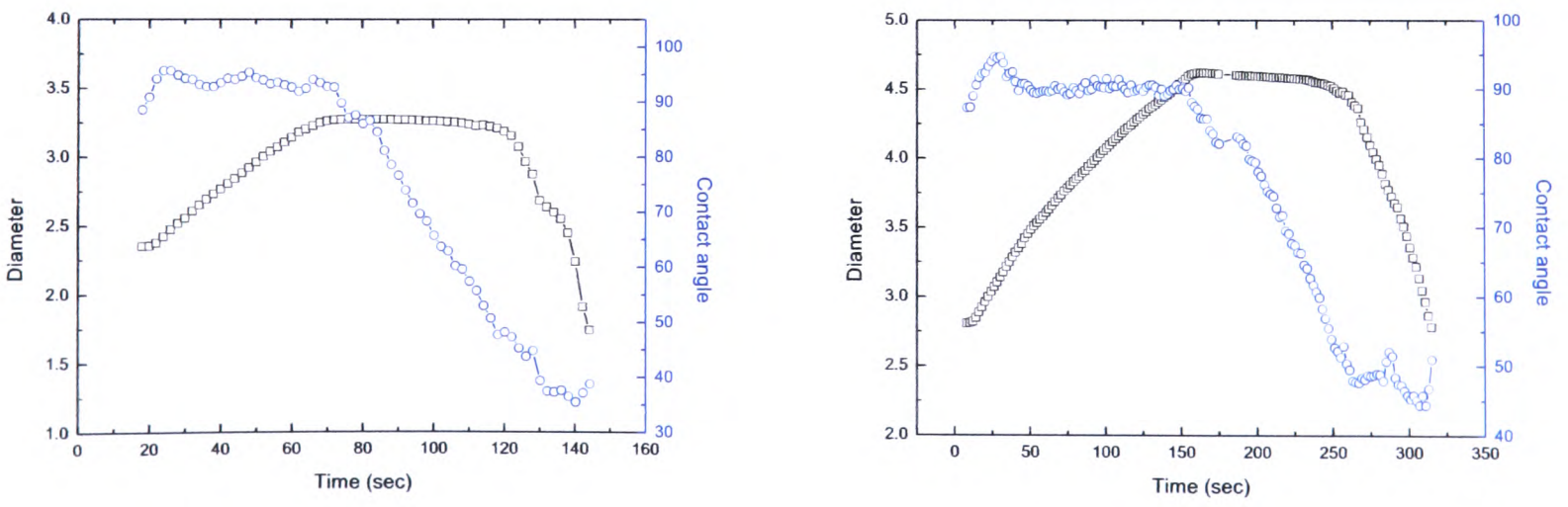

Figure 4.6: *Holes sample (a) (*$1.2\ \mu m$*): Evolution in time of the drop base diameter and contact angle. Base line velocity:* $0.56\ mm/min$ *(left) and* $0.37\ mm/min$ *(right).*

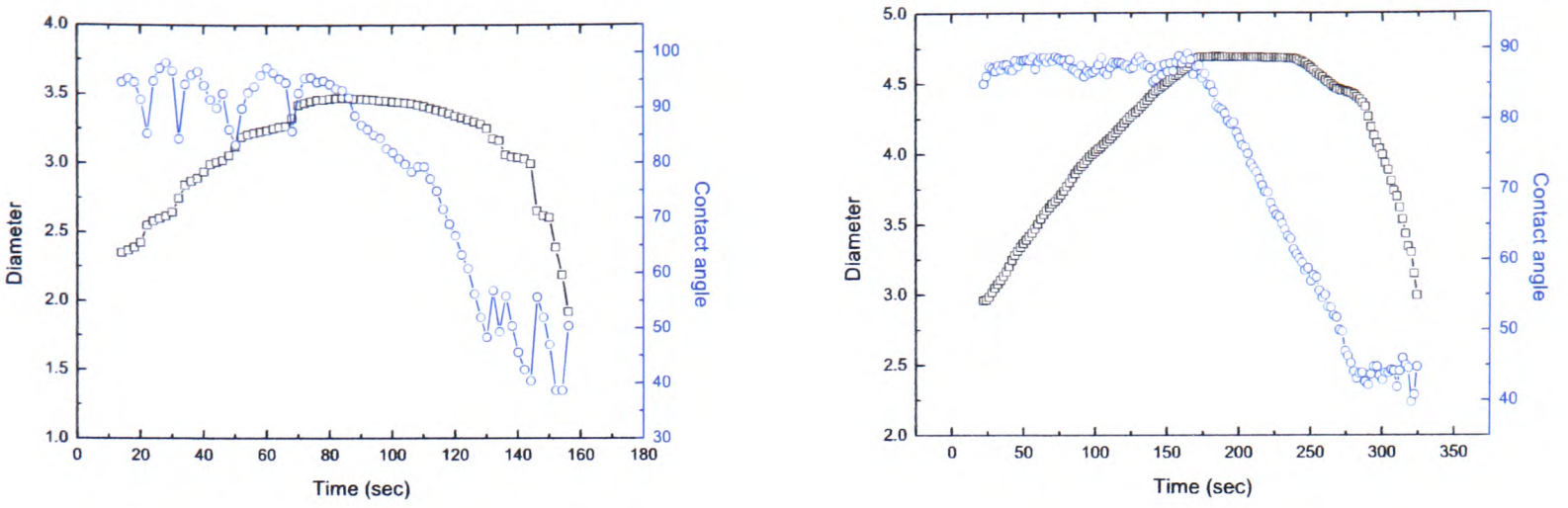

Figure 4.7: *Holes sample (b) (4 μm): Evolution in time of the drop base diameter and contact angle. Base line velocity:* $0.58\ mm/min$ *(left) and* $0.35\ mm/min$ *(right).*

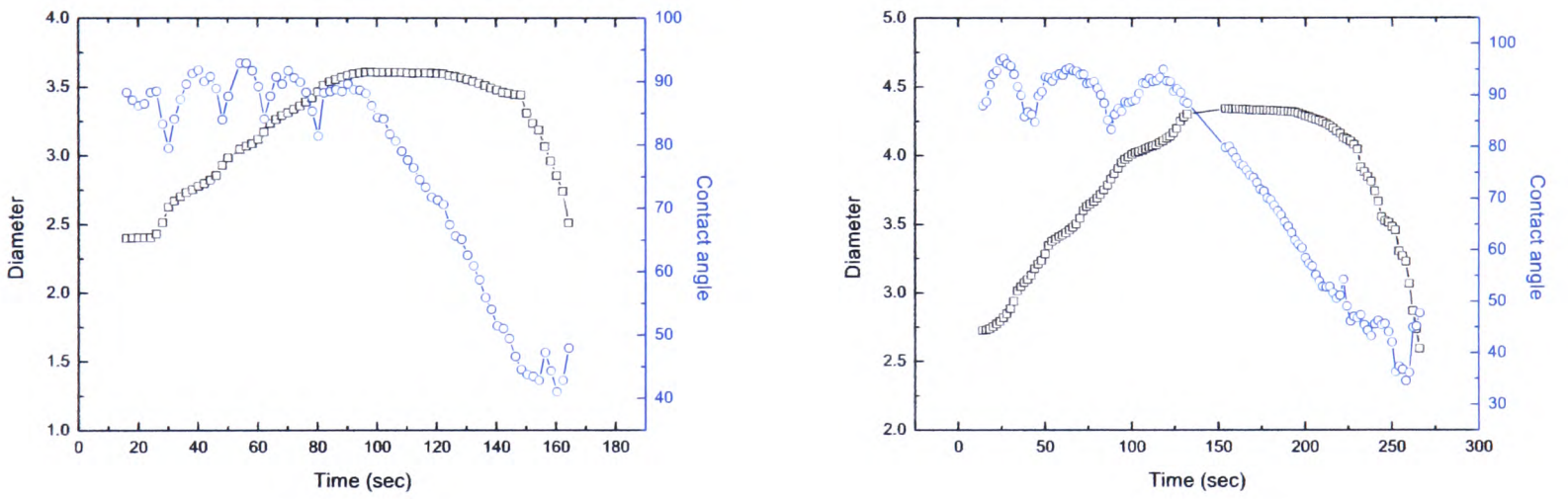

Figure 4.8: *Holes sample (c) (6 μm): Evolution in time of the drop base diameter and contact angle. Base line velocity:* $0.56\ mm/min$ *(left) and* $0.41\ mm/min$ *(right).*

With "pillars" substrates, the study has been focused only on the two extreme cases (a) and (d). First, the case of the smooth substrate is presented in Figure 4.10. The value of the advancing contact angle is much higher than in the case of "holes" substrates as PDMS is more hydrophobic than the photoresist, more than $30\,^{\circ}$ difference. Little fluctuations (no more than $4\,^{\circ}$) of the advancing contact angle are observed, it confirms that the substrate is relatively smooth. On the two other substrates and for each velocity, the advancing contact angle is strongly influenced by the patterned surface. As with "holes" substrates, the evolution of the base diameter is divided into a succession of "steps" while the advancing contact angle oscillates. In all cases, the advancing contact angle fluctuate between $116\,^{\circ}$ and $128\,^{\circ}$, it means that the height of the pillars and the velocity of the triple line have no noticeable influence on its value. This is different

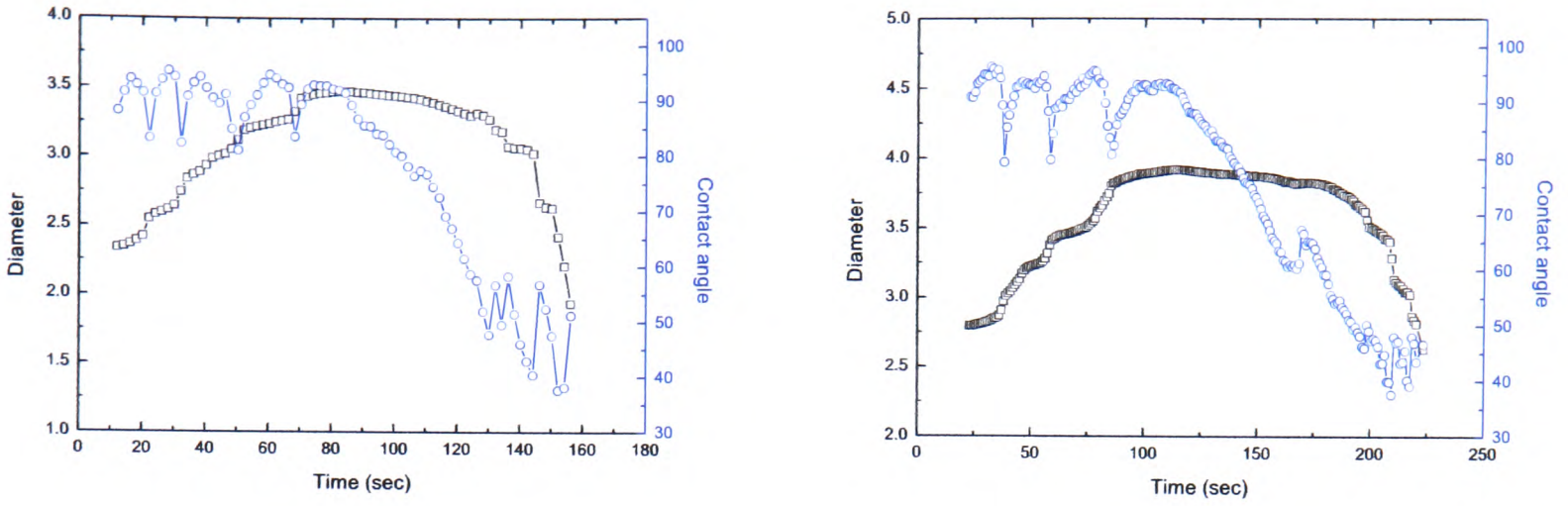

Figure 4.9: *Holes sample (d) (*$11\ \mu m$*): Evolution in time of the drop base diameter and contact angle. Base line velocity:* $0.55\ mm/min$ *(left) and* $0.51\ mm/min$ *(right).*

from the holes substrates.

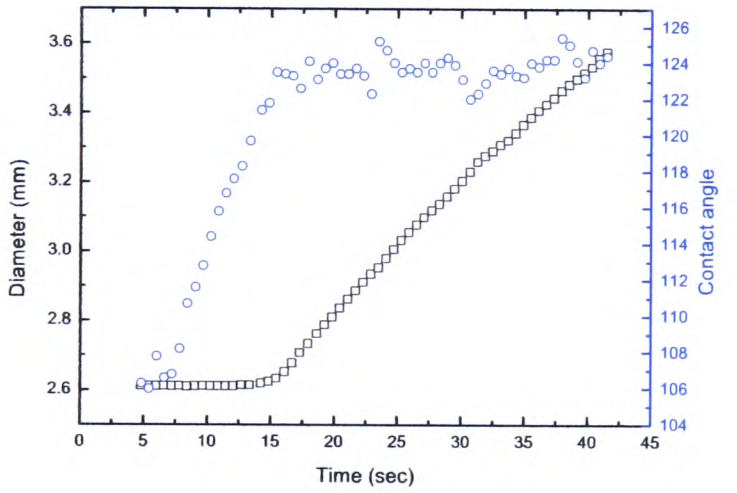

Figure 4.10: *Smooth sample covered with PDMS: Evolution in time of the drop base diameter and contact angle. Base line velocity:* $1.03\ mm/min$.

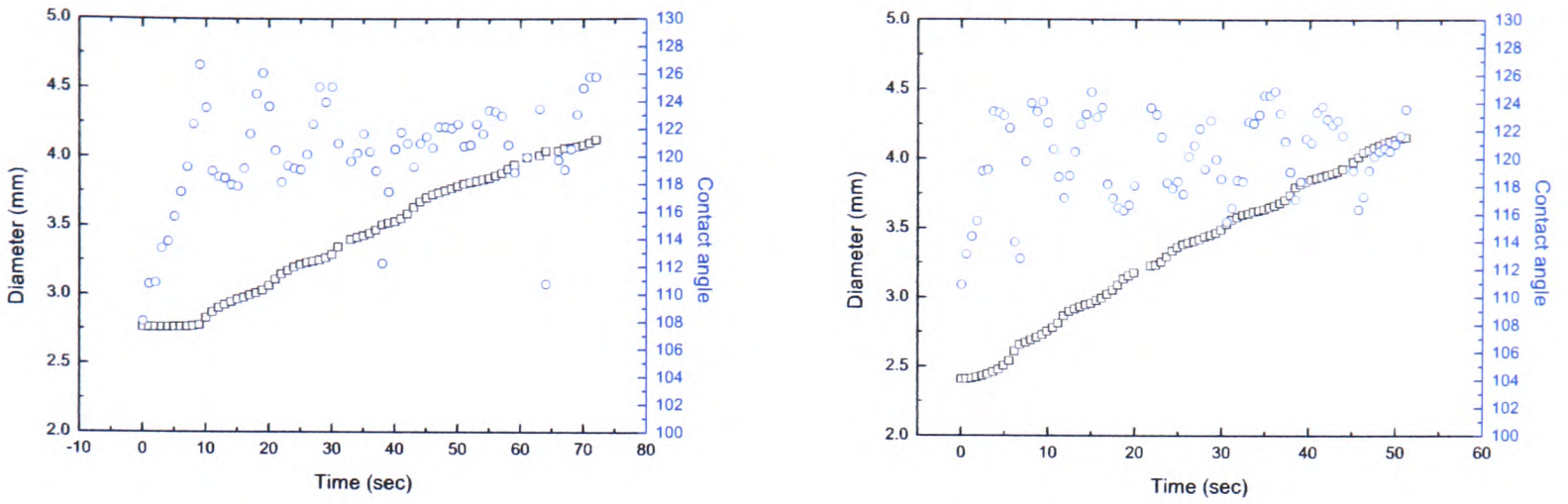

Figure 4.11: *Pillars sample (a) (*$1.2\ \mu m$*): Evolution in time of the drop base diameter and contact angle. Base line velocity:* $0.63\ mm/min$ *(left) and* $1.06\ mm/min$ *(right).*

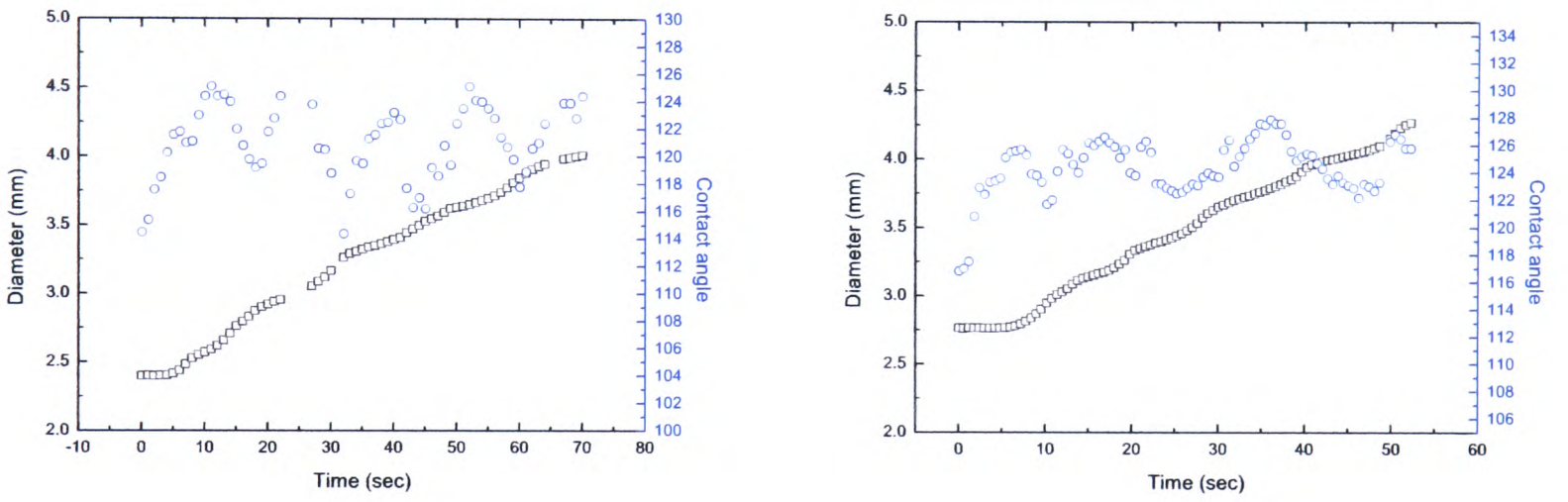

Figure 4.12: *Pillars sample (d) (*$11\ \mu m$*): Evolution in time of the drop base diameter and contact angle. Base line velocity:* $0.74\ mm/min$ *(left) and* $1.1\ mm/min$ *(right).*

4.3 Conclusion

The pinning/depinning phenomenon of the contact line of a Water drop on two kinds of substrates ("holes" and "pillars") was investigated to elucidate the role played by roughness on the dynamics of moving contact lines. The evolution of the advancing/receding contact angle while the drop base diameter increases/decreases suggests that the competition between the unbalanced Young force ($\gamma_{water}(\theta_{adv} - \theta_{eq})$) and the anchoring forces of the defects may be dominating the pinning/depinning process. While noticeable stick-slip behaviour of the contact line was observed for "holes" substrates with larger defects (deeper holes), the pillars height doesn't seem to have any influence in the range studied. As the "holes" and "pillars" substrates

have been made by two different materials, photoresist and PDMS, it's difficult to compare the holes structure to the pillars structure.

Chapter 5
Evaporating binary mixture drops

5.1 Introduction

The wetting behaviour of evaporating pure liquids has been extensively investigated by numerous authors. On the contrary many issues related to binary systems remain to be elucidated. Indeed multicomponent droplets are present in several industrial applications, such as crop-dusting where the wettability and the evaporation of herbicides on targeted surfaces is crucial. In cooling technologies binary systems are also frequently encountered when using binary refrigerants as cooling fluids. The understanding of wettability associated with phase change behaviour is essential for these applications.

In this chapter we present the results of an experimental investigation of binary drops by using Methanol-Water and DMSO-Water drops deposited on a smooth silicon substrate with Nitrogen as the ambient gas. For each mixture, three different compositions have been prepared. First, details on the choice of the studied liquids and their preparation are given. Then the experimental results are presented and analysed before being discussed.

5.2 Materials and procedure

5.2.1 Liquids

Two mixtures have been prepared, namely Water-Methanol and Water-DMSO. These mixtures were chosen based on the surface tension and volatility. On Figure 5.1, it can be seen that Water has the highest surface tension, 72 mN/m, then DMSO, 43 mN/m, and finally Methanol, 25 mN/m. For Water-Methanol mixtures, Methanol is the more volatile component and in the case Water-DMSO mixture Water is the more volatile component. It means that in Water-Methanol mixtures the component the more volatile has the lowest surface tension whereas in the case of Water-DMSO mixtures it is the opposite case. For each case, three concentrations have been prepared: Water-Methanol mixtures with mass to mass concentrations of 10%, 50%

and 80% and Water-DMSO mixtures with mass to mass concentrations of 20%, 50% and 80%. The lowest concentrations differ because of the surface tension variation with Methanol (or DMSO) fraction. On Figure 5.1, it can be seen that the surface tension variation is larger at low concentration with Methanol than with DMSO in the mixture. Ultra pure deionised Water (milliQ) was supplied by the laboratory facilities and DMSO and absolute Methanol 99.8% were purchased from Fisher Scientific. The mixtures were prepared before running each experiment in order to keep the composition unchanged. A microbalance (Mettler Toledo XS205) was used for the preparation of the binary mixtures. A small container (10 mL) was placed on the balance plate and the amount (depending on the concentration) of Water/Methanol/DMSO was added with a micropipette.

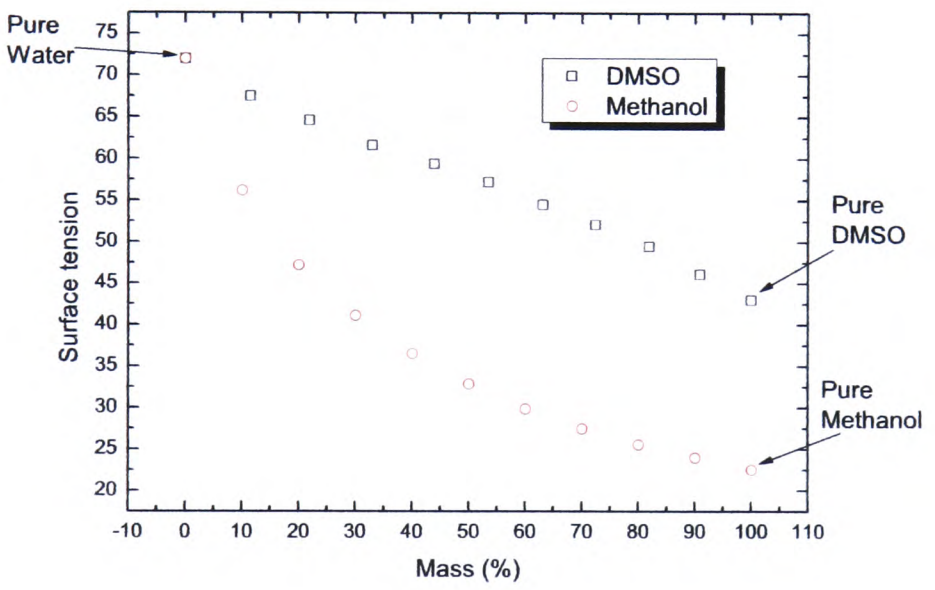

Figure 5.1: *Evolution of the surface tension with mass concentration for Water-Methanol and Water-DMSO mixtures.*

5.2.2 Substrates

For these specific experiments a smooth substrate where no pinning of the contact line occurs is desirable. Due to its very smooth surface, a silicon wafer has been chosen (see details on Figure 5.2). The wafer was precisely cut in 10 mm squares at the Scottish Microelectronics Centre (SMC[1]) to produce identical samples for the experiment. As the silicon has a quite high surface energy (it is completely wet by most liquids), it was decided to coat all the samples with a very thin layer of PDMS (Polydimethylsiloxane) to obtain measurable wetting angles. This

[1] centre part of the University of Edinburgh

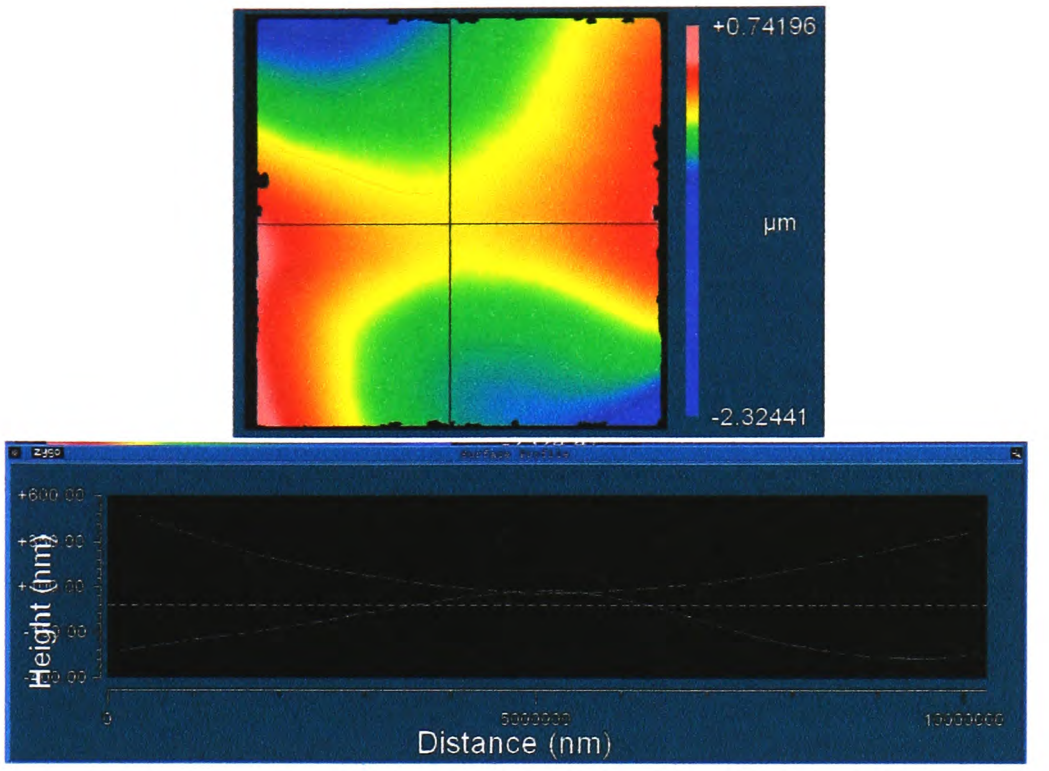

Figure 5.2: *ZYGO analysis of silicon sample coated with a thin layer of PDMS.*

operation does not modify the surface roughness of the silicon. The deposition was done in our institute by Dr Frédéric Madani-Grasset. Firstly, the silicon wafer was cleaned using a piranha solution (mixture composed by one third of H_2O_2 and two thirds of H_2SO_4) to remove any organic products, and then rinsed with a generous amount of deionised water. Secondly, the cleaned silicon samples were immersed in the polymer solution and placed in a vacuum oven (temperature at $110°C$) for 24 hours. Finally, the samples were immersed in Toluene in order to remove the PDMS in excess and leave only a very thin layer of Polymer (the Toluene is a very good solvent of PDMS thus only the closest molecules, strongly anchored to the solid surface, are left). The substrate obtained is still very smooth but with a very low surface energy. On Figure 5.2 the surface profile analysis done by profilometry (ZYGO) is shown. It shows that the silicon wafer surface is slightly curved but very smooth. Before running each experiment, the samples were cleaned following the usual process (see details in sections 3.6.1).

5.2.3 Procedure

For all experiments, the drops were placed inside the "low pressure" chamber. It allows a better control of the external conditions (gas, pressure and temperature) and the possibility of saturation of the atmosphere by one of the two components (see explanation in section 3.2 page 59). To eliminate the influence of humidity, the chamber was filled with Nitrogen. The ambient temperature was maintained at $23°C$ and the pressure at $1000\ mbar$.

The evaporation and wetting of drops made of the prepared mixtures under the above described experimental conditions were systematically investigated.

5.3 Experimental results

First the results obtained for Water-Methanol mixtures are presented. They are divided in three parts:

- free evaporation in pure Nitrogen at atmospheric pressure
- free evaporation within an atmosphere saturated by Water vapour
- free evaporation in pure Nitrogen at lower pressures

Then the study of Water-DMSO mixtures is presented. This latter is only performed in a pure Nitrogen environment at atmospheric pressure.

5.3.1 Water-Methanol

Non saturated atmosphere

As it was introduced in the "Theory Chapter" (section 1.5 page 11), the wettability of a drop (which corresponds to the apparent contact angle) is a function of its surface tension. It means that in the case of binary drop mixtures where the surface tension will change with the composition, the initial contact angle, $\theta_{initial}$, will also differ. Water and Methanol have actually been chosen for their great difference in surface tension, this leads to a large range of $\theta_{initial}$ over the mixture composition. On Figure 5.3, pictures of the drops in their initial state are presented for the two pure components and three concentrations (10%, 50% and 80% fraction in Methanol). It shows a large variation of θ_{app} between each mixture composition. These contact angles measurements versus Methanol concentration are plotted on Figure 5.4. The θ_{app} values for the three fractions of Methanol: (10%, $\theta = 95°$), (50%, $\theta = 72°$) and (80%, $\theta = 60°$) are encompassed by the values of the two pure components, 105° for pure Water drops and 35° for pure Methanol drops. As the surface tension is an interfacial property, this suggests that the composition near the interface is similar to the bulk. As mentioned in Yu *et al.* [11], the plot of the initial contact angle against the drop mixture concentration may serve as a chart to estimate the concentration from contact angle measurements.

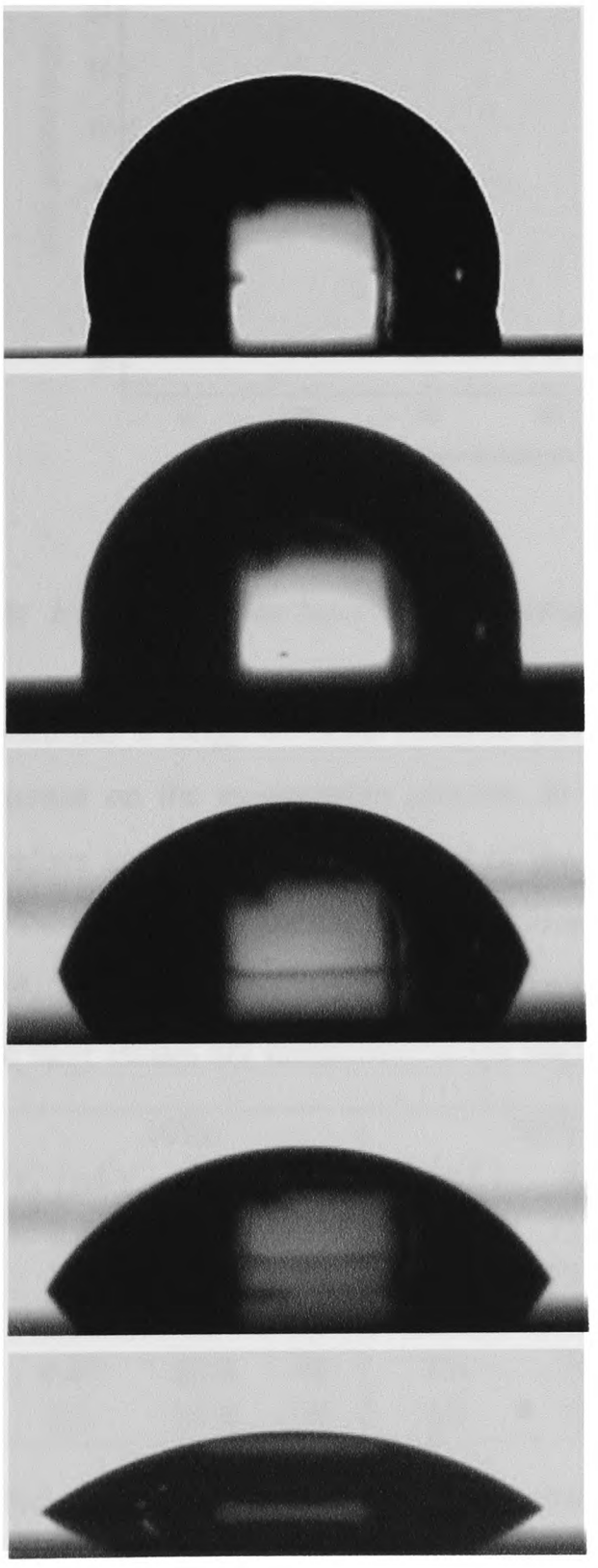

Figure 5.3: *Example of initial sessile drop profile at different water-methanol concentration*

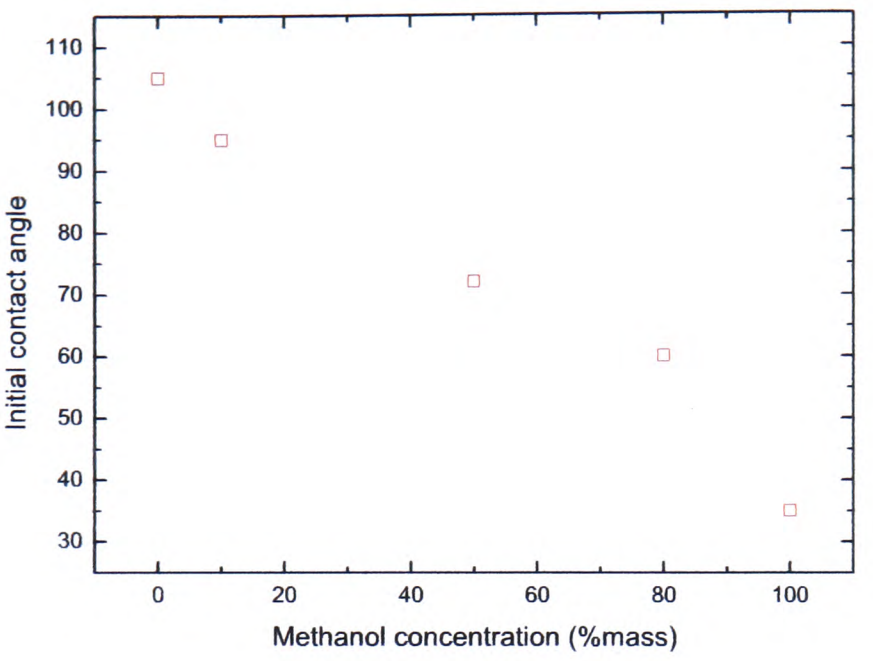

Figure 5.4: *Evolution of the binary mixture Water-Methanol initial contact angle.*

For each concentration a range of drop volumes has been investigated to show if the drop size has an influence on the evaporation process, in particular on the initial and maximum contact angles values and on the general trend of the volume and base diameter. These data are presented in Table 5.1 where for each concentration the values of the initials and maximum contact angles ($\theta_{initial}$ and θ_{max}) are given for five different initial volumes ($V_{initial}$). The results show that their values are insensitive to the initial volume $V_{initial}$.

	10%			50%			80%		
	V_i (μL)	θ_i	θ_m	V_i (μL)	θ_i	θ_m	V_i (μL)	θ_i	θ_m
test 1	2.8	94.7	98.5	4.1	73.8	80.5	5	59	72
test 2	3.3	94.3	99	2.42	73.1	82	2.41	60.2	70
test 3	4.05	95	98	2.63	74.3	80	2.26	59.3	73
test 4	4.47	95.8	98	3.6	75	81	3.54	59.2	70
test 5	5.3	95.2	99	4.9	74	80	4.28	58.7	72

Table 5.1: *Values for the initial and maximum contact angles for various drop volumes*

At the difference of Yu *et al.* [11] and Rowan *et al.* [9] works where they compared drops with identical initial volumes, it was decided to study drops with identical initials base radii, see Figure 5.5 page 81. The reason is that the evaporation rate is proportional to the drop base radius. From all investigated data, the closest initial base diameters have been chosen, studied and presented below.

On Figure 5.5, the evolution in time of the volume, base diameter and apparent contact angle are shown for the three mixtures and the two pure components. The data show the large differences in lifetime for each composition. A drop of pure water takes around 40 minutes to evaporate, while a drop of pure methanol takes 100 seconds. It was thus decided to present the data mixtures on three sets of graphs: $(D(t), \theta(t))$ on Figure 5.6, $(V(t), D(t))$ on Figure 5.7 and $(V(t), \theta(t))$ on Figure 5.8.

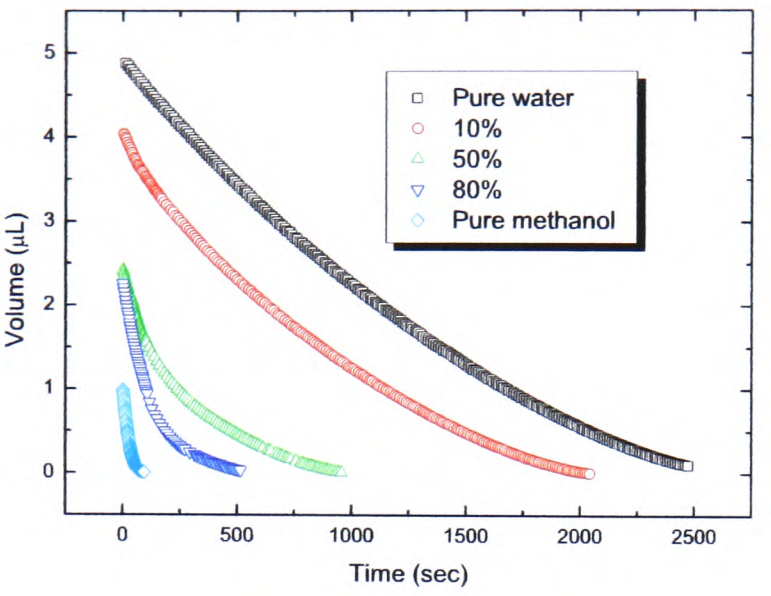

(a)

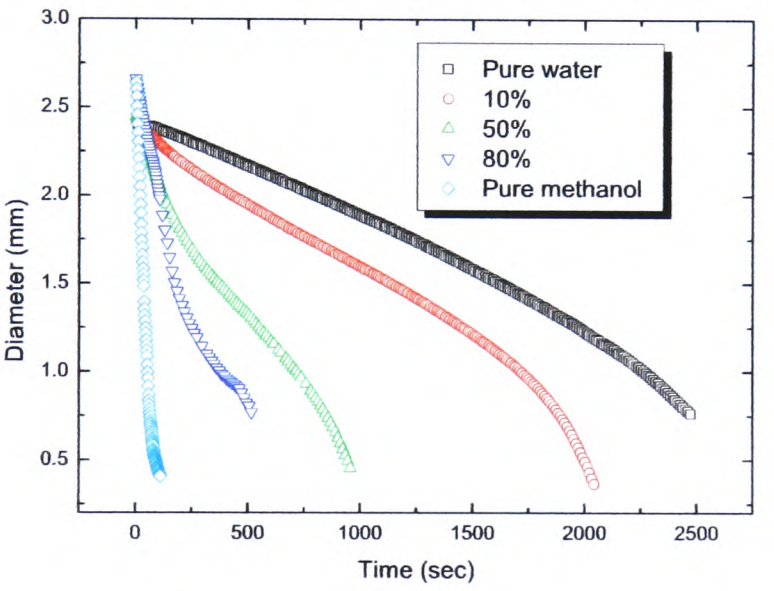

(b)

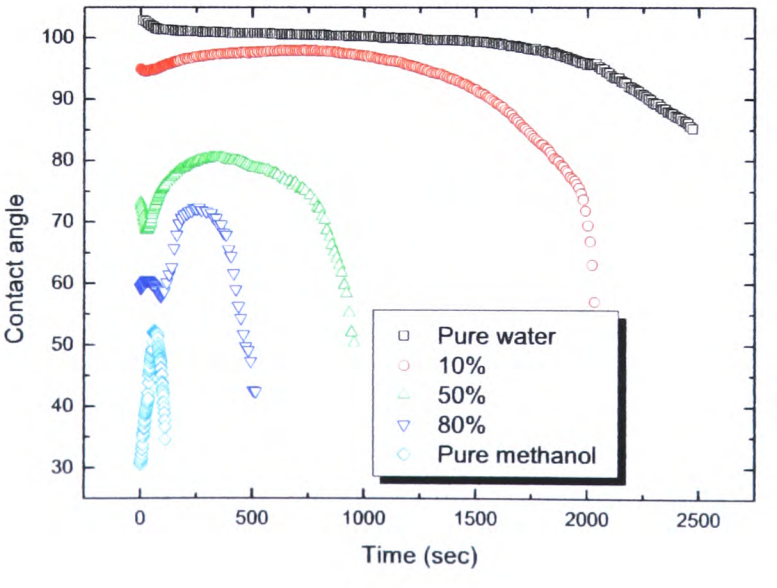

(c)

Figure 5.5: *Evolution in time of the volume (a), contact diameter (b) and contact angle (c) for the three concentrations and the two pure components*

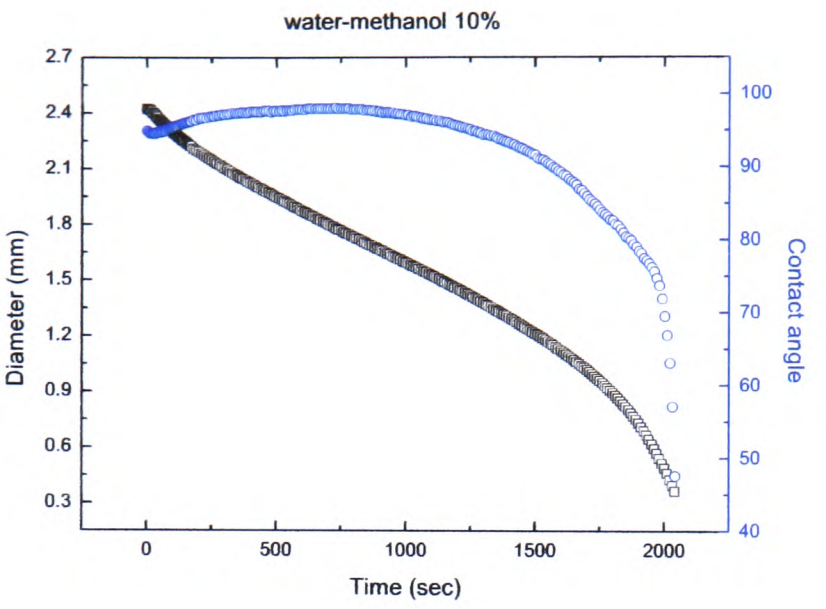

(a)

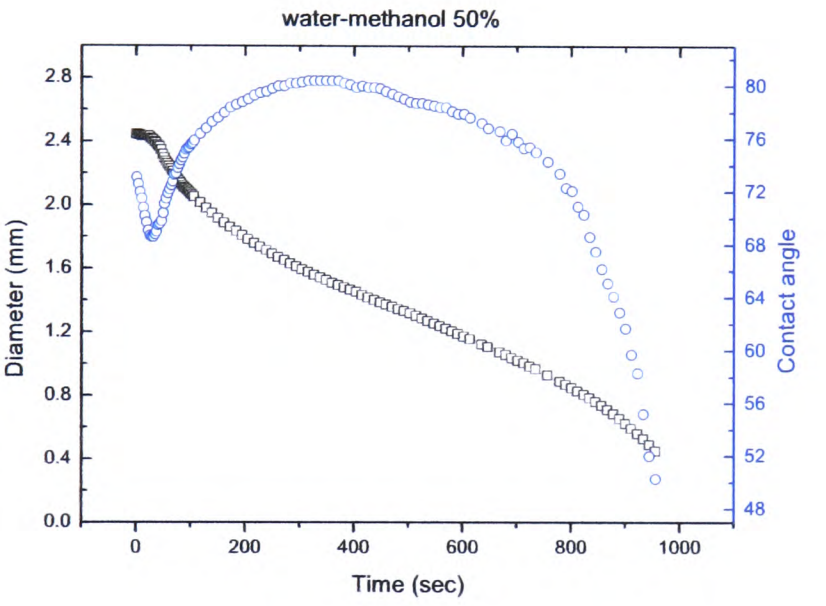

(b)

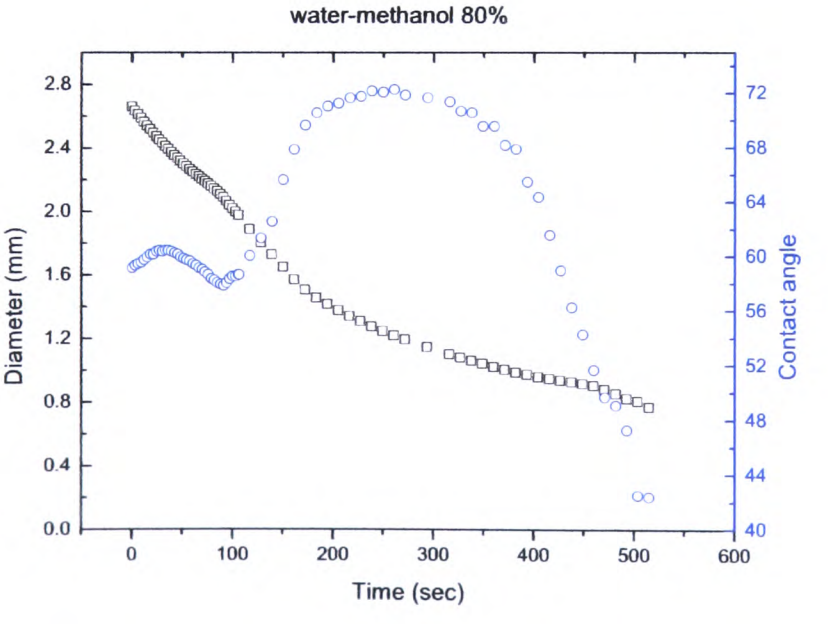

(c)

Figure 5.6: *Evolution in time of the base diameter and contact angle for thee three Water-Methanol mixtures (*10% *(a),* 50% *(b) and* 80% *(c)).*

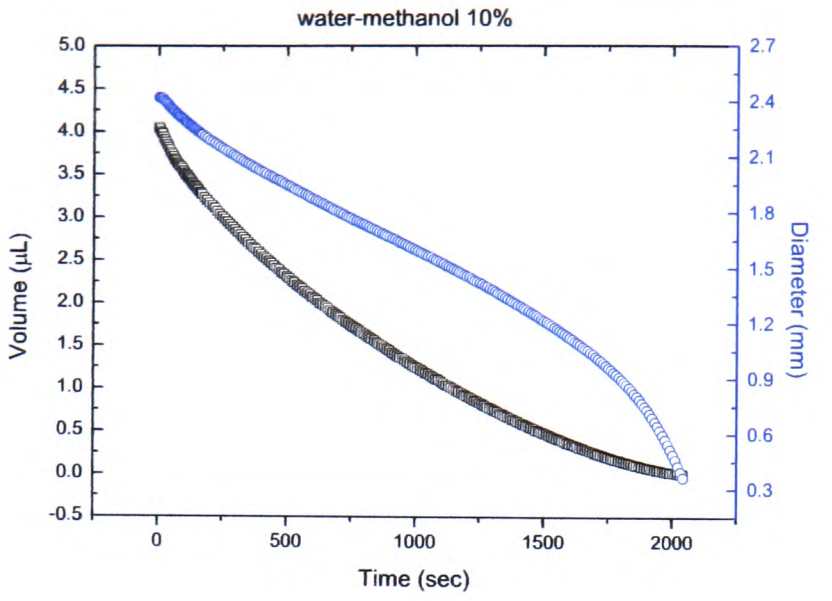

(a)

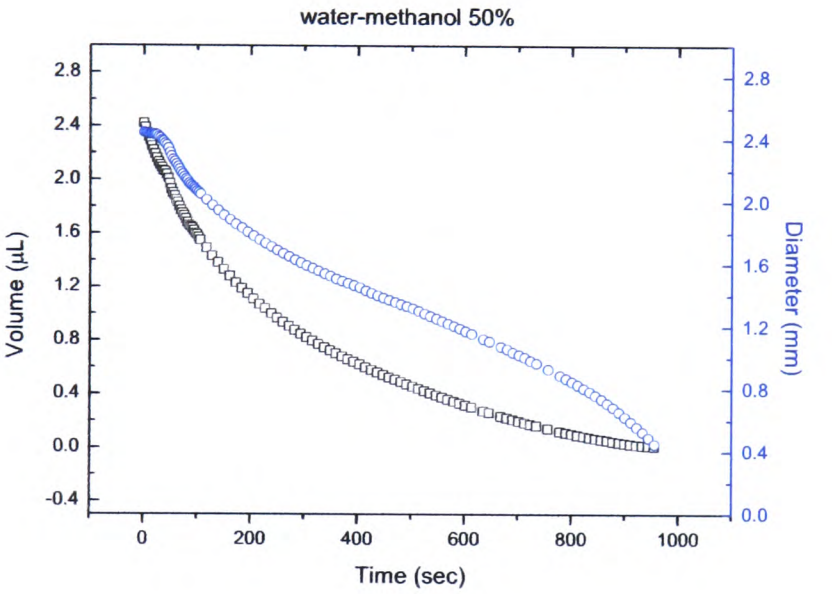

(b)

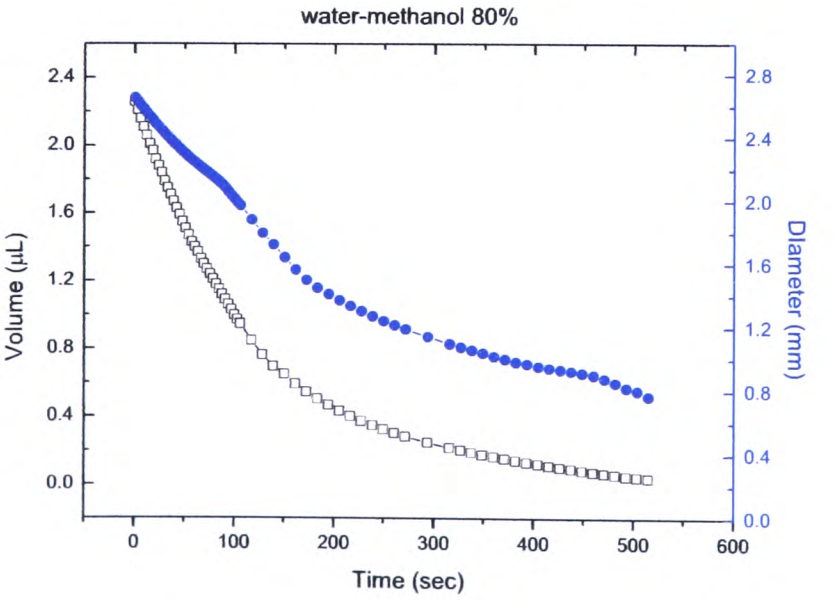

(c)

Figure 5.7: *Evolution in time of the volume and base diameter for the three Water-Methanol mixtures (*10% *(a),* 50% *(b) and* 80% *(c)).*

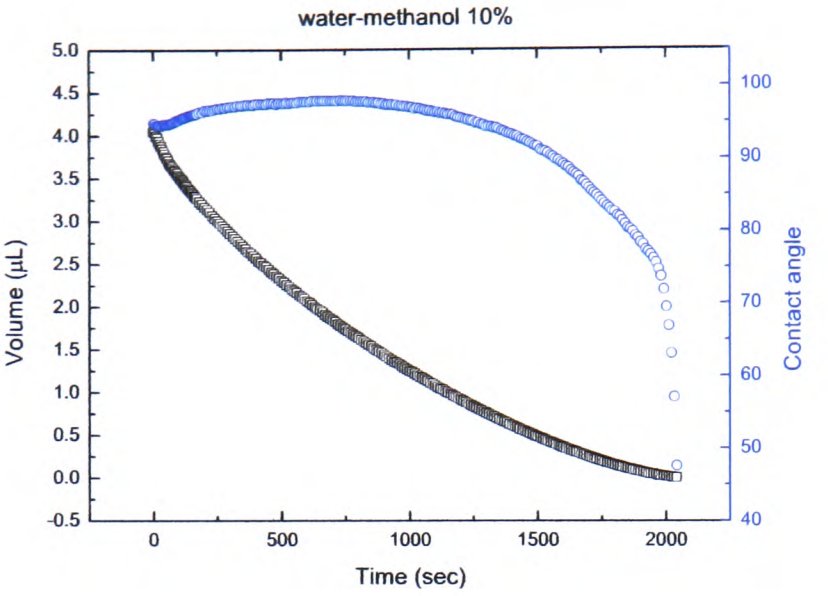

(a)

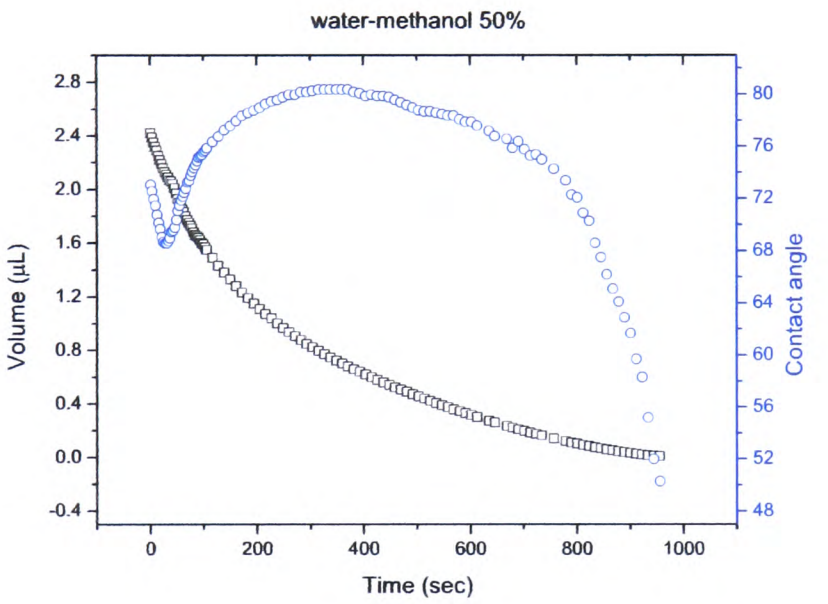

(b)

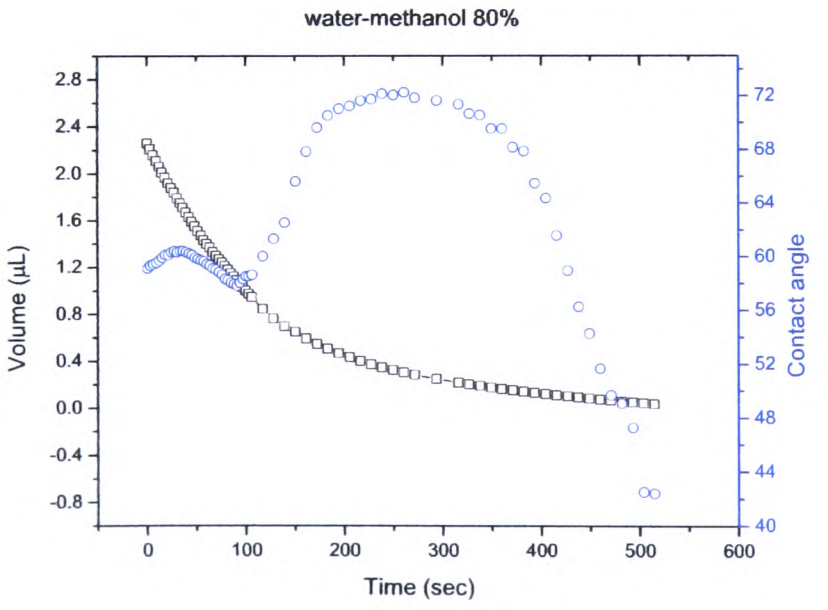

(c)

Figure 5.8: *Evolution in time of the volume and contact angle for the three Water-Methanol mixtures (*10% *(a),* 50% *(b) and* 80% *(c)).*

The plot of the volume against the time (see Figures 5.5, 5.7 and 5.8) shows a rapid evaporation at the beginning with a slow decrease until the drop disappears. To get a better comparison of the volume evolution for each concentration, it has been normalized (by its initial value) and plotted against the normalized time on Figure 5.9. This representation indicates that the evaporation rate is greater for higher initial fraction of Methanol. If we look at the evolution of the base diameter D on either Figure 5.6 or Figure 5.7, D is only constant in the first ten seconds. It means that the triple line is pinned at the very beginning and recedes continuously then after. It confirms that the silicon substrates surfaces are very smooth indeed. From the three parameters investigated here, the behaviour of the contact angle θ is the most characteristic. Through the whole evaporation process the general trends are quite similar, they could be divided into three stages. The first stage ends when θ starts its rise towards its maximum value. For a low concentration in Methanol (10%), this stage lasts for ten seconds while θ is almost constant (slight decreases by half a degree only). For an equal fraction in mass of Water and Methanol, θ decreases rapidly (over $25\ s$) by 5 degrees. For the highest concentration in Methanol θ increases and then decreases slightly in the first $50\ s$. The last two stages are similar in each case. In the second stage, θ tends to its maximum value before the drop shrinks and θ tends to zero in the last stage.

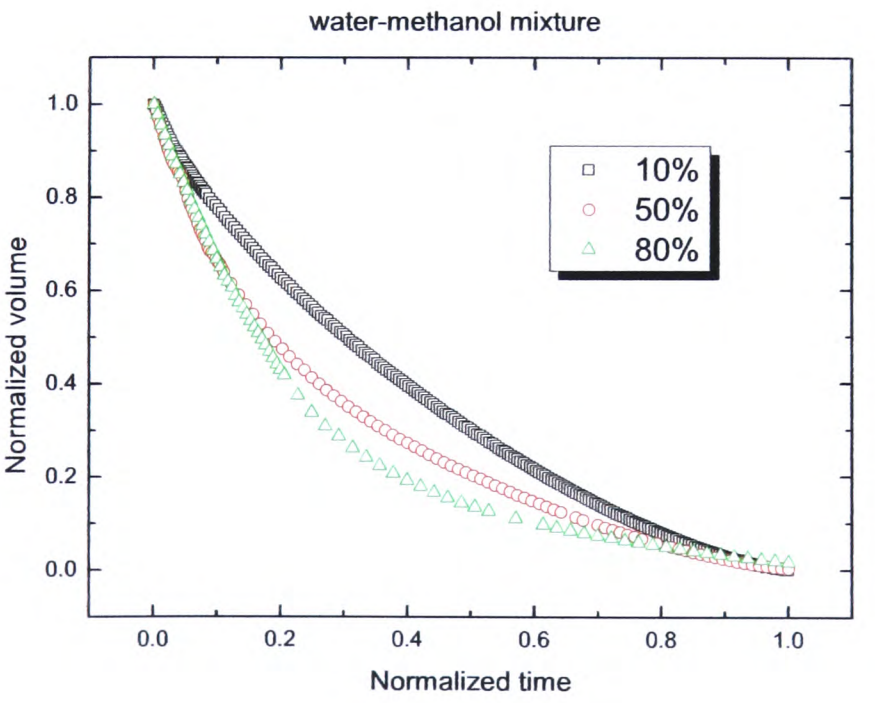

Figure 5.9: *Normalized volumes plotted against normalized times for the three Water-Methanol mixtures.*

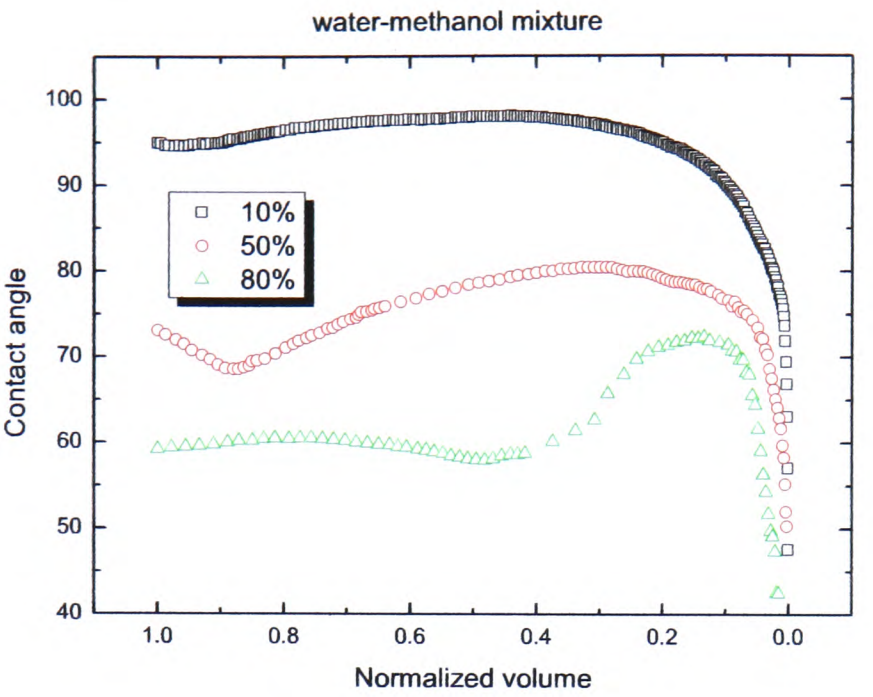

Figure 5.10: *Drops contact angles plotted against the normalized volume for the three Water-Methanol mixtures.*

As it is observed on Figure 5.6 and pointed out on Table 5.1, θ_{max} decreases with the initial concentration of Methanol. It follows the values of the initial contact angle which are function of the drop initial composition. On Figure 5.10, the contact angle is now plotted against the normalized volume. This representation indicates that θ_{max} is reached at different periods of the drop volume evolution. For low concentration the maximum corresponds for almost half of the drop evaporated volume, 70% for the medium concentration and 85% for the highest concentration. This result is expectable if one can imagine that θ_{max} corresponds to a stage where all the Methanol is evaporated and only Water remains. It means that for a lower concentration in Methanol θ_{max} corresponds to a higher fraction of the initial drop volume. This argument could also lead to the conclusion that θ_{max} should be the same as the drop is composed of pure Water only. But this is actually not the case as it was shown above. This result is also in contradiction with previous studies, Yu *et al.* [11] and Rowan *et al.* [9]. In order to investigate these trends, further experiments have been realised with an atmosphere saturated in Water vapour. In this situation only Methanol is forced to evaporate from the mixture.

Saturated atmosphere

As explained in the Experimental Chapter (section 3.2, page 59), the saturation is obtained by placing a small reservoir of Water inside the "low pressure chamber". The experiments were run until equilibrium was clearly established. By equilibrium we mean that the evaporation process stops, i.e all the parameters (θ, D and V) are constants in time. The three parameters (θ, D and V) are plotted against time on two graphs. These results are represented on Figure 5.11 ($D(t)$, $V(t)$) and on Figure 5.12 ($\theta(t)$, $D(t)$). The first Figure shows that the behaviour of the volume, $V(t)$, and the diameter, $D(t)$, are similar for each composition, they decrease towards an asymptotic value which confirms that the evaporation process stops after a while. On Figure 5.12, it is observed, like in the precedent case, that the behaviour of θ at the early times differs for each composition. At low Methanol concentration (10%), θ rises continuously from its initial value to equilibrium θ_{eq}. At 50% the behaviour is very similar to the non saturated case with a few degrees drop before rising to θ_{eq}. And for the highest concentration, θ increases to a maximum before reaching its equilibrium value few degrees below.

From Table 5.2, we can see that, as in the absence of saturation, the initials contact angles, θ_i, and the equilibrium contact angles, θ_{eq}, do not depend on $V_{initial}$. It is aslo important to notice that the equilibrium contact angles, θ_{eq}, also differ for each composition. It varies from 101° at the highest concentration, 10%, to $86 - 87°$ at 50% and 78° at the lowest concentration, 10%. Now if we look at the two Tables 5.1 (page 79) and 5.2, two mains observations emerge.

	10%			50%			80%		
	V_i (μL)	θ_i	θ_m	V_i (μL)	θ_i	θ_m	V_i (μL)	θ_i	θ_m
test 1	1.67	95.8	102	4.4	76	88	7	58	77
test 2	3.26	94.7	101	3.6	75.3	89.2	4.8	58	78.5
test 3	4.72	94.5	100	5.8	74	87.5	5.4	55.5	79
test 4	5.01	95	101	3	75.7	90	3.2	59	78
test 5	6.16	95.2	102	6.8	75	88	7.5	60	79

Table 5.2: *Values for the initial and maximum contact angles for various drop volumes*

First, the values of the initials contact angles, θ_i, are similar for the two cases. This suggests that the presence of a saturated atmosphere doesn't affect the wettability of the drops and the saturation might only play a role in the evaporation process i.e. in the evolution of the drops profiles. Secondly, the values of the equilibrium contact angles, θ_{eq}, in the case of a saturated atmosphere are greater than the values of the maximum contact angles obtained in the absence of saturation.

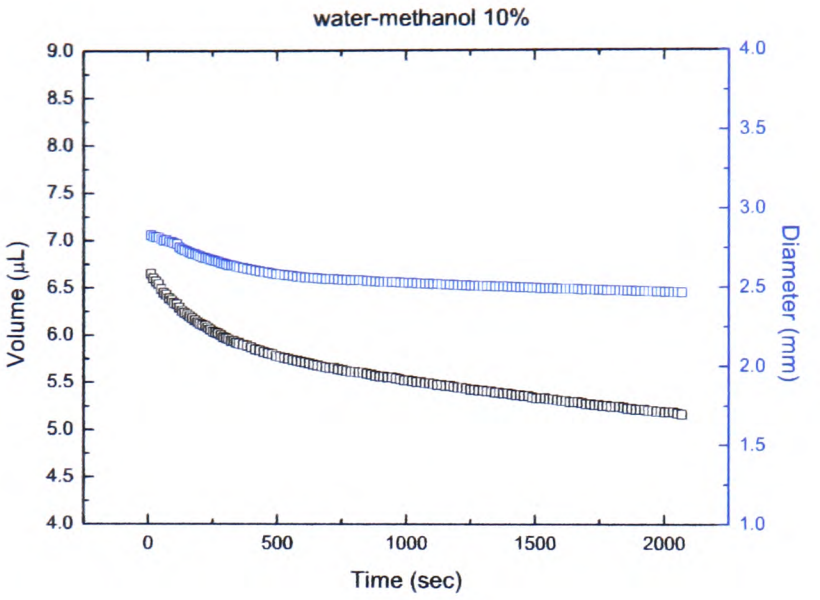

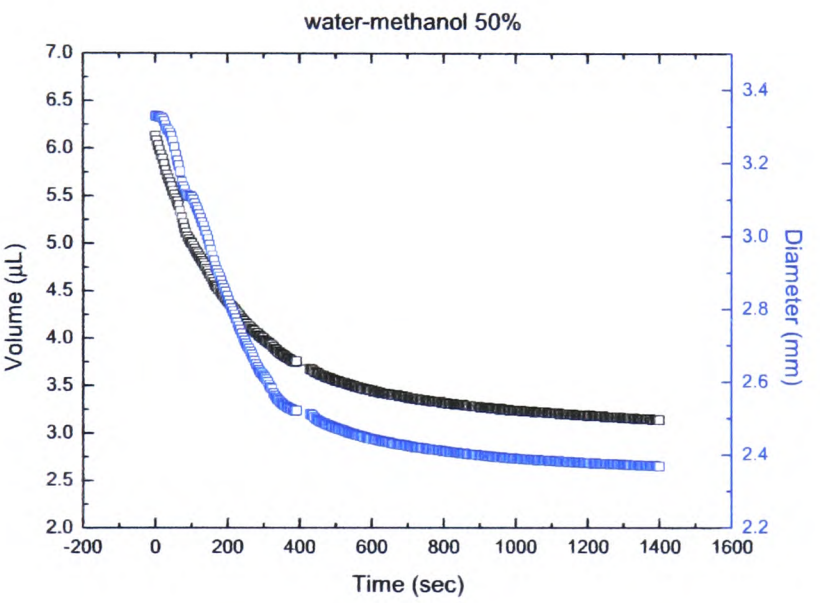

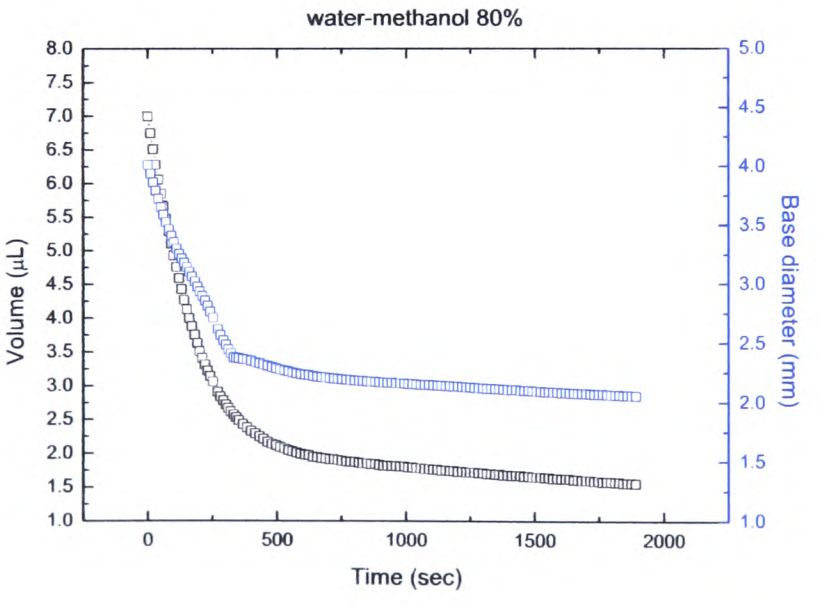

Figure 5.11: *Evolution in time of the volume and base diameter for the three Water-Methanol mixtures in an atmosphere saturated in Water vapour (*10% *(a),* 50% *(b) and* 80% *(c)).*

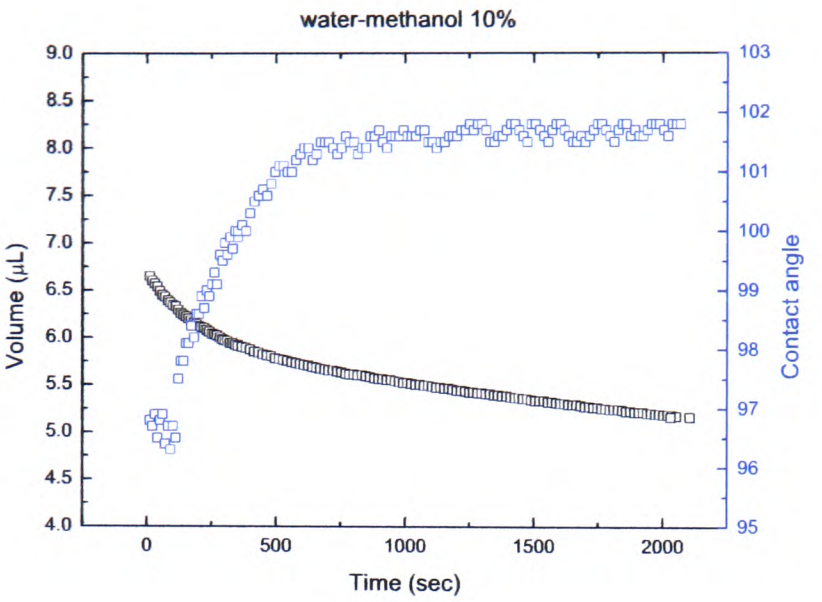

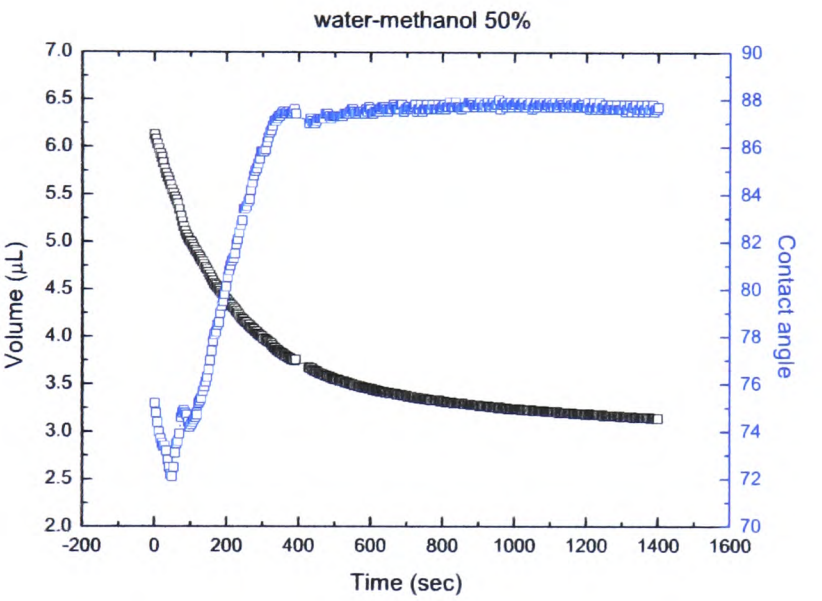

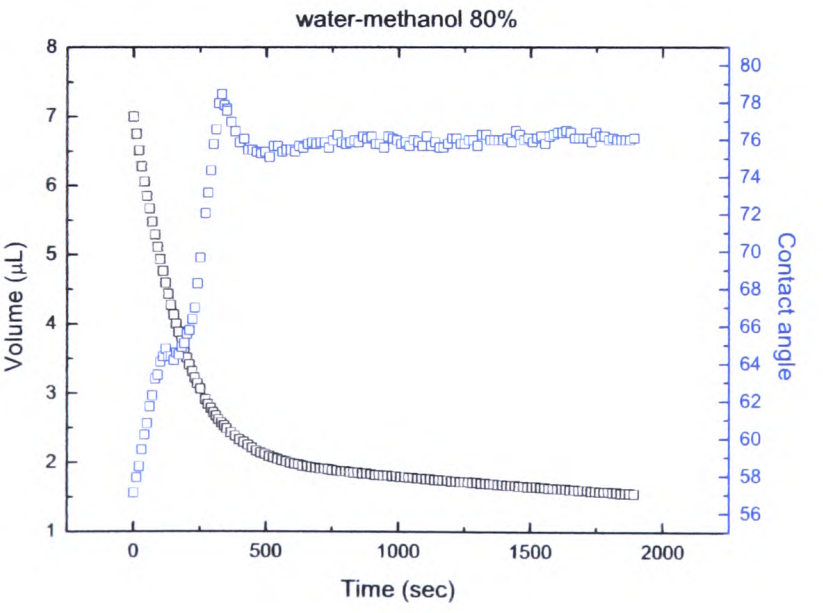

Figure 5.12: *Evolution in time of the volume and contact angle for the three Water-Methanol mixtures in an atmosphere saturated in Water vapour (*10% *(a),* 50% *(b) and* 80% *(c)).*

On Figures 5.13, 5.14 and 5.15, the comparison of the evolution in time of the volume, $V(t)$, the base diameter, $D(t)$, and the contact angle, $\theta(t)$, between the two cases are presented. For the lowest concentration it is difficult to analyse the data as the low amount of Methanol present into the mixture seems to evaporate quickly. But for the two other compositions, strong similarities in the first part of the evaporation process are observed. As in the presence of a saturated atmosphere, the evaporation only corresponds to the evaporation of the Methanol component, the evolutions of $V(t)$ and $D(t)$ suggest that even in the absence of saturated Water vapour, the Methanol seems to be the main component evaporating at the beginning. When most of Methanol seems to have been evaporated the behaviour of the contact angle differs for each case. In the presence of a saturated atmosphere the evolution of the contact angle continues to rise towards its equilibrium value while in the absence of saturation the contact angle stops its progression at a lower value before decreasing. Inside the drop, the Methanol molecules evaporated are replaced by molecules coming from the bulk. These molecules diffuse from the bulk towards the liquid-gas interface. The diffusion coefficient of Methanol molecules into Water is of the order of $2 \times 10^{-9}\ m^2/s$, hence the characteristic time of the diffusion will be:

$$t_{diff} = \frac{L^2}{D} = \frac{0.001}{2 \times 10^{-9}} = 1000\ s, \tag{5.1}$$

where L is the characteristic length which corresponds to the drop size ($1\ mm$). The value of the characteristic time suggests that the diffusion of the Methanol molecules are much slower than the evaporation time of the drop. It means that even if the very beginning of the evaporation process is dominated by the evaporation of Methanol molecules, afterwards the evaporation is composed by Water and Methanol molecules.

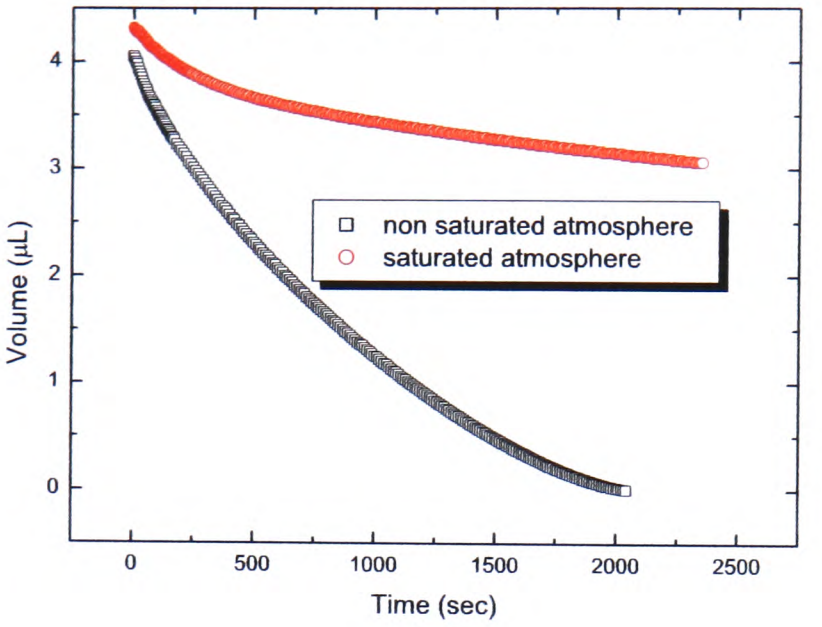

(a)

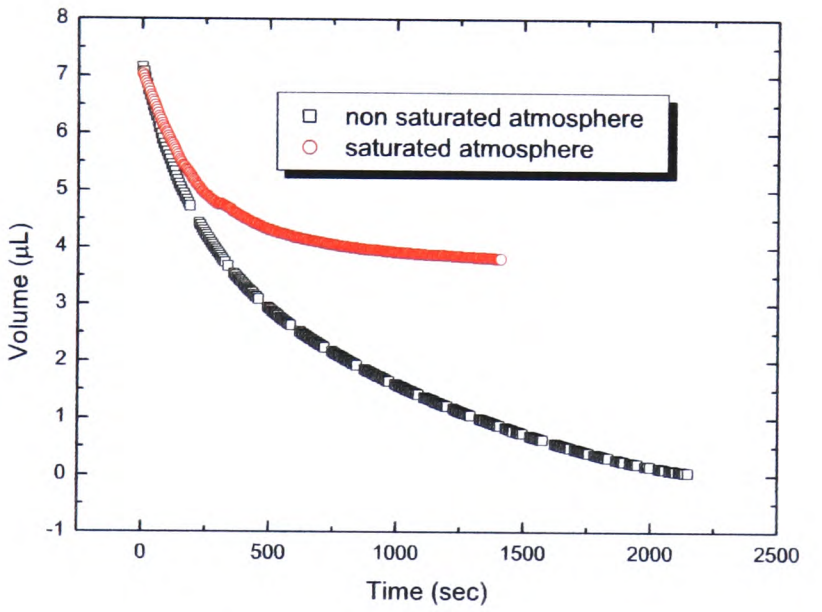

(b)

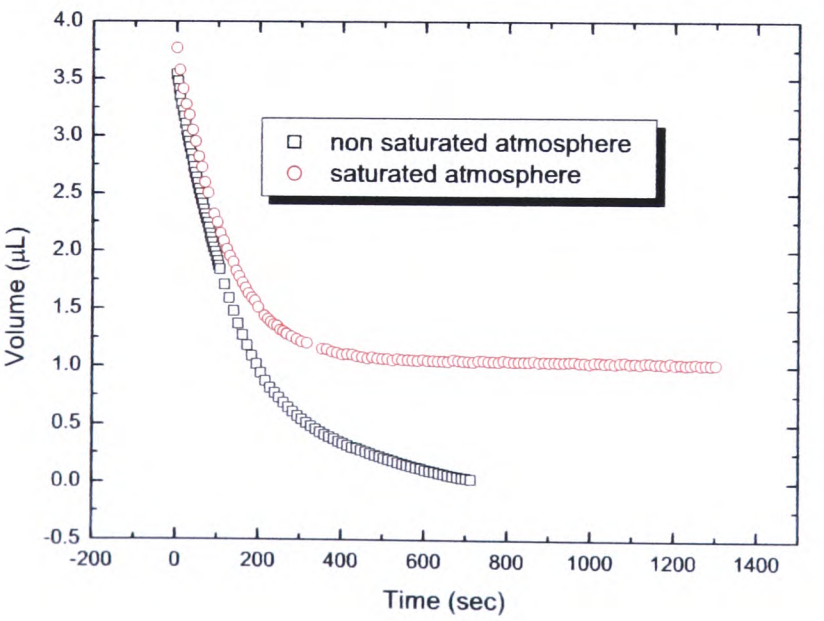

(c)

Figure 5.13: *Comparison of the volume evolution between saturated and non saturated experiments (*10% *(a),* 50% *(b) and* 80% *(c)).*

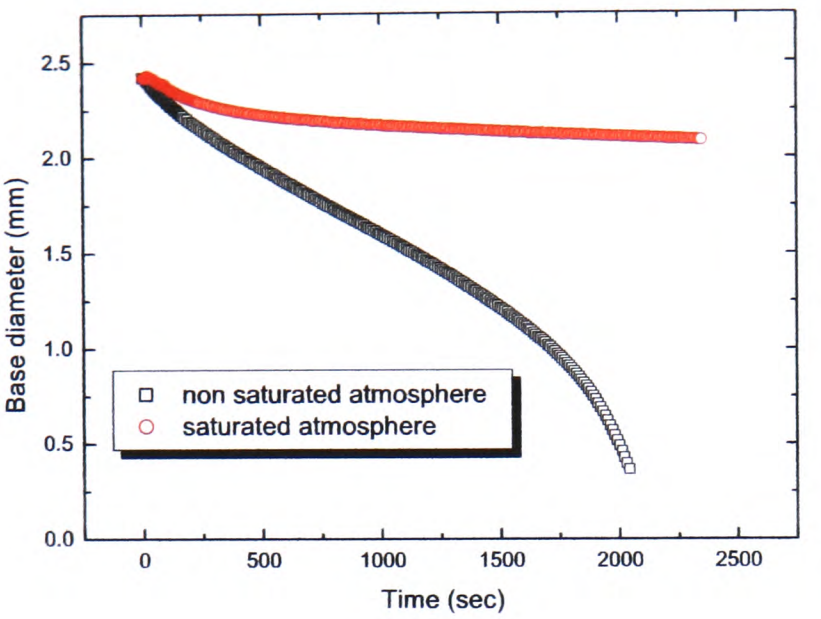

(a)

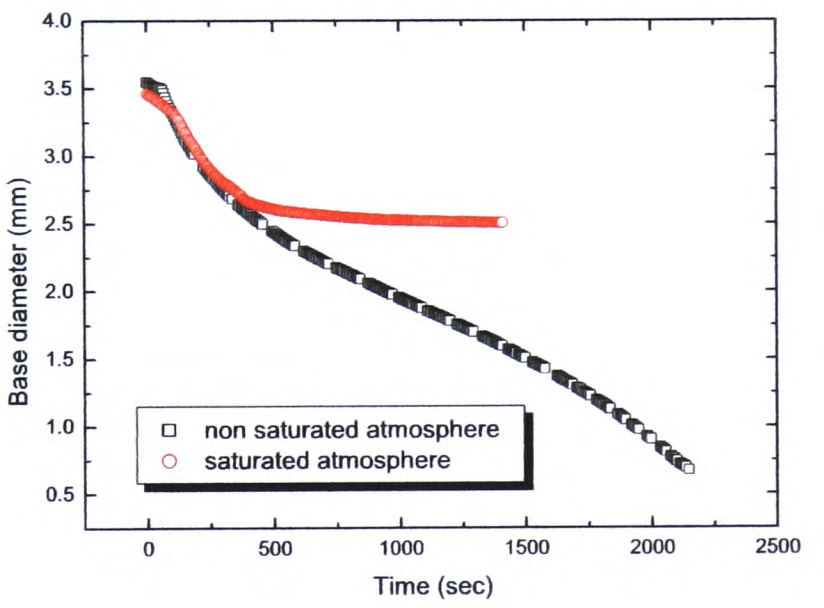

(b)

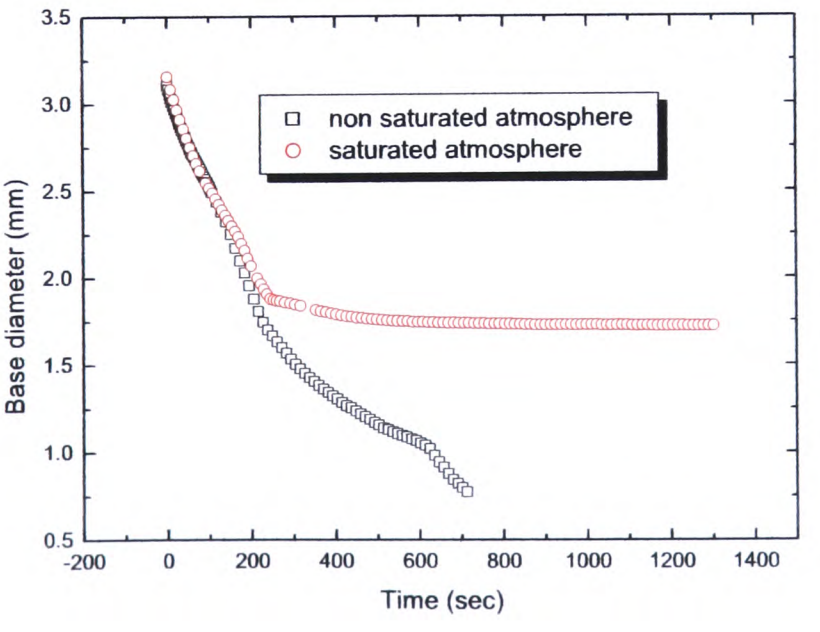

(c)

Figure 5.14: *Comparison of the base diameter evolution between saturated and non saturated experiments (*10% *(a),* 50% *(b) and* 80% *(c)).*

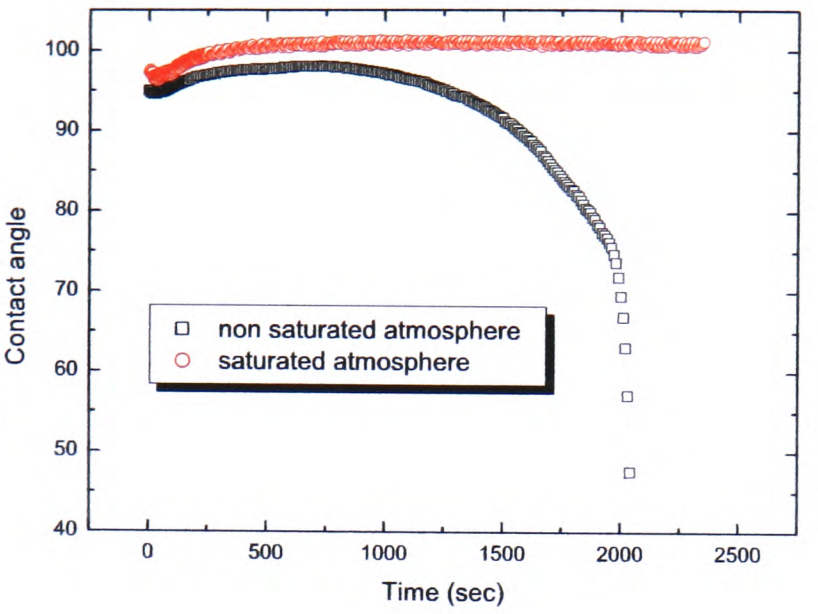

(a)

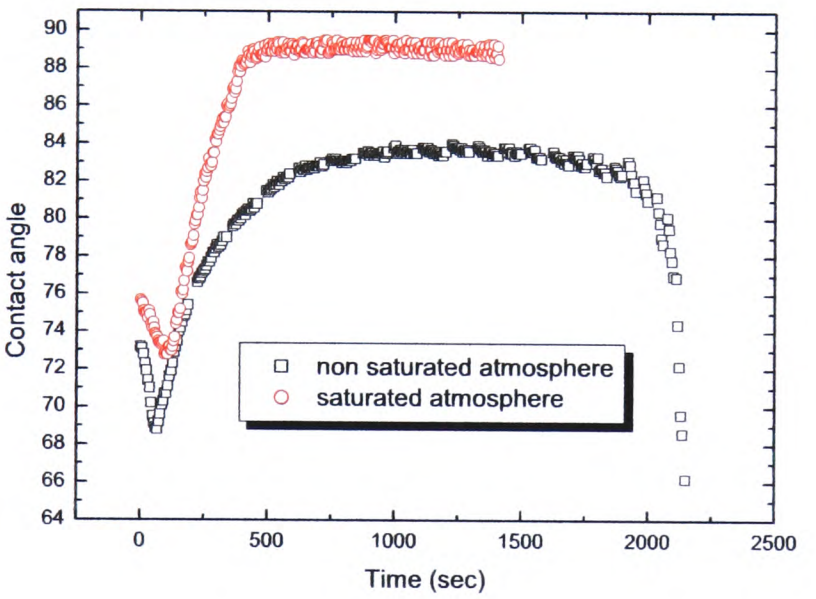

(b)

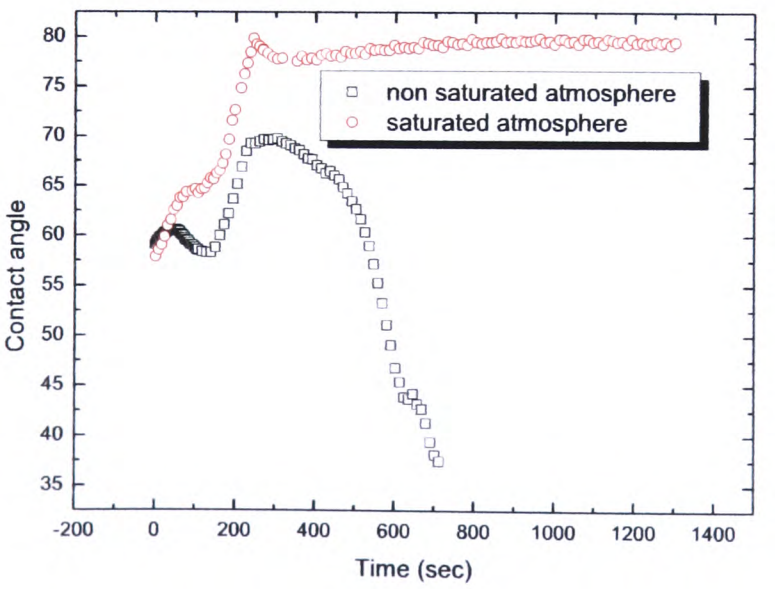

(c)

Figure 5.15: *Comparison of the contact angle evolution between saturated and non saturated experiments (*10% *(a),* 50% *(b) and* 80% *(c)).*

5.3.2 Water-DMSO

The same experiments as in the case of Water-Methanol mixture have been performed with Water-DMSO mixtures. The case of Water-DMSO mixture is an interesting one as DMSO has a lower surface tension than Water but less volatile. On Figure 5.16, the initial contact angles of Water-DMSO and Water-Methanol binary mixtures are plotted against mass fraction. This

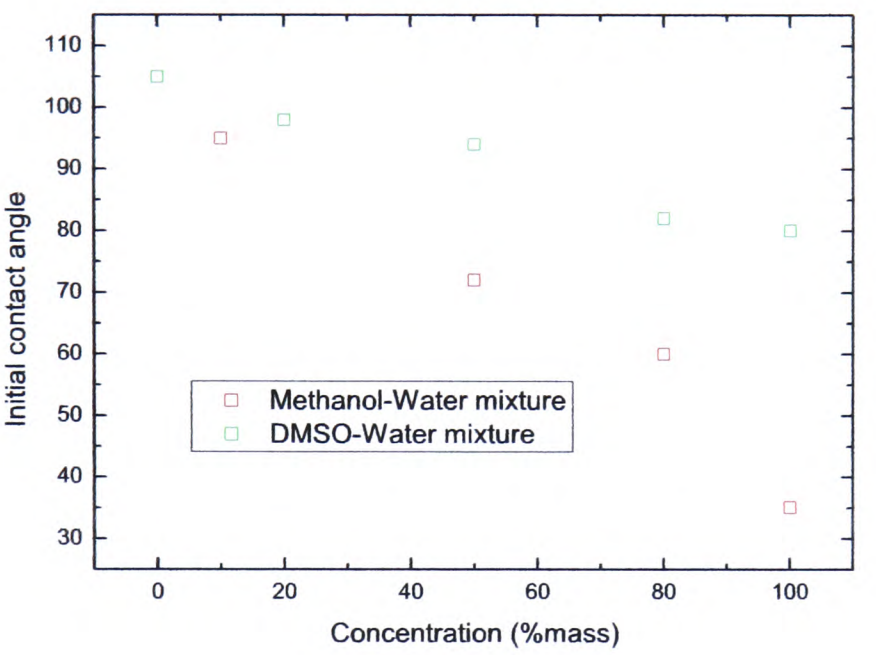

Figure 5.16: *Initial contact angles for DMSO-Water and Methanol-Water binary mixtures.*

shows a decrease of the initial contact angle with higher concentration of DSMO/Methanol. From the evolution of the surface tension of the binary mixture (see Figure 5.1 page 75) where the surface tension decreases with the concentration, these trends were expected. In the case of Water-DMSO mixtures the variation of the initial contact angle is smaller (from 105° to 80°) than in the case of Water-Methanol mixtures (from 105° to 35°). On Figures 5.18 and 5.19, the evolution of the drop diameter, contact angle and volume is represented. The evolution of all the parameters could be divided in two mains stages. In the first stage, all the parameters exhibit a variation, they actually all decrease towards a constant value. In the second stage, all parameters are almost constant, it seems that during this stage the evaporation process stops. In Water-DMSO binary mixture, the more volatile component is Water hence Water is the component which will mainly evaporate in the first stage. This is confirmed by the evolution of the contact angle in time (see Figure 5.18) which decreases continuously in the first stage. It means that the mixture becomes richer in DMSO. When we look at the volatility of DMSO

($P_{sat} = 0.42\ mmHg$ at $20\,°C$), it can be seen that its value is very low compared to the volatility of Water ($P_{sat} = 17.54\ mmHg$ at $20\,°C$). These two orders of magnitude of volatility difference between the two components means that the Water-DMSO mixture is similar to the evaporation of Water-Methanol mixture with an atmosphere saturated in Water vapour where only the Methanol component was forced to evaporate.

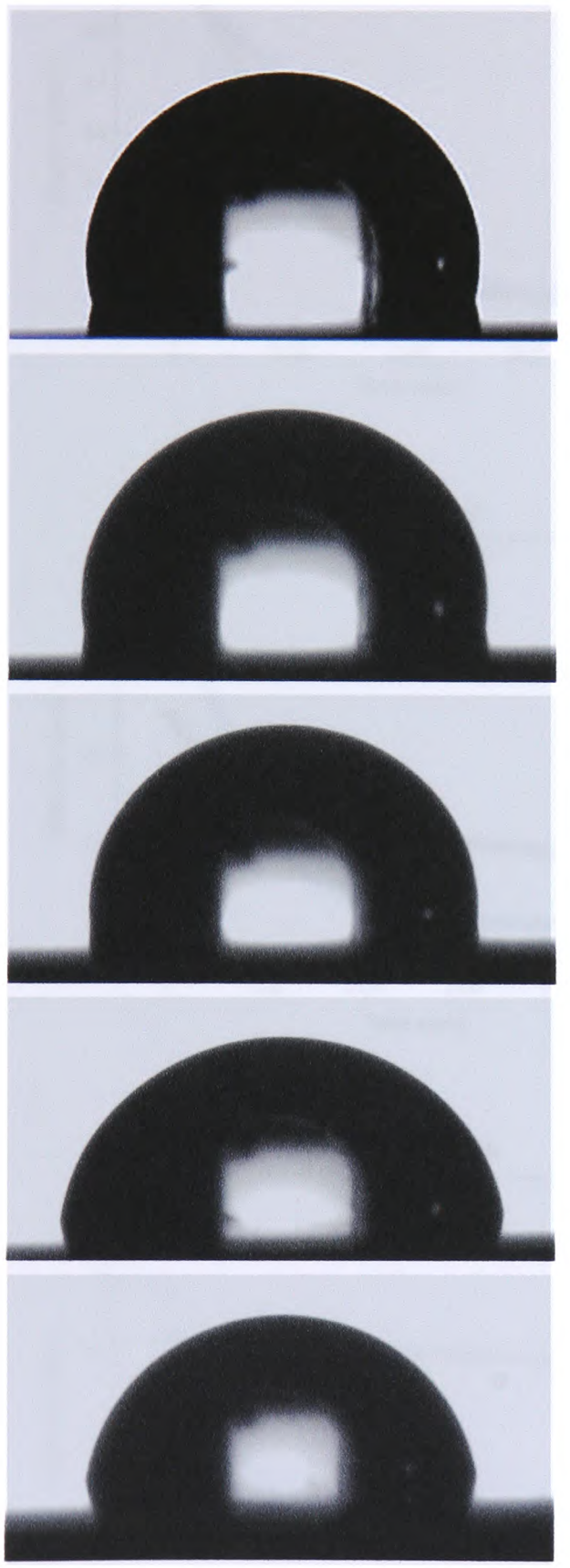

Figure 5.17: *Example of initial sessile drop profile at different Water-DMSO concentration*

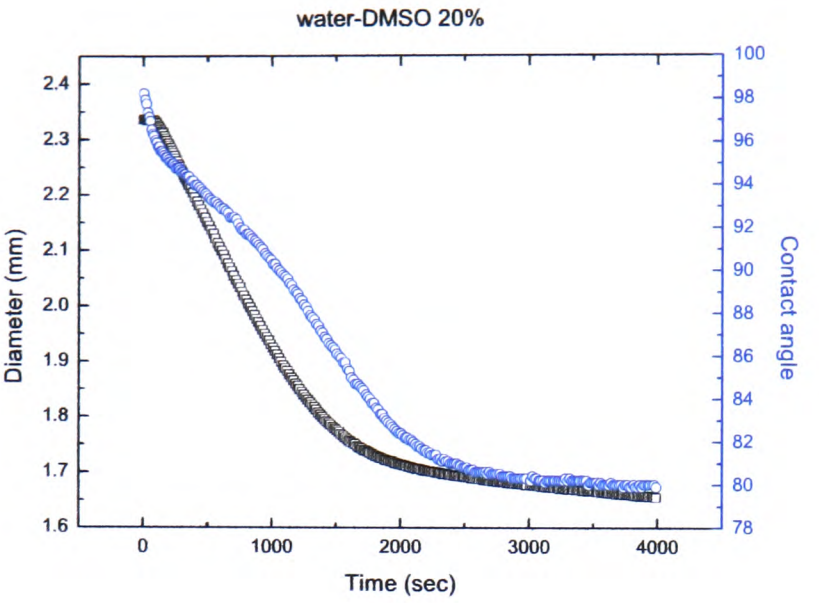

(a)

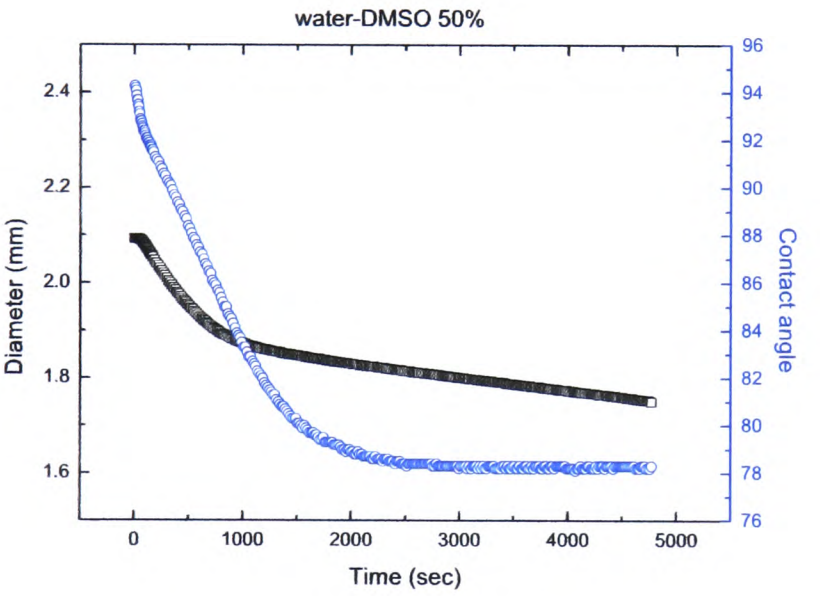

(b)

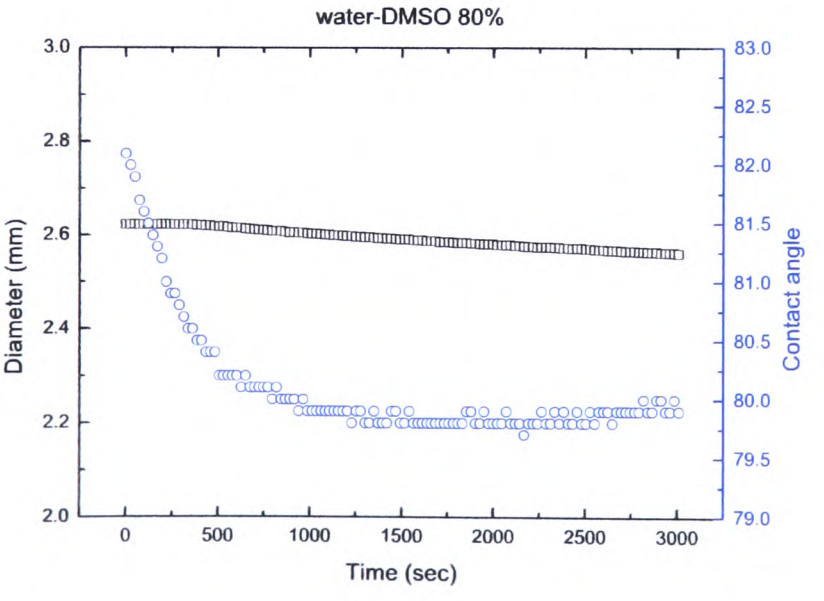

(c)

Figure 5.18: *Evolution in time of the base diameter and contact angle for the three Water-DMSO mixtures (*20% *(a),* 50% *(b) and* 80% *(c)).*

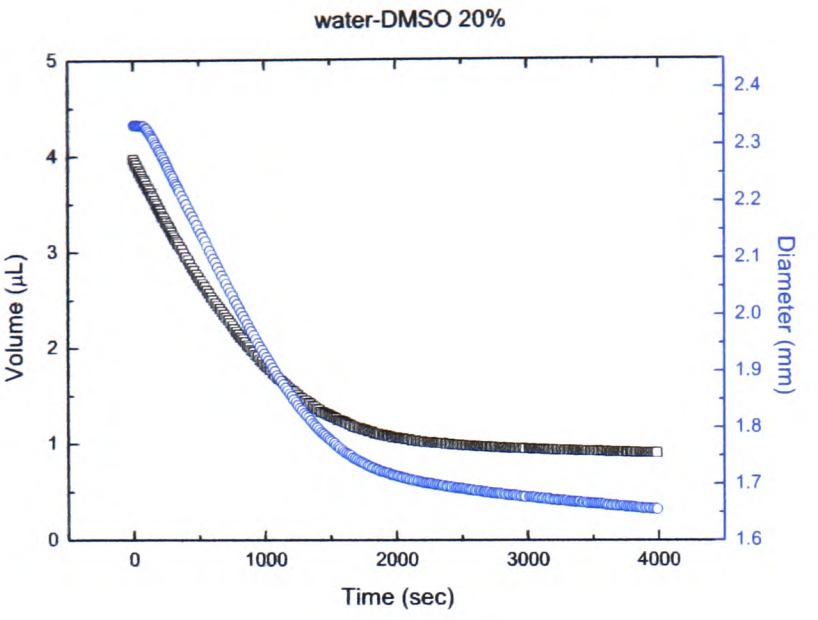

(a)

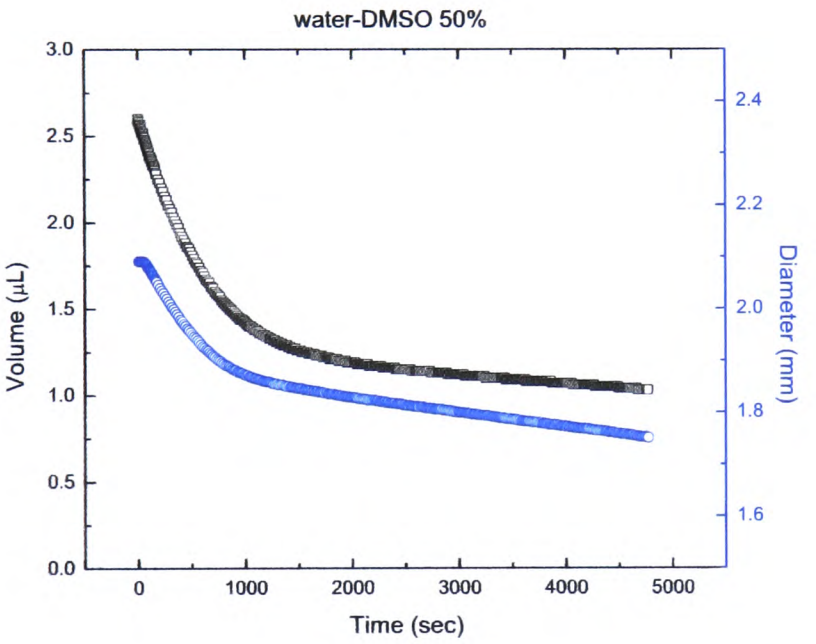

(b)

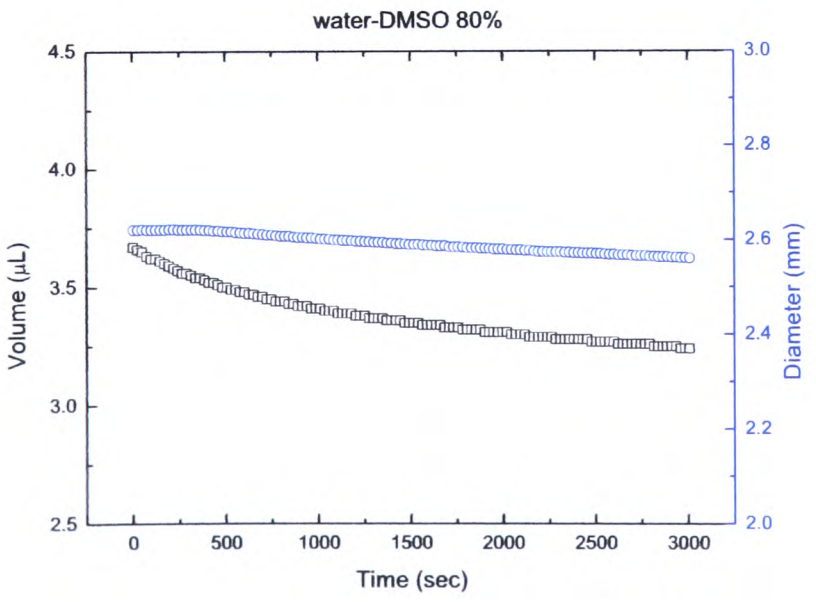

(c)

Figure 5.19: *Evolution in time of the volume and base diameter for the three Water-DMSO mixtures (*20% *(a),* 50% *(b) and* 80% *(c)).*

5.4 Conclusion

The investigation of the evaporation of Water-Methanol and Water-DMSO binary drops have been presented. These drops were deposited on a smooth silicon substrate coated by PMMA where almost no pinning of the triple line was observed. The results suggest that in the first part of the evaporation process the evaporated molecules are mainly the most volatile components. This is confirmed by the "saturated atmosphere" experiment in the case of Water-Methanol mixtures. At the difference of Yu *et al.* [11] (see section 2.4 page 48), the maximum contact angle reached differ with the initial concentration. It might suggest that residual Methanol molecules are present through the whole evaporation process.

Chapter 6
Mathematical model

As it was mentioned in the general introduction, this work has been undertaken in close collaboration with Gavin Dunn, PhD student at the University of Strathclyde under the supervision of Pr. S. Wilson and Dr B. Duffy. In a joint effort between our group in Edinburgh and Strathclyde group, a mathematical model for the case of sessile droplets with a pinned triple line was developed. This chapter presents a detailed summary of the model.

The mathematical model developed assumes spherical cap like droplets with a constant diameter. Due to the axisymmetry of the problem, a 2D model is thought to be sufficient to describe the major mechanism and the underlying physics of the phenomenon (see Figure **??**). The evaporation of the drop is solely driven by the diffusion of its vapour into the ambient gas. The droplet has a constant viscosity, density ρ, surface tension, and thermal conductivity k and the substrate has a constant thickness h^s with constant thermal conductivity k^s. On Figure **??**, the various geometrical parameters are defined as follow (referred to cylindrical polar coordinates (r, ϕ, z)):

- origin on the substrate at the centre of the droplet with the z axis vertically upwards
- the free interface liquid-gas is denoted by $z = h(r, t)$
- the upper surface of the substrate is denoted by $z = 0$
- the lower surface of the substrate is denoted by $z = -h^s$

As it was shown in the "Theory Chapter", when the droplet is small enough (i.e. the radius is smaller than the capillary length), it could be considered as a spherical cap shape. In the case studied, the droplet radius R remains constant because of the contact line pinning by surface roughness. Therefore h is expressed as:

$$h = \sqrt{\frac{R^2}{\sin^2\theta} - r^2} - \frac{R}{\tan\theta}, \tag{6.1}$$

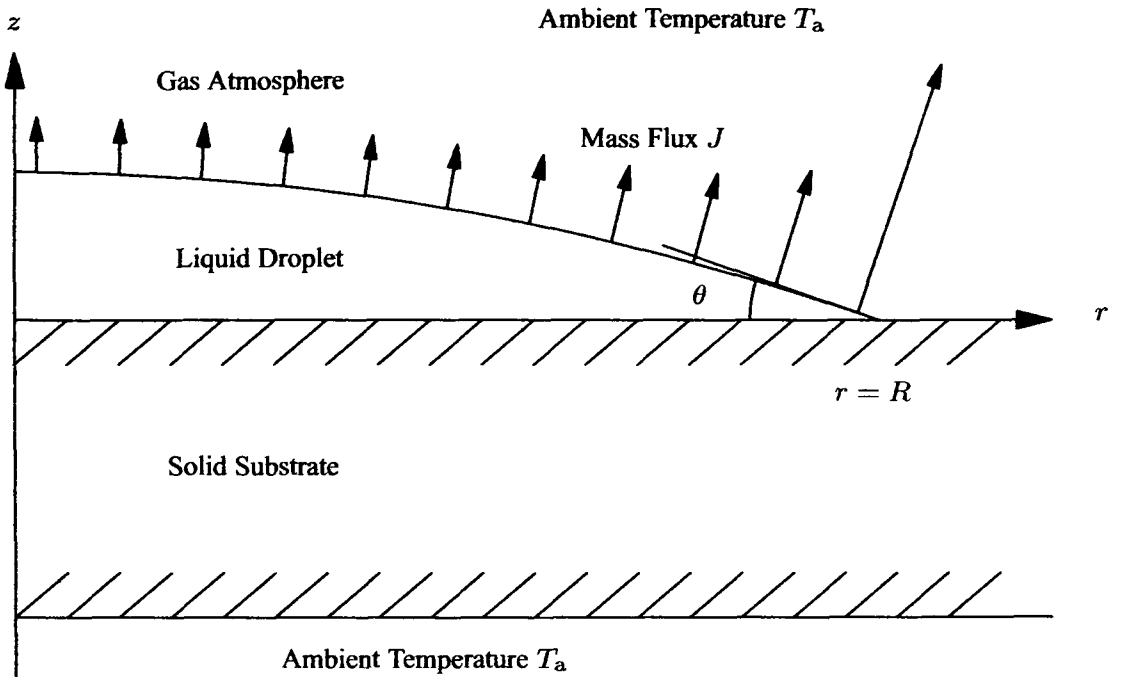

Figure 6.1: *Geometry of the mathematical model.*

with volume $V = V(t)$ and contact angle $\theta = \theta(t)$ related by

$$V = \frac{\pi h_{\rm m}(3R^2 + h_{\rm m}^2)}{6}, \tag{6.2}$$

where $h_{\rm m} = h(0,t) = R\tan(\theta/2)$ is the maximum height of the droplet. The total evaporation rate is given by

$$\rho\frac{{\rm d}V}{{\rm d}t} = -2\pi\int_0^R J(r,t)\, r\sqrt{1+\left(\frac{\partial h}{\partial r}\right)^2}\,{\rm d}r, \tag{6.3}$$

where $J = J(r,t)\,(>0)$ is the local evaporative mass flux from the droplet.

Temperature in droplet and substrate

The atmosphere surrounding the droplet and the lower surface of the substrate is assumed to be at constant ambient temperature $T_{\rm a}$. The temperature of the droplet, denoted by $T = T(r,z,t)$, and the temperature of the substrate, denoted by $T^{\rm s} = T^{\rm s}(r,z,t)$, are governed by the heat equation. For times $t \gg t_T = \rho_L R^2/k$ for the droplet (and equivalently for $t \gg t_T^{\rm s} = \rho_s R^2/k^{\rm s}$ for the substrate) the unsteady term in the heat equation may be neglected and we must solve Laplace's equation:

$$\nabla^2 T = 0, \quad \nabla^2 T^{\rm s} = 0 \tag{6.4}$$

Typical values for t_T, t_∞ and t_T^s are given in Tables 6.1 and 6.2. It is observed that $t_T \ll t_\infty$

	Definition	Acetone	Methanol	Water
l_c (m)	$\sqrt{\sigma/(\rho g)}$	1.75×10^{-3}	1.70×10^{-3}	2.72×10^{-3}
t_T (s)	$\rho c_p h_m^2/k$	4	3	4
t_c (s)	R^2/D	0.17	0.12	0.07
t_∞ (s)		35	80	700

Table 6.1: *Important dimensional parameters of selected liquids for a drop with radius* $R = 1.35\ mm$.

	Definition	Al	Ti	Macor	PTFE
t_t^s (s)	$\rho^s c_p^s (h^s)^2/k^s$	0.01	0.10	1	5

Table 6.2: *Important dimensional parameter of selected substrates.*

and $t_T^s \ll t_\infty$.

No heat transfer by convection has to be considered within the droplet as the rate of convection heat transfer is much smaller than the rate of the conductive heat transfer. It could be shown using an inverse Stanton number $St^{-1} = \rho c_p \bar{u}_r R/k$, which is a ratio of the convective to the thermal diffusive effects. As it is described in Hu *et al.* work [60], the parameters corresponding to water droplets have the following approximate values: height-averaged radial velocity $\bar{u}_r = 1\ \mu$m/s, contact line radius $R = 1\ mm$, $k = 1.4536 \times 10^{-3}\ cal.K^{-1}.cm^{-1}.s^{-1}$ (from Bird *et al.*), $c_p = 1\ cal.g^{-1}.K^{-1}$, and water density $\rho = 1\ g.cm^{-3}$, which gives St^{-1} about 0.02. Therefore the convection term is negligible to the conduction term.

Finally, we assume that the temperature and the heat flux are continuous between the droplet and the substrate, that is

$$-k\frac{\partial T}{\partial z} = -k^{\mathrm{s}}\frac{\partial T^{\mathrm{s}}}{\partial z}, \quad T^{\mathrm{s}} = T \quad \text{on } z = 0 \text{ for } r < R, \tag{6.5}$$

and also constant ambient temperature

$$T^{\mathrm{s}} = T_{\mathrm{a}} \quad \text{on } z = 0 \text{ for } r > R \text{ and } z = -h^{\mathrm{s}}. \tag{6.6}$$

we assume that any energy lost from evaporation is converted into a heat loss:

$$LJ = -k\nabla T \cdot \mathbf{n} \quad \text{on } z = h \text{ for } r < R, \tag{6.7}$$

where L is the (constant) latent heat of evaporation and $\mathbf{n} = (-h_r, 0, 1)/\sqrt{1 + h_r^2}$ is the unit

normal to the droplet.

Concentration of vapour in the atmosphere

The local evaporative mass flux from the droplet J depends on the rate-limiting step, which can be either the transfer rate across the liquid-gas interface or the diffusion of the saturated vapour layer into the ambient gas. As it is mentioned by Popov *et al.* [72], the transfer rate across the liquid-gas interface is characterized by a time scale of the order of 10^{-10} s and the diffusion process characterized time scale is of the order of R^2/D (where D is the diffusion coefficient for the liquid vapour in ambient gas and R is the characteristic length of the drop), which is of the order of seconds for water drops. The evaporation process can be considered quasi-steady. Indeed, the ratio of the time required for the vapour-phase water concentration to adjust to the changes in the droplet shape (R^2/D) to the droplet evaporation time t_∞ is of the order of $c_{\text{sat}}(1-H)/\rho \simeq 10^{-5}$, i.e. the vapour concentration adjusts rapidly compared to the evaporation time.

The concentration of vapour, denoted by $c = c(r, z, t)$, is defined as the mass of vapour per unit volume of atmosphere surrounding the droplet. For times $t \gg t_c = R^2/D$ (see Table 6.1) c is governed by Laplace's equation.

$$\nabla^2 c = 0, \tag{6.8}$$

At the free surface of the droplet we assume that the atmosphere is saturated with vapour and hence

$$c = c_{\text{sat}}(T) \quad \text{on } z = h \text{ for } r < R, \tag{6.9}$$

where the saturation value of the concentration $c_{\text{sat}} = c_{\text{sat}}(T)$ is an increasing function of temperature, approximated accurately by

$$c_{\text{sat}} = \sum_{i=0}^{4} \alpha_i (T_{\text{a}} - T)^i, \tag{6.10}$$

where the coefficients $\alpha_0 = 1.93 \times 10^{-2}, \alpha_1 = 1.11 \times 10^{-3}, \alpha_2 = 2.78 \times 10^{-5}, \alpha_3 = 3.78 \times 10^{-7}$ and $\alpha_4 = 2.59 \times 10^{-9}$ are chosen to fit experimental data given by Raznjevic [73]. But in the case of small temperature differences, the saturation value of the concentration

$c_{sat} = c_{sat}(T)$ could be assumed as a linearly increasing function of temperature given by

$$c_{sat}(T) = c_{sat}(T_a) + \left.\frac{\mathrm{d}c_{\mathrm{sat}}}{\mathrm{d}T}\right|_{T=T_{\mathrm{a}}} (T - T_{\mathrm{a}}) \tag{6.11}$$

Far from the droplet the concentration of vapour approaches its ambient value, i.e.

$$c \to H c_{\mathrm{sat}}(T_{\mathrm{a}}) \tag{6.12}$$

as $(r^2 + z^2)^{1/2} \to \infty$, where H is the relative saturation (known as relative humidity in the case of water vapour) of the atmosphere.

On the dry part of the substrate there is no mass flux, that is,

$$\frac{\partial c}{\partial z} = 0 \quad \text{on } z = 0 \text{ for } r > R, \tag{6.13}$$

Once c is known the local evaporative mass flux from the droplet is given by

$$J = -D\nabla c \cdot \mathbf{n} \quad \text{on } z = 0 \text{ for } r < R, \tag{6.14}$$

where D is the diffusion coefficient of vapour in the atmosphere.

To determine the transfer rate across the liquid-gas interface the kinetic theory is used. This is known as the Hertz-Knudsen (Prosperetti & Plesset [34]) relation and leads to a linear relation between the transfer rate and the departure from equilibrium at the interface:

$$J = v_{\mathrm{k}}(c_{\mathrm{sat}}(T) - c) \tag{6.15}$$

where $v_{\mathrm{k}} = \alpha\sqrt{R_{\mathrm{g}}T_{\mathrm{a}}/2\pi M}$ is a typical kinetic velocity. Here, α, is an accommodation coefficient usually assumed to be close to unity, R_{g} is the universal gas constant and M is the molecular mass of the vapour.

Because of the continuity of the evaporative flux at the interface we equate (6.14) and (6.15) to give

$$-D(\mathbf{n} \cdot \nabla c) = v_{\mathrm{k}} \left(c_{\mathrm{sat}}(T_{\mathrm{a}}) - c + \left.\frac{\mathrm{d}c_{\mathrm{sat}}}{\mathrm{d}T}\right|_{T=T_{\mathrm{a}}} (T - T_{\mathrm{a}}) \right) \tag{6.16}$$

on $z = h, r < R$.

Solution procedure

In the special case $\alpha_i = 0$ for $i = 1 \ldots 4$ when $c_{\mathrm{sat}} = c_{\mathrm{sat}}(T_{\mathrm{a}})$, the saturation concentration is constant and we recover the model developed by Deegan *et al.* [1]. Based on a numerical solution obtained using a finite element method, Hu and Larson [7] approximated the evaporation rate for this case as

$$\rho \frac{\mathrm{d}V}{\mathrm{d}t} = -\pi R D c_{\mathrm{sat}}(T_{\mathrm{a}})(0.27\theta^2 + 1.30). \tag{6.17}$$

This approximation is consistent with the analytic results

$$\rho \frac{\mathrm{d}V}{\mathrm{d}t} = -4 R D c_{\mathrm{sat}}(T_{\mathrm{a}}) \qquad \text{on } \theta = 0, \text{ and} \tag{6.18}$$

$$\rho \frac{\mathrm{d}V}{\mathrm{d}t} = -2\pi R D c_{\mathrm{sat}}(T_{\mathrm{a}}) \qquad \text{on } \theta = \frac{\pi}{2}. \tag{6.19}$$

In general, the problem for c involves the free-surface temperature and has to be solved numerically. This was done using the Matlab-based numerical analysis package Comsol Multiphysics (formerly Femlab). The domain radius is chosen to be 160 times the radius of the droplet and following Hu and Larson [7] the mesh points are densely populated at the contact line. Comparison with Equation 6.17 in the special case $c_{\mathrm{sat}} = c_{\mathrm{sat}}(T_{\mathrm{a}})$ suggests that this setup ensures at most 1% numerical error. At each time step we solve the system of equations outlined above to obtain $\mathrm{d}V/\mathrm{d}t$. Euler's forward method is then used to estimate V, and hence θ, h and the geometry at the next time step.

In the following two chapters, the present model will be confronted to the experimental results. First, the mathematical model will be compared to the experimental results for validation, then it will be applied as a complementary tool to better understand the various mechanisms involved during the evaporation process of sessile drops.

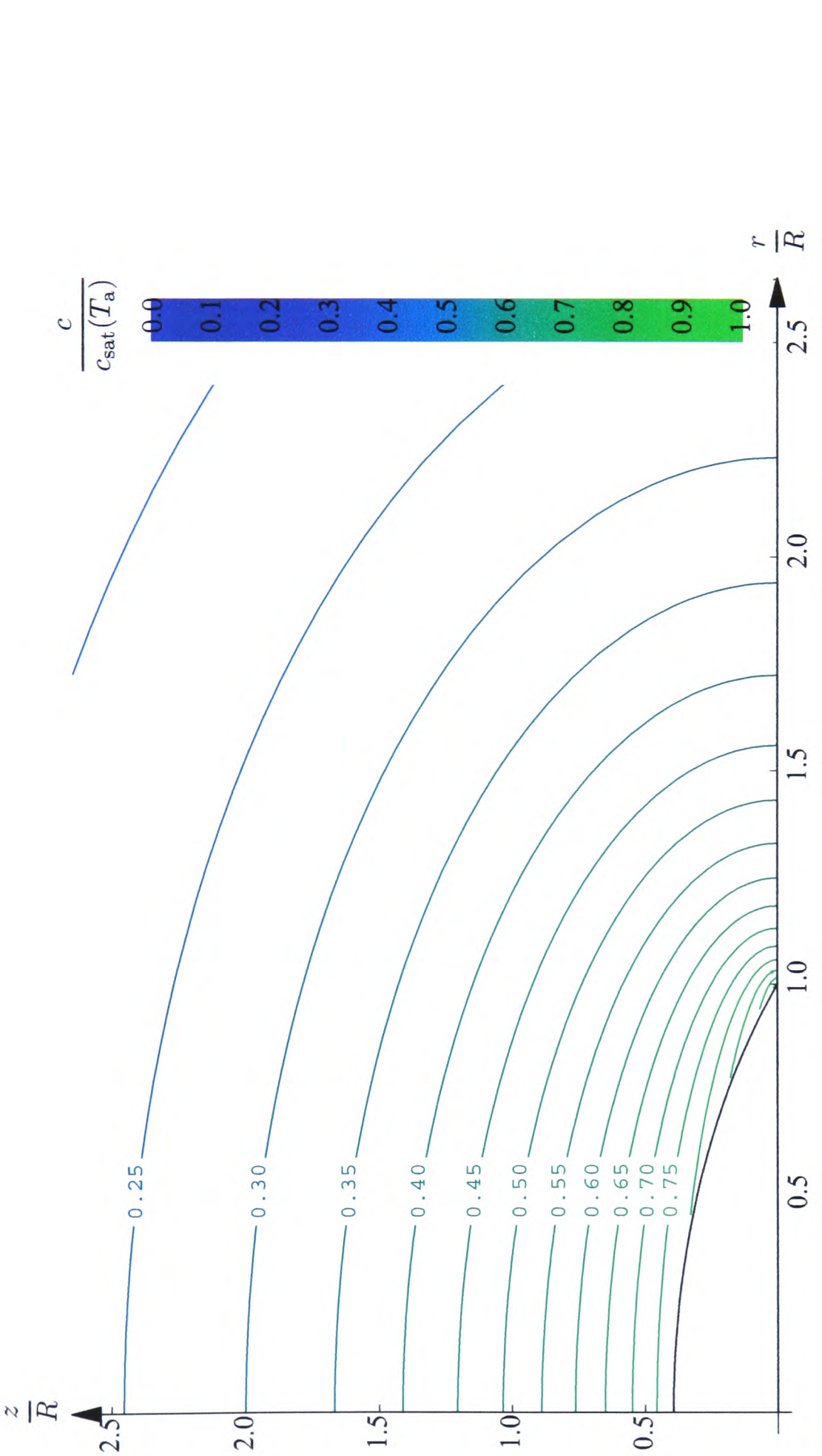

Figure 6.2: *Theoretical prediction of the model showing concentration contours in the atmosphere for a methanol droplet of radius* $R = 1.35\,\mathrm{mm}$, *with contact angle* 43° *on an aluminium substrate.*

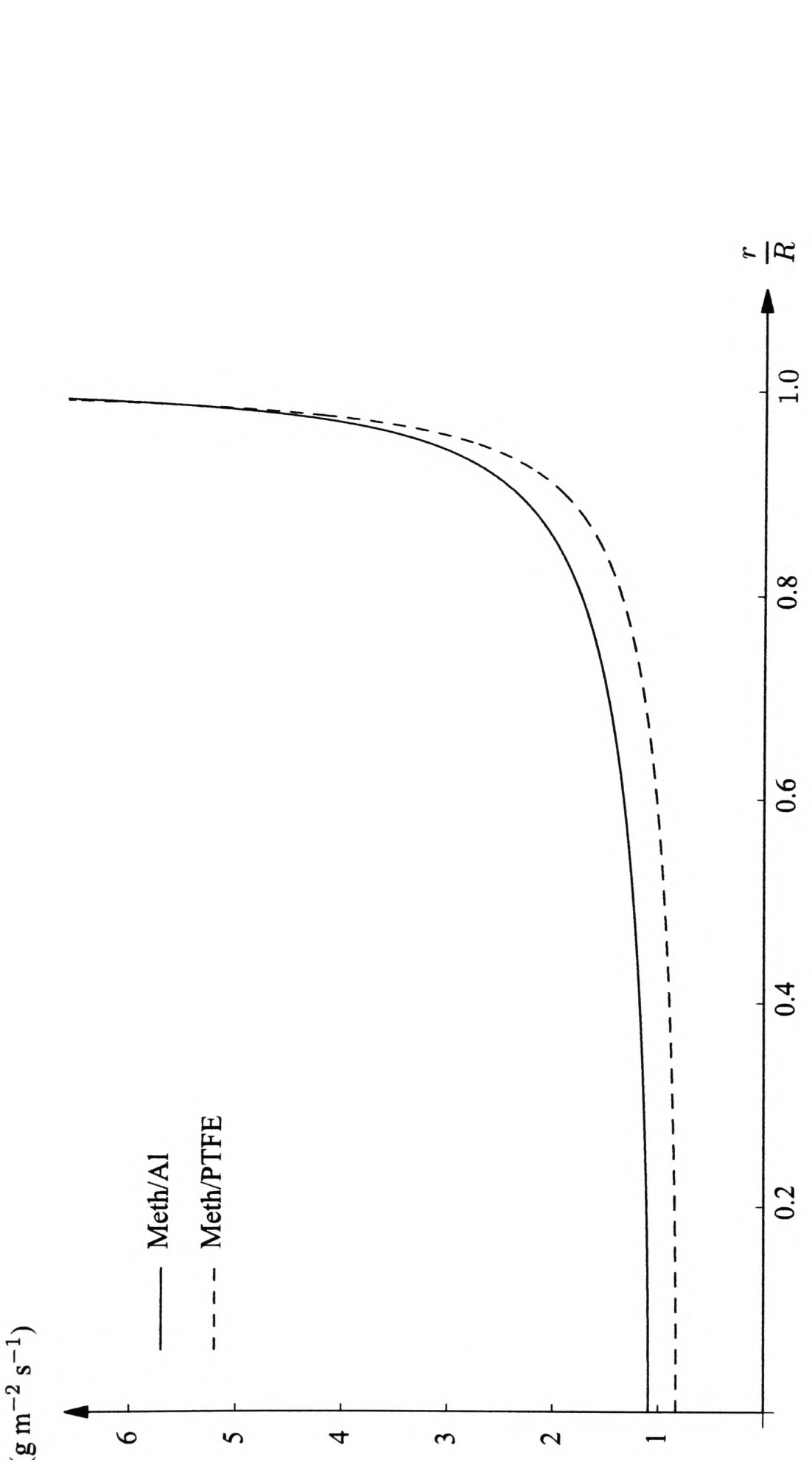

Figure 6.3: *Theoretical prediction of the model for the evaporative mass flux of a methanol droplet with radius* $R = 1.35\,\mathrm{mm}$ *and initial contact angle* $43°$*, on aluminium and PTFE substrates. The atmosphere has temperature* $T_\mathrm{a} = 295\,\mathrm{K}$ *and relative saturation* $H = 0$*.*

Chapter 7
Influence of the pressure and ambient gas on the evaporation.

This chapter presents the results of an experimental study of evaporating sessile drops in a controlled environment. The experimental setup allowed the investigation of the evaporation rate of sessile drops under reduced pressure (40 to 1000 mbar) and various ambient gases. Sessile drops of initial volume 2.5 μL are deposited on substrates and left to evaporate in a controlled atmosphere. The effect of reducing pressure on the evaporation rate as well as changing the ambient gas is studied. Three different gases are used; namely Helium, Nitrogen and Carbon Dioxide. The role of vapour diffusion as a limiting mechanism for evaporation is studied and the experimental results are compared to the mathematical model.

7.1 Experimental conditions

All performed experiments presented in this chapter have been realised with pure deionised Water drops resting on Aluminium substrates. The Aluminium substrate has a dimension of $10 \times 10 \times 1\ mm$ ($l \times w \times t$) and a high thermal conductivity (237 $W/m.K$). The surface roughness of the substrate was analysed with a profilometer using light interferometry (see details in section 3.3 page 61), the rms (root mean square) was found to be 306 nm (relatively rough), in this case the Water drop triple line was found to pin during most of the evaporation process (see Figure 7.1). In order to control the ambient gas and pressure, the experiment was performed in a "low pressure" chamber. A full description of this chamber is given in the "Experimental Chapter" section 3.2 page 59. Three gases have been chosen because of their diffusion properties with respect to Water vapour (see Table 7.1 for details), namely Carbon Dioxide, Nitrogen and Helium. The pressure was varied in the range of 40 $mbar$ to 1000 $mbar$. All experiments were carried out in an environment where the room temperature was controlled with an air conditioning unit with a precision of $\pm 1\,°C$, the ambient temperature was kept at $22\,°C$ during all experiments.

	Helium	Nitrogen	Carbon Dioxide
Diffusion coeffcient, cm^2/s	82	25	16

Table 7.1: *Experimental values of the diffusion coefficient (water vapour into gas) for each gas at atmospheric pressure and at* $25\,°C$ *[26].*

7.2 Experimental results

Before looking at the experimental results, a short comment on the experimental analysis is presented. As it has been shown in previous studies [46, 48, 49], the evaporation rate is proportional to the drop radius. Hence a relatively rough substrate has been chosen where the drops contact line will remain pinned during the main part of the evaporation process. This can be observed on Figure 7.1 where a photography of the drop profile has been taken periodically (every 150 s). The evolutions of the drop diameter and volume are plotted against time on Figure 7.2. Their evolutions could be divided in two stages. In the first stage the base diameter is constant while the volume decreases linearly. Finally the drop diameter and volume decrease until disappearance. The evaporation rate calculation is based only on the first stage where the diameter is constant, see Figure 7.2. On Figure 7.3, the evaporation rates are plotted against the drop base radius. In agreement with earlier works [46, 48, 49], the results show a linear trend as a function of R. Therefore all the experiments have been performed with a similar drop size (2.7 mm in diameter). The study has only focused on the variations of the evaporation rates over a large range of pressures, not on the evolution of the drop geometry (diameter or contact angle).

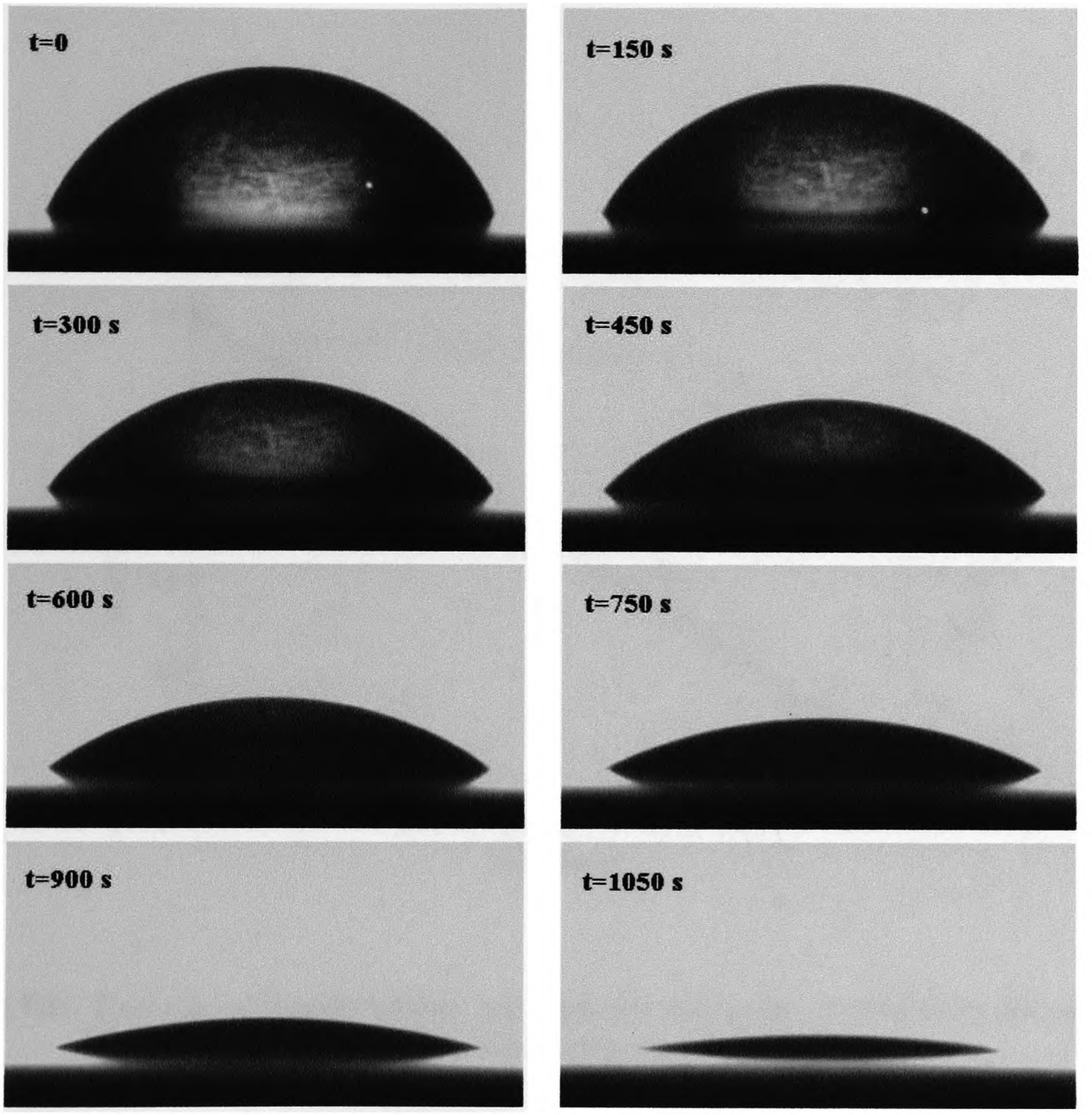

Figure 7.1: *This is an example of a pinned evaporative Water droplet deposited on Aluminium substrate. Pictures taken every 150 seconds.* $P = 1000$ *mbar and* $T = 22\,^{\circ}C$.

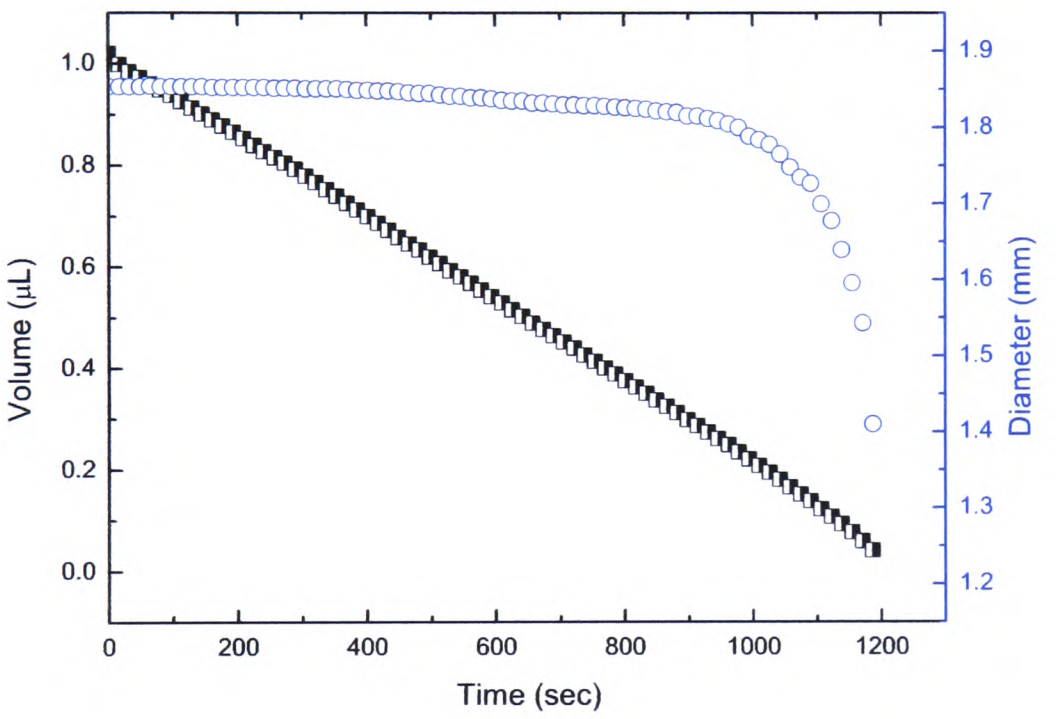

Figure 7.2: *Example of droplet volume and diameter evolutions in time (here the case of a Water drop on an Aluminium substrate is illustrated).*

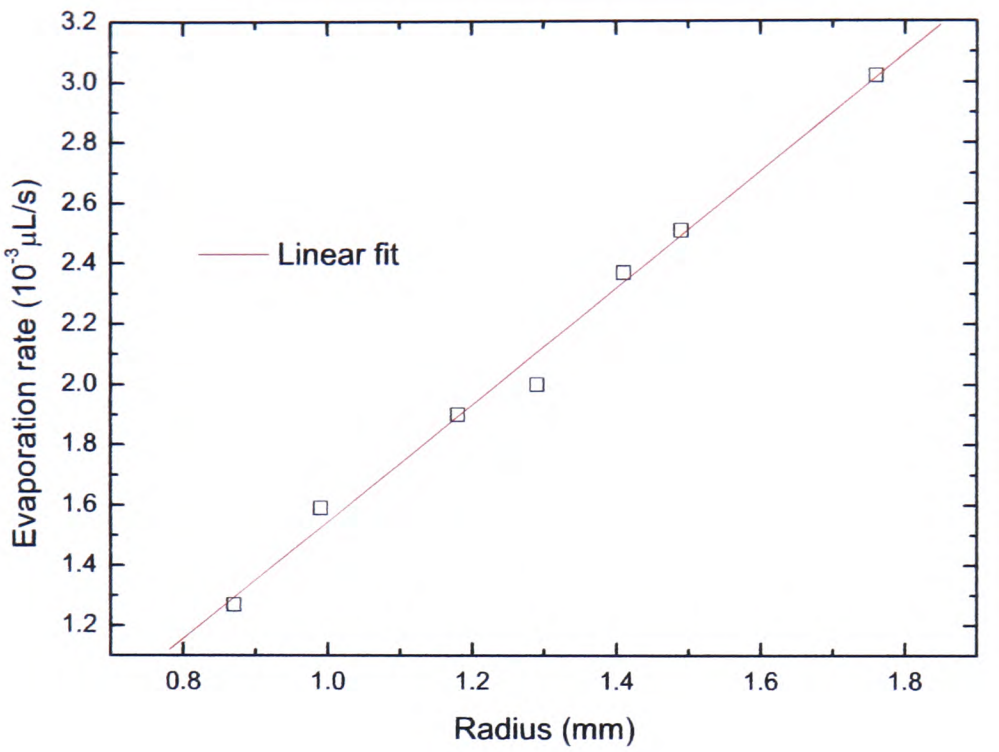

Figure 7.3: *Evolution of a Water drop evaporation rate as a function of the base radius.*

The effect of reducing the pressure on the evaporation rate is first investigated. The results shown on Figure 7.4 correspond to the case of Nitrogen as the ambient gas.

On a linear scale (top graph in Figure 7.4) the evaporation rate is found to increase exponentially as the pressure is reduced. The evaporation rate increases from $30 \times 10^{-4}\ \mu L/s$ at atmospheric pressure to more than $400 \times 10^{-4}\ \mu L/s$ at the lowest investigated pressure (around $50\ mbar$). When these data are plotted on a logarithmic scale (bottom graph in Figure 7.4), the data set can be reasonably fitted with a straight line. It means that the correlation of the evaporation rate to the pressure could be expressed as follows: $dV/dt = aP^b$. These experimental data will be confronted to the theory based on diffusion in the discussion section.

As previously mentioned in the introduction section, the diffusion coefficient depends on the nature of the ambient gas. In order to investigate the influence of varying the diffusion coefficient it is decided to change the ambient gas. The same experiment, as described above, is realized with two other gases: Helium and Carbon Dioxide. It is worth noticing on Figure 7.5 that the evaporation rates for Helium are greater than the ones for Nitrogen and Carbon Dioxide respectively. It is also observed on Figure 7.5 (logarithmic scale) that the evolutions of the evaporation rates with the pressure are similar and parallel.

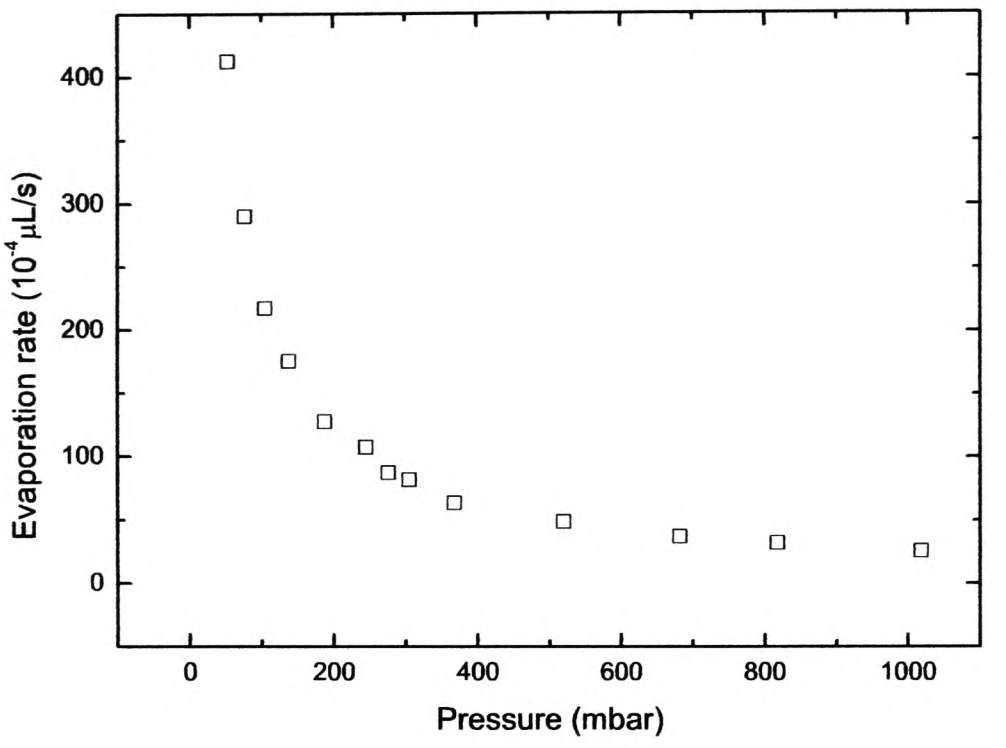

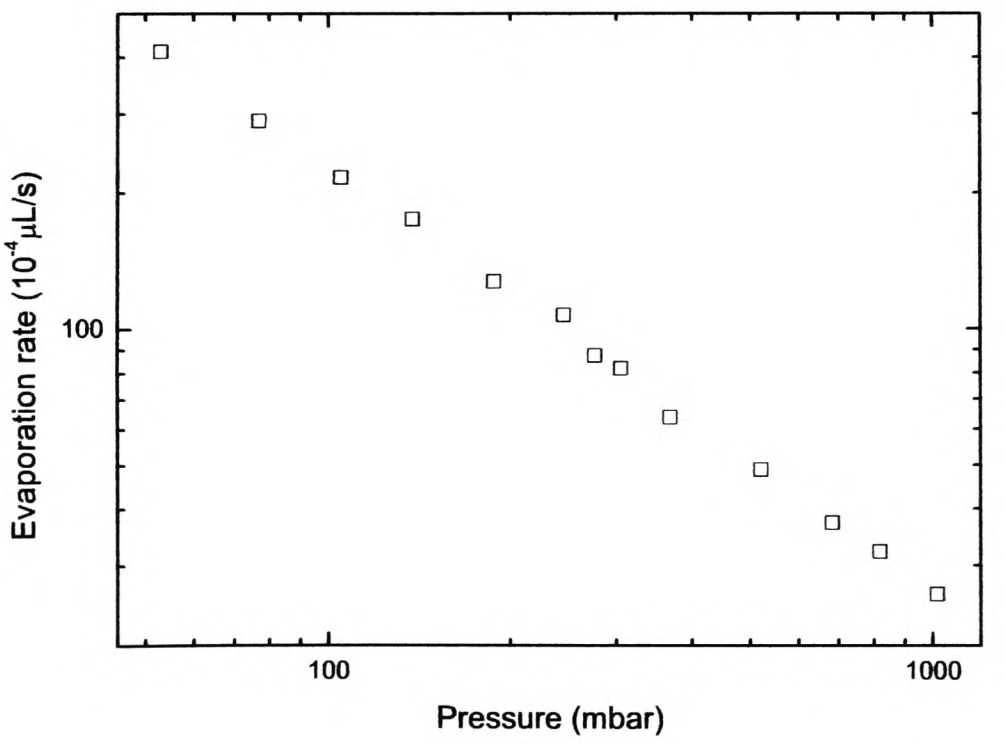

Figure 7.4: *Experimental measurement of the evaporation rate against ambient pressure (from* 40 *mbar to* 1000 *mbar). Water drops with an initial volume of* 2.5 μL.

The difference between each case seems to be proportional to the values of the diffusion coefficient of Water vapour into these gases, see Table 7.1 page 109.

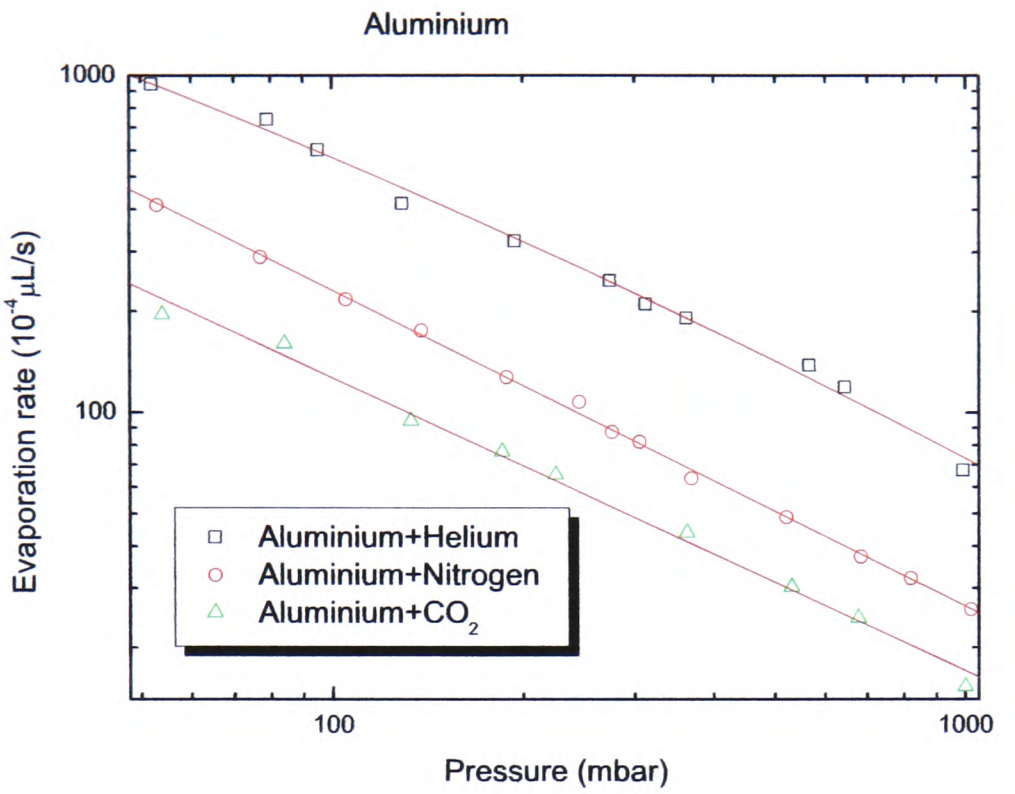

Figure 7.5: *Evolution of a Water drop evaporation rate as a function of the base radius.*

The fact that the evaporation rate for Helium is larger than that of Nitrogen and Carbon Dioxide indicates that the evaporation is mainly controlled into the ambient. The substrate being a good thermal conductor does not seem to have a major influence.

7.3 Discussion

When a drop is deposited on a substrate, it evaporates spontaneously (if the environment is not saturated). The evaporation process in this situation is thought to be diffusion limited. The model presented in the previous chapter is based on this assumption. In this case the process can be regarded as quasi steady-state. The vapour concentration at the interface is usually assumed to be the saturation value $c_v(T_s)$ and zero far from the drop. The driving force for the evaporation and diffusion is the concentration gradient between the interface and far from the drop. In order to be able to estimate the evaporative mass flux, J, the diffusion coefficient as well as the saturation concentration at the interface needs to be properly estimated (see Equation 6.14 page 104). The diffusion coefficient will depend on the nature of the ambient gas as well

as ambient pressure. The saturation concentration at the interface will mainly depend on the liquid temperature of the drop. In the "Theory" chapter (section 7.1 page 109) it is shown that the theory describing diffusion in binary gas mixture has been well developed. Solving the Boltzmann equation Chapman and Enskog [26] derived the following expression for the diffusion coefficient in a binary gas system:

$$D_{AB} = \frac{0.00266T^{3/2}}{PM_{AB}^{1/2}\sigma_{AB}^{2}\Omega_{D}} \tag{7.1}$$

where D_{AB} is the diffusion coefficient ($cm^2.s^{-1}$), T is the temperature (K), P is the pressure (bar), σ_{AB} is the characteristic length (A) and Ω_D is the diffusion collision integral (dimensionless).

The expression of the binary diffusion coefficient shows a well known result: D_{AB} is inversely proportional to pressure and depends on the nature of the ambient gas. Equation 7.1 is used to estimate the diffusion coefficient for each gas in the range of investigated pressure. The so estimated diffusion coefficients are plugged into the expression of J (Equation 6.14 page 104) to calculate the evaporation rate:

$$\rho\frac{\mathrm{d}V}{\mathrm{d}t} = -2\pi\int_{0}^{R} J(r,t)\, r\sqrt{1+\left(\frac{\partial h}{\partial r}\right)^{2}}\,\mathrm{d}r \tag{7.2}$$

The obtained evaporation rates for the three gases in the range of investigated pressure are then compared to the experimental data on Figure 7.6. It is observed that the mathematical model overestimates the evaporation rates but the trends are very similar. These similarities are also revealed on Figure 7.7 where the diffusion coefficients have been fitted. This overestimation is not fully understood yet but one explanation could be the humidity formation by the molecules evaporated from the droplet.

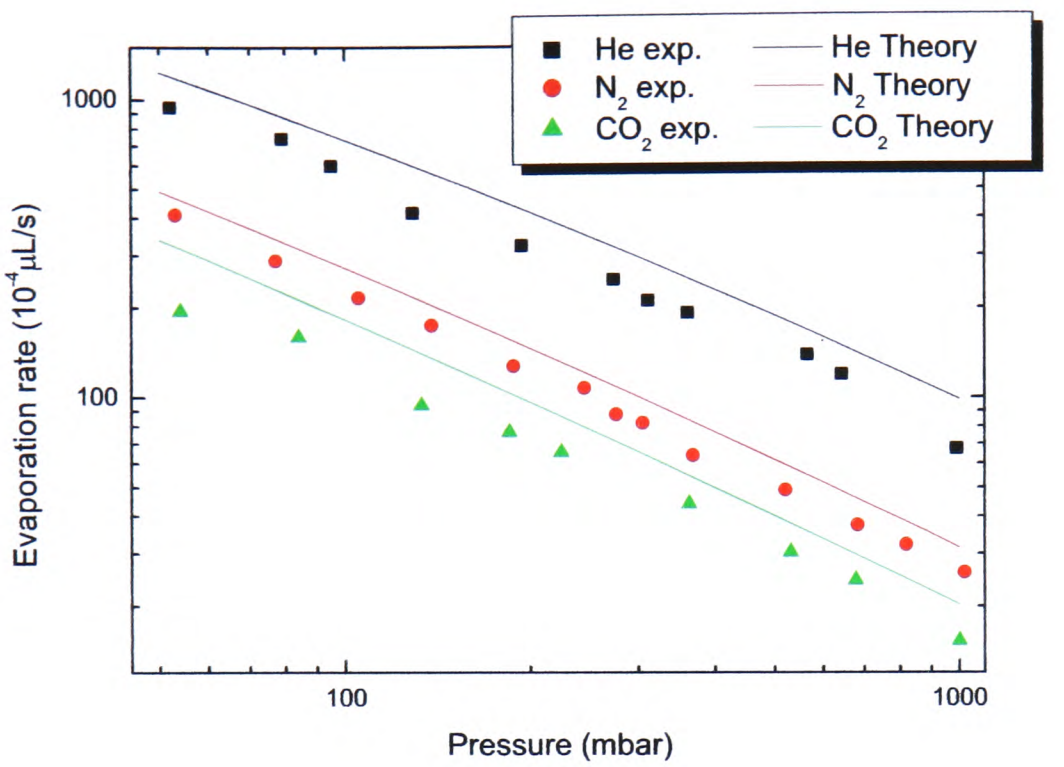

Figure 7.6: *Comparison between experimental results and theory.*

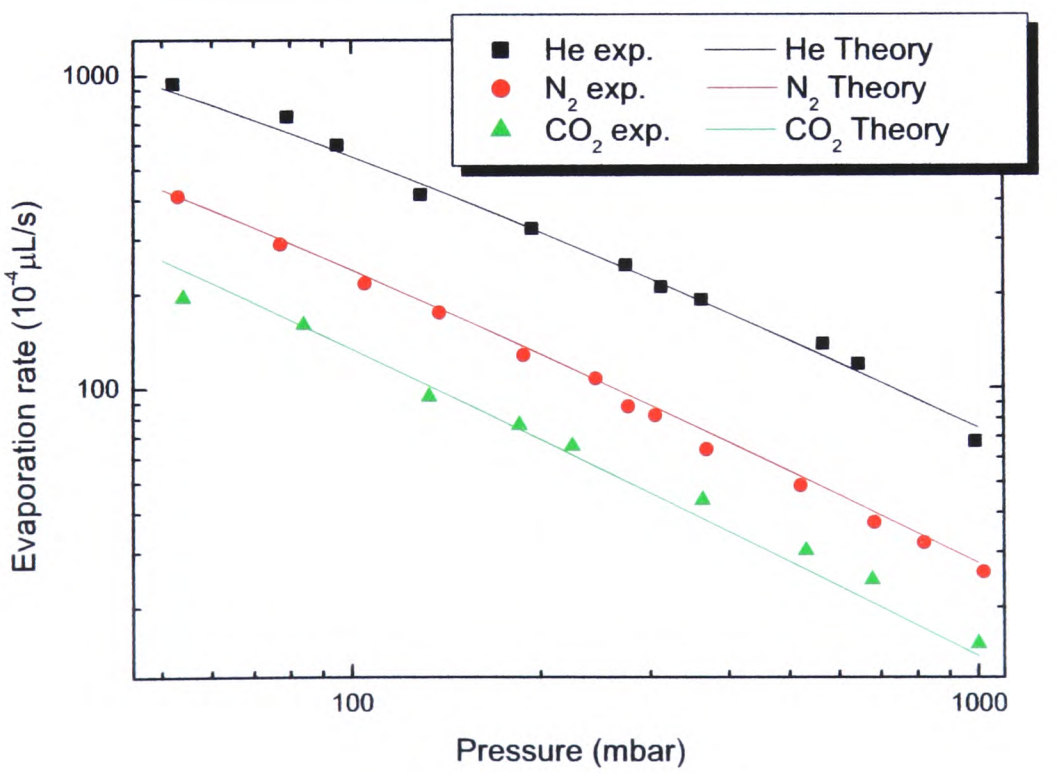

Figure 7.7: *Comparison between experimental results and theory.*

7.4 Conclusion

In this chapter an experimental study is undertaken to investigate the evaporation of pinned sessile drops. The role of vapour diffusion as a limiting mechanism for evaporation is investigated. The ambient pressure as well as the nature of the ambient gas is varied to look at the effect of changing the diffusion coefficient. A diffusive theoretical model is used to compare the obtained experimental data for the evaporation rate. When using ambient gases with higher diffusion coefficient, higher evaporation rates are observed.

Chapter 8
Effect of substrate thermal properties

8.1 Introduction

In the present chapter, two mains investigations on the influence of substrate thermal properties will be presented. In all experiments, four different materials based on their thermal conductivity have been used. The first investigation has been undertaken at atmospheric pressure. The experiments have been performed with three liquids (Water, Acetone and Methanol) for various drop sizes. In the second investigation, Water drops (R = 1.35 mm) are used and evaporating in an atmosphere for a range of pressures (from 40 $mbar$ to 1000 $mbar$). Three gases were used: Helium, Nitrogen and Carbon Dioxide. The above mentioned conditions will allow us to investigate the precise role played by substrates thermal properties in the evaporation of drops.

8.2 Experimental conditions

8.2.1 Liquids

The three liquids used for this experiment were deionised Water, Acetone and Methanol. They were chosen because of their volatility and wetting properties. Acetone and Methanol were purchased from Fisher Scientific (Loughborough, United Kingdom). Acetone has a purity of 99% and Methanol 99.8%. Deionised Water was supplied by a high purification system, the "Barnstead NANOpure Diamond" system (Dubuque, Iowa USA). It supplies Water with a resistivity of 18.2 $m\Omega/cm$. More details on the physical properties of used liquids are given in Table 8.1.

As the three liquids have very different surface tension (Water in comparison with Acetone and Methanol, see Table 8.1), depositing drops of identical volumes generates sessile drops sizes (base diameter and contact angle) with large differences. To keep the spherical shape, sessile drops radii have to be less than the capillary length, κ^{-1}, (see Table 8.1). This corresponds to a volume less than 8 μL for water drops for example.

		Water	Acetone	Metahnol
γ	mN/m	71.99	22.72	22.07
ρ	kg/m^3	998	788	790
κ^{-1}	mm	2.71	1.71	1.69
$Viscosity$	$mPa.s$	0.890	0.306	0.544
Cp	$J/mol.K$	75.3	126.3	81.1
k^l	$W/m.K$	0.604	0.161	0.203
L	J/kg	2.45×10^6	5.49×10^5	1.20×10^6
c_{sat}	kg/m^3	1.94×10^{-2}	0.637	0.186
dc_{sat}/dT	$kg/m^3.K$	1.11×10^{-3}	2.84×10^{-2}	1.50×10^{-3}
D	m^2/s	2.46×10^{-5}	1.06×10^{-5}	1.50×10^{-5}

Table 8.1: *Values of the physical parameters for the different liquids used.*

8.2.2 Substrates

In order to isolate the effect of thermal conductivity of the substrate, four samples were chosen and prepared to satisfy the following:

- a large range of thermal conductivity, four orders of magnitude,
- identical surface energy,
- non ideal rough surfaces to pin the triple line but with a similar surface roughness to obtain equivalent contact angles.

From the wide range of available materials, four substrates were selected according to their thermal conductivity: PTFE (2.5 $W/m.K$), Macor (1.46 $W/m.K$), Titanium (21.9 $W/m.K$) and Aluminium (237 $W/m.K$). Full details on their properties are given in Table 8.2. PTFE (polytetrafluoroethylene) is a fluoropolymer and characterised with a very low surface energy and thermal conductivity. Macor is a brand name for a machinable glass ceramic. It is a white, porcelain-like (in appearance) material composed of approximately 55% fluorophlogopite mica and 45% borosilicate glass. Its thermal conductivity is similar to the one of glass. Titanium and Aluminium are both metals. Titanium has a lower thermal conductivity compared to Aluminium. Selected materials have then been surface analysed to compare their surface roughness similarities. This task has been achieved using a microscope interferometer (see details in 3.6 page 61) and an example of surface topography can be seen on Figure 8.1. It is found that the substrates have the same order of magnitude of roughness, i.e. between 240 nm (PTFE) and 440 nm (Titanium).

		PTFE	Macor	Titanium	Aluminium
k^s	$W/m.K$	0.25	1.46	21.9	237
C_p	$J/g.K$	1	0.79	0.523	0.897
ρ	kg/m^3	1200	2520	4507	2700
$Surface\ roughness$	nm	240	276	440	306

Table 8.2: *Substrates physical properties*

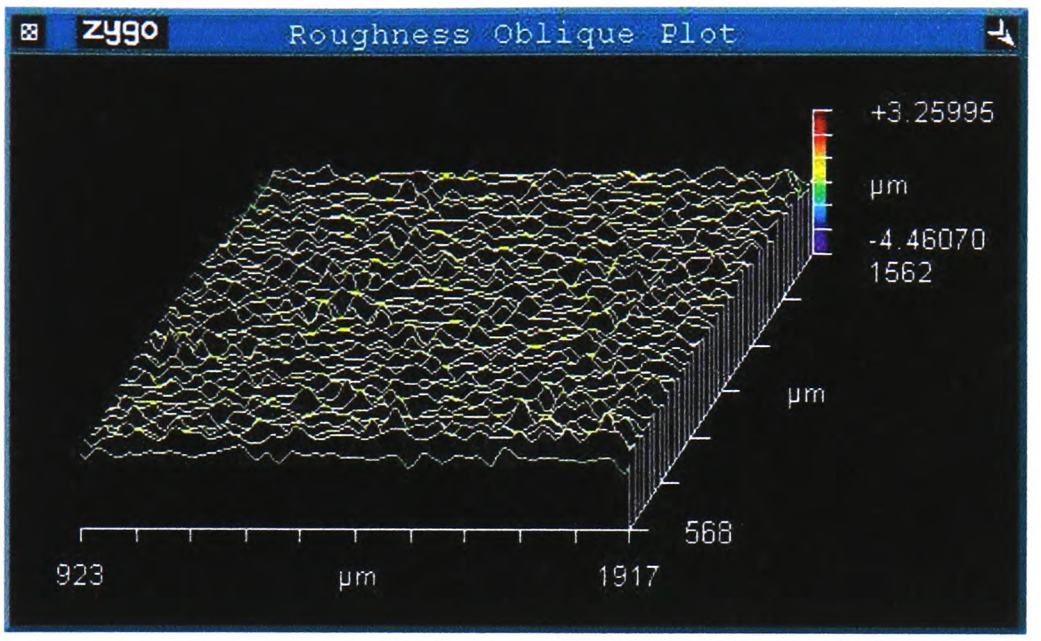

Figure 8.1: *Surface roughness profile (Aluminium sample).*

The four substrates have all the same dimensions, $10 \times 10 \times 1mm$ (see picture 8.2).

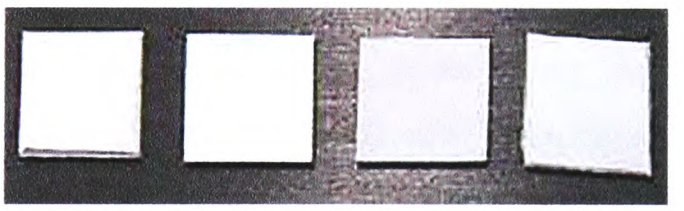

Figure 8.2: *Top view of the four substrates used. From the left side: Aluminium, Titanium, Macor and PTFE*

In order to get the same surface energy a very thin layer of Aluminium, 3 μm, was deposited on all substrates. As Aluminium has the highest thermal conductivity, the thin layer does not alter the thermal conductivity of the substrates. This process has been performed at the Scottish Microelectronics Centre (Research Centre part of the University of Edinburgh). For this process, thermal evaporation technique was used. The material to be deposited is placed on an electric resistance to melt and raise its vapour pressure. The target surface is cooler and faces the material. It allows the up coming particles to form a solid layer. This is done in high vacuum to allow the particles to travel as freely as possible and reduce the impurities.

In the case of Methanol and Acetone, the substrates had also to be coated with a thin layer of Parafilm® (does not modify the thermal conductivity). Their surface tension is too low and so they wet completely the Aluminium surfaces. The Parafilm® decreases the surface energy and hence the initials contact angles are enhanced (see Figures 8.3(a) and 8.3(b)).

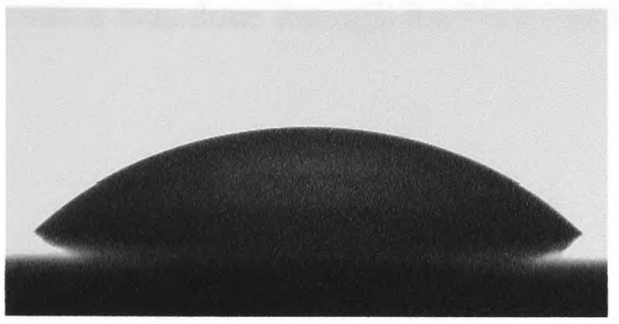

(a) Initial Metahnol drop shape on a Aluminium substrate (covered with Parafilm).

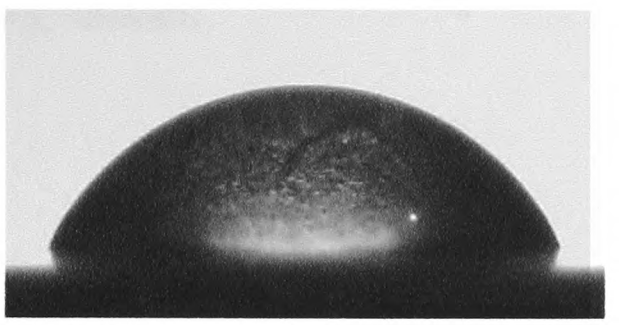

(b) Initial Water drop shape on a Titanium substrate (Aluminium coated).

Figure 8.3: *Illustration of Water and Metahnol initial drop shape.*

As no specific requirements are needed to clean the four materials, the cleaning process is the same as for the two previous experiments. Ten minutes immersion in an Acetone ultrasonic bath, rinsing with deionised water and drying under a Nitrogen flow.

8.2.3 Temperature measurements

To measure the temperature profile inside and around the droplets, miniature thermocouples were used (purchased from Omega Engineering, Manchester, United Kingdom), 0.025 mm in diameter and 0.125 mm at the junction. Such small dimensions minimize the interaction between the wire and the liquid interface (see Figure 8.4). It also allows performing measurements close to the interface and the triple line. The response time is 0.05 seconds and the accuracy is $\pm 0.01\,^{\circ}C$. These thermocouples were very fragile and hence difficult to manipulate. It was necessary to keep the wires lengths short to overcome surface tension and pierce the liquid surface. The thermocouples are attached to a small plastic tip (see top left picture in Figure 8.4) to unable them to be introduced into the drop. Finally the wires were connected to a data acquisition system. The temperatures data were stored into a PC via a data acquisition system (data logger from Pico Technology Ltd, United Kingdom). It recorded the temperature evolution in time (see for example Figure 8.6 page 125).

Two kinds of measurement were performed with the thermocouples: inside and outside the environmental cell. Due to the design and use of the low pressure chamber, the position of the thermocouple was fixed. Only the drop could move up and down (see cell description section

3.2 page 59). As the step of the z-axis step motor was not small enough the measurement could only be done into the sessile drop bulk (see bottom pictures in Figure 8.4). The measurement which were not performed inside the cell allowed to move precisely the thermocouple into the droplet. The thermocouple was positioned using a double axis stage. In both cases the visualisation was done through the DSA100 imaging software.

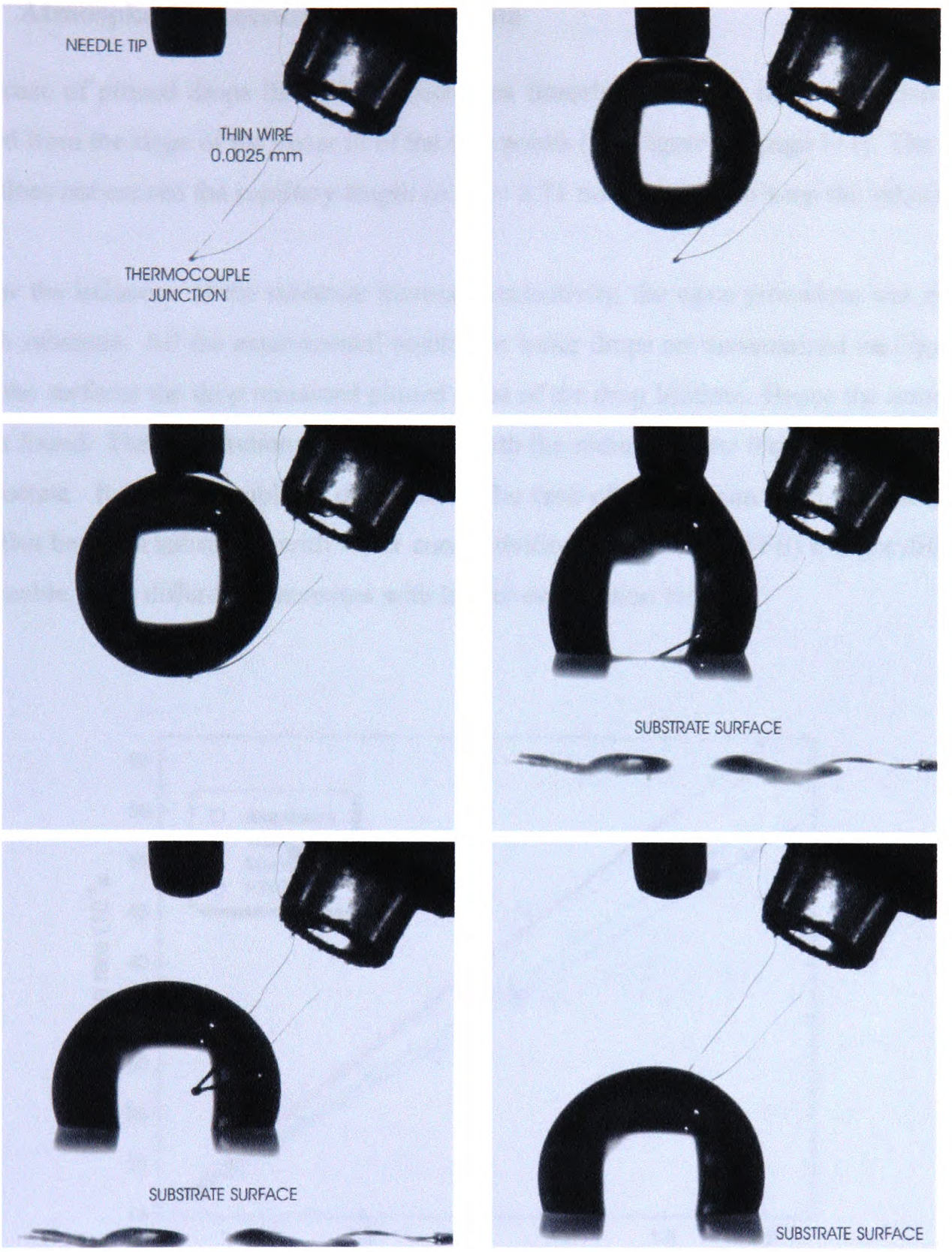

Figure 8.4: *Steps of the temperature measurements process in the low pressure chamber. On the first picture, the positions of both the needle tip and the thin thermocouple before the drop formation are shown. They are both fixed, only the substrate can move up and down. The drop is then injected and the sample lifted to pick it up. Once the sessile droplet is formed, measurement can only be obtained along a vertical position by moving the sample stage.*

8.3 Experimental results

8.3.1 Atmospheric pressure measurements

In the case of pinned drops the volume decreases linearly with time, the evaporation rate is deduced from the slope of the linear fit of the data points (see Figure 7.2 page 111). The droplet radius does not exceed the capillary length ($\kappa^{-1} = 2.71$ mm) in order to keep the spherical cap shape.

To show the influence of the substrate thermal conductivity, the same procedure was repeated on each substrate. All the experimental results for water drops are summarized on Figure 8.5. On all the surfaces the drop remained pinned most of the drop lifetime. Hence the same linear trend is found. The evaporation rate increases with the radius and the thermal conductivity of the substrate. It is not possible to differentiate the case of Aluminium from the one of Titanium. But between substrates with lower conductivities (Macor and PTFE) a slight difference is noticeable. This difference increases with higher evaporation rates.

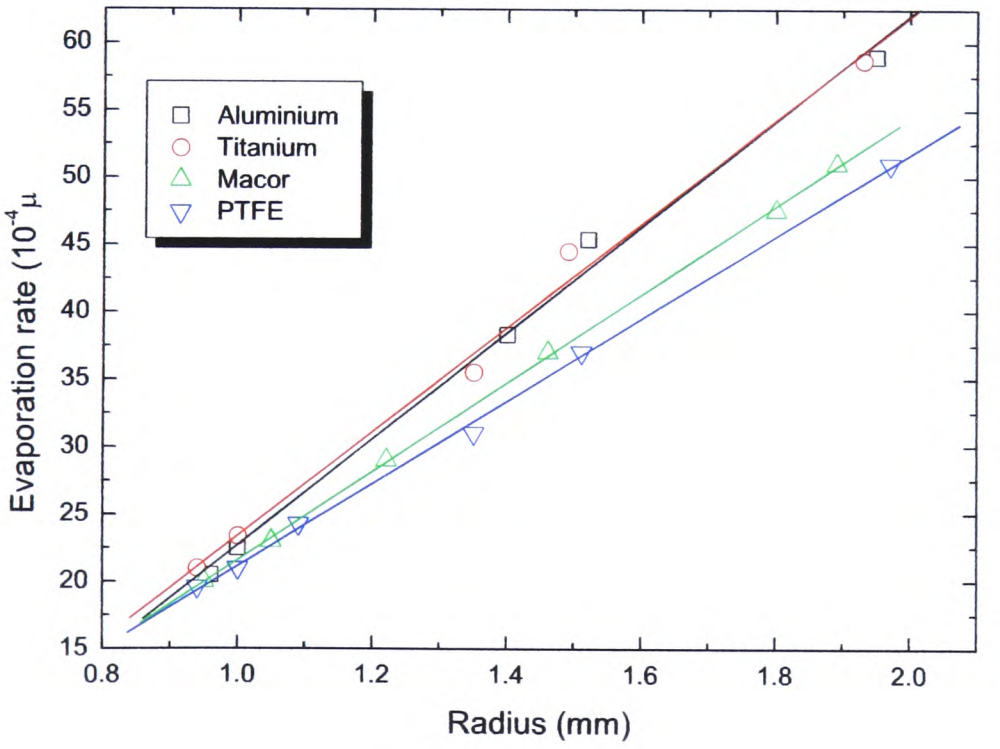

Figure 8.5: *Evolution of Water drops evaporation rates as a function of the base radius.*

These evaporation rates data were completed with temperature measurements. Instead of looking at the absolute temperature of the drop bulk, the temperature difference between the ambient gas and the drop was investigated. An example of temperature measurement is illustrated on

Figure 8.6. A thin thermocouple is introduced into the drop bulk for few hundreds seconds to measure any fluctuation. On the graph in Figure 8.6, it is observed that the temperature is almost constant over the measurement period. The temperature difference between the drop and the atmosphere is then determined. All these data are reported on Figure 8.7. It can be first noticed that the temperature is slightly influenced by the drop size (small changes in the case of PTFE for larger drops). It is also found that on both Aluminium and Titanium the temperature difference is negligible. It is however higher for Macor and highest for PTFE. The temperature decreases due to the loss of energy needed by the evaporation. From these results it is worth noticing that there is virtually no difference between Aluminium and Titanium despite an order of magnitude difference in thermal conductivity (see Table 8.2 page 120).

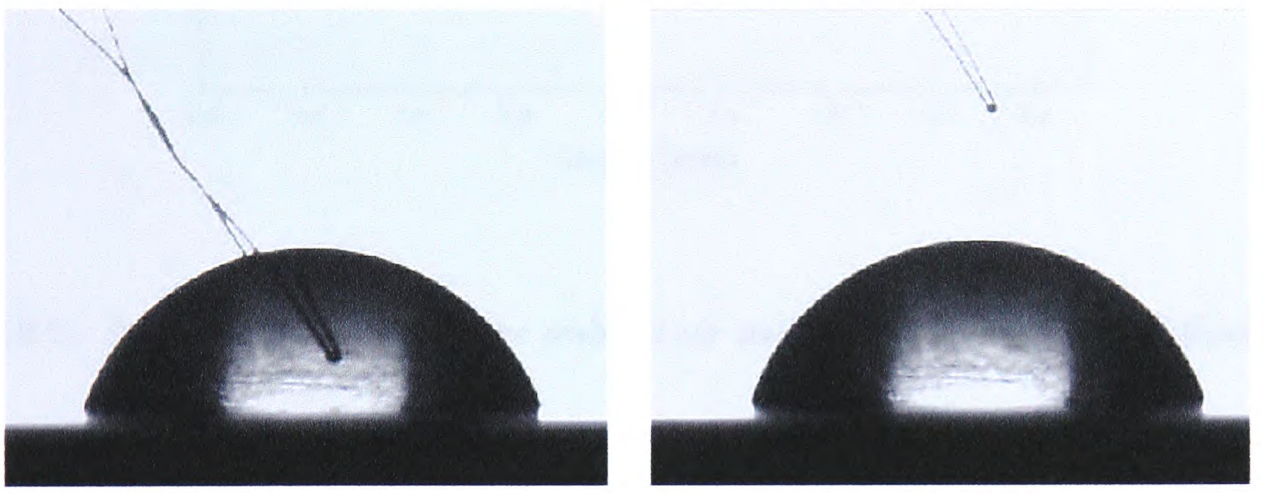

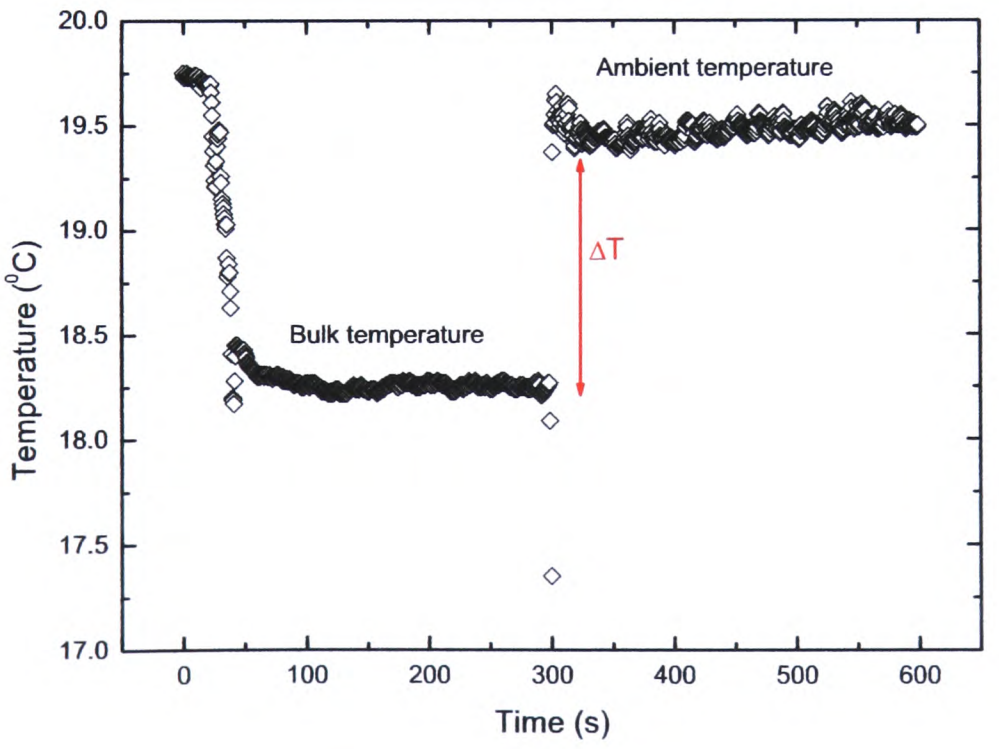

Figure 8.6: *Example of temperature measurement between the ambient gas and the drop bulk.*

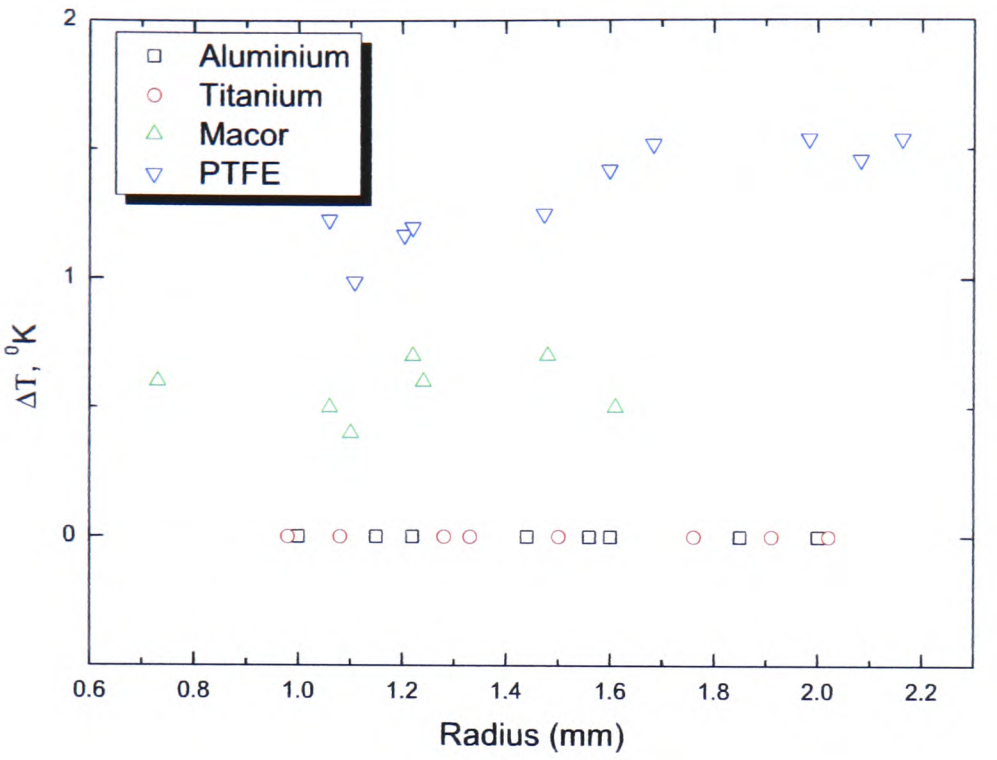

Figure 8.7: *ΔT measured between the ambient air and the water droplet for different base radii on each substrates.*

Complementary temperature measurements have been performed to understand the primary instants of the evaporation process. In this case, the thermocouple is stuck on the substrate surface, the drop hanging from the delivery needle is then gently deposited on the substrate on the top of the thermocouple, see Figure 8.8. The temperature measurements presented on Figures 8.9 and 8.10 represent the evolution of the temperature before and after the deposition of the pendant drop. It means that the first stage corresponds to the ambient temperature and the second to the drop bulk temperature. Two kinds of measurement have been performed depending on the formation time of the hanging drop. As it can be seen on Figure 8.9 after about 20 seconds the measured temperature drops at the very moment of the drop deposition. The temperature is found to increase afterwards then slightly decrease and reach a steady state. On Figure 8.10, a similar drop has been hanging for a shorter period of time. The bulk temperature at the deposition is now higher and decreases towards a steady state after $50\ s$. This experiment shows that over the time the drop has been hanging, the evaporation process starts and hence the cooling effect. This is revealed by the value of the temperature at the very moment of the drop deposition. It also confirms that the steady state is reached relatively quickly, no more than $50\ s$.

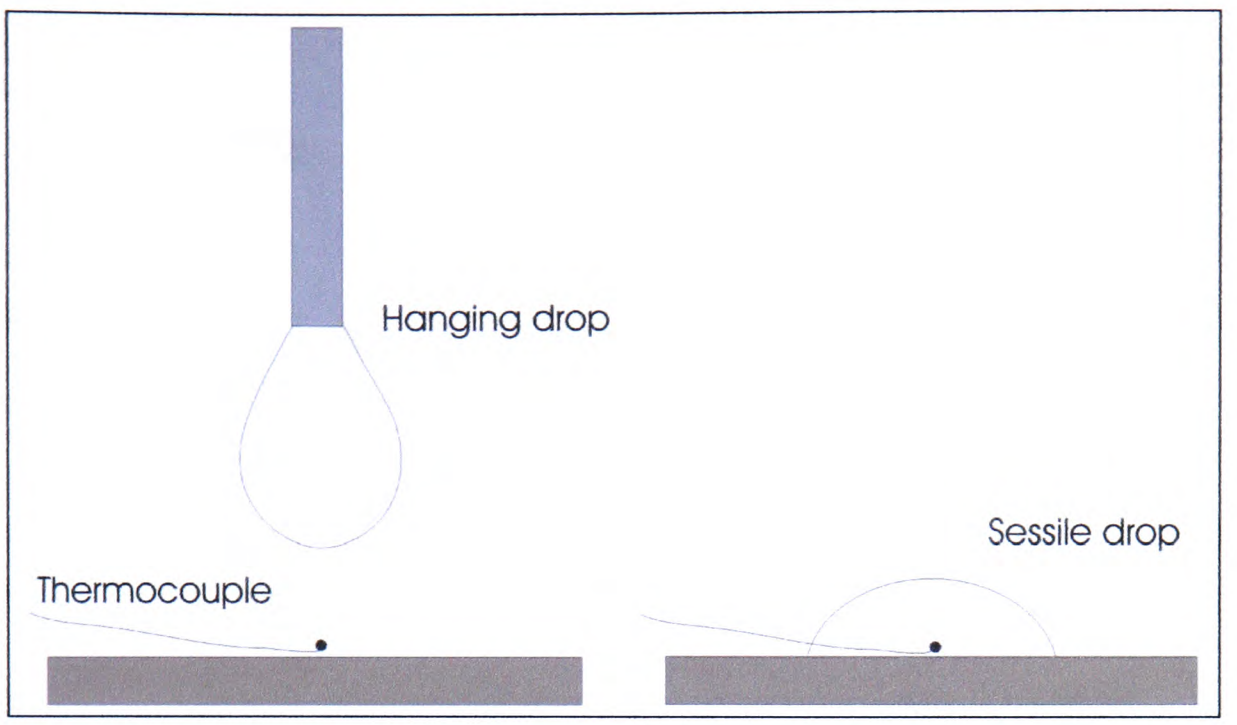

Figure 8.8: *Scheme of the drop deposition on substrate (thermocouple)*

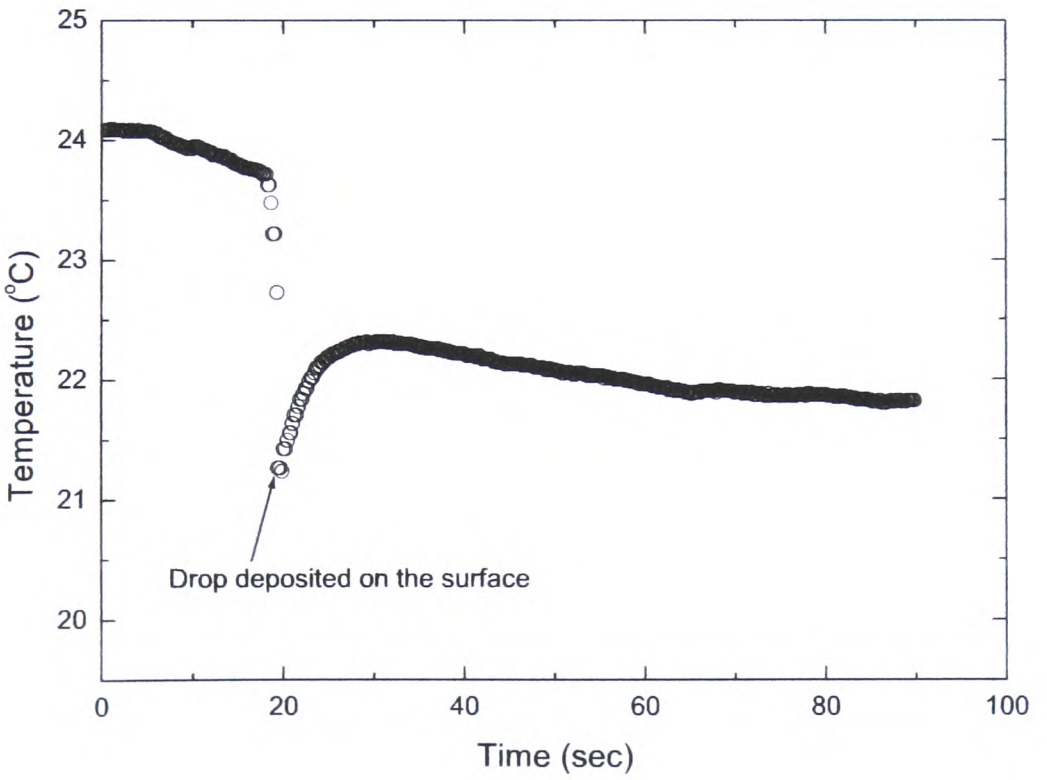

Figure 8.9: *Temperature evolution as Water drop is deposited on PTFE substrate on top of the thermocouple.*

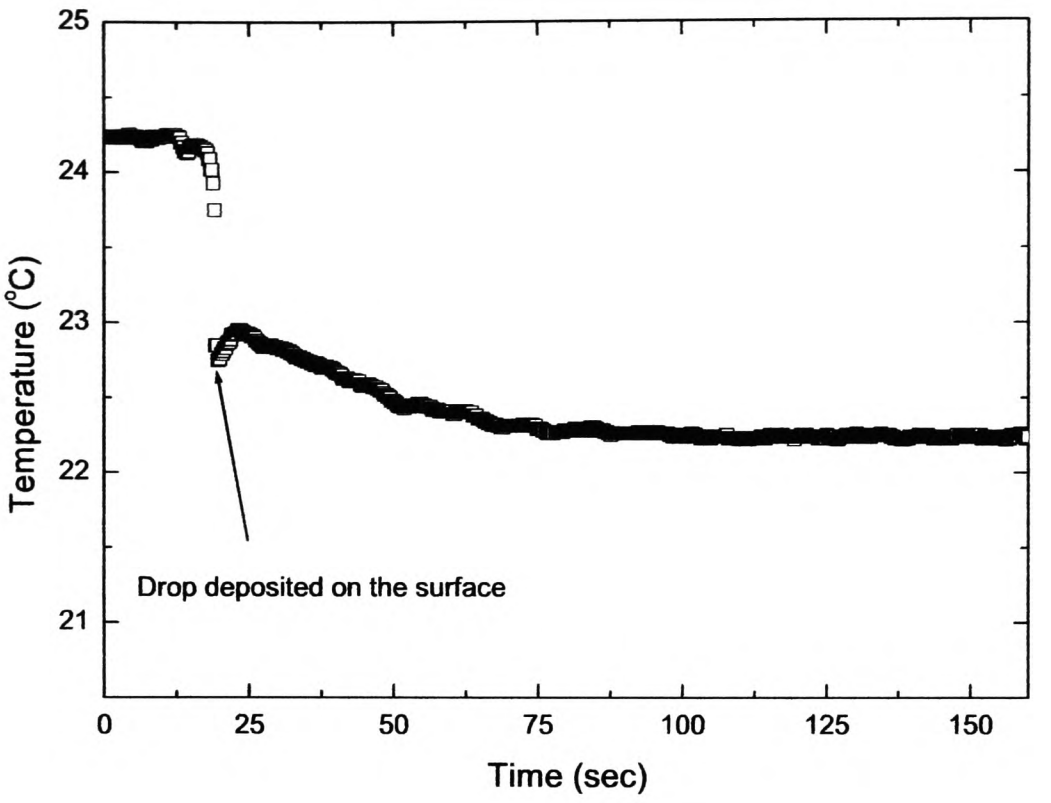

Figure 8.10: *Temperature evolution for a similar drop (Figure 8.9) which has been hanging for a shorter period of time.*

In order to gain more insight into the investigated problem, various liquids were used on the two extreme substrates in terms of thermal conductivity (Aluminium and PTFE). Acetone and Methanol have been selected. Their thermo-physical properties as well as wettability are different (see Table 8.1 page 119). They are more volatile than Water, their saturation pressure at room temperature is 10 times higher than that of Water.

The evaporation rates of drops of various sizes (ranging from 0.5 to 8 μL not to exceed the capillary length) are measured on Aluminium and PTFE. The results presented on Figure 8.11 show that for each liquid the evaporation rate on Aluminium is always higher than on PTFE. The difference in evaporation rates on the two substrates increases with the liquid volatility.

Again, these results were completed with temperature measurements inside the drops. The experiments undertaken with Acetone and Methanol were more difficult. Due to the high evaporation rate and low initial contact angle the contact line depinning occurred after only 20 seconds. The tests were realised with the largest volume (6 μL) to have more time to introduce the thermocouple into the droplet. The values are summarized in Table 8.3. In agreement with the results obtained with Water, the temperature difference decreases with the thermal conductivity.

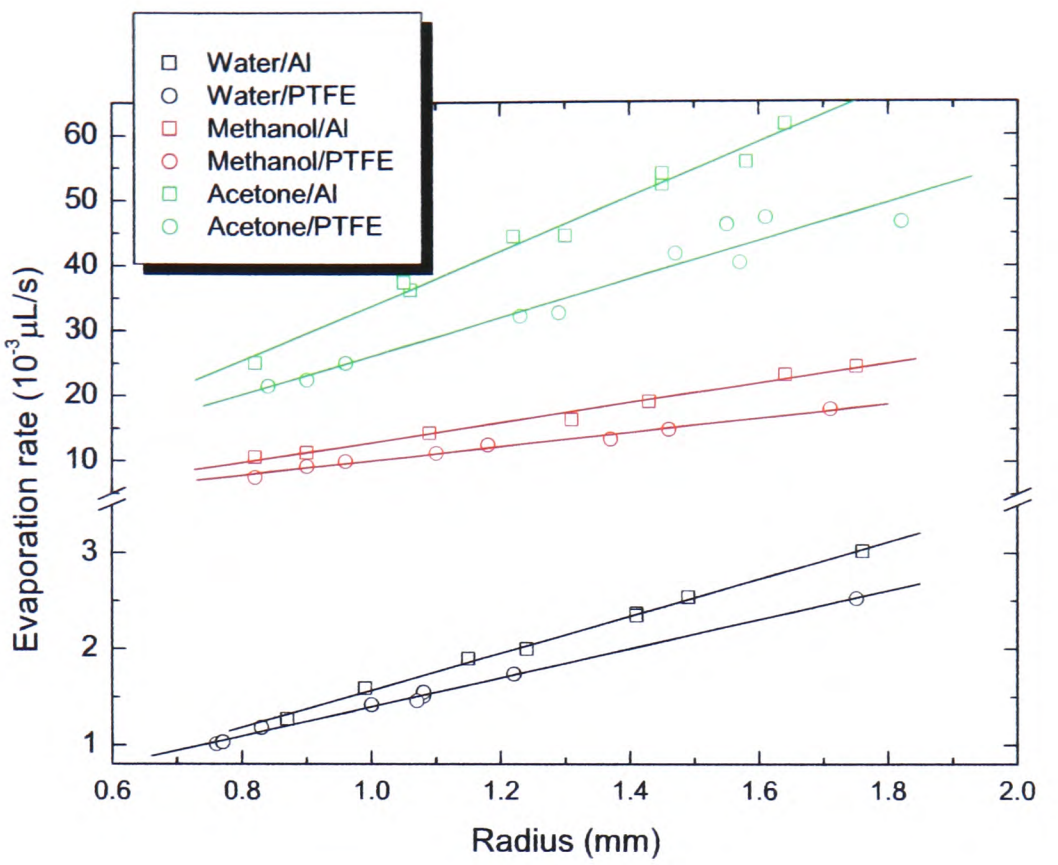

Figure 8.11: *Comparison of the evolution of the evaporation rate with the radii between Acetone, Methanol and Water on both Aluminium and PTFE substrates.*

However with Acetone and Methanol the temperature variations in the case of Aluminium is not negligible anymore. The temperature drops by $3.6\,°C$ for Methanol and $4\,°C$ for Acetone.

	$\Delta T(K)$		
	Water	Methanol	Acetone
Al	0	3.6	4
Ti	0	–	–
Macor	0.6	–	–
PTFE	1.3	6.9	8.6

Table 8.3: *Temperature difference between the ambient air and the droplet bulk.*

It is clear from the above findings that the evaporation rate is influenced by the thermal properties of the substrate. Furthermore a strong evaporative cooling is revealed for higher evaporation rates.

8.3.2 Reduced pressure

Following these very interesting results it was decided to look at the case of higher evaporation rates. As it has been demonstrated in the previous chapter one way of enhancing evaporation is to reduce the surrounding pressure. It was decided to run all the experiments with similar size Water drops as Acetone and Methanol are far too volatile to be used in a low pressure environment. The results are presented in Figure 8.12. In agreement with the results demonstrated in the previous chapter, the evaporation rates obtained are greater with Helium than Nitrogen and Carbon Dioxide. The evaporation rates are ranging from $20 \times 10^{-4} \mu L/s$ at atmospheric pressure to $1000 \times 10^{-4} \mu L/s$ at the lowest pressures ($\sim 40\ mbar$) on an Aluminium substrate. When the drops evaporate in a Carbon Dioxide environment, the evaporation rate exhibits a noticeable difference mainly at the lowest pressure. As expected, this difference increases with Nitrogen and Helium gases. It confirms the precedent results that Water drops evaporation exhibit higher evaporation rates when resting on higher thermal conductive substrates. It is also important to notice that, at the difference of atmospheric pressure measurements, a difference appears between Aluminium and Titanium substrates at high evaporation rates. It means that at lower pressures the thermal conductivity of Titanium starts to have a limiting effect.

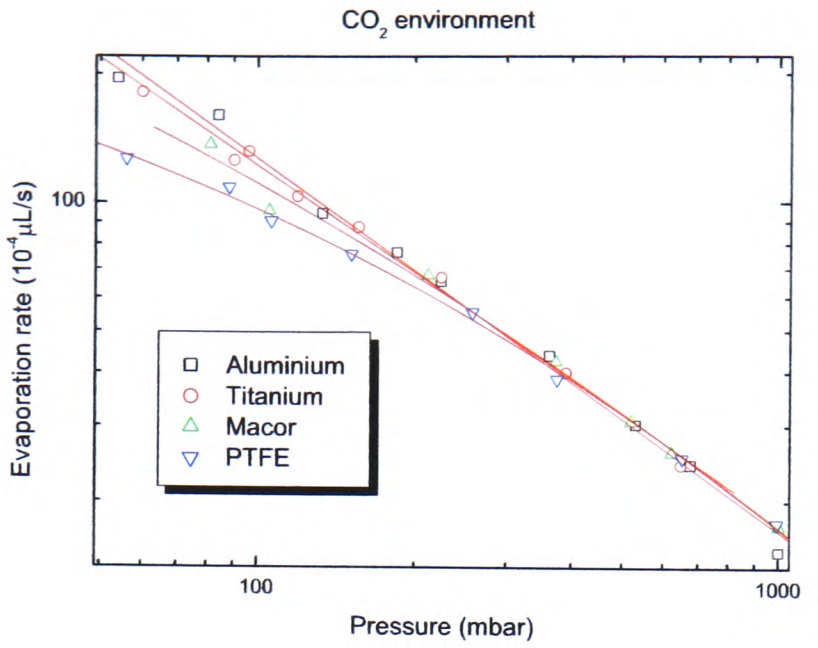

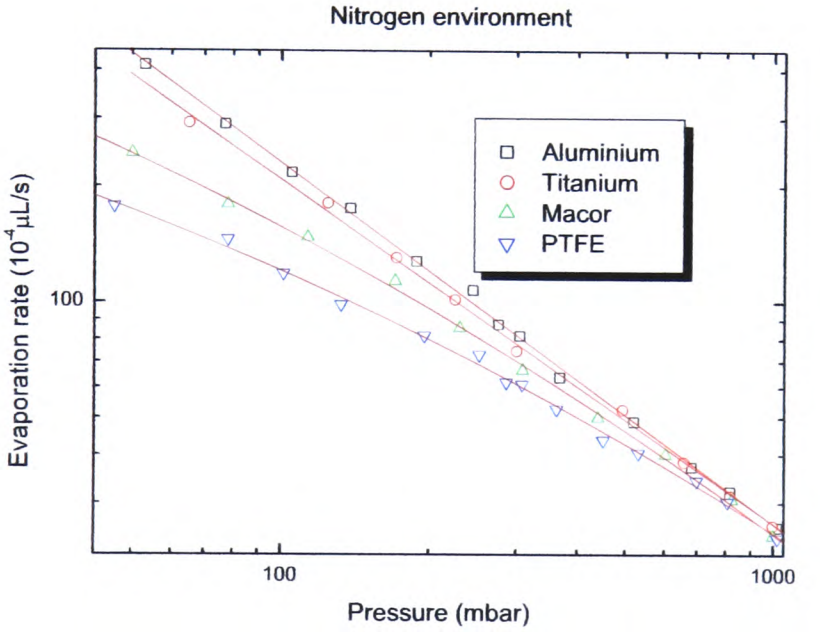

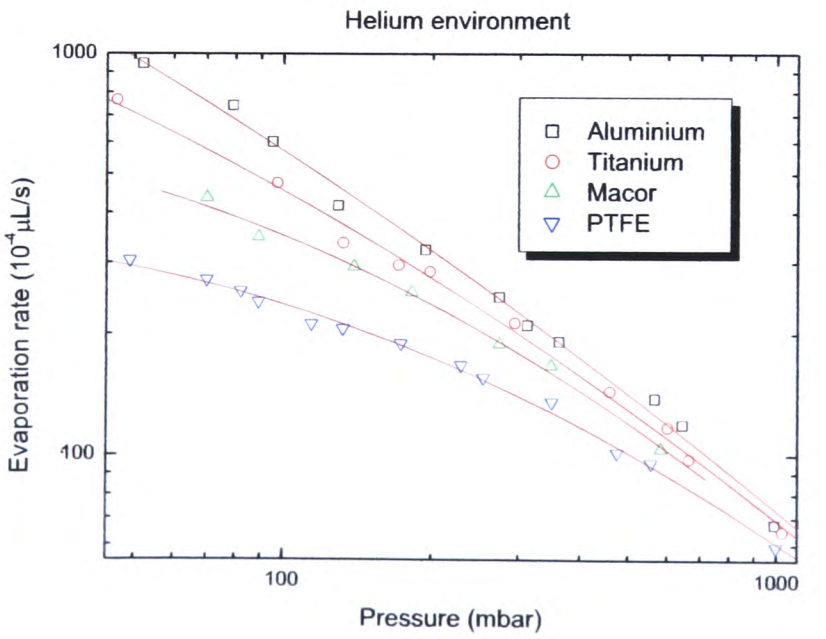

Figure 8.12: *Evaporation rates of Water drops on each substrate in three different environments (He, N_2 and CO_2) for different pressures at ambient temperature (22 °C).*

Again, temperature measurements have been undertaken in an attempt to demonstrate the cooling effect. These measurements have been performed in an Helium environment for the lowest and highest thermal conductivity substrates, PTFE and Aluminium respectively. As explained in the experimental description part, these measurements, which have been performed inside the "low pressure " chamber, were much more challenging. The accuracy is poorer and the temperatures indicated are to be considered as trend values. Nevertheless, these data reveal a great variation of the bulk temperature over the range of investigated evaporation rates. On Figure 8.13, the trend of the temperature measurement is very similar to the evaporation rate one. There is an important decrease of the temperature at high evaporation rates even with the drops resting on Aluminium.

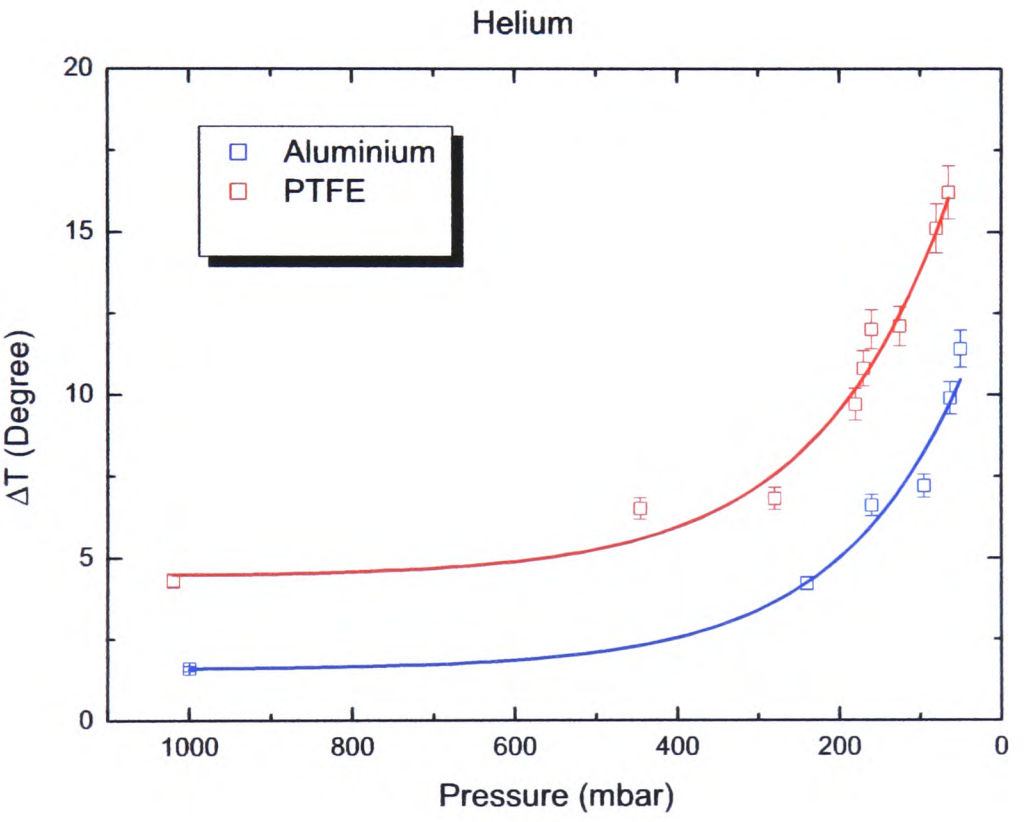

Figure 8.13: *Bulk temperature measurements of evaporative Water drops on both Aluminium and PTFE in a Helium environment for different pressures at ambient temperature (22 °C).*

8.4 Discussion

In the previous chapter, it was shown that there is a good agreement between the mathematical model and the experimental data. The model is hence applied to the substrates and liquids used in the present study. On Figure 8.14, the theoretical (lines) and experimental (symbols) evaporation rates for Acetone, Methanol and Water drops are plotted against the drop base radius. A good agreement between the theory and the experiment is observed. On Figure 8.15, theoretical temperature profiles in the drop and substrate are plotted for the three liquids deposited on Aluminium and PTFE. A gradient of temperature is only observed with the PTFE substrate. Due to the high thermal conductivity of Aluminium the temperature at the solid-liquid interface is maintained at 295 K. With PTFE substrates, the temperature at the solid-liquid interface varies with the liquid used. For Acetone droplets the temperature is around 290.5 K, 291 K with Methanol and 293.8 K with Water. The comparison between the corresponding temperature of the drop bulk and the experimental measurements (see Table 8.3 page 129) shows a relatively good agreement.

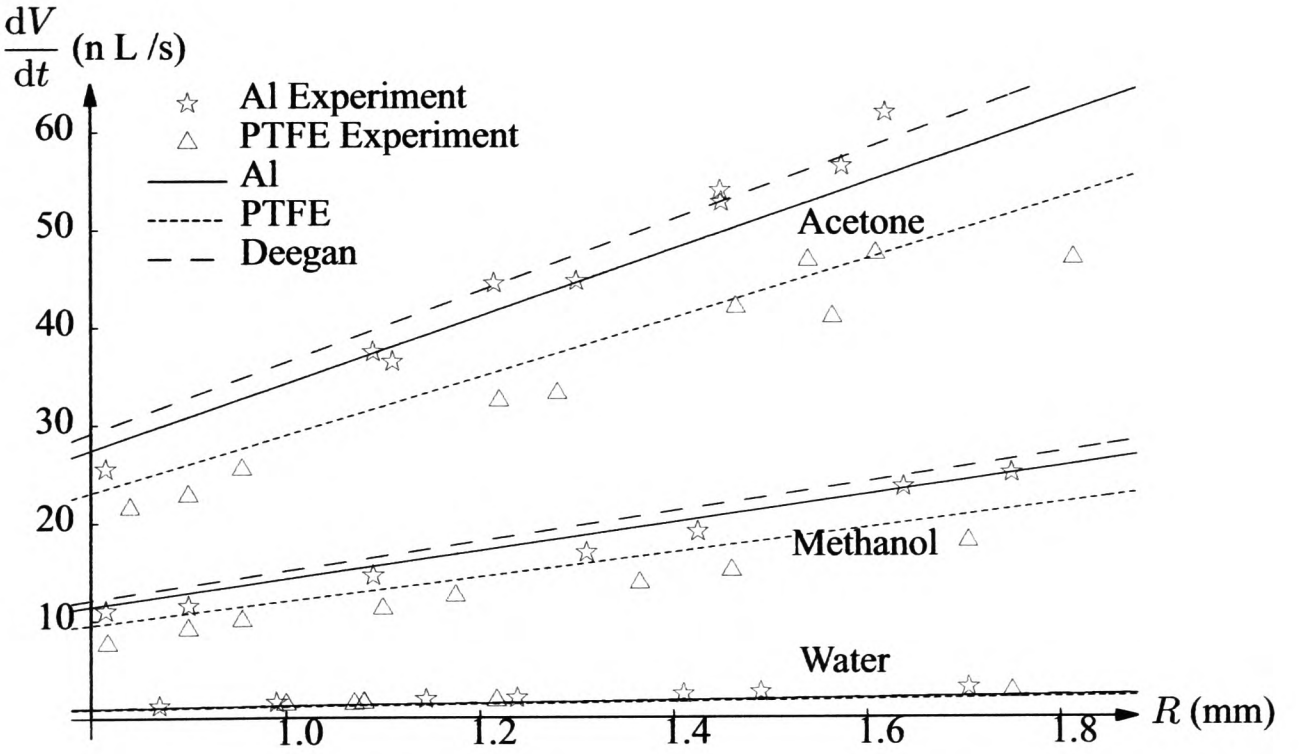

Figure 8.14: *Comparison between experimental results and theoretical predictions of both and Deegan models for the volume V plotted as a function of time t for a methanol droplet with radius $R = 1.43\,\mathrm{mm}$ evaporating into air at temperature $T_a = 295\,\mathrm{K}$ on aluminium and PTFE.*

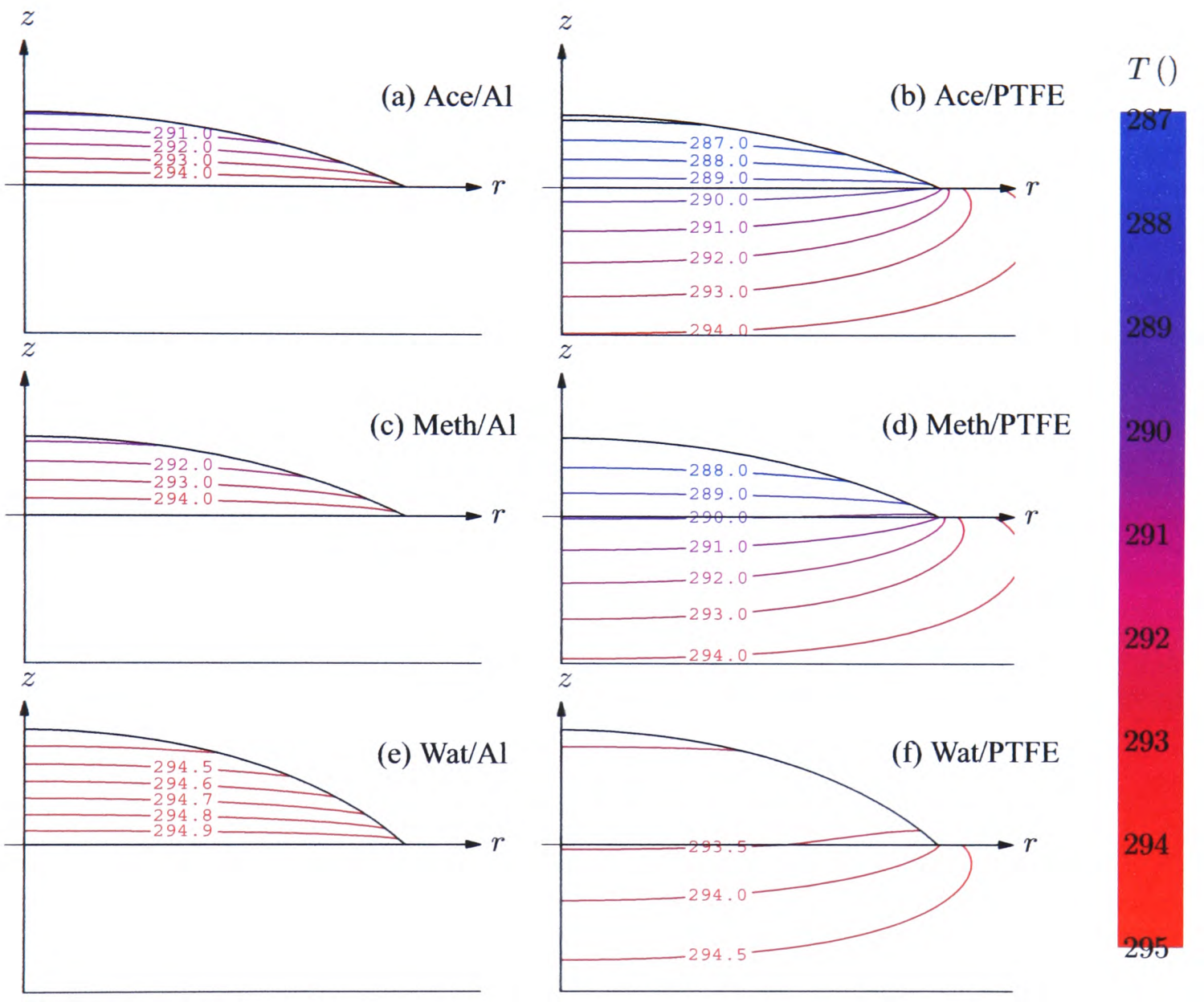

Figure 8.15: *Theoretical prediction of the model for the temperature profile in the drop and the substrate for Acetone, Methanol and Water droplets of radius R=1.35 mm resting on Aluminium and PTFE substrates. The atmosphere has temperature* $T_a = 295\ K$.

The model has also been run for Water drops resting on the four different substrates evaporating into the three gases for the range of experimentally investigated pressure (from 40 to 1000 $mbar$). The comparison between the theoretical results and the experimental measurements are plotted on Figure 8.16. A remarkable agreement is found for the two extreme thermal conductivity (Aluminium and PTFE) but with Macor and Titanium the theory slightly overestimates the experimental data. The corresponding bulk temperature estimation have been plotted on Figure 8.17. A general decrease of the temperature of the drop is observed with higher evaporation rate. On Figures 8.18 and 8.19, the evaporation rate and the drop bulk temperature against the surrounding pressure are plotted on the graph. It shows clearly that the cooling of the drop increases with evaporation rate but has also a limiting effect. When Water droplets are resting on PTFE substrates, the temperature and the evaporation rate are lower than for droplets resting on Aluminium substrates.

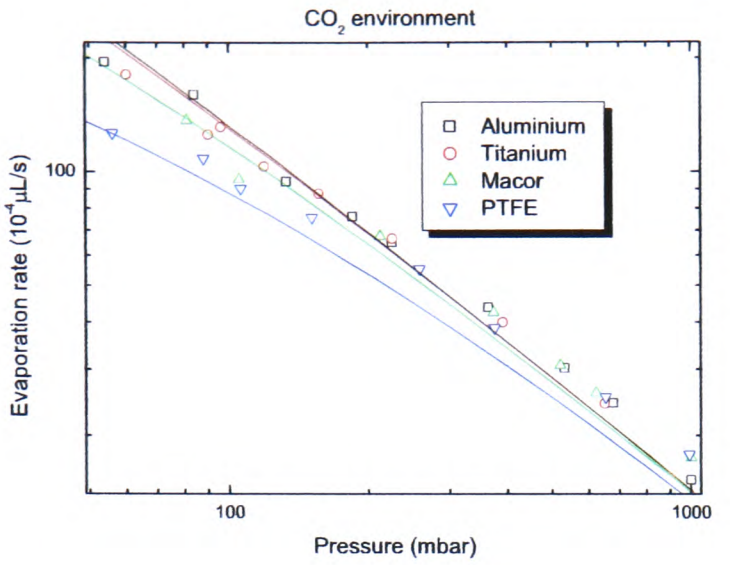

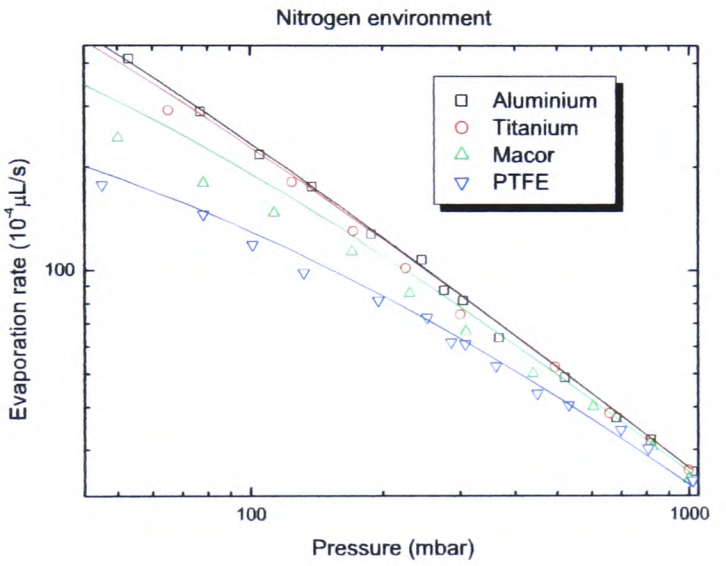

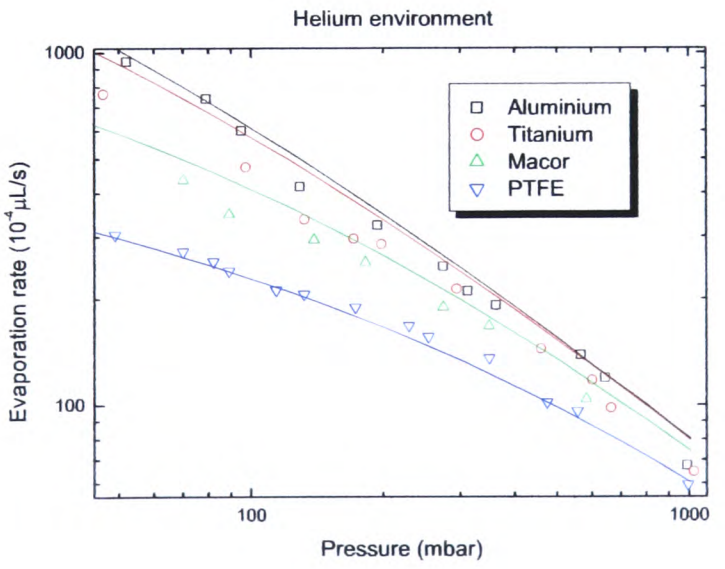

Figure 8.16: *Theoretical evaporation rates of Water drops on each substrate in three different environments (He, N_2 and CO_2) for different pressures at ambient temperature (22 °C).*

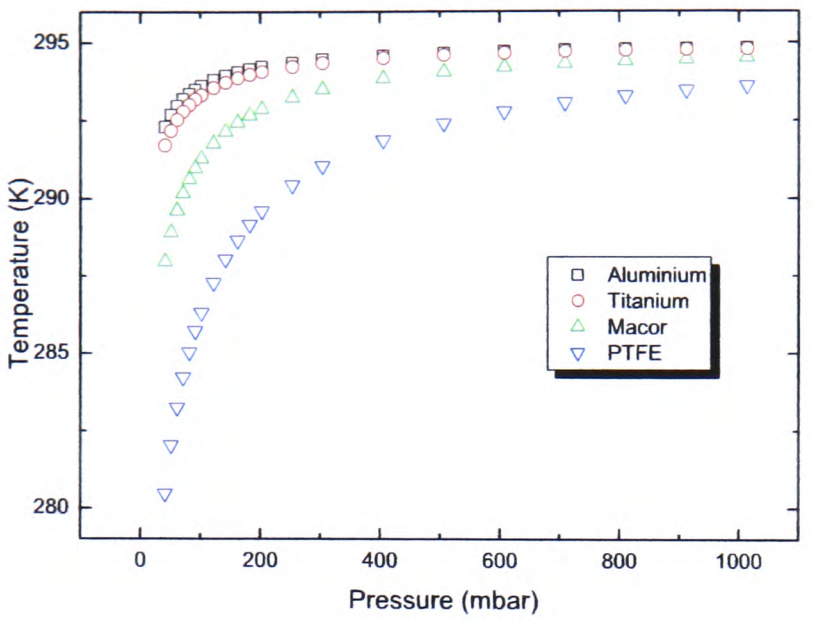

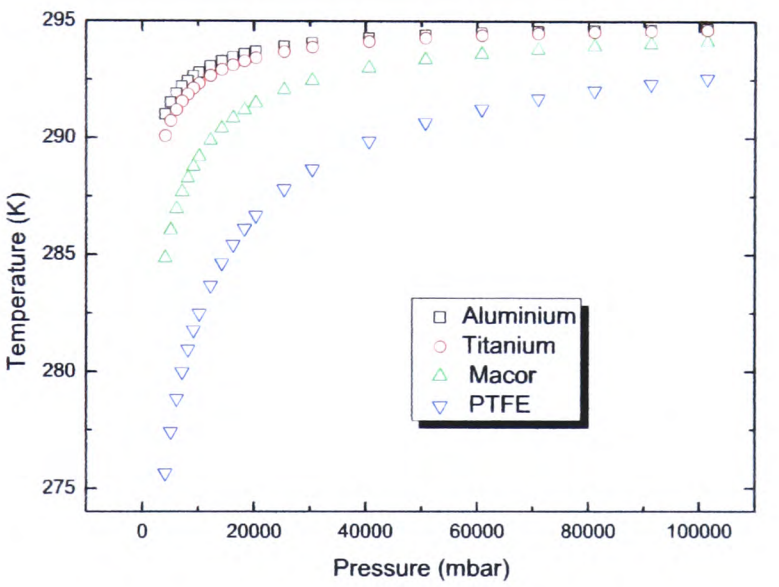

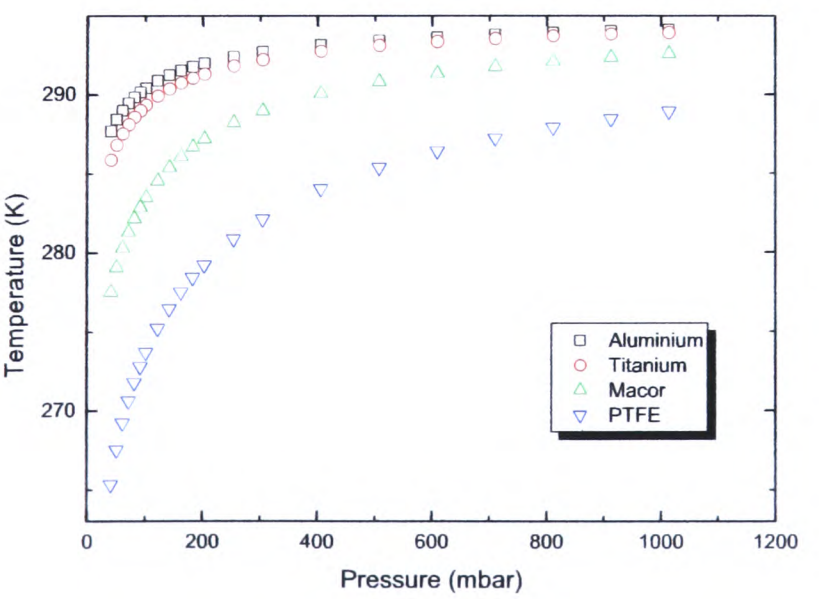

Figure 8.17: *Theoretical bulk temperature estimation of evaporative Water drops resting on Aluminium, Titanium, Macor and PTFE. Three different environments (He, N_2 and CO_2) with pressure ranging from 50 to 1000 $mbar$.*

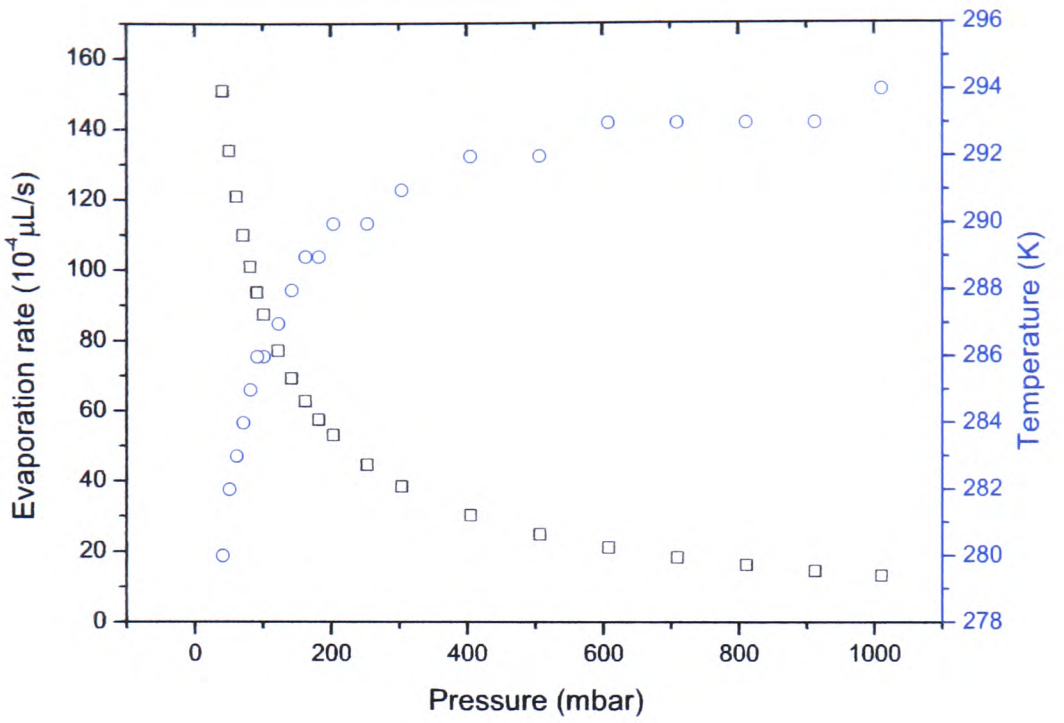

Figure 8.18: *Theoretical evaporation rate and bulk temperature against the surrounding pressure for Water drops resting on Aluminium. Helium is the ambient gas.*

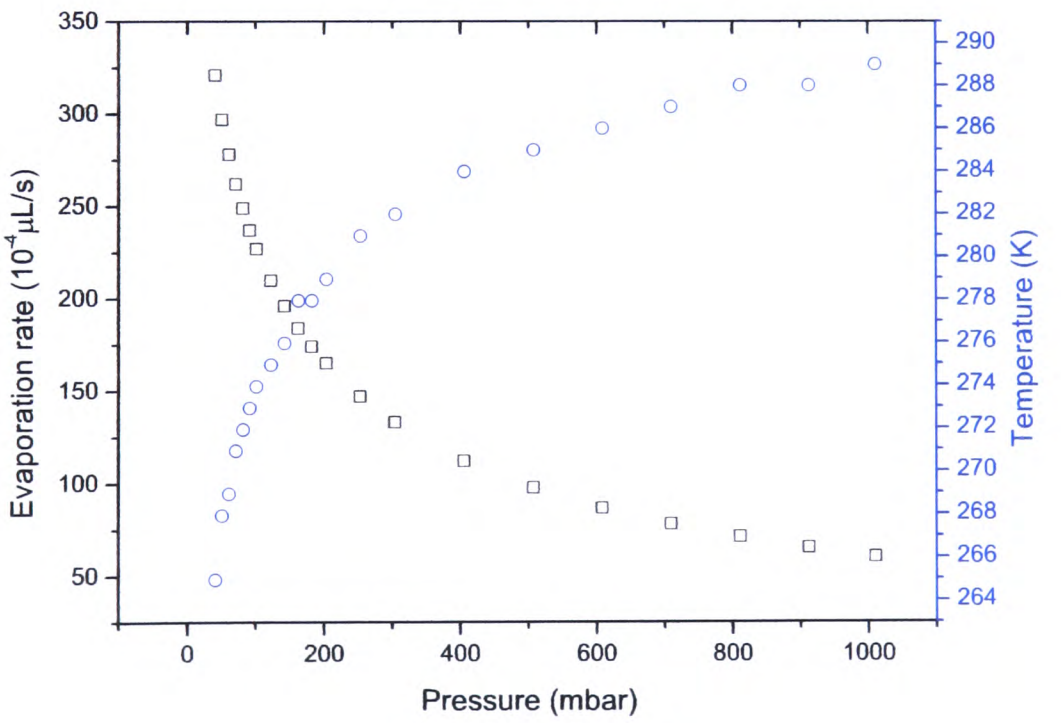

Figure 8.19: *Theoretical evaporation rate and bulk temperature against the surrounding pressure for Water drops resting on PTFE. Helium is the ambient gas.*

8.5 Conclusion

The evaporation of a drop in a gaseous phase is accompanied by a cooling effect. This latter being the result of the difference in energy consumed by the evaporation process (latent heat) and the energy supplied from the environment. When the drop is deposited on a substrate, different situations can be encountered depending on the nature of the substrate and its interaction with the liquid. It is important to note that by depositing the drop, a new interface is created (liquid-solid) and the evaporation interface (liquid-vapour) is also altered depending on the wettability of the liquid to the substrate. Two extreme cases can occur:

- A perfect thermal insulating substrate; in this case the evaporation rate will be modified according to the change of the liquid-vapour interface area. It is important to note that in this situation a cooling effect of the drop will be unavoidably observed due to the latent heat of evaporation.

- A perfect thermal conducting substrate, in this second case the evaporation rate is altered by two effects: the first is similar to the previous one (surface area change because of drop deposition) and the second mechanism which might be more important is the heat transfer between the substrate and the drop. The energy required for evaporation is brought in this case by conduction from the ambient (the gas phase) as well as heat conduction through the substrate. As a result the evaporation rate is enhanced compared to the thermally isolating substrate. Following this simple analysis it can be deduced that the evaporation of a sessile drop is limited by the diffusion process of vapour in the gaseous phase in the perfectly thermal conducting substrate case.

Chapter 9
Infrared measurements

As it was shown in the last three chapters, in the presence of evaporation the temperature of the drop is not uniform. Temperature measurements obtained with the thin thermocouples show these variations but were technically limited, the liquid-gas temperature measurements were not feasible. In order to realise these measurements, thermography technique was used. Preliminary infra-red (IR) measurements of the interfacial temperature have been undertaken on three liquids: Water, Methanol and FC72 (coolant liquid) respectively.

The three liquids have been chosen regarding their volatility: Water (2.34 kPa), Methanol (17 kPa) and FC72 (31 kPa). All drops were deposited on the same substrate, silicon wafer covered with a thin layer of polymer to decrease its surface energy and increase the contact angle (details on this substrate is given in the chapter on the binary mixture 5.2.2 page 75). All the experiments have been performed at ambient conditions, the evaporation process was driven by the diffusion of the liquid vapour into the surrounding atmosphere. A top view of the liquid-gas interface temperature was obtained by using a FLIR SC3000 thermal camera. The IR camera has a thermal sensitivity of $20mK$ at $30°C$, an accuracy of 1% or $1\ K$ of full scale for temperatures up to $150°C$ and 2% or $2\ K$ of full scale for temperatures above $150°C$. At the difference of thermocouples, IR technique is a nondestructive test (NDT) method. The IR method of measuring temperature is based on the fact that all objects, above absolute zero, emit infrared, radiant heat, at a rate that is directly related to the temperature of the object. The IR sensor detects the wavelength of the energy emitted by an object and by the use of integral equations, the temperature can be obtained once the body material and surface quality are known.

The radiant energy incident on a surface is partially reflected, partially absorbed and partially transmitted through the material. If we call r, a and t the ratio of the energy reflected, absorbed and transmitted to the total incident energy, one gets:

$$r(\lambda) + a(\lambda) + t(\lambda) = 1 \tag{9.1}$$

Reflection, absorption and transmission for a material depend on the radiation wavelength (λ). The surface of an object is really important in determining the reflection from it. A special body that has $a = 1$ and $r = t = 0$ at all wavelengths is called black body. A body does not only absorb radiation, but also emits it. Usually good absorbers are also good emitters. Emissivity is defined as the ratio of the body radiant energy to the black body one. Usually absorption (a) and emission (ϵ) are a function of temperature and the bodys nature as well as wavelength. The Kirchhoff principle states that the ratio between emission and absorption for a body is only a function of temperature and wavelength:

$$\epsilon = F(\lambda, T, B), \quad a = G(\lambda, T, B) \quad \epsilon/a = \Phi(\lambda,\ T) \tag{9.2}$$

The emission coefficient for a black body is called ϵ_0. Grey bodies are those which emit radiation with the same spectral distribution as a black body but of reduced intensity; i.e. grey bodies have a lower emission coefficient. Therefore, knowing ϵ_0, the Kirchhoff principle allows us to get the emission or absorption of a grey body once the other of these two is known. Selective emitters are those with an emissivity that is a function of the wavelength. For selective emitters spectral emission ($\epsilon(\lambda)$) is not equal to total emission (emissivity). Grey bodies are those with equal spectral and total emission. The Stefan law of radiation for a black body is:

$$q_0 = \int_0^\infty \epsilon_0 d\lambda = \sigma_0 T^4 \tag{9.3}$$

where q_0 is the total radiant heat flux from the black body. The black body spectral emission ϵ_0 is given by the Planck law:

$$\epsilon_0(\lambda,\ T) = \frac{2hc^2}{\lambda^5} \frac{1}{e^{\frac{hc}{kT}} - 1} \tag{9.4}$$

where h is the Planck's constant, k the Boltzmann's constant and c the speed of light.

What the IR camera measures is the heat flux emitted by a body. By this measurement and knowing the body emissivity and surface characteristics, one can infer the body temperature. The advantages and disadvantages of the IR technique can be found in specialised books such as Kaplan [10] and will not be repeated here. However, it must be said that the strong advantages for the present application are due to the quite small target size to be analysed and the great spatial resolution achievable with IR cameras.

Basically, the drops were deposited on smooth silicon substrates and let free evaporate. The whole evaporation process was recorded through an IR camera to get the liquid-gas interface

temperature profile. With Water drops, see Figure 9.1, the temperature field agrees with the measurements obtained with the thermocouple. But with the two other liquids, surprising and unexpected features have been observed. Even if the phenomenon was better observed on the experimental movies, the presence of these thermal wave could be seen on Figures 9.2 and 9.3.

As it was shown in the study of binary drops (see Chapter 6), the difference in behaviour of the pure components (water, methanol) is intriguing. Moreover the increase of the contact angle for methanol throughout the drop lifetime, till near the end, is unexpected. Infrared measurements of the interfacial temperature revealed that whilst the surface temperature of water remains uniform, the evaporation of methanol droplets exhibits wave trains in temperature profile. These thermal waves are found to spin around in a circular fashion. Such findings raise the possibility of a wavy interface and also internal waves, which could contribute to the difference in wetting behaviour.

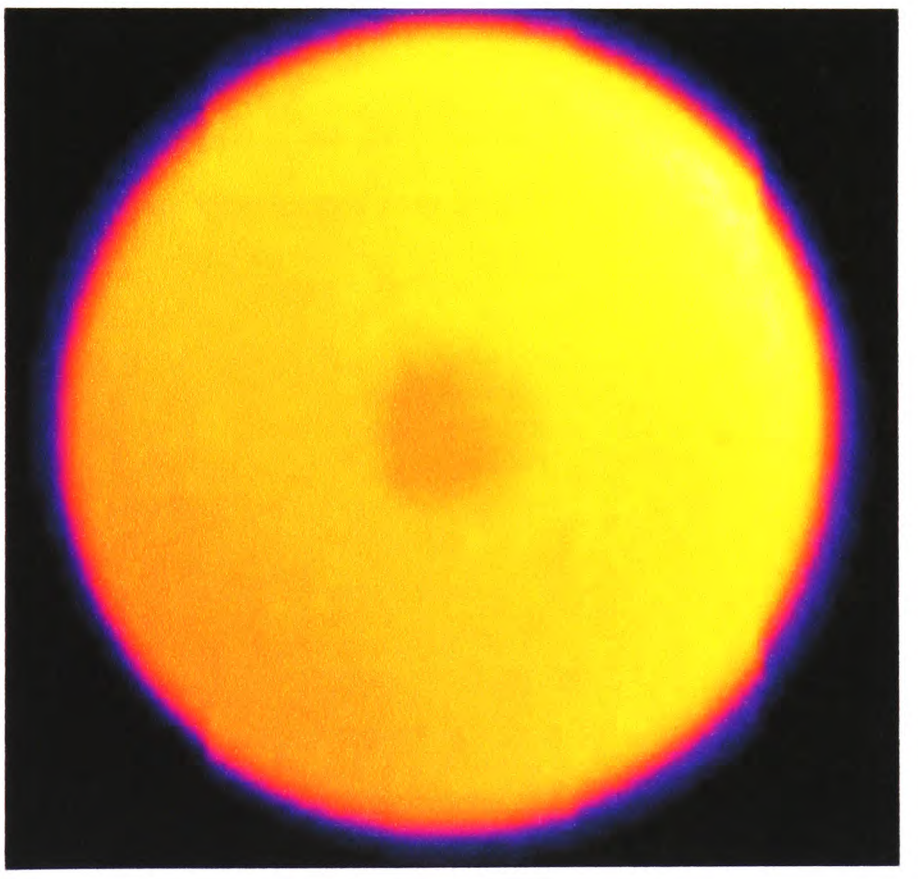

Figure 9.1: *Thermography imaging of a Water sessile drop (top view).*

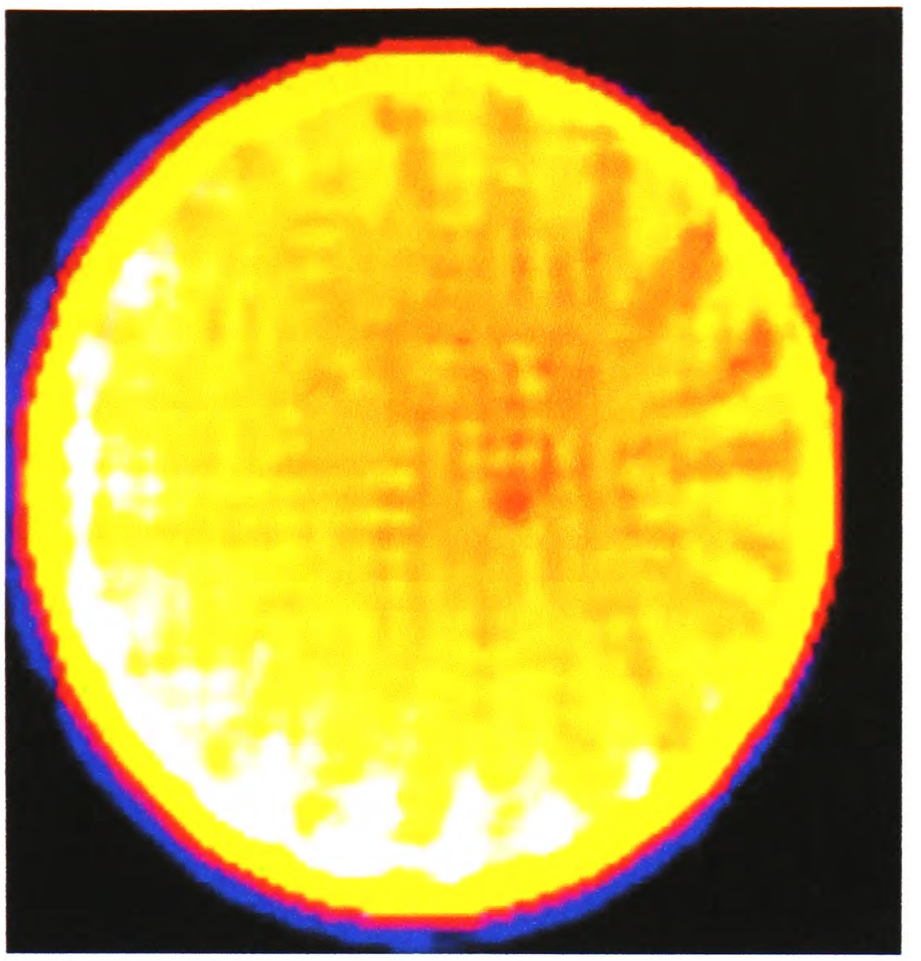

Figure 9.2: *Thermography imaging of a Methanol sessile drop (top view).*

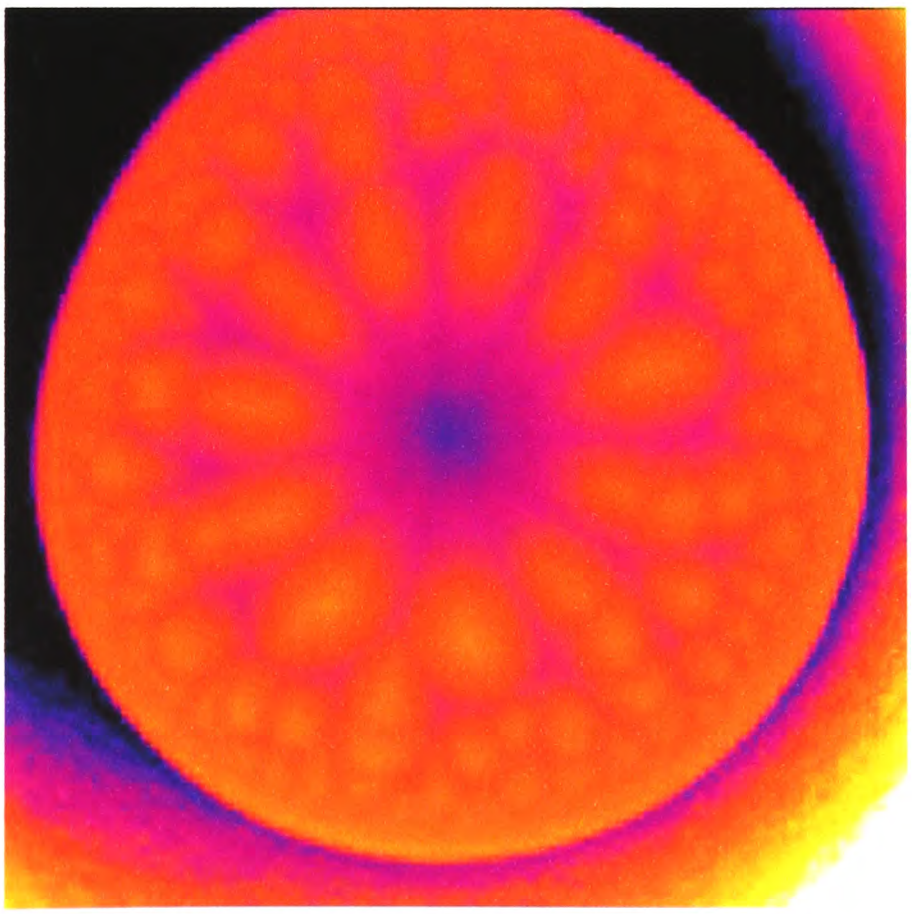

Figure 9.3: *Thermography imaging of a FC72 sessile drop (top view).*

Conclusions

A study of evaporating sessile drops have been presented. Many aspects of the evaporation mechanisms involved have been experimentally investigated and a mathematical model has been developed for particular conditions. This work focused on sessile drops in the particular case of partial wetting, the apparent contact angle was essentially rather than $15\,^{\circ}$, and only for spontaneous evaporation, no heat was supplied hence the evaporation process was solely driven by the deviation from the equilibrium pressure. Depending on the studied phenomenon, great care has been taken in the choice and preparations of the different liquids and substrates. Our interest in the liquids volatility property and the substrates surface roughness and energy was particularly important.

Before investigating the role played by each phase (solid, liquid and gas) in the heat and mass transfers involved, two particular cases have been studied: surface roughness influence on wetting and evaporating binary mixture drops behaviour respectively. In the first case, two kinds of patterned surfaces have been built, one with holes structure and the other with pillars structure. The experiments undertaken with Water drops deposited on "holes" and "pillars" substrates showed the pinning/depinning phenomenon of the contact line. The evolution of the advancing/receding contact angle while the drop base diameter increases/decreases suggests that the competition between the unbalanced Young force ($\gamma_{water}(\theta_{adv} - \theta_{eq})$) and the anchoring forces of the defects may be dominating the pinning/depinning process. Unfortunately, as the "holes" and "pillars" substrates have been made by two different materials, photoresist and PDMS, it is difficult to compare the holes structure to the pillars structure. Future works have to be focused on the preparation of structured surfaces with identical materials. And in order to study the influence of high evaporation rates by reducing the pressure, a new feature has to be set up to allow the formation and deposition of the drops after the pressure is reduced. Hence the problem due to the expansion of the air trapped between the substrate and the drop will be removed. In the second case, the evaporation of Water-Methanol and Water-DMSO binary drops have been investigated. These drops were deposited on a smooth silicon substrate coated by PMMA where almost no pinning of the triple line was observed. The results suggested that in the first part of the evaporation process the evaporated molecules were mainly the ones of the most volatile components. This was confirmed by the "saturated atmosphere" experiment

in the case of Water-Methanol mixtures. We also concluded that residual Methanol molecules were present through the whole evaporation process.

To understand the different mechanisms of the heat and mass transfers involved in the evaporation of pure liquid drops deposited onto a substrate, a mathematical model has been developed in close collaboration with Glasgow group (Pr S. Wilson, Dr B. Duffy and G. Dunn) and compared to the experimental results. This investigation had been divided in two steps. First, an experimental study was undertaken to investigate the evaporation process by looking at the role of vapour diffusion as a limiting mechanism. The ambient pressure as well as the nature of the ambient gas was varied to look at the effect of changing the diffusion coefficient. The comparison with the mathematical model showed that in the absence of any heat supplied, the evaporation process was effectively limited by the diffusion of the liquid vapour into the ambient gas. When using ambient gases with higher diffusion coefficient, higher evaporation rates were observed. Then the interaction between the substrate and the drop has been largely investigated through the use of solids with four orders of magnitude in thermal conductivity, liquids with three different volatilities and a large range of evaporation rates. It confirmed that the evaporation of a drop in a gaseous phase was accompanied by a cooling effect. This latter being the result of the difference in energy consumed by the evaporation process (latent heat) and the energy supplied from the environment. When the drop was deposited on a substrate, different situations can be encountered depending on the nature of the substrate and its interaction with the liquid. It is important to note that by depositing the drop, a new interface is created (liquid-solid) and the evaporation interface (liquid-vapour) is also altered depending on the wettability of the liquid to the substrate. Two extreme cases can occur. First, a perfect thermal insulating substrate; in this case the evaporation rate will be modified according to the change of the liquid-vapour interface area. It is important to note that in this situation a cooling effect of the drop will be unavoidably observed due to the latent heat of evaporation. Then a perfect thermal conducting substrate, in this second case the evaporation rate is altered by two effects: the first is similar to the previous one (surface area change because of drop deposition) and the second mechanism which might be more important is the heat transfer between the substrate and the drop. The energy required for evaporation is brought in this case by conduction from the ambient (the gas phase) as well as heat conduction through the substrate. As a result the evaporation rate is enhanced compared to the thermally isolating substrate. Following this simple analysis it can be deduced that the evaporation of a sessile drop is limited by the diffusion process of vapour in the gaseous phase in the perfectly thermal conducting substrate case. This

shows that the thermal conductivity of the substrate has to be taken into account to estimate the sessile drops evaporation rates. Complementary informations on the drop temperature field of volatile liquids has been brought by infra red measurements. These preliminary measurements of the interfacial temperature revealed that whilst the interfacial temperature of a water drop on a silicon substrate remains fairly uniform, the interfacial temperature of methanol and FC72 drops on the same substrate exhibit wave-like structures which rotate in the azimuthal direction. These novel thermal waves may cause both interfacial and internal waves and affect the wetting behaviour, and will hopefully be the subject of future work. New techniques as micro PIV has to be employed in order to characterise this phenomenon by another mean than thermography and bring new essential informations.

However, the first improvement of the model to be considered will be the introduction of the thermocapillary effect as Marangoni stress along the liquid-vapour interface of evaporating droplets is certainly one of the mechanisms occurring during the evaporation process. Indeed, the fluid flow inside a droplet may play an important role on the overall transport phenomena. This has not been systematically investigated and many questions remain to be elucidated. Marangoni effects result from the gradients along the interface, the gradients can be generated by imposed temperature or self generated by the evaporation process. The occurrence and magnitude of the above phenomenon depends on the applied constraints (Heating/Saturation) as well as the system undergoing evaporation namely the liquid and the substrate on which it lies. Hu and Larson [60] have modeled Marangoni effects in evaporating drops. The authors concluded that Marangoni effects are more important at higher contact angles (40 °). They concluded that thermocapillary becomes weak and cease at lower contact angles (14 °). This result indicates that thermocapillary effects might play a role in the early stages of evaporation. As the drop evaporation progress, the contact angle quickly gets to smaller values and the Marangoni effects would cease.

Appendix A
A kinetic model of diffusion

Considering a binary gas mixture in which the molecules A of one species are very similar to the molecules B. If the composition gradient is in one direction, molecules A diffuse down to lower concentration. Mixture temperature and pressure are uniform and the mass average velocity is zero.

The average thermal speed of the molecules is $\bar{C}$. Then the average rate at which the molecules cross the $x = x_0$ is $N\bar{C}$ where N is the molecular density (molecules per unit volume). Prior to crossing the x_0-plane, the molecules travel a distance close to the mean free path l, al, where a is a number on the order of one.

The net mass flux at the plane x_0 is the difference between the flux of molecules travelling from the left hand side and the molecules travelling from the right hand side. As the molecules travel a distance al prior crossing, the fraction of A correspond to N_A/N at $x_0 - al$ and N_A/N at $x_0 + al$ respectively. We thus obtain:

$$j_A\Big|_{x_0} = \eta\left(N\bar{C}\right)\left(\frac{M_A}{\mathcal{N}}\right)\left(\frac{N_A}{N}\Big|_{x_0-al} - \frac{N_A}{N}\Big|_{x_0+al}\right) \tag{A.1}$$

where η is a constant of proportionnality and $\frac{M_A}{\mathcal{N}}$ is the mass of molecule A ($\mathcal{N}$ is the Avogadro's number).

$$\begin{aligned} j_A\Big|_{x_0} &= \eta\left(N\bar{C}\right)\left(\frac{M_A}{\mathcal{N}}\right)\left(-2al\frac{d(N_A/N)}{dx}\Big|_{x_0}\right) \\ &= -2\eta a(\bar{C}l)\rho\frac{dm_A}{dx}\Big|_{x_0} \end{aligned} \tag{A.2}$$

The expression of the diffusion coefficient is then:

$$D_{AB} = -2\eta a(\bar{C}l) \tag{A.3}$$

References

[1] R. D. Deegan, O. Bakajin, T. F. Dupont, G. Huber, S. R. Nagel, and T. A. Witten, "Contact line deposits in an evaporating drop," *Physical Review E*, vol. 62, pp. 756–765, July 2000.

[2] C. Bourgès-Monnier and M. E. R. Shanahan, "Influence of evaporation on contact angle," *Langmuir*, 1995.

[3] P. G. de Gennes, "Wetting: statics and dynamics," *Reviews of modern physics*, 1985.

[4] R. G. Picknett and R. Bexon, "The evaporation of sessile or pendant drops in still air," *Journal of colloid and interface science*, 1977.

[5] O. E. Ruiz and W. Z. Black, "Evaporation of water droplets placed on a heated horizontal surface," *Journal of Heat Transfer*, vol. 124, pp. 854–863, Oct. 2002.

[6] R. D. Deegan, O. Bakajin, T. F. Dupont, G. Huber, S. R. Nagel, and T. A. Witten, "Capillary flow as the cause of ring stains from dried liquid drops," *Nature*, vol. 389, pp. 827–829, Oct. 1997.

[7] H. Hu and R. G. Larson, "Evaporation of a sessile droplet on a substrate," *J. Phys. Chem. B*, vol. 106, pp. 1334–1344, Sept. 2001.

[8] H. Hu and R. G. Larson, "Analysis of the microfluid flow in an evaporating sessile droplet," *Langmuir*, vol. 21, pp. 3963–3971, Jan. 2005.

[9] S. M. Rowan, M. I. Newton, F. W. Driewer, and G. McHale, "Evaporation of microdroplets of azeotropic lquids," *Journal of physical chemistry B*, 2000.

[10] K. Sefiane, L. Tadrist, and M. Douglas, "Experimental study of evaporating water-ethanol mixture sessile drop: influence of concentration," *International journal of heat and mass transfer*, 2002.

[11] A. K. H. Cheng, D. M. Soolaman, and H. Yu, "Evaporation of microdroplets of ethanol-water mixtures on gold surfaces modified with self-assembled monolayers," *J. Phys. Chem. B*, 2006.

[12] R. N. Wenzel, "Resistance of solid to wetting by water," *Industrial and Engineering Chemistry*, 1936.

[13] R. N. Wenzel, "Surface roughness and contact angle," *Journal of Physical Chemistry*, 1949.

[14] A. B. D. Cassie and S. Baxter, "Wettability of porous surfaces," *Transaction of the Faraday Society*, 1944.

[15] D. Pesach and A. Marmur, "Marangoni effects in the spreading of liquid mixture on a solid," *Langmuir*, 1987.

[16] A. Marmur, "Thermodynamic aspects of contact angle hysteresis," *Advances in colloid and interfaces science*, 1994.

[17] J. Bico, C. Marzolin, and D. Quéré, "Pearl drops," *Europhysics letters*, 1999.

[18] J. Bico, C. Tordeux, and D. Quéré, "Rough wetting," *Europhysics letters*, 2001.

[19] S. Shibuichi, T. Onda, N. Satoh, and K. Tsujii, "Super water-repellent surfaces resulting from fractal structure," *The journal of physical chemistry*, 1996.

[20] T. Onda, S. Shibuichi, N. Satoh, and K. Tsujii, "Super-water-repellent fractal surfaces," *Langmuir*, 1996.

[21] C. Neinhuis and W. Barthlott, "Characterization and distribution of water-repellent, self cleaning plant surfaces," *Annals of botany*, 1997.

[22] W. Chen, A. Fadeev, H. M. C., D. Öner, J. Youngblood, and J. McCarthy, "Ultrahydrophobic and ultralyophobic surfaces: Some comments and examples," *Langmuir*, 1999.

[23] D. Öner and J. McCarthy, "Ultrahydrophobic surfaces. effects of topography length scales on wettability," *Langmuir*, 2000.

[24] J. Bico, U. Thiele, and D. Quéré, "Wetting of textured surfaces," *Colloids and surfaces A*, 2002.

[25] J. Lee, B. He, and N. Patankar, "A roughness-based wettability switching membrane device for hydrophobic surfaces," *Journal of Micromechanics and Microengineering*, vol. 15, pp. 591–600, 2005.

[26] R. C. Reid, J. M. Prausnitz, and B. E. Poling, *The properties of Gases and Liquids*. McGraw-Hill, 1987.

[27] R. Defay, I. Prigogine, A. Bellemans, and D. H. Everett, *Surface Tension and Adsorption*. Longmans, 1966.

[28] *Handbook of Surface and Colloid Chemistry*. CRC Press, 1997.

[29] R. E. Johnson and R. H. Dettre, "Wettability and contact angles," *Surface and Colloid Science*, 1969.

[30] T. S. Meiron, A. Marmur, and I. S. Saguy, "Contact angle measurement on rough surfaces," *Journal of Colloid and Interface Science*, 2004.

[31] R. E. Johnson and R. H. Dettre, "Conatct angle, wettability and adhesion," *Advances in chemistry series*, 1964.

[32] C. Lam, R. Wu, D. Li, M. Hair, and A. W. Neumann, "Study of the advancing and receding contact angles: liquid sorption as a cause of contact angle hysteresis," *Advances in Colloid and Interface Science*, 2002.

[33] P. De Gennes, F. Brochard-Wyart, and D. Queré, *Gouttes, Bulles, Perles et Ondes*. Belin, 2002.

[34] A. Prosperetti and M. S. Plesset, "The stability of an evaporating liquid surface," *Phys. Fluids*, 1984.

[35] E. Sultan, A. Boudaoud, and M. Ben Amar, "Evaporation of a thin film: Diffusion of the vapour and marangoni instabilities," *Journal of Fluid Mechanics*, 2005.

[36] *A heat transfer textbook.* Phlogiston press, 2004.

[37] L. H. Tanner, "The spreading of silicone oil drops on horizontal surfaces," *Journal of physics D: applied physics*, 1979.

[38] L. Leger and J. F. Joanny, "Liquid spreading," *Reports on progress in physics*, 1992.

[39] G. McHale, S. M. Rowan, M. I. Newton, and M. K. Banerjee, "Evaporation and the wetting of low-energy solid surface," *Journal of physical chemistry*, 1998.

[40] H. P. Kavehpour, B. Ovryn, and G. H. McKinley, "The microscopic and macroscopic structure of the precursor layer in spreading viscous drops," *Physic review letter*, 2002.

[41] A. M. Cazabat, M. P. Valignat, S. Villette, J. De Connick, and F. Louche, "The mechanism of spreading: a microscopic description," *Langmuir*, 1997.

[42] A. Oron, S. H. Davis, and S. G. Bankoff, "Long-scale evolution of thin liquid films," *Review of modern physics*, 1997.

[43] P. Ehrhard and S. H. David, "Non-isothermal spreading of liquid drops on horizontal plates," *Journal of fluid dynamics*, 1991.

[44] D. Bonn, J. Eggers, J. Meunier, and E. Rolley, "Wetting and spreading," *Physical review E*, 2007.

[45] M. de Ruijter, T. D. Blake, A. Clarke, and J. De Coninck, "Droplet spreading: a tool to characterise surfaces at the microscopic scale," *Journal of petroleum science and engineering*, 1999.

[46] K. S. Birdi, D. T. Vu, and A. Winter, "A study of the evaporation rates of small water drops placed on a solid surface," *Journal of physical chemistry*, 1989.

[47] S. M. Rowan, M. I. Newton, and G. McHale, "Evaporation of microdroplets and the wetting of solid surfaces," *Journal of Physical Chemistry*, 1995.

[48] A. K. Panwar, S. K. Barthwal, and S. Ray, "Effect of evaporation on the contact angle of a sessile drop on solid substrates," *Journal of adhesion science and technology*, 2003.

[49] R. D. Deegan, O. Bakajin, T. F. Dupont, G. Huber, S. R. Nagel, and T. A. Witten, "Contact line deposits in an evaporating drop," *Physical review E*, 2000.

[50] H. Y. Erbil, G. McHale, and M. I. Newton, "Drop evaporation on solid surfaces: Constant contact angle mode," *Langmuir*, 2002.

[51] G. McHale and M. I. Newton, "Frenkel's method and the dynamic wetting of heterogeneous planar surfaces," *Colloid and surfaces A*, 2002.

[52] H. Y. Erbil and Y. Avci, "Simultaneous determination of toluene diffusion coefficient in air from thin tube evaporation and sessile drop evaporation on a solid surface," *Langmuir*, vol. 18, pp. 5113–5119, 2002.

[53] M. di Marzo, P. Tartarini, Y. Liao, D. Evans, and H. Baum, "Evaporative cooling due to a gently deposited droplet," *International Journal of Heat and Mass Transfer*, 1993.

[54] S. Chandra, M. di Marzo, Y. M. Qiao, and P. Tartarini, "Effect of liquid-solid contact angle on droplet evaporation," *Fire Safety Journal*, 1996.

[55] M. di Marzo and D. D. Evans, "Evaporation of a water droplet deposited on a hot high thermal conductivity surface," *Trans. ASME, J. Heat transfer*, 1989.

[56] M. Klassen, M. di Marzo, and J. Sirkis, "Infrared thermography of dropwise evaporative cooling," *ASME HTD*, 141.

[57] M. Klassen and M. di Marzo, "Transient cooling of a hot surface by droplets evaporation," *NIST-GCR*, 1990.

[58] E. F. Crafton and W. Z. Black, "Heat transfer and evaporation rates of small liquid droplets on heated horizontal surfaces," *International journal of heat and mass transfer*, 2004.

[59] N. N. Lebedev, *Special functions and their applications*. Prentice-Hall, 1965.

[60] H. Hu and R. G. Larson, "Analysis of the effect of marangoni stresses on the microflow in an evaporating sessile droplet," *Langmuir*, vol. 21, pp. 3972–3980, Jan. 2005.

[61] A. Marmur, "Contact angle hysteresis on heteregeneous smooth surfaces," *Journal of colloid and interface science*, 1994.

[62] S. Brandon and A. Marmur, "Simulation of conatct angle hysteresis on chemically heterogeneous surfaces," *Journal of colloid and interface science*, 1996.

[63] A. Marmur, "Contact angles in constrained wetting," *Langmuir*, 1996.

[64] S. Brandon, A. Wachs, and A. Marmur, "Simulated contact angle hysteresis of a three dimensional drop on a chemically heterogeneous surface: a numerical example," *Journal of colloid and interface science*, 1997.

[65] A. Marmur, "Contact-angle hysteresis on heterogeneous smooth surfaces: theoretical comparison of the captive bubble and drop methods," *Colloids and surfaces A*, 1997.

[66] G. Wolansky and A. Marmur, "The actual contact angle on heterogeneous rough surface in three dimensions," *Langmuir*, 1998.

[67] G. Wolansky and A. Marmur, "Apparent contact angles on rough surfaces: the wenzel equation revisited," *Colloids and surfaces A*.

[68] A. Marmur, "Wetting on hydrophobic rough surfaces: to be heterogeneous or not to be?," *Langmuir*, 2003.

[69] B. N. J. Persson, O. Albohr, U. Tartaglino, A. I. Volokitin, and E. Tosatti, "On the nature of surface roughness with application to contact mechanics, sealing, rubber friction and adhesion," *Journal of physics: condensed matter*, 2005.

[70] D. Quéré, A. Lafuma, and J. Bico, "Slippy and sticky microtextured solids," *Nanotechnology*, vol. 14, pp. 1109–1112, 2003.

[71] D. Quéré, "Rough ideas on wetting," *Physica A: Statistical Mechanics and its Applications*, vol. 313, pp. 32–46, Oct. 2002.

[72] Y. O. Popov, "Evaporative deposition patterns: spatial dimensions of the deposit," *Physical Review E*, 2005.

[73] *Handbook of Thermodynamic Table*. Begell House Publisher, 1995.